The neurochemistry underlying higher cognitive functions in the primate fronto-striatal network

By

Seyed-Alireza Hassani

Dissertation

Submitted to the Faculty of the

Graduate School of Vanderbilt University

in partial fulfillment of the requirements

for the degree of

DOCTOR OF PHILOSOPHY

in

Psychology

May 12, 2023

Nashville, Tennessee

Approved:

Thilo Womelsdorf, PhD

Carrie K. Jones, PhD

Alexander Maier, PhD

Mark Wallace, PhD

Acknowledgements

First and foremost, I would like to sincerely thank my PhD supervisor and scientific mentor, Dr. Thilo Womelsdorf. Starting from when we met, during my undergraduate studies, he showed excitement in my ideas and fostered my curiosity about the brain and cognition. He spent countless hours supporting me and my scientific endeavors and with great patience and care has taught me much, scientific and otherwise.

I would like to thank my committee members, Dr. Carrie K. Jones, Dr. Alexander Maier and Dr. Mark Wallace for their invaluable feedback and support.

I especially would like to thank Dr. Carrie K. Jones for her wisdom and support as a collaborator in our cholinergic projects. I would also like thank Dr. Paul Tiesinga and Dr. Matthijs van der Meer for their computational support as collaborators. Last but not least, I would like to thank our collaborators Dr. Janusz Pawliszyn and the Pawliszyn lab, in particular Dr. Sofia Lendor, for their support in the neurochemical sampling.

I would like to thank all past and present lab members and co-authors for providing invaluable scientific and social support. I would like to thank Dr. Mariann Oemisch in particular for her mentorship and training, Dr. Benjamin Voloh for making difficult times in my life bearable and being a wonderful role model, Adam Neumann for his patience, experimental support and for pushing me to be better, Dr. Kianoush Banaie Boroujeni and Robert Louie Treuting for their impact on my research and friendship, and Dr. Marcus Watson and Dr. Christopher Thomas for their invaluable technical support and friendship.

Finally, I would like to thank my friends and family from the bottom of my heart. My friends for helping keep me sane and grow in unexpected ways. My parents who gave up comfortable lives and promising futures to give me and my sister the best future possible, my sister for her unconditional love, my loving partner, Elizabeth Senft who has supported me and loved me through even the hardest parts of my studies and our wonderful dog Cabbages.

Table of Contents

Page

List of Figures

List of Tables

Chapter 1 Introduction

Neuromodulators add a dynamic component to the neural computations of neurons. These compounds act at metabotropic receptors and alter synaptic, neuronal and circuit behavior through intracellular second messenger systems. Their actions can have profound effects on synaptic plasticity, firing behavior of individual neurons, and even larger scale circuit activity like local field potentials observable in circuits ranging from invertebrate central pattern generators all the way to the primate neocortex (Bargmann, 2012; Marder, 2012; Marder et al., 2014; Thiele and Bellgrove, 2018). They are thought to define internal 'states' which adjust local neural activity to best support particular behaviors and actions.

1.1 Neuromodulatory systems

The characteristics of major neuromodulatory systems, namely norepinephrine (NE), acetylcholine (ACh), dopamine (DA) and serotonin (5-HT), well supports their ability to influence a large number of local circuits in a non-uniform manner. Throughout this document, I will focus on the noradrenergic and cholinergic systems and their involvement in the prefrontal cortex (PFC), anterior cingulate cortex (ACC) and the striatum.

1.1.1 Neuromodulatory projections

First, neuromodulatory nuclei project to multiple brain regions spanning the cortex, basal ganglia, hippocampus, cerebellum and even other neuromodulatory nuclei (Foote et al., 1983; Mesulam et al., 1983; Aston-Jones and Cohen, 2005a; Newman et al., 2012; Nomura et al., 2014; Avery and Krichmar, 2017). The pontine locus coeruleus (LC), the primary source of NE in the brain innervates the entirety of the cortex, including the PFC, ACC and hippocampus, as well as parts of the basal ganglia although with notably sparser projections (Foote et al., 1983; Aston-Jones and Cohen, 2005a; Nomura et al., 2014). The basal forebrain (BF), one of two sources of ACh, innervates the cortex, including the PFC, ACC hippocampus, amygdala and more while the brainstem cholinergic system innervates the basal ganglia including the ventral tegmental area

(VTA) as well as the cortex to a much lesser extent (Mesulam et al., 1983; Newman et al., 2012). Furthermore, the LC has projections to the BF while cholinergic stimulation of the LC is known to elicit a neural response (Berridge and Foote, 1991; Avery and Krichmar, 2017).

Although the BF is known to be made up of several smaller nuclei (Avery and Krichmar, 2017) the LC has, until recently, been thought of as a homogenous nucleus. However, recent results from both *ex vivo* and *in vivo* experiments have demonstrated different LC cell populations based on waveforms and encoding, as well as distinct sub-populations of cells projecting to specific targets (Chandler et al., 2014; Totah et al., 2018; Bari et al., 2020; Breton-Provencher et al., 2022; Su and Cohen, 2022).

1.1.2 The adrenoceptors of the noradrenergic system

Second, they have a wide range of receptor families, with different sensitivities for their respective neuromodulators, that couple with different g proteins and interact with various intracellular signaling pathways and transcription factors (Caulfield, 1993; Arnsten, 2000). For NE, there are three families of adrenoceptors: the β, α1 and α2 with the lowest to highest affinity for NE in that order. The β adrenoceptors are coupled to G_s and have a facilitatory interaction with cAMP while in contrast the α2 adrenoceptors are $G_{i/o}$ coupled with an antagonistic relationship with cAMP signaling. The role of cAMP on neural activity flips when comparing posterior, sensory cortices to the PFC such that the α2 adrenoceptors enhance PFC function but impair sensory cortical activity while β adrenoceptors enhance sensory cortical activity with some evidence of supporting a β1 mediated disruption of PFC function (Arnsten, 2000; Ramos et al., 2005). The α1 adrenoceptors are $G_{q/11}$ coupled and behave in an opposite manner to α2 adrenoceptors, enhancing sensory processing while having a negative impact on PFC function (Datta et al., 2019).

The well-defined differences in adrenoceptor sensitivity for NE combined with their frequently opposing actions lends the noradrenergic system to a Yerkes-Dodson style inverted-U function (Yerkes and Dodson, 1908) with too high or too low concentrations resulting in suboptimal behavior (Aston-Jones and Cohen, 2005a; Arnsten, 2015). The α2 adrenoceptors also

have the added function of being pre-synaptic auto-receptors for the noradrenergic system, however, they are expressed predominantly post-synaptically (U'Prichard et al., 1979; Arnsten and Pliszka, 2011). Previous work shows that auto-receptor activation reduces the slower tonic firing of the LC, associated with arousal (Rajkowski et al., 1994), while leaving glutamate-driven phasic responses, associated with stimulus driven activation (Aston-Jones and Cohen, 2005a), intact suggesting that auto-receptor activation does not simply lead to a non-discriminant reduction in LC activity (Aston-Jones et al., 1991a).

1.1.3 The muscarinic receptors of the cholinergic system

The cholinergic system contains two major families of receptors: the ionotropic nicotinic receptors and the metabotropic muscarinic receptors. I will focus on the neuromodulatory actions of ACh through the muscarinic receptors as nicotinic receptors allow for direct depolarization. The muscarinic ACh receptors (mAChRs) themselves contain 5 subtypes (M_1-M_5) which can be further split into M_1-like mAChRs paired with $G_{q/11}$ (M_1, M_3 and M_5), generally associated with promoting neural excitability, and M_2-like mAChRs paired with $G_{i/o}$ (M_2 and M_4), generally associated with reducing neural excitability (Caulfield, 1993; Lucas-Meunier et al., 2003; Langmead et al., 2008; Brown, 2010; Jones et al., 2012; Thiele, 2013). Although M_1 receptors bind to $G_{q/11}$, depending on its phosphorylation state, the β-arrestin signaling pathway could instead be activated (DeFea, 2008; Tobin, 2018).

The M_1 mAChRs are the most prevalent of the muscarinic receptors and are expressed post-synaptically throughout the brain, for example in the hippocampus, striatum, and the cortex including the PFC and ACC (Mrzljak et al., 1993; Langmead et al., 2008; Tsolias and Medalla, 2022). The M_2 mAChRs are expressed in the hippocampus, striatum and cortex, including the PFC, primarily as pre-synaptic auto-receptors (Mrzljak et al., 1993; Rouse et al., 1997; Tsolias and Medalla, 2022). The M_3 mAChRs are expressed in the cortex and hippocampus while the M_5 mAChRs are expressed in the substantia nigra, with both being expressed to a lesser degree than the M_1 mAChRs (Langmead et al., 2008; Jones et al., 2012). The M_4 mAChRs are expressed most prominently in the striatum both post- and pre-synaptically (Langmead et al., 2008; Jones et al., 2012). Notably, pharmacological targeting of muscarinic receptors has led to adverse side effects

through peripheral receptor activation credited to the M_2 and M_3 mAChRs (Foster, 2022), although there is evidence for M_1 mAChR involvement as well (Cruickshank et al., 1994; Rook et al., 2017). The mAChR localization and activation in posterior sensory cortices differ from the PFC, however, in contrast to the noradrenergic system, they do not seem to have different post-synaptic effects, but rather seem to serve different functions (Herrero et al., 2008; Galvin et al., 2018; Dasilva et al., 2019a), although excessive mAChR stimulation has been shown to disrupt PFC functions like rule selectivity (Major et al., 2018).

1.1.4 Spatial scale of neuromodulatory action

Third, there is evidence to suggest that the release of neuromodulators may take part in synaptic spillover or utilize a volume-transmission mechanism allowing for the activation of extra-synaptic receptors and those expressed by distal neurons (Umbriaco et al., 1994; Mrzljak et al., 1995; Mather et al., 2016; Disney and Higley, 2020). This is in opposition to wire-transmission referring to communication between a pre- and post-synaptic neuron (Sarter and Lustig, 2020). Through such mechanisms, a spatial gradient of neuromodulatory concentration is created with the site of release containing the highest concentration. This, combined with the variable sensitivities of different receptor families can create interesting patterns of receptor activation. One theory posits that this exact process, with noradrenergic spillover stimulating β receptors at the point of release with $\alpha1$ and $\alpha2$ receptors being activated in the proximal and distal periphery respectively, creating a so-called 'hotspot' (Mather et al., 2016) with recent empirical evidence to support it (Ghosh and Maunsell, 2022).

1.1.5 Receptor densities

Lastly, the specific pattern of expression of both muscarinic and noradrenergic receptors varies between brain regions and plays an important role in their ability to exert control over local circuits. For the various neuromodulatory receptor sub-types, expression profiles vary across regions and laminae (Zilles et al., 2004; Palomero-Gallagher et al., 2008; Froudist-Walsh et al., 2021; Rapan et al., 2022). The laminar distribution of most neuromodulatory receptors seems to be well preserved between different areas in the macaque, with the notable exception of the M_2

mAChR (Rapan et al., 2022). This seems to also be consistent in the human ACC, where the expression of M_1, M_3, $\alpha1$, and $\alpha2$ receptors is highest in layers 2-4 with some differences in the expression density of noradrenergic (primarily $\alpha1$) receptors between the dorsal and ventral banks (Palomero-Gallagher et al., 2008). In the primate, amongst the cortical regions, the ACC seems to boast the highest raw concentrations of multiple neuromodulatory receptors among which are the M_1, $\alpha1$, $\alpha2$ and other dopaminergic and serotonergic receptors (Froudist-Walsh et al., 2021). On the other hand, there was no observable difference in the expression of cholinergic or noradrenergic receptors, except for M_3 mAChRs, between dorsal and ventral sub-divisions of area 46 (Rapan et al., 2022). There is, however, a significantly higher expression of $\alpha2$ adrenoceptors along the entire principal sulcus relative to surrounding areas (Rapan et al., 2022). Note that not all major neuromodulatory families of interest were always accounted for in the above studies but they do provide invaluable data for the receptors that are reported.

The identity of the cell type, whether they are excitatory or inhibitory in nature for example, is also an important variable that determines neuromodulatory action on local circuits. Within the striatum, the M_1 mAChR is widely expressed and the M_2 mAChR is primarily pre-synaptic while the M_4 mAChR is the primary subtype responsible for regulating dopaminergic signaling and is highly expressed in D1 containing direct pathway spiny neurons (Hersch et al., 1994; Moehle and Conn, 2019). Cortically, in rhesus macaques, a comparative anatomy study found M_1 expression in both the lateral PFC and ACC to be extensive with almost all parvalbumin, calretinin and calbindin positive interneurons showing M_1 with no area differences, while expression in excitatory neurons was higher in the lateral PFC than the ACC (Tsolias and Medalla, 2022). On the other hand, post-synaptic M_2 expression was higher in the ACC than the lateral PFC for interneurons and lower for excitatory neurons, while pre-synaptic M_2 expression co-localized with the spines of excitatory, but not inhibitory, neurons more in the layer 3 of the lateral PFC compared to ACC (Tsolias and Medalla, 2022). This suggests strong cholinergic influence on both circuits with the ACC likely to experience more inhibitory outcomes from M_1 and M_2 mAChR stimulation than the lateral PFC. Lastly, in dorsolateral PFC (dlPFC) layer 3 excitatory synapses also show strong localization and responsiveness to M_1 stimulation (Galvin et al., 2020a). The dense expression of mAChRs in both the ACC and lateral PFC suggests they play a crucial role for local circuit functioning which is supported by many studies showing severe behavioral consequences

after exposing these circuits to scopolamine, a muscarinic antagonist (Bartus and Johnson, 1976; Zhou et al., 2011).

Within the noradrenergic system, α2 adrenoceptors are documented to play a role in controlling dopamine release (Trendelenburg et al., 1994; Hara et al., 2010). Cortically, the α2 and α1 adrenoceptors are also documented at the dlPFC layer 3 excitatory spines where they have enhancing and detrimental effect on synaptic efficacy respectively (Wang et al., 2007; Datta et al., 2019). Previous reports using rodents suggest that α but not β adrenoceptors enhance interneuron driven inhibitory action on pyramidal cells (Kawaguchi and Shindou, 1998). While another study showed NE selectively depresses excitatory action on inhibitory interneurons in the rat PFC (Wang et al., 2013). More recently, the cell-type localization of adrenoceptors was reported for the macaque frontal eye field (FEF) which results suggest may be extended to area 46 (Lee et al., 2020). It was found that α2A and β2 adrenoceptors were the most abundant relative to α1 and β1 adrenoceptors although all were found on both excitatory and inhibitory neurons consistent with previous results in primate dlPFC and mouse medial PFC (Liu et al., 2014; Xing et al., 2016). Furthermore, β, α1, and α2 expression in calbindin positive interneurons was significantly higher than both calretinin and parvalbumin positive interneurons. Lastly, long range projecting excitatory neurons were found to have a greater expression of all adrenoceptors than other excitatory neurons (Lee et al., 2020). This suggests that NE plays an important role in the PFC's capability to exert influence over other brain regions.

These characteristics of neuromodulatory systems allow for widespread and non-uniform action on local circuits across cortical and subcortical regions. This enables them to modulate behavior dependent on the current internal state of the individual.

1.2 Neuromodulators and behavior

What are the actual behavior and cognitive processes that these neuromodulatory systems support? We can explore this question from two complementary perspectives: disease states with loss of neuromodulatory neurons as well as exogenous compounds that activate, antagonize, modify or otherwise interact with existing neuromodulatory receptors. Both approaches allow for

the observation of changes in behavior that can provide insights into the specific contribution of each system or receptor to specific aspects of cognition.

1.2.1 The role of neuromodulators in psychiatric disorders

Extensive loss of neuromodulatory neurons is observed in the post-mortem brains of individuals with Alzheimer's disease (AD), Parkinson's disease and more (Whitehouse et al., 1981; Mesulam et al., 1983; Delaville et al., 2011). Furthermore, the extent of neuronal loss in neuromodulatory nuclei has been described to precede and predict the disease progression in AD (Schmitz and Nathan Spreng, 2016; Fahnestock and Shekari, 2019). Similarly, deafferentation or lesioning of neuromodulatory nuclei can lead to profound behavioral deficits that parallel symptoms in disease states.

For example, selective lesions of the nucleus basalis of Meynert or of cholinergic inputs to the PFC impaired spatial working memory (WM) and attention but not learning, decision making or episodic memory in macaques (Voytko et al., 1994; Croxson et al., 2011). In rats, cholinergic lesions of the BF disrupted visual attention and shifted latencies to maintain response accuracy (speed-accuracy tradeoff) to a stimulus of an unknown modality (visual vs auditory), while more specific lesions of the nucleus basalis magnocellularis disrupted feature binding while leaving learning and retrieval intact (Muir et al., 1992; Turchi and Sarter, 1997; Botly and de Rosa, 2009). In contrast, lesioning of the LC in rats impaired performance in a visual detection task only with increased attentional demand through the addition of distractors or temporal unpredictability (Dalley et al., 2001). The same study found elevated ACh tone in the PFC being significantly attenuated after dissociating performance with reward while NE, which was only elevated transiently after task onset, maintained high tone throughout after the dissociation of reward from performance. Studies have also compared cholinergic and noradrenergic lesions to better dissociate their functionality in cognition. In rats, noradrenergic but not cholinergic deafferentation of the medial PFC disrupted performance in an intra-/extra-dimensional set shifting task (McGaughy et al., 2008). Although these studies suggest distinct functions for the cholinergic and noradrenergic systems, a recent study found that lesions to both the LC and BF were required to induce memory deficits in rats although WM disruption only required LC lesions (Leo et al., 2023).

These studies suggest that ACh is critical for acuity and attention-based behaviors while NE helps adjust behavior in light of changing task rules and environmental statistics.

1.2.2 Pharmacological intervention

Due to the variability in the observable symptoms of individuals based on progression, co-morbidity and other variables, accurate diagnoses have remained a major challenge for psychiatric disorders. The research domain criteria (RDoC) project attempts to resolve this by providing guidelines for the classification of mental disorders based on the behavioral and cognitive processes that brain networks have been identified to support (Cuthbert and Insel, 2013). This is partially based on the heavy overlap in the, often multiple, cognitive processes that are disrupted in different psychiatric disorders (Millan et al., 2012). Individual cognitive processes that are impacted to some degree in multiple disorders may reflect insults to one or more neuromodulatory systems. Thus, the RDoC framework may assist in the association of particular cognitive processes to neuromodulatory perturbations. Neuromodulatory receptors are common targets for pharmacological interventions aimed at addressing and reducing psychiatric symptoms. The goal of these pharmacological agents is often to supplement reduced neuromodulatory tone by (1) increasing the longevity of endogenous neuromodulators, (2) directly acting as agonist or antagonist at the orthosteric site on receptors, or (3) potentiating endogenous neuromodulatory receptors through actions at allosteric sites.

The degradation of ACh in the synaptic cleft is conducted by the enzyme acetylcholine esterase. Compounds that disrupt the activity of this enzyme are referred to as acetylcholine esterase inhibitors (AChEIs), which have achieved mild success in the treatment of AD symptoms (Li et al., 2019; Marucci et al., 2021). One such compound is donepezil, and although it is FDA approved for the treatment of dementia in AD, due to overlapping symptoms across disorders, its efficacy has also been studied in attention deficit hyperactivity disorder (ADHD), schizophrenia, and more (Sugimoto, 2001; Yoo et al., 2007). Studies utilizing donepezil in primates provide evidence for the cholinergic system's involvement in multiple cognitive domains such as attention and vigilance (Rupniak et al., 1997; Tsukada et al., 2004a; Hassani et al., 2021), working memory (Buccafusco and Terry, 2004; Callahan et al., 2013) and even reasoning and problem solving

(Vardigan et al., 2015). While rodent studies support these findings, they also robustly test learning and memory enhancement with donepezil (Luine et al., 2002; Spowart-Manning and van der Staay, 2005; Bartko et al., 2011). For the noradrenergic system, NE is not degraded but is removed from extracellular space through the norepinephrine transporter which is targeted by drugs such as methylphenidate and atomoxetine. These drugs are FDA approved for the treatment of ADHD and have been shown in rodent studies to increase both dopaminergic and noradrenergic tone in PFC but only methylphenidate increases striatal dopamine (Bymaster et al., 2002; Swanson et al., 2006; Koda et al., 2010; Kodama et al., 2017). Empirical evidence suggests that both methylphenidate and atomoxetine confer their pro-cognitive benefits in the PFC through α2 adrenoceptors (Andrews and Lavin, 2006; Koda et al., 2010), or alternatively through striatal dopamine (Swanson and Volkow, 2002; Kodama et al., 2017), or both (Gamo et al., 2010). Studies in primates, supported by rodent studies, implicates these drugs with enhanced attention, impulse control, WM, distractor filtering and more (Chamberlain et al., 2006; Seu et al., 2009; Gamo et al., 2010; Kodama et al., 2017; Callahan et al., 2019; Higgins et al., 2020).

Alternatively, neuromodulatory receptors can be directly targeted with agonists or antagonists. However, because receptors from the same neuromodulatory system respond to the same endogenous actor (e.g. NE or ACh), their orthosteric sites are similar and thus make the development of receptor selective compounds difficult. For example guanfacine, an α2A adrenoceptor selective agonist still has affinity for α2B and α2C sub-types although at 15-60 times lower affinity (Uhlen and Wikberg, 1991; Uhlen et al., 1994). Nevertheless, guanfacine has provided great insight into the mechanism of the α2A adrenoceptor mediated enhanced in spatial WM (Wang et al., 2007). Clinically, guanfacine is FDA approved for the treatment of ADHD but has been explored for schizophrenia, autism spectrum disorder and more (Arnsten and Jin, 2012). Outside of WM enhancement, primate studies show guanfacine is capable of enhancing associative learning, attention and distractor filtering as well (O'Neill et al., 2000; Wang et al., 2004, 2007; Hassani et al., 2017). Although successful in the case of guanfacine, other drugs with lower specificity, such as Xanomeline, an M_1/ M_4 mAChR agonist suffer from peripheral side effects despite having highly efficacious pro-cognitive effects (Thorn et al., 2019).

Unlike orthosteric binding sites, pharmacological agents with affinity towards allosteric sites can be far more selective. Allosteric compounds for various metabotropic receptors have shown promise as pharmacological agents (Foster and Conn, 2017), with mAChR allosteric compounds raising a lot of excitement for the treatment of AD, schizophrenia and other disorders (Korczyn, 2000; Conn et al., 2009; Jones et al., 2012; Tobin, 2018). In particular, a number of M_1 mAChR positive allosteric modulators (PAMs) have been developed with several undergoing clinical trials. Studies in primates and rodents have shown that M_1 PAMs enhance WM, learning, executive functioning, attention and more with dramatically less dose-limiting adverse effects than non-PAM alternatives (Shirey et al., 2009; Chambon et al., 2012; Uslaner et al., 2013, 2018; Lange et al., 2015a; Vardigan et al., 2015; Rook et al., 2018a).

Due to the heavy overlap in symptoms and cognitive deficits between psychiatric disorders, the same compounds are explored as therapeutic agents in multiple disorders (Yoo et al., 2007; Arnsten and Jin, 2012; Millan et al., 2012; Melancon et al., 2013). This strongly suggests the involvement of neuromodulatory systems in multiple disorders as the mechanism of cognitive deficits but also therapeutic targets.

1.3 The fronto-striatal network

The fonto-striatal network, namely the dlPFC, ACC and caudate nucleus of the striatum (CD) are critical and heavily interconnected brain regions for the performance complex tasks. There is strong reciprocal connectivity between the ACC and dlPFC (Arikuni et al., 1994; Barbas, 2000; Heilbronner and Hayden, 2016; Nácher et al., 2018), both of which send excitatory projections to the striatum in a topographic manner (Haber and Knutson, 2010). The fronto-striatal network supports functions such as credit assignment, updating object and action values, maintaining of abstract rules, shifting behavioral strategies and more (Buckley et al., 2009; Morris et al., 2016; Asaad et al., 2017; Hikosaka et al., 2017; Izquierdo et al., 2017; Bartolo and Averbeck, 2020; Monosov et al., 2020; Boroujeni et al., 2022). In support of their function, neurons in these areas encode object and feature values (Kim and Hikosaka, 2013; Atallah et al., 2014; Bichot et al., 2015; Asaad et al., 2017; Oemisch et al., 2019; Boroujeni et al., 2020), reward expectation

(Kennerley et al., 2009; Kaping et al., 2011; Monosov, 2017), and reward prediction errors (RPEs) (Matsumoto et al., 2007; Glimcher, 2011; Oemisch et al., 2019).

1.3.1 Insights from lesion studies

Lesion studies can help reveal the functional role of different brain regions in a variety of behaviors. In humans and monkeys, lesions of the ACC disrupt the integration of history about rewards of feedback needed for the optimization of behavior as well as impair shifting behavioral strategies and response sets, particularly after erroneous outcomes when such adjustments are most needed (Kennerley et al., 2006; Buckley et al., 2009; Gläscher et al., 2012; Sheth et al., 2012; Kuwabara et al., 2014; Mansouri et al., 2020). Comparatively, in human and monkey lesion studies, dlPFC lesions disrupted maintenance of task rules in WM, conflict monitoring and selective attention of relevant feature dimensions (Mansouri et al., 2007, 2020; Rossi et al., 2007; Buckley et al., 2009; Minamimoto et al., 2010; Gläscher et al., 2012). As for the striatum, studies in monkeys with selective lesions of the ventral striatum resulted in deficits in utilizing reward to learn stimulus values (Rothenhoefe et al., 2017) while selective lesioning of the medium striatum resulted in deficits for the updating of stimulus values after reversal events (Clarke et al., 2008). These studies provide strong evidence for the dissociable contributions of the individual areas within the fronto-striatal network for robust and flexible behavior.

1.3.2 Convergent neuromodulation

The fronto-striatal network is critical in the regulation of neuromodulators. The LC and serotonergic raphe nucleus have strong reciprocal projections to the PFC and ACC (Aston-Jones and Cohen, 2005a; Avery and Krichmar, 2017), and the BF works in concert with the ACC to implement action plans (Khalighinejad et al., 2020). As described previously (see section 1.1.5), the neuromodulatory influence of the PFC and ACC involves expression of neuromodulatory receptors on the vast majority of neurons, with particularly dense expression on interneurons and excitatory projection neurons (Goldman-Rakic et al., 1990; Lee et al., 2020). While striatal dopamine, critical for RPE signaling (Schultz et al., 1997; Glimcher, 2011), is partially regulated by both cholinergic (Cachope et al., 2012; Cachope and Cheer, 2014; Moehle et al., 2017; Mohebi

et al., 2022) and noradrenergic signals (Trendelenburg et al., 1994; Hara et al., 2010). Although neither the dlPFC nor the ACC has particularly dense expression of neuromodulatory receptors relative to other areas within the PFC, perhaps with the exception of M_2 mAChRs (Rapan et al., 2022), layer 3 dlPFC recurrent connections between pyramidal neurons are documented to be particularly sensitive to neuromodulatory actions (Arnsten et al., 2010; Cools and Arnsten, 2022).

These recurrent connections between pyramidal neurons support the maintenance of information in WM through persistent 'delay' activity. Furthermore, these excitatory NMDA synapses are morphologically unique, with elongated post-synaptic spines expressing leaky channels that lead to low fidelity conduction by default (Arnsten et al., 2010). However, through intracellular signaling cascades, these synapses can be dynamically strengthened through the actions of α2A adrenoceptors (Arnsten and Goldman-Rakic, 1985; Li and Mei, 1994; Mao et al., 1999; Wang et al., 2007), M_1 mAChRs (Zhou et al., 2011; Major et al., 2015; Galvin et al., 2020a), nicotinic (α7) cholinergic receptors (Yang et al., 2013), nicotinic (α4/β2) cholinergic receptors (Sun et al., 2017), and mGluR3 metabotropic glutamate receptor (Jin et al., 2018). Alternatively, these synapses may be weakened by the over stimulation of NE or dopamine in an inverted-U manner through the activation of α1 adrenoceptors (Datta et al., 2019), β adrenoceptors (Ramos et al., 2005), and D1 dopaminergic receptors (Vijayraghavan et al., 2007, 2016; Wang et al., 2019). These synapses demonstrate how the simultaneous action of multiple neuromodulators may converge to modulate local circuit activity and demonstrate the interconnected nature of the neuromodulatory systems.

1.4 The multi-modulatory brain

Neuromodulatory systems heavily interact with one another. They can do this directly, for example through innervation from one neuromodulatory nucleus to another (Jones and Cuello, 1989; Aston-Jones et al., 1991b; Avery and Krichmar, 2017), or through convergent actions on local circuits (for example, see 1.3.2). It is therefore difficult to probe the behavioral contributions of single receptor sub-type or even a single neuromodulatory system in behavior. A trade-off exists between identifying receptor-specific contributions to the modulation of single neurons and local circuits and confidence in the manipulation being causal and sufficient for behavioral adjustment.

Both are ultimately required to gain a better understanding of receptor-specific contributions to cognition and developing efficacious interventions for the clinical population.

1.4.1 The interaction between multiple neuromodulatory systems

As already described, neuromodulatory receptors are abundant throughout the brain and fronto-striatal network and converge on individual neurons and even synapses (see sections 1.1.5 and 1.3.2). Activation of these receptors is not only non-mutually exclusive, but rather likely due to the overlap in the activity of neuromodulatory nuclei. Although serving different functions, neurons in the LC, BF, dopaminergic ventral tegmental area and serotonergic raphe nucleus may respond to similar sensory-evoked events such as reward acquisition and presentation of surprising or salient stimuli (Aston-Jones et al., 1994; Mirenowicz and Schultz, 1994; Parikh et al., 2007; Bromberg-Martin et al., 2010; Glimcher, 2011; Bouret and Richmond, 2015; Hangya et al., 2015; Luo et al., 2015; Monosov et al., 2015; Breton-Provencher et al., 2022). Furthermore, even outside of their respective nuclei, neuromodulators may interact through hetero-receptors. A well-documented example of such a case is the cholinergic mediated release of dopamine in the striatum (Zhang and Sulzer, 2004; Cachope and Cheer, 2014). A recent study shows that the activity of cholinergic interneurons and dopaminergic release are linked in the striatum independent of the firing rate of dopaminergic neurons in the ventral tegmental area (Mohebi et al., 2022). This suggests that the application of even receptor-specific pharmacological agents could implicate other neuromodulatory systems.

A special relationship also exists between NE and dopamine due to dopamine being the pre-cursor molecule to the synthesis of NE. This also means that they are similar enough structurally that the norepinephrine transporter is capable of removing dopamine from extracellular space (Morón et al., 2002; Devoto et al., 2020). Furthermore, noradrenergic terminals releasing NE have been shown to contain dopamine, with LC activity being linked to extracellular dopamine in the PFC (Devoto et al., 2005, 2019, 2020).

1.4.2 Making multi-modulator measurements

The strong interactions between the neuromodulatory systems suggests that in order to understand the role of one neuromodulatory system on cognition and behavior, we should ideally be measuring as many neuromodulators as possible. This would not only lead to more confident results by ruling out confounds and contributions of other neuromodulatory systems, but also be informative about the simultaneous and convergent actions of neuromodulatory systems. Several theories and models take into account the multi-modulatory nature of the brain (e.g. Yu and Dayan, 2005; Doya, 2008).

Methodological advances in the past few decades for neuromodulatory detection have mostly focused on increasing temporal resolution, specialized for a few compounds at most (Heien et al., 2004; Dale et al., 2005; Jacobs et al., 2010). Recent optical methods using fluorescent proteins such as dLight are promising (Patriarchi et al., 2018; Salinas et al., 2022) with more generic metabotropic (g-protein coupled receptor) tracking likely to be the future, although currently not capable of tracking multiple neuromodulatory signals to my knowledge (Jing et al., 2019). Thus, micro-dialysis still remains the most widely used method capable of reporting multiple neuromodulators *in vivo* during active behavior (Anderzhanova and Wotjak, 2013; Kennedy, 2013). It is by no means a perfect method however, and has certain weaknesses and barriers to entry such as requiring a long stabilization period before recording.

1.5 Thesis overview

Probing the contribution of neuromodulatory systems on the fronto-striatal network and its cognitive functions is a worthwhile endeavor that could help forward our basic science understanding of neuromodulators as well as better support clinical populations. My work outlined here attempts to support studying the multi-modulator brain and parse out the contributions of individual receptor sub-types through the comparative use of specific and non-specific pharmacological agents.

In the second chapter, we describe efforts for the development of a multi-modulator measurement technique to supplement micro-dialysis (Hassani et al., 2019). A critical focus was

placed on multi-site recordings for reasons described above such that asymmetries in neuromodulatory tone and activity could be captured. We report concentrations of glutamate, ACh, dopamine, and choline simultaneously in the dlPFC, premotor cortex and CD in a stable and reliable manner in two monkeys. Since then, continued work with our collaborators has allowed us to report serotonin and GABA as well. Expanding the space of available tools for multi-modulatory measurements is critical for more accessible and creative experiments that will undoubtedly reveal more about the individual, synergistic and antagonistic role of neuromodulatory systems.

In the third chapter, we utilize the AChEI donepezil to explore how the cholinergic system modulates multiple facets of higher order cognition (Hassani et al., 2021). By evaluating the variable contributions of such a non-specific drug on different cognitive domains, we can learn more about the role of the endogenous cholinergic system. Our results suggest that the peak of inverted-U curves of the dose – performance relationship in two tasks varies based on their cognitive demands. Thus, the 'optimal' donepezil dose promoting improved cognitive flexibility and improved attentional filtering differed from one another.

In the fourth chapter, we utilize a more specific M_1 PAM utilizing the same behavioral setup as chapter three in order to isolate the M_1 specific contributions of cholinergic neuromodulation on behavior relative to the unspecific AChEI donepezil (Hassani et al., 2023, *in review*). We find that the M_1 potentiation by an M_1 PAM is important for enhancing cognitive flexibility but not attentional mechanisms.

In the fifth chapter, we utilize the non-WM contribution of α2A adrenoceptors on cognition by identifying and utilizing an efficacious dose of guanfacine for enhancing selective attention and cognitive flexibility (Hassani et al., 2017). Using hybrid Bayesian-reinforcement learning models we propose a non-WM mechanism of α2A action involving enhanced scaling of RPE signals.

In the sixth chapter, we empirically show that RPE signals in the fronto-striatal network are indeed enhanced with guanfacine in order to improve cognitive flexibility (Hassani and Womelsdorf, 2023, *in prep*). Simultaneous single unit recordings in the dlPFC, ACC and CD

reveal that guanfacine does not change firing rate statistics or the proportion of neurons encoding task, outcome or latent (model-derived) learning relevant variables, but instead results in enhanced outcome and RPE encoding to allow for faster behavioral adjustments after unexpected outcomes. Furthermore, fast spiking putative inhibitory neurons were specifically identified as contributing to the enhanced outcome encoding observed after guanfacine administration.

Chapter 2 Multi-Neuromodulator Measurements across Fronto-Striatal Network Areas of the Behaving Macaque using Solid-Phase Microextraction

2.1 Abstract

Different neuromodulators rarely act independent from each other to modify neural processes but are instead co-released, gated, or modulated. To understand this interdependence of neuromodulators and their collective influence on local circuits during different brain states, it is necessary to reliably extract local concentrations of multiple neuromodulators in vivo. Here we describe results using solid phase microextraction (SPME), a method providing sensitive, multi-neuromodulator measurements. SPME is a sampling method that is coupled with mass spectrometry to quantify collected analytes. Reliable measurements of glutamate, dopamine, acetylcholine and choline were made simultaneously within frontal cortex and striatum of two macaque monkeys (*Macaca mulatta*) during goal-directed behavior. We find glutamate concentrations several orders of magnitude higher than acetylcholine and dopamine in all brain regions. Dopamine was reliably detected in the striatum at tenfold higher concentrations than acetylcholine. Acetylcholine and choline concentrations were detected with high consistency across brain areas, within monkeys and between monkeys. These findings illustrate that SPME microprobes provide a versatile novel tool to characterize multiple neuromodulators across different brain areas in vivo to understand the interdependence and co-variation of neuromodulators during goal directed behavior. Such data will be important to better distinguish between different behavioral states and characterize dysfunctional brain states that may be evident in psychiatric disorders.

2.1.1 New and noteworthy

Our manuscript reports a reliable and sensitive novel method for measuring the absolute concentrations of glutamate, acetylcholine, choline, dopamine and serotonin in brain circuits in-vivo. We show that this method reliably samples multiple neurochemicals in three brain areas

simultaneously while nonhuman primates are engaged in goal directed behavior. We further describe how the methodology we describe here may be used by electrophysiologists as a low barrier to entry tool for measuring multiple neurochemicals.

2.2 Introduction

Extracellular concentrations of neuromodulators influence firing regimes, input-output relationships and neural interactions in local circuits and long-range brain networks (Marder, 2012; Thiele and Bellgrove, 2018), and are dysregulated in virtually all psychiatric disorders (Millan et al., 2012; Avery and Krichmar, 2017). Accumulating evidence suggests that these fundamental roles of neuromodulators for circuit functioning are unlikely realized by single neuromodulators operating in isolation. Rather, neuromodulatory systems are heavily intertwined (Gobert et al., 1998; Avery and Krichmar, 2017; Moehle et al., 2017), and operate simultaneously on individual cells and circuits (Arnsten et al., 2010; Marder, 2012; Hassan et al., 2015; Santana et al., 2018). In each circuit, local mechanisms exert control over the release of neuromodulators from terminals of brainstem-originating projection neurons. This local control proceeds through activation of pre-synaptic glutamatergic receptors (Wang et al., 1992; Ghersi et al., 2003; Pittaluga et al., 2006; Luccini et al., 2007; Grilli et al., 2009; Pittaluga, 2016). These insights suggest that an understanding of the contribution of neuromodulators to circuit functioning requires measuring, simultaneously, multiple neuromodulators in conjunction with ongoing glutamatergic neurotransmitter concentrations and action. Consistent with this conclusion single neuromodulator theories often fail to account for all observable symptoms in psychiatric diseases (Remy et al., 2005; Halliday et al., 2014; Bohnen et al., 2015).

Despite the accumulating evidence for the interdependence of neuromodulator actions, few methods exist for their simultaneous measurement in vivo and across multiple brain areas (**Appendix A, Table A1;** https://github.com/att-circ-contrl/SPME_paper_SI.git). Most of these existing neurochemical sensing methods allowing multi-neuromodulator sampling have a barrier to entry by requiring specialized equipment and trained experts preventing data collection by scientists who are otherwise interested in the role of endogenous and exogenous neuroactive chemicals in cognition and psychiatric disorders. Electrochemical methods such as fast scan cyclic

voltammetry (FSCV) and amperometry have sub-second temporal resolution, but are limited to the measurement of a few compounds (Dale et al., 2005; Jacobs et al., 2010) and are challenging and not robust for wide-spread in vivo application in nonhuman primates yet, although several labs have recently reported success (Quintero et al., 2007; Schluter et al., 2014; Disney et al., 2015; Yoshimi et al., 2015; Schwerdt et al., 2017; Vartak et al., 2017; König et al., 2018). Imaging techniques such as positron emission tomography (PET) are also limited to the measurement of one or a few compounds simultaneously (Fisher et al., 1995). Microdialysis (MD) paired with mass spectrometry is the most commonly used method for measuring multiple neuromodulators in awake behaving animals. MD provides a data collection method which is then analyzed post hoc to identify and quantify collected analytes. It operates with a semi-permeable membrane which allows for the continuous collection of the available extracellular neuromodulators through passive diffusion, and can even be used to locally release pharmacological agents (Watson et al., 2006; Buck et al., 2009; Perry et al., 2009; Anderzhanova and Wotjak, 2013; Kennedy, 2013). However, MD does have several disadvantages. MD disrupts the tissue during its initial placement of the probe or a guiding cannula resulting in damage-induced release of neuromodulators that can last several hours before stable measurements become possible. Moreover, MD has low affinity for hydrophobic compounds and comparatively broad spatial and temporal resolution that is in the range of 200-400 μm in diameter and 10-20 minutes, respectively. These values are dependent on the surface area of the permeable membrane, the exact method of MD, flow rate, resolution of detection methods for analytes of interest, tissue tortuosity and more (Watson et al., 2006; Anderzhanova and Wotjak, 2013; Kennedy, 2013).

Here, we set out to address some of these limitations with a novel protocol for measuring multiple neuromodulators in vivo in discrete 20 minute intervals using probes optimized for solid phase microextraction (SPME) (Pawliszyn, 2000, 2012). SPME probes are thin (200 μm) wires of arbitrary length coated with an inert porous polymeric matrix using biocompatible binder on one end where molecules with appropriate size and affinity migrate via passive diffusion and are retained by weak intermolecular interactions (*see* Methods). SPME provides an alternate method for data collection which can then be analyzed by tools such as mass spectrometers. This method has been shown to extract in neural tissue dynamic changes in dopamine (DA) and serotonin (5-HT) levels with comparable precision to MD (Cudjoe et al., 2013; Cudjoe and Pawliszyn, 2014).

Additionally, due to the similarity of SPME probes to commonly used microelectrodes in electrophysiological recordings, relatively minor adjustments will allow for the adaptation of conventional microelectrode driving systems for SPME use. This, combined with post collection analysis through standard chemistry facilities makes SPME an attractive and easy-to-use tool for electrophysiology labs.

SPME has the potential to be a powerful new tool to compliment the mentioned methods well suited for neurochemical profiling that spans both multiple neuromodulators as well as multiple brain regions simultaneously. Such data will allow for global observation of slow neuromodulator dynamics that could better inform our hypotheses and help relate global neuromodulator levels to electrophysiology and behavior.

Thus, the ability of SPME to report major neuromodulators as well as glutamate and GABA were tested in two behaving rhesus macaques. Probes were repeatedly and simultaneously inserted into two cortical regions and the striatum to observe inter-areal differences between extracellular neuromodulator concentrations. We found that extracellular concentrations of glutamate, dopamine, acetylcholine and choline could be reliably distinguished and differed systematically between brain regions.

2.3 Materials and methods

2.3.1 Animals

Data was collected from two 8 year-old male rhesus macaques (*Macaca mulatta*) weighing 8-12 kg. All animal care and experimental protocols were approved by the York University Animal Care Committee and were in accordance with the Canadian Council on Animal Care guidelines. Details regarding the experimental setup, recording procedures, and reconstruction of recording sites have been described previously (Oemisch et al., 2015). Briefly, animals were implanted with a 20 mm by 28 mm recording chamber over the frontal region of the right hemisphere guided by stereotaxic coordinates (Paxinos et al., 2000) and MR images. The animals were seated in a custom made primate chair and head stabilized with their eyes 65cm away from a 21’ LCD monitor

refreshed at 85 Hz. Eye traces were collected by a video-based eye-tracking system (Eyelink 1000 Osgoode, Ontario, Canada, 500 Hz sampling rate). The animals were engaged in an over-trained attention tasks in which they would use saccadic eye movements to acquire juice reward (**Appendix A, Fig A1;** https://github.com/att-circ-contrl/SPME_paper_SI.git). The specifics of the task are described elsewhere (Hassani et al., 2017). Both animals showed stable performance and acquired similar reward volumes on all recording days. In both tasks, stimulus presentation and reward delivery was controlled through MonkeyLogic (http://www.brown.edu/Research/monkeylogic/).

2.3.2 SPME protocol and Fabrication of SPME Probes

We provide a visual overview of the complete SPME protocol used here in **Appendix A, Fig A2** (https://github.com/att-circ-contrl/SPME_paper_SI.git) and delineate the chemical materials, LC-MS/MS analysis, and detailed quantitation of neuromodulators in **Appendix A** (https://github.com/att-circ-contrl/SPME_paper_SI.git) and in a companion paper (Lendor et al., 2019b). All measurements used miniaturized SPME probes that were manufactured by repeated dip-coating of stainless steel wires in a suspension of extracting phase in a binder. This general procedure reported previously (Gómez-Ríos et al., 2017), has been modified to fit the purpose of *in vivo* brain sampling (Lendor et al., 2019b). The 3 mm long tip of the wire was acid-etched down to approx. 100 µm to create a recession capable of accommodating thicker layer of coating without significantly increasing the total probe diameter. The extracting phase was an in-house synthesized hydrophilic-lipophilic balance polymer functionalized with benzenesulfonic acid to introduce strong cation exchange properties (HLB-SCX). The monodispersed polymeric particles with diameter of approx. 1 µm were suspended in the binder consisting of 7% polyacrylonitrile dissolved in N,N-dimethylformide (w/v), ensuring the particles-to-binder ratio at 15% (w/v). The extracting phase suspension was prepared one day before the probe coating, homogenized by sonication and stirred at 800 rpm overnight. Several layers of coating were deposited on the modified wires, resulting in total coating thickness of ≈50 µm and total probe diameter of 195 µm. The average pore size of the extracting phase was measured at 1.2nm. Before the use, the probes were cleaned with the mixture of methanol, acetonitrile and 2-propanol (50:25:25, v/v/v), activated in the mixture of methanol and water (50:50. v/v) and sterilized in steam for 15 min at 121°C.

During the sampling, SPME probes were inserted into sheathing cannulas to protect the coating and prevent it from extracting compounds on the way to the target brain area. The cannulas underwent the same cleaning and sterilization procedure as the probes and then the lengths of both components of the SPME assembly were adjusted to 60-70 and 70-80 mm for the probes and cannulas, respectively.

2.3.3 MRI Guided Electrophysiological Mapping of Target Tissue

The anatomical coordinates of the brain regions of interest were first identified through 3 T MR images. The MR images were then verified with extracellular electrophysiological recordings of the target areas, which provided the gray and white matter boundaries for the cortical sites and the dorsal most aspect of the head of the caudate nucleus. Tungsten microelectrodes were 200 μm thick with an impedance of 1-2 MΩ. All electrodes, SPME probes and their accompanying guiding cannulas were driven down into the brain and later out using software-controlled precision microdrives (Neuronitek, ON, Canada). Electrodes were connected to a multichannel acquisition processor (Neuralynx Digital Lynx system, Inc., Bozeman, Montana, USA) which was used for data amplification, filtering and acquisition of spiking activity. Spiking activity was obtained by applying a 600-8000 Hz bandpass filter, with further amplification and digitization at a 32 KHz sampling rate. For every recording day, electrodes were lowered until the first detection of spiking activity (indicative of gray matter) at the depth suggested by the MR images.

2.3.4 SPME Sampling and Post-Processing Procedures

All three SPME assemblies (example of sampling using one assembly in **Fig 2.1A-C**) were simultaneously driven to 200 μm above the point of first spiking detection. SPME assemblies were located ~1 mm away from the electrode penetration location. Then, only the SPME probes were inserted 3 mm into the areas of interest. On average macaque cortical thickness is only 2 mm while the head of the caudate at the point of sampling was well over 3 mm. An extraction duration of 20 min was selected to reflect stable extraction time profiles for all compounds of interest. The kinetics of target analyte extraction, for example glutamate and dopamine, can be visualized in vitro through extraction time profiles (Lendor et al., 2019b) (**Fig 2.1D-E**). Brain homogenate was

spiked with known concentrations of target analytes and four replicates were collected during which multiple probes were placed in the homogenate and sequentially removed at reported times after initial insertion and quantified (LC-MS/MS procedure described below). These extraction time profiles reflect the quantifiable concentration of collected analyte over time, which is captured in sequence by a linear "kinetic" regime, a "dynamic" regime and an "equilibrium" regime over extraction time. These labels are used to describe the various rates of analyte adsorption by the SPME fibre, where the kinetic regime reflects the fastest adsorbtion of the target analyte, the equilibrium regime reflects a period of only marginal further analyte collection and an intermediate dynamic regime (Ouyang and Pawliszyn, 2007). These extraction kinetics provide information about the time it takes until equilibrium is reached in a concentration independent manner that is helpful in estimating a lower limit for extraction times to collect quantifiable analyte concentrations. After the 20 min extraction event, all SPME probes were driven back 3 mm into the guiding cannulas and all SPME assemblies were withdrawn from the brain (**Fig 2.1A-C**). The microdrives were then removed from the chamber to enable unclamping of the SPME probes, a brief wash and then storage in glass vials surrounded by dry ice until placing them into a -80°C freezer. One entire sampling event (one extraction in 3 different brain areas together with assembling the SPME probes and cannulas, driving into and out of brain, washing and preparing for storage) was performed within 50 min, except for the first sampling event in each sampling day. The first sampling event, with the area identification using electrophysiology recording, was performed within 75 min. The removal of the SPME microprobe from the gray matter and the positioning of a new SPME microprobe in the same location limits the temporal continuity of sampling. We believe that further optimizing of the SPME microprobe switching procedure with e.g. pre-loaded SPME probes will allow replacing SPME fibres within 2-10 min. Alternatively, SPME microprobes could be used in spatially separate but adjacent guiding tubes (separation of ~300μm), which would allow to switch sampling from one to other probe without temporal delays.

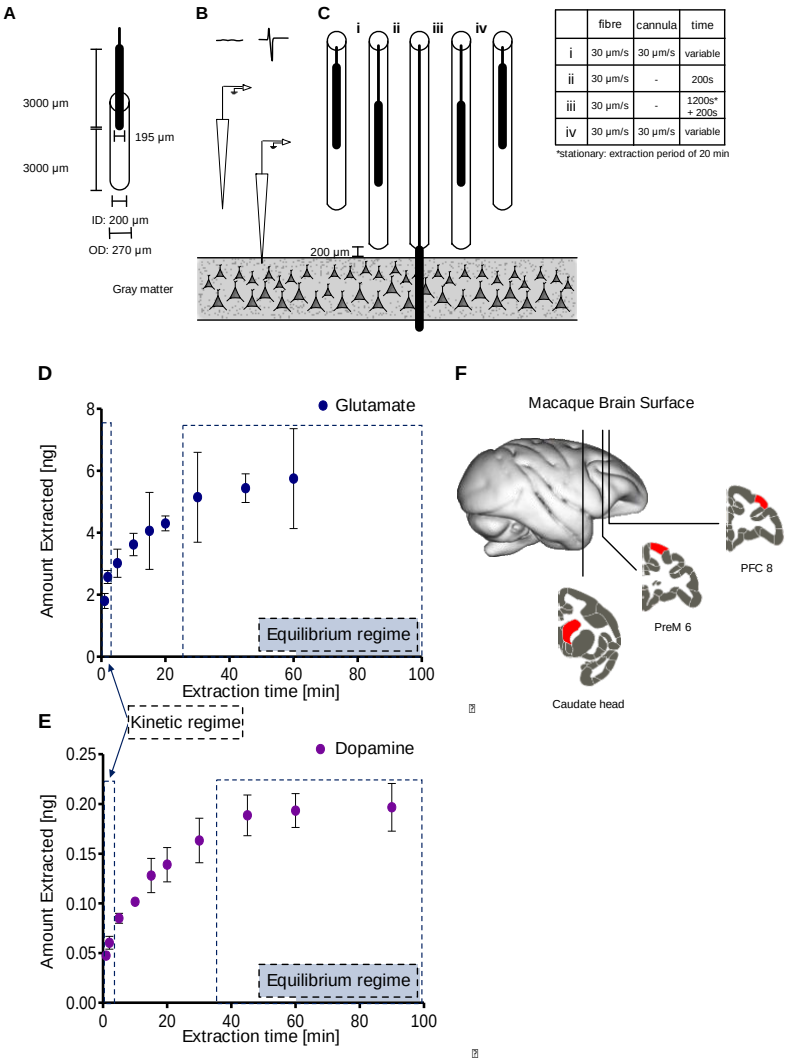

Fig 2.1 SPME sampling procedure, extraction time profiles and measurement locations.
(A) Dimensions of the SPME probe and the accompanying cannula. There was a 3000 µm buffer from the opening of the cannula and the start of the SPME coating. The SPME coating spanned 195 µm at the tip. The SPME coating made up the terminal 3000 µm of the entire probe and was placed in a cannula with an internal diameter of 200 µm and an external diameter of 270 µm. (B) Tungsten microelectrodes were lowered into the brain guided by 3 T magnetic resonance (MR) images in order to map the depth at which detectable spiking was observed matching expectations from the MR images. (C) SPME probes and their accompanying cannulas in all brain areas were then simultaneously lowered to 200 µm above the point of first observable firing in the target brain region and the SPME probes were lowered to expose only the 3000 µm SPME coating. After 20 minutes of extraction, the SPME probes were then retracted 3000 µm back into the cannula and the probes plus their accompanying cannulas were removed from the brain. The table inset into the figure provides the velocities and times of each probe and cannula as they transitioned between the extraction steps. (D) In vitro extraction quantities of Glutamate in ng and (E) Dopamine in ng over time utilized to select in vivo extraction times. The linear "kinetic" regime and "equilibrium" regime are labelled with the dynamic range being in between. (F**)** Anatomical locations of SPME sampling events in the right hemisphere of two Rhesus Macaques. Target brain regions are highlighted in red and include two cortical regions, prefrontal cortex (PFC) area 8 and premotor cortex (PreM) area 6 as well as a subcortical region: the head of the caudate.

2.3.5 Neuromodulator detection and quantitation

Detection and quantitation of neuromodulators followed previously established procedures described in **Appendix A** (https://github.com/att-circ-contrl/SPME_paper_SI.git). In brief, SPME probes were defrosted and desorbed in an aqueous solution containing water, acetonitrile, methanol, formic acid and deuterated isotopologues of target neuromodulators as internal standards (IS). Chromatographic separation of target compounds was conducted as previously reported (Cudjoe and Pawliszyn, 2014). Tandem mass spectrometry (MS/MS) was performed with electrospray ionization with two MS/MS transitions for each neuromodulator and one for each IS (Lendor et al., 2019b).

Stock solutions of all target neuromodulators were prepared and used to generate standard calibration curves and to calculate the amounts of neuromodulator extracted by each experimental SPME probe. Conversion of the amount of neuromodulator extracted to in-brain concentrations was done using matrix-matched external calibrations. LOD is defined as 3 times the signal obtained from blank samples.

2.4 Results

During all measurements animals were engaged in a cognitively demanding task with stable behavioral performance to minimize state dependent fluctuations of basal extracellular concentrations of neuromodulators. Three brain regions were selected to provide a sample of extracellular neuromodulatory concentrations. Two cortical regions: prefrontal cortex (PFC) area 8, premotor cortex (PreMC) area 6 and the head of the caudate nucleus (CD) were selected (**Fig 2.1F**). In 3 daily sessions, we sampled 3 times per session simultaneously from all three areas. Monkey As had an additional 3 days of recording with one sample collected on each day. Overall we collected and analyzed 12 probes in monkey As and 9 probes in monkey Ke. We were specifically interested in major neuromodulators and neurotransmitters but successfully measured other compounds such as amino acids (e.g. glutamine, taurine, phenylalanine etc) that we do not discuss here.

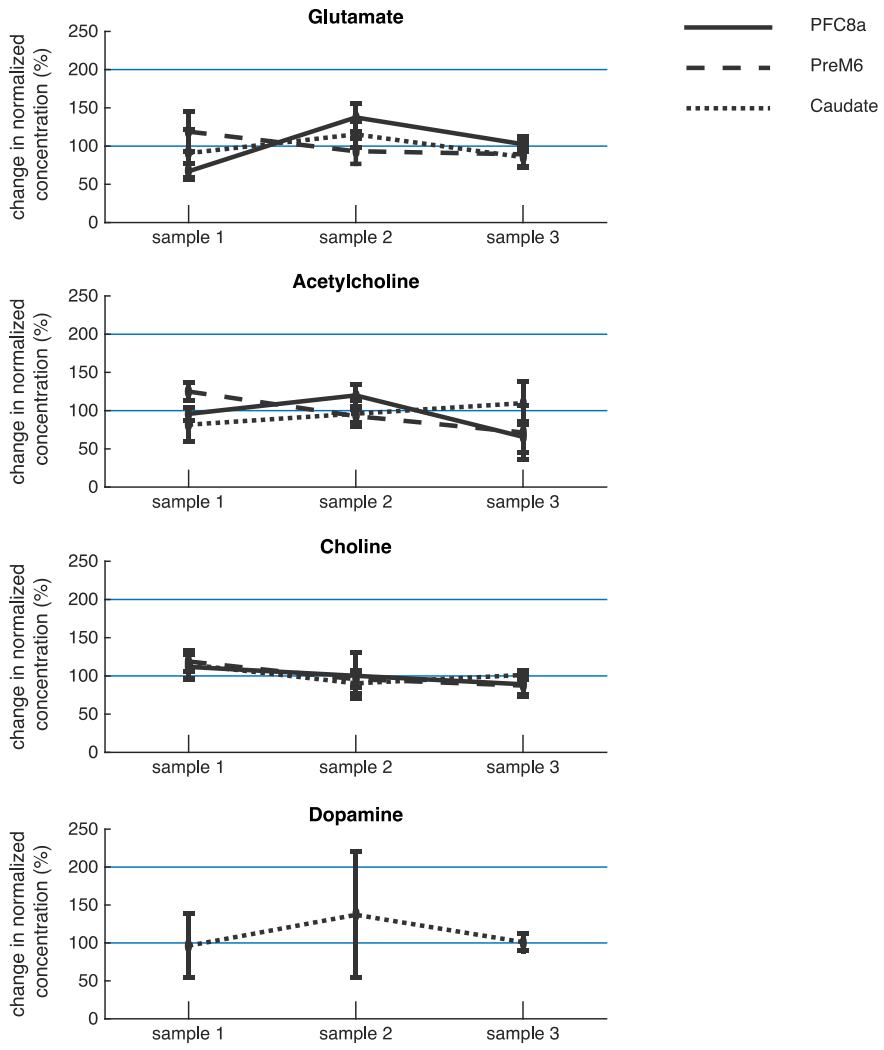

Fig 2.2 Changes in SPME sampling over time.
Changes in the normalized concentrations of the observed neuromodulators across daily sampling sessions in each sampled brain region. The median concentration of (A) Glutamate (B) acetylcholine (C) choline and dopamine (D) with standard error of the median plotted for each sampling time and location. Data was normalization for each subject separately and for the respective neurochemical and area combinations. Sampling locations are represented by different lines: solid line for the prefrontal cortex, dashed line for the premotor cortex and dotted line for the caudate nucleus. Sampling events were 20 minutes in length and the time between the end of one sampling event to the start of the next sampling event was 40 minutes (STD 2 minutes) making the second sampling event 40 minutes and the third 100 minutes from the initial measurement. No significant change was observed for any neuromodulator in any brain region (Wilcoxon rank sum test). Note that a single prefrontal choline data point was excluded in this analysis for being >4 standard deviations from the median (data point is present in **Fig 2.3a**).

To allow comparison of the SPME extraction results to those typically reported in microdialysis studies, we calculated the relative change in measured concentrations across the three successive sampling events per session pooled across monkeys to enhance the statistical power of the analysis (**Fig 2.2**). Relative to the end of the first sampling event, the second and third

sampling events started after 40 minutes and 100 minutes respectively. We expected that the variability of measurements (indexed as standard error of the median) is comparable to repeatedly measured microdialysis of an identical, active brain state. We found that measured concentrations did not change significantly across sampling events for any compound area combination (Wilcoxon rank sum test; **Fig 2.2**).

We found that four target neurotransmitters and neuromodulators were reliably detected in each animal: glutamate, dopamine, acetylcholine, and choline. Serotonin was also detected on several probes but always near the limit of detection (LOD) and therefore was excluded from analyses here (Lendor et al., 2019b). Glutamate concentrations were several orders of magnitude higher than all other observed compounds of interest in all areas and both animals. Relative to glutamate, choline concentrations were >15 times lower, DA concentrations were >700 lower and ACh concentrations were >8300 times lower (**Fig 2.3**).

Glutamate concentrations (across areas), measured as median ± standard error, ranged from 159,147 (±19,395) to 233,659 ng/mL (±33,917) in monkey As, and from 135,523 (±22,945) to 184,333 ng/mL (±33,516) in monkey Ke. In both monkeys, glutamate concentrations were highest in the head of the caudate, which was significantly different from glutamate concentrations in the premotor cortex in monkey As (kruskal-wallis test with Tukey's HSD correction, $p = 0.048$) but not in monkey Ke (kruskal-wallis test with Tukey's HSD correction, $p = 0.847$, n.s.). Glutamate concentrations between the caudate and PFC, as well as the PFC and premotor cortex were not significantly different for either animal. Comparisons between monkeys showed no significant differences between the glutamate concentrations in any of the measured areas (**Fig 2.3**).

In addition to glutamate, dopamine could be reliably detected in both monkeys in the caudate at concentrations of 232 ng/mL (±47) in monkey As, and 226 ng/mL (±31) in monkey Ke. These concentrations were similar between monkeys (Wilcoxon rank sum test $p = 1$, n.s.). Dopamine was not found above detection limits in frontal cortex.

Acetylcholine measurements in the three brain areas ranged from (across areas) 25 (±2) to 36 ng/mL (±5) in monkey As, and from 29 (±2) to 36 ng/mL (±4) in monkey Ke. In monkey As,

extracellular ACh concentrations between the caudate and premotor cortex were significantly different (kruskal-wallis test with Tukey's HSD correction, $p = 0.008$). Cortical areas were not significantly different from one another (kruskal-wallis test with Tukey's HSD correction, $p = 0.476$, n.s.) nor was there a significant difference between the caudate and PFC (kruskal-wallis test with Tukey's HSD correction, $p = 0.145$, n.s.). In monkey Ke, only one cortical region had concentrations of ACh above detection limits, which approached significant difference to the concentrations measured in the caudate (Wilcoxon rank sum test, $p = 0.08$). Measurements of extracted ACh in the pre-motor cortex of monkey Ke were consistently below detection limits (**Fig 2.3**).

We also measured choline which is a main product of the enzymatic breakdown of the highly regulated ACh and which is a main indicator of attentional modulation of cholinergic activity in frontal cortex (Parikh et al., 2007). Choline concentrations ranged across areas from 2,914 (±590) to 5,078 ng/mL (±675) in monkey As, and 3,408 (±3,705) to 5,533 ng/mL (±860) in monkey Ke. Choline concentrations between the caudate and premotor cortex were significantly different in monkey As (kruskal-wallis test with Tukey's HSD correction, $p = 0.030$), but not in monkey Ke (kruskal-wallis test with Tukey's HSD correction, $p = 0.729$, n.s.). All other area comparisons were not significant for both monkeys. Comparisons of choline concentrations between monkeys were not significant in any of the measured areas.

Overall, serotonin concentrations were not observed as reliably as the other reported neurochemicals and therefore were excluded from the main analyses. However, in monkey As, serotonin was observed near the LOD in the prefrontal cortex as well as the caudate in a subset of probes. Within the 9 probes placed in both areas, serotonin was detected in 22% of samples (2/9 probes) in the prefrontal cortex and 33% of samples (3/9 probes) in the caudate nucleus. Serotonin observations ranged from 149 ng/mL to 232 ng/mL with a median of 171 ng/mL (±18.5 ng/mL; standard error of the median) with a LOD of 100 ng/mL. The proximity of the measurements to the LOD suggest that the other probes likely collected concentrations of serotonin below the detection threshold. No serotonin observations were made in monkey Ke.

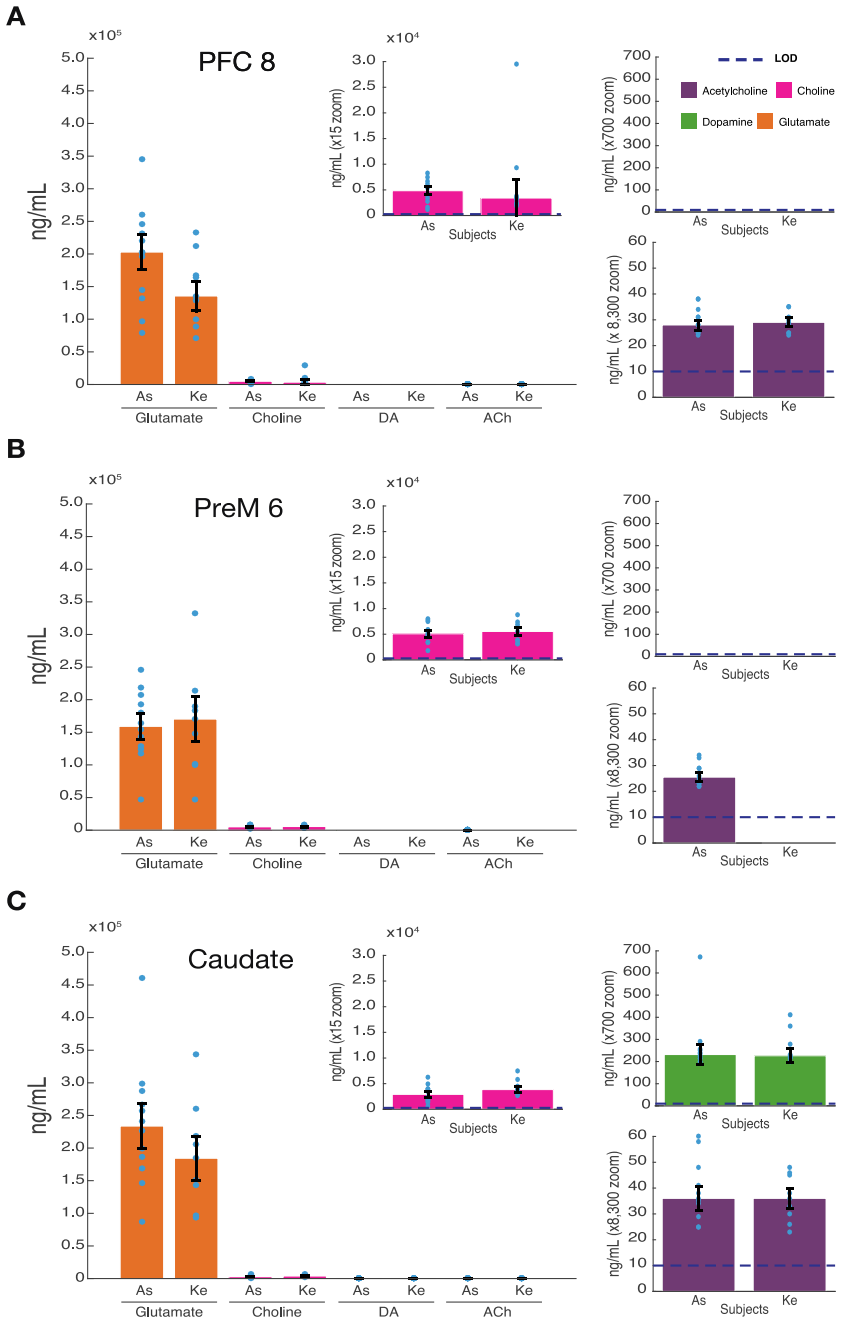

Fig 2.3 SPME sampling of the macaque brain.
SPME probes extract from the cortex (PFC and PreM6) as well as the caudate of two adult macaques after 20 minutes of extraction within the respective brain region. Median and standard error of the median of n= 12 probes for animal As and n= 9 probes for animal Ke with no data excluded. Four neuromodulators were reliably measured: glutamate, dopamine, acetylcholine, and choline (orange, green, purple, red respectively). All brain regions had high concentrations of glutamate and relatively much lower concentrations of acetylcholine and choline extracted (with the exception of animal Ke PreM6 lacking detectable acetylcholine). The only tested region to yield measurable dopamine was the caudate. The dashed blue line depicts the limit of detection (LOD).

2.5 Discussion

We demonstrated the reliable measurements of glutamate, dopamine, acetylcholine and choline simultaneously within cortical and subcortical regions of awake and behaving macaques using coated microprobes optimized for solid phase microextraction. Glutamate concentrations were several orders of magnitude higher than dopamine, acetylcholine and choline across brain regions. Extracellular concentrations of choline, dopamine and acetylcholine were detected at >15, >700, and >8,300 times lower than glutamate respectively. Dopamine was readily detected in the caudate but not observed at detectable concentrations in the cortical regions measured. Acetylcholine concentrations showed a statistical trend of being different between the caudate and measured cortical areas and with high consistency between monkeys. Choline concentrations, a product of acetylcholine degradation as well as a precursor for its synthesis, were negatively correlated with acetylcholine ($R = -0.355$; $p = 0.01$). Together, these findings provide new and rare insights about the neurochemical circuit profiles during an active brain state in three areas of the primate fronto-striatal network.

The high consistency of measured concentrations within animals, between brain areas and between monkeys suggests that SPME microprobes could provide a versatile neuro-technique for understanding how variations of the neurochemical milieu relate to local and long-range circuit operations and ultimately cognitive functioning.

2.5.1 Extracellular Concentrations of Glutamate, Dopamine, Acetylcholine and Choline.

Our results revealed particularly high levels of glutamate within all measured brain regions (PFC, PreMC, and CD) relative to other neuromodulators. This finding is consistent with its ubiquitous role as major excitatory neurotransmitter. This holds true even in the caudate which consists exclusively of GABAergic neurons, but receives glutamatergic inputs from the cortex (Haber and Knutson, 2010). Tonic concentrations of glutamate within the striatum have been previously reported to be comparable to that of the hippocampus, prefrontal cortex and other cortical areas due to glutamatergic inputs, extra-synaptic release and glial release (Moghaddam, 1993; Ascenzo et al., 2006; Moussawi et al., 2011). In contrast, classical neuromodulators such as

DA and ACh, are released in extracellular space through volume transmission where they are highly regulated and may bind to receptors on multiple neurons (Vizi, 2000; Syková, 2004; Santello et al., 2012; Schwartz and Javitch, 2013). This regulation may help explain the relatively low observed concentrations of DA and ACh and may be a large source of extracellular choline through the enzymatic breakdown of ACh.

Extracellular DA was measured well above the detection threshold in the striatum. In combination with glutamatergic and cholinergic concentrations, our results show promise in the application of SPME to further our understanding of the relationship between glutamatergic inputs to the striatum and the neuromodulatory ACh and DA signals impinging on striatal circuits. Such circuits are strongly involved in hypo- and hyperkinetic diseases (Millan et al., 2012; Halliday et al., 2014). Dopaminergic signals did not exceed the detection threshold in either cortical regions. The presence of DA in the PFC is well documented (Goldman-Rakic et al., 1990; Watanabe et al., 1997; Vijayraghavan et al., 2007) and we thus conclude that DA most likely has failed to exceed our detection limit. The difference between the detection success of DA in the caudate vs PFC and PreM cortex may be due to differences in available DA, release concentrations and dynamics (Holloway et al., 2019). A possible explanation for the lack of detectable cortical DA is the susceptibility of catecholamines to oxidation. This may be partially addressed by faster coupling of sample collection to quantitation by MS.

Few previous studies have documented ACh concentrations in vivo in non-human primates due to its rapid breakdown by acetylcholinesterase and the challenges of neurochemical testing in primates (Kreitzer, 2009; Schwartz and Javitch, 2013; Zapata et al., 2013). ACh plays a major role in organizing local circuits, deployment of attention, locomotion and reward through different receptors present in cortical and subcortical regions (Granger et al., 2016; Howe et al., 2017; Moehle et al., 2017). It has been difficult to discern which ACh concentration corresponds to efficient endogenous circuit operations. Our finding of measurements in all sampling locations except for premotor cortex in monkey Ke, is therefore a promising starting point for future studies comparing ACh concentrations, in conjunction with other neuromodulators, during different cognitive states. The fast turn-around of ACh due to AChE however, likely leads to an underestimation of ACh concentrations by SPME. Although AChE cannot traverse the porous

SPME coating due to its size (~7.6nm diameter), preventing any enzymatic degradation of trapped ACh, the dynamic equilibration process continuously leads to a transfer of ACh out of the SPME coating following the concentration gradient of the rapidly depleted ACh into the extracellular space as discussed in the case of calibration in the coating approach (Zhang et al., 2007a; Alam and Pawliszyn, 2016).

Amongst other sources, choline is created as a byproduct of ACh degradation by AChE. Choline is also a precursor for the synthesis of ACh. Given this relationship, a negative correlation between choline concentrations and ACh is expected which we indeed observed in our dataset. Despite the difference in the measured concentrations of choline and acetylcholine, other studies with similar differences have demonstrated the relationship of ACh and choline to behavior within the cortex (Parikh et al., 2007). Future studies may focus on quantifying this relationship across a wider range of brain states.

Many factors may contribute to variation in measured concentrations of neuromodulators including behavioral state, the specific brain region measured and individual differences amongst others. Importantly, different methods may yield different estimates of absolute extracellular concentrations. For example, comparable measurements of extracellular glutamate via MD or voltammetry as opposed to electrophysiological estimates can differ by orders of magnitude and may be attributed to differences in probe size, or sensitivity to different sources of glutamate (Moussawi et al., 2011).

2.5.2 Reliable Measurement of Individual Differences of State Specific Neuromodulatory Tone.

Our results suggest that SPME probes provide reliable and sensitive measurements in consecutive sampling events within an experimental session and between sessions on consecutive days. These results were obtained while we controlled brain states across measurement events by engaging animals in a cognitive task. This experimental control could have contributed to the comparable extracellular levels of neuromodulators from sample to sample within *and* between days from similar brain locations (**Fig 2.2**) (Marder et al., 2014; Reimer et al., 2014, 2016;

McGinley et al., 2015). The reproducibility of multiple measurements at the same anatomical location within and between days suggests that the SPME penetrations did not significantly disturb tissue (Cudjoe et al., 2013). This conclusion contrasts with reported experience from microdialysis measurements, where the initial placement of the probe or guiding cannula causes transient measurement instabilities that can require several hours of settling time before reliable, steady state neuromodulator concentrations are measurable (Watanabe et al., 1997; Kodama et al., 2002, 2015, 2017; Moussawi et al., 2011). These waiting periods must be taken into account when designing microdialysis experiments for in vivo tracking of neuromodulators during behavioral tasks in awake and restrained animals. Furthermore, the reliability of observations for the reported neurochemicals with SPME is extremely high and outperforms many reported microdialysis studies. We present 100% reliability in reporting glutamate and choline concentrations in all brain regions and subjects. Acetylcholine concentrations were reported with 100% reliability in one animal and 92% (11/12 probes) in the other within the prefrontal cortex, 0% reliability (below detection threshold) in one animal and 83% (10/12 probes) in the other within the premotor cortex and 100% reliability in one animal and 92% (11/12 probes) in the other within the caudate. Dopamine concentrations were reported with 100% reliability in both animals in the caudate and were not observed above detection thresholds in the cortex.

2.5.3 Qualities and Advantages of SPME.

Our results illustrate several inherent advantages of using SPME to measure neurochemical profiles in brain circuits (Lendor et al., 2019b). As illustrated in **Appendix A, Table A1** (https://github.com/att-circ-contrl/SPME_paper_SI.git), SPME complements or outperforms alternative techniques in various domains. Practically, the arbitrary length of the wire where the SPME coating is placed allows for robust placement within the brain. The narrow diameter of the SPME probe that is within the range common to electrodes for electrophysiological recordings, allows for repeated, simultaneous sampling at multiple sites without observable changes to detected extracellular neuromodulator levels using 20-minute sampling times.

Spatial Resolution. In principle, the spatial resolution of the SPME measurements are capable of reflecting laminar concentration gradients across areas as small as several tens of

micrometers. In our protocol we coated 3mm in length with 50 μm of thickness and desorbed the entire area into an organic solvent mixture for subsequent LC-MS/MS analysis. However, with the use of other techniques, such as desorption electrospray ionization (DESI), which represents a direct-to-MS approach (Deng et al., 2014), much smaller areas of the SPME matrix may be analyzed at a time allowing for laminar or near-laminar resolution. Direct coupling of SPME fibres to MS is the preferred mode, as it provides the most rapid analysis thus preventing diffusion of compounds within the coating and smearing the imprinted layer information. If diffusion of molecules within the fibre is high, it can be prevented by, for example, the inclusion of a divider between two halves of the coating. This would allow the simultaneous measurement of separated compartments of a cortical column. The absolute spatial resolution of SPME is difficult to estimate as SPME operates through diffusion and dynamic equilibration similar to MD. As a consequence, the sampled volume will depend on sampling time, the compound's diffusion coefficient, as well as the target tissue and its properties affecting the rate of diffusion such as tortuosity (Syková, 2004).

Temporal Resolution. Several factors determine the appropriate extraction time using SPME. Depending on the goals of an experimenter, resolutions below 5 minutes may be achieved as the detection limit is reached within the first few minutes for most compounds tested (**Fig 2.1D-E**). As sampling continues, the SPME coating will eventually reach an equilibrium point with the external environment (**Fig 2.1D-E**). In principle, sampling times beyond a stable equilibrium point will result in the same extracted values of compounds. However, in the brain there is no single stable equilibrium point and thus, even with long sampling times, there will be some variation in extracted concentrations. Within the dynamic regime, we can still calculate environmental concentrations from which sampling occurred given knowledge of the extraction time and the dynamic range. The lower limit of this dynamic range that can be informative is determined by the coating's physicochemical characteristics and sample's properties and in practice also volume of desorption and sensitivity of the MS. The analytical technique's sensitivity also practically determines the thickness of the SPME coating as thinner coatings could in principle increase temporal resolution but would extract less compounds overall requiring higher sensitivity to detect. With higher sensitivity, less time is required for the thin coating to extract sufficient amounts to exceed limits of detection and quantitation. This then means that the compound with regards to

which the sensitivity is the lowest, limits the temporal resolution because it will have the slowest-to-reach detectable concentration. But as long as the detection threshold is exceeded, the extraction time profiles allow for the calculation of the equilibrium concentration even with pre-equilibrium sampling. However, making measurements in the dynamic range requires consistency of extraction times as differences in time will lead to variations of extraction yields in a range that can be estimated from the SPME extraction time profiles (**Fig 2.1D-E**). Given the dynamic nature of brain networks and the lack of a stable equilibrium point, we expect consistency in brain states to be one of the biggest factors in reducing replicated variability. Moreover, SPME measurements are inherently an average of the temporal dynamics of the target tissue milieu. This means that due to the bi-directional exchange of neuromodulators from the extracellular space and the SPME coating, longer periods of stable concentration gradients will be more strongly reflected in the extracted measurements.

Utility and Ease of Use. SPME based microprobe extraction allows for multiple simultaneous measurements that can be reliably repeated within the same measurement sessions at the same locations with no evidence of damage induced disruption of the neurochemical environment. Another critical advantage of SPME over comparable MS-analysis based methods such as MD is its ease of use and accessibility. Due to their similar size to recording microelectrodes used for electrophysiology, little adjustment is required for conducting SPME measurements using existing acute microelectrode positioning systems. Measurements in deeper structures should use an accompanying guide tube (**Fig 2.1C**) as travelling through non-target tissue will result in unwanted chemical collection. Beyond the collection, a chemistry core could apply LC-MS/MS to the probes allowing for relatively easy quantitation of extracellular compounds of interest.

Detection Methods. SPME is ultimately a sampling method, much like MD, that provides data for analytical tools such as chromatography and mass spectrometry. In fact, once SPME analytes have been desorbed from the probe into a solvent, data provided by SPME and MD are treated very much the same. Thus, the advancement in detection limits and reliability of post-hoc analytical methods utilized by MD also benefit SPME, and vice versa. However, SPME sample

analysis is more reliably and conveniently coupled to LC-MS/MS as it lacks issues such as high salt content of collected dialysate that MD suffers from (Guihen and Connor, 2009).

Extension of SPME measurements beyond classical neuromodulators. A unique advantage of SPME over alternative methods of in vivo detection of compounds within the brain is its potential affinity for hydrophobic compounds. Although MD is capable of collecting metabolomics data similarly to SPME (Zhang et al., 2007b; Li et al., 2012; Anderzhanova and Wotjak, 2013), the artificial cerebra-spinal fluid that is commonly traversing the semi-permeable membrane better facilitates the collection of hydrophilic molecules. This means that molecules that cross the semi-permeable membrane and are therefore collected and quantified through LC-MS are much more likely to be hydrophilic. SPME, in contrast, provides balanced analyte coverage, which means that in principle certain SPME matrix coatings have similar affinity for both hydrophilic or hydrophobic compounds (Reyes-garcés et al., 2018). Data collected here includes other neurochemicals of interest such as amino acids (e.g. glutamine, taurine, phenylalanine, etc) that we reliably detected but do not discuss here. In practice, the detection of very polar molecules such as monoamines and catecholamines requires coating chemistry that facilitates hydrophilic compound extraction. Comparatively many lipids play important roles in intracellular signaling and have been suggested to provide biomarkers for psychiatric disorders (Yehuda et al., 1999; Tamiji and Crawford, 2011), therefore making SPME a potentially versatile and comprehensive tool for brain neurochemistry studies.

2.5.4 Future direction and improvements to the SPME neurochemical sensing.

The next immediate steps for the continued testing of SPME's utility as a neurochemical sampling method is to evaluate its ability to report behavioral state dependent changes in extracellular neuromodulator concentrations. Similar testing as described here will be conducted with varying, stable behavioral states such as passive engagement, active task engagement, and drowsy/sleepiness. We predict that the various brain regions tested will display different changes in neuromodulator concentrations as a function of behavioral state.

Several improvements to the protocol can be made in order to make SPME more informative. Using a more sensitive MS would reduce detection thresholds and increase sensitivity in detecting compounds not successfully measured here such as GABA, serotonin or norepinephrine. This would be very impactful, especially in the case of serotonin for reasons discussed above. Additionally, efforts could be made to improve the extracting phase synthesis and functionalization protocols and increase the extracting capabilities of SPME probes. Moreover, in order to decrease the MS background and interferences in the range of small molecules, derivatization strategy could be considered.

For GABA, the most promising strategy is post-desorption derivatization by reagent increasing the compound's hydrophobicity resulting in better MS signal such as benzoyl chloride (Wong 2016). Catecholamine and acetylcholine detection may be improved by optimizing the post-sampling analysis pipeline. Improvements can be made at several steps in order to better preserve and quantify catecholamines: (1) faster coupling of sampling to desorption (2) trying various antioxidant solutions and other preservatives for maintaining catecholamine integrity and (3) faster analysis of the desorbed analytes. Faster coupling of sampling to desorption could be achieved through a more stream-lined process of fibre placement and retraction involving a static cannula maintained through several sampling events. This mechanism would also allow for a faster replacement of SPME probes resulting in a shorter delay between consecutive measurements.

A preliminary experiment using both spiked artificial cerebra-spinal fluid (aCSF) and lamb brain homogenate with very high, known concentrations of all target compounds yielded detectable concentrations of all target compounds indicating that the extracting phase of the SPME probe is capable of capturing all compounds of interest. Furthermore, simultaneously collected replicates displayed very little loss of collected compounds over several days within a -80°C freezer (data not shown). Various strategies were compared for storage and placement of extraction fibres in desorption solvent prior to -80°C storage seemed most reliable for many compounds and will be the storage method utilized in the future. Such findings neither support nor antagonize the suggested strategies for improving SPME yield and sensitivity in primates as detection properties within the aCSF and lamb brain homogenate may not accurately reflect those observed in vivo in primates. This is likely contributed to by the dynamic and highly regulated nature of target

compounds within the extracellular space of the brain and the dynamic equilibrium between the extracting phase of the SPME probes and the extracellular environment. Further tests of the possible differences between these mediums and improvement strategies to SPME probes are subject for future studies.

2.5.5 Implications for Understanding and Treating Psychiatric Disease States.

Most psychiatric disorders are accompanied by neuromodulatory dysregulation (Millan et al., 2012). However, this fact is seldom studied in a multi-modulatory manner with a single or few nuclei or neurochemicals being observed at a time. This is an increasingly evident problem because models attributing symptoms of a disorder to a single neuromodulator often fall short in explaining many symptoms (Remy et al., 2005; Bohnen et al., 2015). For example, in Parkinson's disease, outside of the well characterized dopaminergic deficits, there is evidence for deficits in noradrenergic, cholinergic and serotonergic systems as well (Halliday et al., 1990, 2014; Moehle et al., 2017). Many cognitive deficits observed within Parkinson's disease are linked to such non-dopaminergic deficits. Such findings emphasize the need to simultaneously observe multiple neuromodulatory systems. Thus the simultaneous measurement of multiple neuromodulators, in multiple brain regions within healthy and clinical populations will allow for a better understanding of the underlying causes of symptoms and progression of psychiatric disorders (Millan et al., 2012; Kao et al., 2015; Avery and Krichmar, 2017).

A better understanding of psychiatric disorders through multi-modulator methods may also lead to more accurate understanding of the action of pharmacological agents. Previously, many studies aimed at identifying the locus of action of a pharmacological agent have used local injection methods such as iontophoresis or microinjections (Lapiz and Morilak, 2006; Wang et al., 2007). Although highly informative about the role of neuromodulators in modulating the activity of individual cells and circuits, this approach does not allow physiologically realistic exploration of a systemically administered pharmacological agent. Pharmacological agents are often administered in some systemic fashion and even with highly specific receptor affinities, may interact with multiple neuromodulatory systems through the actions of heteroreceptors (Gobert et al., 1998; Millan et al., 2015; Avery and Krichmar, 2017). Multi-modulator measurements, as

described here, will allow for a better understanding of pharmacological agents, as well as provide novel insights into the development of more effective drugs or combinations of drugs to better treat the clinical population.

2.6 Conclusion.

We described a novel SPME protocol capable of simultaneous, multi-modulator measurements of multiple brain regions. Our results suggest that SPME both supplements current methods of neuromodulator detection and allows for novel measurements previously not possible for the investigation and dissection of neuromodulatory systems, their role in physiological brain processes and their modulation by pharmacological agents.

2.7 Acknowledgments

This research was supported by grants from the Canadian Institutes of Health Research (CIHR), the Natural Sciences and Engineering Research Council of Canada (NSERC) and the Ontario Ministry of Economic Development and Innovation (MEDI). We thank Dr. Hongying Wang for invaluable help with animal care. We thank Thermo Scientifc for providing the triple quadrupole mass spectrometer TSQ Quantiva used in this work as a loan to our laboratory. The authors thankfully acknowledge Pfizer Canada Inc., Merck Canada Inc., Quebec Consortium for Drug Discovery (CQDM), Brain Canada, and Ontario Brain Institute for the grant “Solid phase microextraction-based integrated platform for untargeted and targeted in vivo brain studies”.

2.8 Conflicts of interest

None of the authors have any conflict to disclose.

2.9 Author contributions

Seyed-Alireza Hassani and Sofia Lendor together collected all data and conducted statistical analysis of the collected data. Seyed-Alireza Hassani trained and handled the animals, prepared the MRI mapping and managed sampling equipment. Sofia Lendor prepared all SPME probes and

conducted all chemical analyses/quantification of collected compounds. Ezel Boyaci contributed to the preparation of SPME probes and quality control. Janusz Pawliszyn and Thilo Womelsdorf contributed to the collection of data and analyses. All authors contributed to the writing, visualization and editing of the manuscript.

Chapter 3 Dose-Dependent Dissociation of Pro-cognitive Effects of Donepezil on Attention and Cognitive Flexibility in Rhesus Monkeys

3.1 Abstract

BACKGROUND: Donepezil exerts pro-cognitive effects by non-selectively enhancing acetylcholine (ACh) across multiple brain systems. Two brain systems that mediate pro-cognitive effects of attentional control and cognitive flexibility are the prefrontal cortex and the anterior striatum which have different pharmacokinetic sensitivities to ACh modulation. We speculated that these area-specific ACh profiles lead to distinct optimal dose-ranges for donepezil to enhance the cognitive domains of attention and flexible learning.

METHODS: To test for dose-specific effects of donepezil on different cognitive domains we devised a multi-task paradigm for nonhuman primates (NHPs) that assessed attention and cognitive flexibility. NHPs received either vehicle or variable doses of donepezil prior to task performance. We measured donepezil intracerebral and how strong it prevented the breakdown of ACh within prefrontal cortex and anterior striatum using solid-phase-microextraction neurochemistry.

RESULTS: The highest administered donepezil dose improved attention and made subjects more robust against distractor interference, but it did not improve flexible learning. In contrast, only a lower dose range of donepezil improved flexible learning and reduced perseveration, but without distractor-dependent attentional improvement. Neurochemical measurements confirmed a dose-dependent increase of extracellular donepezil and decreases in choline within the prefrontal cortex and the striatum.

CONCLUSIONS: The donepezil dose for maximally improving attention differed from the dose range that enhanced cognitive flexibility despite the availability of the drug in two major brain systems supporting these functions. These results suggest that in our small cohort of adult monkeys donepezil traded improvements in attention for improvements in cognitive flexibility at a given dose range.

3.2 Introduction

The acetylcholinesterase (AChE) inhibitor donepezil (Aricept) is one of few FDA approved cognitive enhancers that aims to address a wide range of cognitive deficits in subjects with mild cognitive impairment or dementia (Sugimoto, 2001; Mori, 2002; Sharma et al., 2020). Basic research suggests that the cognitive domains that can be enhanced with AChE inhibitors range from selective attention, working memory, response inhibition, learning, and long-term memory (Yoo et al., 2007; Floresco and Jentsch, 2011; Cools and Arnsten, 2022). Consistent with these reports, clinical studies assessing donepezil at one or two doses across larger cohorts of subjects with varying stages of Alzheimer's disease have found improvements of compound scores of cognitive testing batteries (Rogers et al., 1998; Pratt and Perdomo, 2002; Foldi et al., 2005; Yoo et al., 2007; Li et al., 2019). It is, however, not clear whether the standard doses of donepezil used in clinical studies improve multiple cognitive domains directly, or whether at a particular effective dose its major route of action is to enhance arousal, which then provides an indirect, overall cognitive advantage for attention, working memory, learning and memory processes (Everitt and Robbins, 1997; Floresco and Jentsch, 2011). Assessing whether donepezil affects multiple cognitive domains simultaneously at a given dose is important for evaluating its therapeutic efficiency and to identify cognitive domains that should be targeted in drug discovery efforts for improved future cognitive enhancers.

One potential limitation of donepezil and other AChE inhibitors is that they increase acetylcholine (ACh) concentrations non-selectively across multiple brain systems. Such a non-selective ACh increase has shortcomings when brain systems are differently sensitive to ACh action so that the same donepezil dose that is optimally affecting one brain system might over- or under-stimulate another brain system. In primates, muscarinic ACh subreceptors relevant for attention and memory functions (Langmead et al., 2008; Lange et al., 2015b; Dean and Scarr, 2020; Foster et al., 2021), have enhanced densities in prefrontal cortex (PFC) (Froudist-Walsh et al., 2021), suggesting that PFC may be more sensitive to modulation by AChE inhibitors than posterior brain areas. Moreover, a comparison of transcription factor (CREB) activation of the PFC and the striatum to muscarinic modulation by Xanomeline has reported a 10-fold higher receptor sensitivity of the striatum (Thorn et al., 2019), consistent with other studies reporting

significantly higher muscarinic binding potential and higher AChE activity in the striatum than in other cortical regions (Tsukada et al., 2004b). It is unclear how these differences affect ACh modulation of attention functions that depend on the PFC (Cohen et al., 2007) and on flexible learning functions that are dependent on the striatum (Williams and Eskandar, 2006; Amita and Hikosaka, 2019). One consequence of the brain area specific sensitivity to ACh levels could be that a *Best Dose* for enhancing cognitive functions supported by the striatum might not sufficiently stimulate the PFC, and that a *Best Dose* for enhancing PFC functions might overstimulate the striatum.

To test for these possible implications of brain region-specific ACh action, we devised a drug testing paradigm for monkeys that assessed the effects of three different doses of donepezil across different domains of arousal, attention, and cognitive flexibility in a single testing session. We evaluated the attention domain with a visual search task that varied the number and perceptual similarity of distracting objects and quantified the domain of cognitive flexibility with a learning task asking monkeys to flexibly adapt to new feature-reward rules and avoid perseverative responding. This assessment paradigm goes beyond existing nonhuman primate studies of donepezil that so far have found enhanced short-term memory using delayed match-to-sample tasks (Rupniak et al., 1997; Buccafusco et al., 2003, 2008; Buccafusco and Terry, 2004; Yoo et al., 2007; Floresco and Jentsch, 2011; Callahan et al., 2013; Lange et al., 2015b; Vardigan et al., 2015; Li et al., 2019), enhanced arousal and non-selective speed of processing (Rupniak et al., 1997; Lange et al., 2015b), or no consistent effect (Tsukada et al., 2004b) (surveyed in **Appendix B, Table B1**), and takes into account that studies in rodents report positive donepezil effects across a wider range of domains including reversal learning (Csernansky et al., 2005), paired associate learning (Bartko et al., 2011), object discrimination (Prickaerts et al., 2005), novelty detection (Luine et al., 2002) and variable results on serial choice tasks indexing attention functions (Romberg et al., 2011) (surveyed in **Appendix B, Table B2**). With our design we found that donepezil improves interference control over distractors at doses that caused an overall slower responding (i.e. reduced speed of processing) and peripheral side effects. In contrast, a lower dose of donepezil caused no clear attentional effect but improved cognitive flexibility. These findings document domain-specific dose-response effects of donepezil for attention and cognitive flexibility.

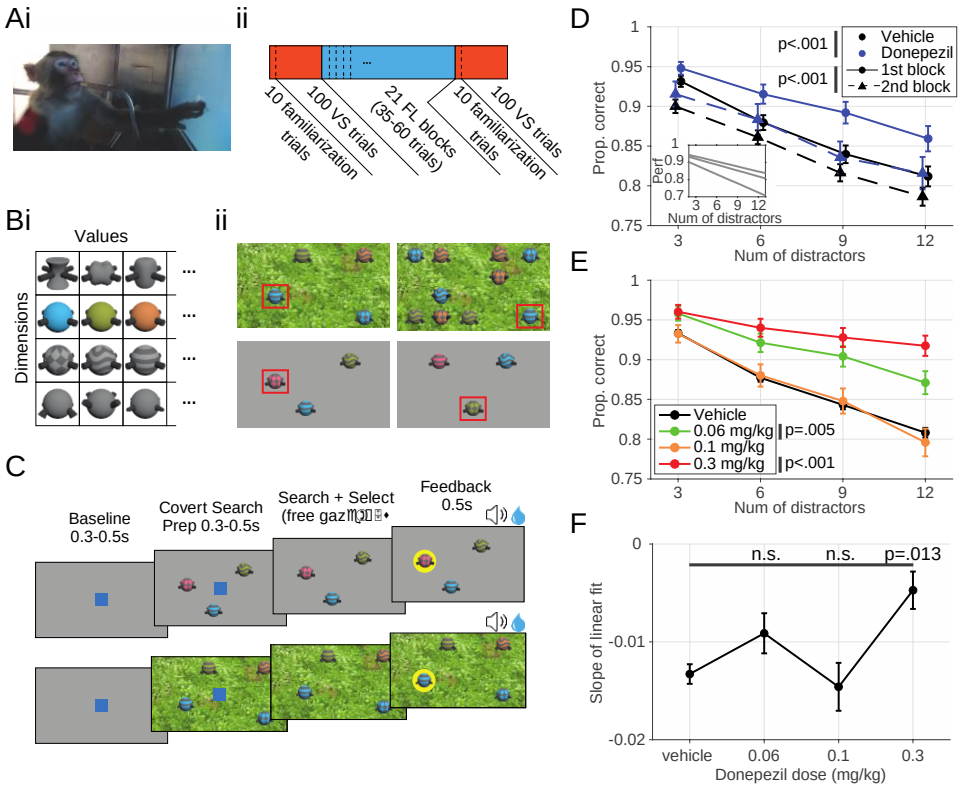

Fig 3.1 Task design, meta-structure and visual search performance as a function of distractor number. (**A**) **i**. Picture of one of the subjects working in the custom-built kiosk, interacting with the touchscreen and receiving fluid reward. **ii.** The meta structure of the Multi-task. Each experimental session consists of 3 super-blocks of VS, FL and VS respectively. Each VS block is preceded by 10 familiarization trials which is identical to a VS trial but without any distractors. Each VS block contains trials with 3/6/9/12 distractors randomly selected and counterbalanced over the block. In contrast, each FL block will contain 0/1 irrelevant feature dimensions in addition to the relevant feature dimension (the dimension with the rewarded feature value) counterbalanced over the session. (**B**) **i**. From the grand pool of quaddles which includes four feature dimensions and a variable number of feature values (9 shapes, 9 patterns, 8 colors, and 11 arms), three feature values from three feature dimensions are chosen. This 3x3 pool is then counterbalanced for dimension presentation and feature reward association and is utilized for 2 weeks of data collection where all presented quaddles are selected from this 3x3 pool. **ii.** Example trials. Two example VS trials (top) within the same block with 3 distractors (left) and 9 distractors (right). Each VS block will contain one of 5 backgrounds, with the VS blocks in the same day never having the same background. All distractors and target objects in VS blocks are three dimensional objects and distractors may be duplicated in each trial. Quaddles are spatially randomly presented at the intersections of a 5x4 virtual grid pattern on screen. The red box highlights the rewarded target object, which is invariable within the VS block, in these examples. Two example FL trials (bottom) within the same block containing 2D quaddles (1 distracting dimension plus the relevant dimension). The rewarded feature value in this block is the checkered pattern independent of what color feature value it is paired with. Quaddles may be presented in 8 possible locations in a circle each being 17 degrees of visual radius away from the center of the screen. The red box signifies the rewarded target object, which is a variable combination of the rewarded feature value (the checkered pattern in this example) with a random feature value of the distractor dimension (color in this example). (**C**) The trial structure for both the FL (top) and VS (bottom) blocks of the task are very similar. A trial is initiated by a 0.3-0.5s touch and hold of a blue square (3° visual radius wide) after which the blue square disappears for 0.3-0.5s before task objects, which are 2.5° visual radius wide, are presented on screen. Once the task objects are on screen, the subject is given 5s to visually explore and select an object via a 0.2s touch and hold. A failure to make a choice within the allotted 5s results in an aborted trial and did not count towards the trial count. Brief auditory feedback and visual feedback (a halo around the selected object) are provided upon object selection, with any earned fluid reward being provided 0.2s following object selection and lasting 0.5s along with the visual feedback. Non-rewarded trials had a different auditory tone and a light blue

halo around the selected, non-rewarded object. Rewarded objects had a higher pitch auditory tone, a light yellow halo around the selected rewarded object and had an accompanying fluid (water) reward. (**D**) Average VS performance by distractor number for vehicle and all donepezil doses combined, both separated by the first vs second VS block. VS performance was significantly different for block number ($F(1,1722) = 22.19$, $p < .001$) as well as condition ($F(1,1722) = 19.0$, $p < .001$). The inlet shows individual monkey average VS performance linear fits. **(E**) Average VS performance by distractor number between vehicle and 0.06, 0.1, and 0.3 mg/kg donepezil doses for the first VS block ($F(3,896) = 10.77$, $p < .001$). Both the 0.06 and 0.3 mg/kg doses were significantly different from vehicle (Tukey's, $p = .005$ & $p < .001$ respectively). Error bars here reflect standard deviation in this panel. (**F**) The set size effect of VS performance by distractor number for each condition. The 0.3 mg/kg dose set size effect was significantly shallower from the vehicle set size effect ($H(3) = 11,46$, $p = .010$; Tukey's, $p = .013$).

3.3 Methods and materials

3.3.1 Nonhuman Primate Testing Protocol

Three adult male rhesus macaques were separately given access to a cage-mounted Kiosk Station that provided a touchscreen interface inside the animal's housing unit to perform cognitive tasks (**Figure 3.1A**) (Csernansky et al., 2005) (see **Appendix B**). The behavioral tasks was controlled by the Unified Suite for Experiments (USE) (Watson et al., 2019b).

3.3.2 Drugs and Procedures

We used donepezil (Sigma-Aldrich ,catalog number D6821; St. Louis, MO, USA) in three doses: 0.06, 0.1 and 0.3 mg/kg to operate within the dosing range of previous studies reporting pro-cognitive effects (surveyed in **Appendix B, Tables B1-2**). At this IM range, plasma concentrations of donepezil are roughly the same when dosing with ~10x the concentration via PO (Lange et al., 2015b). Animals received saline as vehicle control, or a dose of donepezil IM injection 30 minutes prior to starting task performance taking into account its expected 1h half-life (Shiraishi et al., 2005). Administration was double-blinded. Drug side effects were assessed 15 min following drug administration and after completion of the behavioral performance with a modified Irwin Scale (Irwin, 1968; Patel et al., 1997; Andersen et al., 2003; Gould et al., 2020) for rating autonomic nervous system functioning (salivation, etc.) and somato-motor system functioning (posture, unrest, etc.). Monkeys' behavioral status was video-monitored throughout task performance (**Figure 3.1A**).

3.3.3 Behavioral Paradigms

Monkeys performed in each experimental session a visual search (VS) task to measure attentional performance metrics and a feature-reward learning (FL) task to measure cognitive flexibility metrics. Each performance day was made up of an initial set of 100 trials of VS, a set of 21 learning blocks with 35-60 trials each of the FL task, and a second set of 100 trials of the VS task (**Figure 3.1Aii**). Details of both tasks are provided in **Appendix B**. The VS task required monkeys to find and touch a target object among 3, 6, 9, or 12 distracting objects in order to receive fluid reward **(Figure 3.1B**). The target was the object that was shown in 10 initial trials without distractors. Targets and distractors were multidimensional, 3D rendered Quaddle objects (Watson et al., 2019b) that shared few or many features of different features dimensions (colors, shapes, arms, body patterns), which rendered search easier when there was no or few similarities among features of targets and distractors, or more difficult if the target-distractor (T-D) similarity was high (**Figure 3.2A**). The FL-task required monkeys to learn through trial-and-error which object feature is rewarded in blocks of ~35-60 trials (**Figure 3.1C**). The rewarded feature changed un-cued and switched to a new feature of the same or different feature dimensions, which makes the task similar to conceptual set shifting tasks (Moore et al., 2006; Buckley et al., 2009), but different by using a larger set of features that varied within and across sessions in order to vary task difficulty. In each trial three objects were shown that varied either in features of one feature dimension (e.g. having different colors or body shapes), or that varied in features of two feature dimensions (e.g. having different colors and body shapes). Choosing the object with the correct feature was rewarded with a probability of 0.8. Blocks where only 1 feature dimension varied (*1D blocks*) were easier as there was lower attentional load than in blocks with 2 varying feature dimensions (*2D blocks*).

3.3.4 Neurochemical Confirmation of Drug Effect

To evaluate the levels of donepezil in brain structures that are necessary for successful attention and learning performance, we measured the ACh metabolite choline and donepezil concentrations in the prefrontal cortex and the anterior striatum (caudate nucleus) 15 min after administering a low and high dose of donepezil (0.06 and 0.3 mg/kg, IM) in a separate experiment.

Measures of donepezil were made at the time when we observed dose-limiting side effects at the 0.3 mg/kg dose and the two tested doses were accompanied by pro-cognitive effects in our task (see results). We used microprobes that sampled the local neurochemical milieu with the principles of solid phase micro-extraction (SPME) (Lendor et al., 2019b) followed by quantification of the concentrations with liquid chromatography and mass spectrometry (Lendor et al., 2019b). The detailed procedures used here are described in (Hassani et al., 2019) and in **Appendix B**.

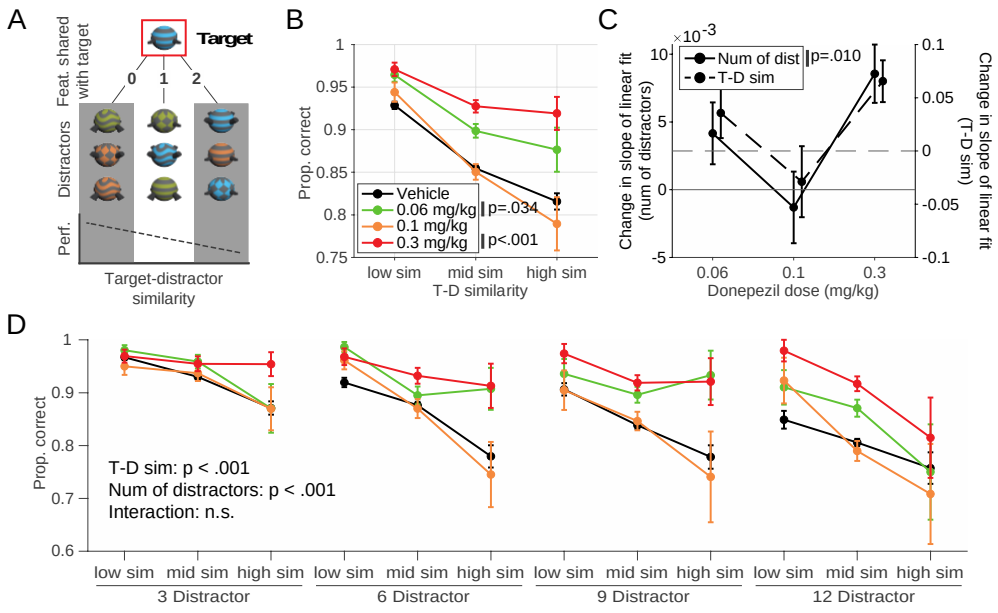

Fig 3.2 Visual search task performance and change in difficulty through increasing distractor numbers and target-distractor similarity.
(**A**) A visual description of the target-distractor similarity measure in the VS task. For an example target in the red square, 3 example distractors are presented with 0, 1 and 2 features in common respectively from left to right. The cartoon plot below shows the impact of the average target-distractor similarity of an individual trial on performance. (**B**) Similar to **Figure 1D**, but here we plot average VS performance by T-D similarity. There was a significant effect of T-D similarity on performance ($F(2,627) = 16.17$, $p < .001$) as well as condition with both the 0.06 and 0.3 mg/kg donepezil doses being significantly different from vehicle ($F(3,267) = 7.75$, $p < .001$; Tukey's $p = .034$ and $p < .001$ respectively). (**C**) The change in the slope of VS performance with 0.06, 0.1 and 0.3 mg/kg donepezil relative to vehicle. The change in slope by distractor number is plotted on the left y axis (same data as **Figure 1F**) ($H(3) = 11.46$, $p = .010$) while the change in slope by T-D similarity is plotted on the right y-axis ($H(3) = 2.8$, n.s.). (**D**) A visualization of the combined effect of distractor number and T-D similarity on performance. From left to right, each cluster of lines represents increasing distractor numbers while data within each line represents low, medium and high T-D similarity from left to right respectivel. Both distractor number ($F(3,2615) = 28.85$, $p < .001$) and T-D similarity ($F(2,2615) = 64.59$, $p < .001$) impact VS performance with no significant interaction ($F(6,2615) = 0.69$, n.s.).

3.3.5 Statistical Analysis

Data were analyzed with standard nonparametric and parametric tests as described **Appendix B**.

3.4 Results

Each monkey was assessed in 38 sessions total including 17 vehicle days and 7 days with each dose (0.06, 0.1 and 0.3 mg/kg). Drug side effects were noted following IM injections of the 0.3 mg/kg dose in the first 30 min post injection as changes in posture, sedation, vasoconstriction and paleness of skin, but no adverse effects persisted beyond 30 min. (**Appendix B, Table B3**). First, we confirmed that monkeys performed the visual search (VS) task at high 84.4% (± 0.54) accuracy (monkeys Ig: 85.2% ±0.81; Wo: 88.3% ±0.94; Si: 79.8% ±0.97) and showed the expected set-size effect evident in decreased accuracy and slower reaction times with increasing numbers of distractors (**Figure 3.1D**, **Appendix B, Figure B1** and **B2**). When targets were more similar to distractors (high T-D similarity) VS performance decreased from 92.9% (±0.4) to 85.5% (±0.3) and 81.6% (±1.0) for low, medium and high T-D similarity, respectively ($H(2) = 169.48$, $p < .001$) (**Figure 3.2B**). In the feature learning (FL) task, the monkeys reached learning criterion faster in the easier 1D (low distractor load) condition (avg. trials to ≥80% criterion: 12.5 ± 0.2 SE), than in the 2D (high distractor load) condition (avg. trials to ≥80% criterion: 15.6±0.2) (**Figure 3.3A**, **Appendix B**).

3.4.1 Dose-dependent improvement of visual search accuracy and slowing of choice reaction times

Donepezil significantly improved accuracy of the visual search task ($F(1,1722) = 18.95$, $p < .001$)(**Figure 3.1D**), but on average slowed search reaction times ($F(1,1722) = 4.83$, $p = .028$)(**Appendix B, Figure B1B**). The slower choice reaction times were evident already to the single target object in the 10 target familiarization trials (**Appendix B, Figure B1A**). These main behavioral drug effects were evident prominently in the first visual search block (**Figure 3.1D, Appendix B, Figure B1A**). We therefore focused our further analysis on the first search block.

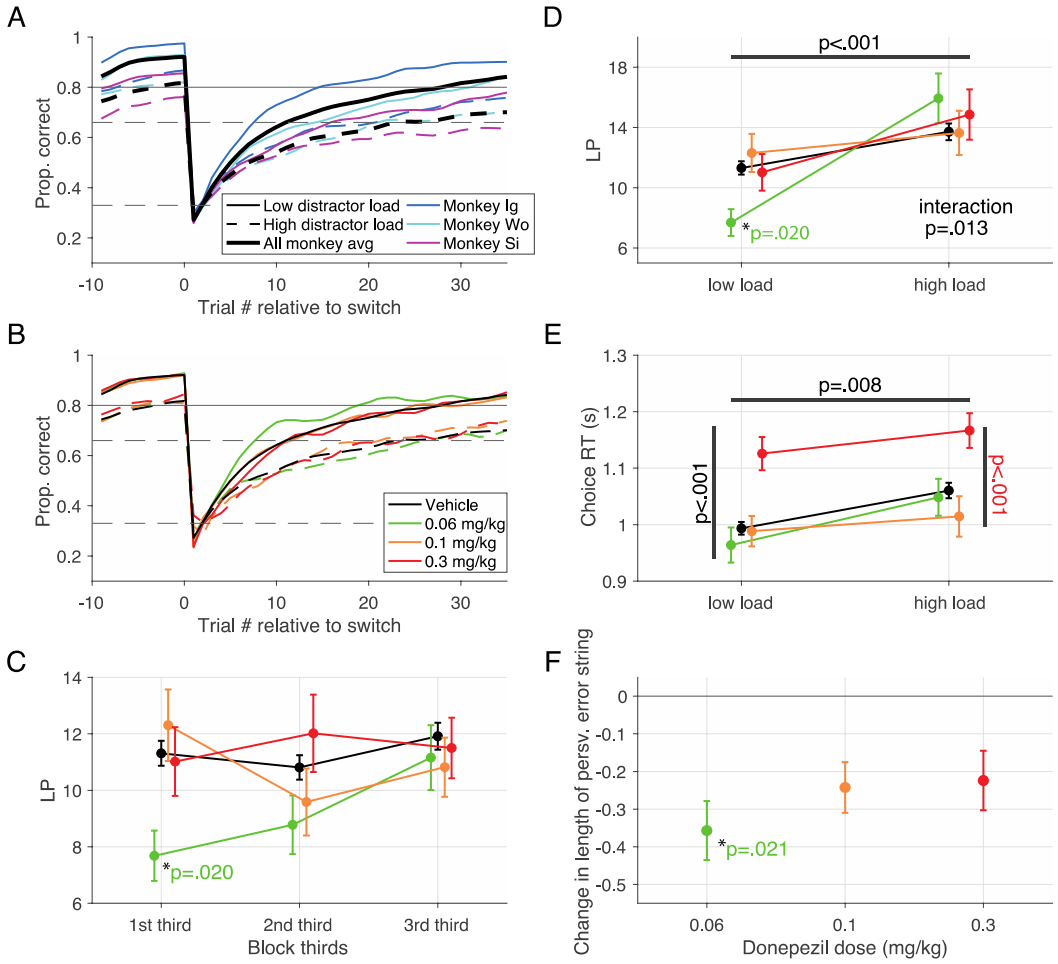

Fig 3.3 Feature learning task learning curves and performance.
(**A**) Average learning curves of each monkey and all monkeys combined for both low and high distractor load conditions. In all instances, monkeys learned faster and with higher plateau performance in low distractor load blocks relative to high distractor load blocks. (**B**) All monkey average learning curves for vehicle, 0.06, 0.1 and 0.3 mg/kg donepezil doses for both low and high distractor load conditions. (**C**) Temporal progression of learning speed (LP) for vehicle, 0.06, 0.1 and 0.3 mg/kg donepezil doses for the low distractor load condition only. At the 0.06 dose, donepezil allows for faster learning in the low attentional load blocks ($F(3,602) = 3.3$, $p = .020$). Similar to the VS task, donepezil's enhancement is only visible early on and relatively close to its i.m. administration. (**D**) Average learning speed of vehicle and donepezil doses for low and high distractor load blocks across sessions reveals an interaction between drug condition and distractor load ($F(3,1052) = 3.59$, $p = .013$). (**E**) The same as D but for choice RTs instead of learning speed. The 0.3 mg/kg donepezil dose slows choice reaction times in both low and high distractor load blocks (Condition $F(3,1052) = 12.3$, $p < .001$; Tukey's, $p < .001$). (**F**) Change in the length of perseverative errors from vehicle, where feature values in the distracting dimension were the target of the perseverations. Error bars reflect SEMean for inter-monkey variability. Donepezil at the 0.06 mg/kg dose significantly reduces perseveration length in the distracting dimension ($p = .021$); other donepezil doses trends towards this as well.

The improved accuracy of visual search was dose-dependent ($F(3,896) = 10.77$, $p < .001$). The 0.06 mg/kg dose enhanced performance by 2.5% ±1.0, 4.4% ±1.3, 6.1% ±1.4 and 6.3% ±1.6 (mean ±SD) for 3/6/9/12 distractor trials, respectively (Tukey's, $p = .005$). The 0.3 mg/kg dose enhanced performance by 2.7% ±1.0, 6.3% ±1.2, 8.5% ±1.3 and 11.0% ±1.4 (mean ±SD) for

3/6/9/12 distractor trials respectively (Tukey's, $p < .001$) (**Figure 3.1E**). Thus, we found larger improvement the more distractors interfered with the target search. We confirmed this by fitting a regression line across performance at different number of distractors, which revealed overall significantly shallower slopes with donepezil (slopes: -0.013 ±0.001, -0.009 ±0.002, -0.015 ±0.003 and -0.005 ±0.002 for vehicle, 0.06, 0.1, and 0.3 mg/kg of donepezil respectively ($H(3) = 11.46$, $p = .01$)). Pairwise comparison showed that the 0.3 mg/kg drug dose and the vehicle condition showed significantly different slopes (Tukey's, $p = .013$)(**Figure 3.1F**).

In contrast to improving visual search accuracy, donepezil slowed down reaction times across all distractor conditions at the 0.3mg/kg dose relative to vehicle by on average 100 ms ±40, 238 ms ±79, 208 ms ±99, 264 ms ±102 (mean ± SD) for 3/6/9/12 distractors respectively ($F(3, 896) = 15.15$, $p < .001$, Tukey's, $p < .001$) (**Appendix B, Figure B1C**). The slope of the regression over different number of distractors did not differ between 0.3 mg/kg dose and vehicle which shows the reaction time effect is a non-selective effect that is independent of distractors (regression slope on RTs: 0.061 ±0.002, 0.065 ±0.007, 0.067 ±0.007 and 0.076 ±0.009 ($H(3) = 3.37$, n.s.) for vehicle, 0.06, 0.1, 0.3 mg/kg of donepezil respectively (**Appendix B, Figure B1D**).

Across sessions visual search accuracy was correlated with reaction times only for the vehicle (Pearson, ρ: -0.30, $p < .001$) and 0.1 mg/kg donepezil dose condition (Pearson, ρ: -0.46, $p = .034$), but not for the 0.06 and 0.3 mg/kg dose conditions in which monkeys showed improved accuracy, which suggests the accuracy improvement is independent from a slowing of reaction speed (**Appendix B, Figure B2A-B**).

We next tested whether improved interference control over increasing number of distractor objects was likewise evident when increasing the similarity of distractor and target features (**Figure 3.2A**). First, we confirmed that higher target-distractor similarity overall reduced performance ($F(2,672) = 16.17$, $p < .001$, **Appendix B**). Donepezil significantly counteracted this similarity effect and improved performance at the 0.06 and 0.3 mg/kg doses ($F(3,672) = 7.75$, $p < .001$, Tukey's, $p = .034$ and $p < .001$ respectively). This finding shows that the beneficial effect of donepezil significantly increased when there was higher demand to control perceptual interference from distracting objects (**Figure 3.2B**). This was also evident as a statistical trend of a shallower

regression slope at 0.06 and 0.3 mg/kg doses of donepezil, which indicates less interference from distracting features when they were similar to the target (**Figure 3.2C**) ($H(3) = 2.79$, n.s.; slope changes relative to vehicle for 0.06, 0.1 and 0.3 mg/kg doses were: +0.0357 ±0.0236, -0.0289 ±0.0334, -0.0656 ±0.0197). The improved search performance with donepezil for visual search with higher target-distractor similarity and with a higher number of distractors was evident in significant main effects, but there was no interaction, suggesting they improved performance independently of each other ($F(2, 2615) = 64.59$, $p < .001$; $F(3,2615) = 28.85$, $p < .001$; $F(6,2615) = 0.69$, n.s. respectively)(**Figure 3.2D**). This independence was also suggested by the absence of a correlation of the target-distractor similarity effect and the number-of-distractor effect (Pearson, n.s.) (**Appendix B, Figure B3**).

3.4.2 Dose-dependent improvement of flexible learning performance

Donepezil also improved feature learning performance, but only at the 0.06 mg/kg dose (**Figure 3.3B**) and most pronounced for the first third of the behavioral session ($F(3,602) = 3.3$, $p = .020$; **Figure 3.3C**). We therefore focused further analysis on the first third of the learning blocks, which revealed that the learning improvement at the 0.06 mg/kg dose was significant for the low distractor load condition (significant interaction effect of drug condition and distractor load (Condition x Distractor Load $F(3, 1052) = 3.59$, $p = .013$); and for vehicle, 0.06, 0.1 and 0.3 mg/kg donepezil doses the trials to criterion were 11.3 ±0.4, 7.7 ±0.9, 12.3 ±1.3 and 11.0 ±1.2 trials long with the 0.06 mg/kg dose and vehicle being significantly different ($p = .020$, Bonferroni correction)(**Figure 3.3D**). There was no change in learning speed with other doses at low or high distractor load.

Beyond learning speed, we found overall slower choice reaction times at the 0.3 mg/kg donepezil dose (**Figure 3.3E**) (main effect of drug condition: ($F(3,1052) = 12.29$, $p < .001$). While reaction times were overall slower at high distractor load ($F(1,1052) = 7.18$, $p = .008$) there was no interaction with drug dose ($F(3,1052) = 0.26$, n.s.). After visually inspecting the results we separately tested the 0.3 mg/kg dose of donepezil and found it led to significantly slower choice reaction time than vehicle (Tukey's, $p < .001$)(**Figure 3.3E**). The changes in choice reaction times did not correlate with changes in learning performance (number of trials to criterion) at any drug

condition, indicating they were independently modulated (Pearson, all n.s.)(**Appendix B, Figure B2D**).

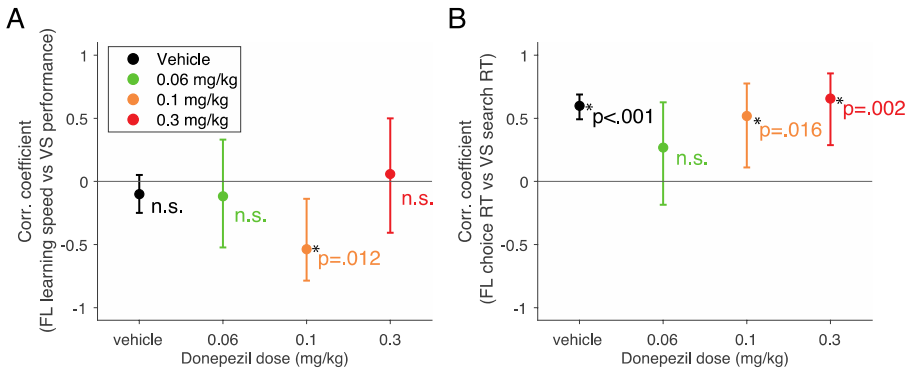

Fig 3.4 The relationship between the visual search task and the feature learning task.
(**A**). Correlation coefficients between FL learning speed (LP) and VS performance for vehicle, 0.06, 0.1 and 0.3 mg/kg donepezil doses. Only the 0.1 mg/kg donepezil dose had a significant correlation between FL and VS task performance (Pearson, ρ: -0.54; p = 0.012). No doses showed a significant change in correlation from vehicle. (**B**) Same as figure A but for FL choice RTs and VS search RTs. Although vehicle, 0.1 and 0.3 mg/kg donepezil doses had a significant correlation between choice and search RTs, we found no significant change in correlation relative to vehicle.

We predicted that the faster learning at the 0.06 mg/kg donepezil dose could be due to a more efficient exploration of objects during learning, which would be reflected in reduced perseverative choices of unrewarded objects. Overall, perseverative errors (defined as consecutive unrewarded choices to objects with the same feature dimension) made up 20% of all errors. As expected, we found significantly shorter sequences of perseveration of choosing objects within distractor feature dimensions at the 0.06 mg/kg dose of donepezil (**Figure 3.3F**). For 0.06, 0.1 and 0.3 mg/kg doses the average length of perseverations in the distractor dimension was: 2.1 ±0.1, 1.8 ±0, 1.9 ±0.1 and 1.9 ±0.1 trials with the difference between vehicle and the 0.06 dose being significant (p = .021). Perseverative choices in the target feature dimension were not different between conditions (for 0.06, 0.1 and 0.3 mg/kg donepezil doses the avg. perseveration length in the target dimension was: 1.7 ±0, 1.7 ±0, 1.6 ±0, and 1.7 ±0 trials (n.s.).

3.4.3 Dissociation of attention and learning improvements, but slowing is correlated

The effects of donepezil on feature learning and visual search might be related, but we found that learning speed and search accuracy was not correlated at those doses at which the drug

improved learning and search (0.06 mg/kg dose) or improved only visual search (0.3 mg/kg dose) (Pearson, all n.s.). A significant correlation was found only for the 0.1 mg/kg dose (Pearson, ρ: -0.54; p = .012) (**Figure 3.4A**). Learning at low or high distractor load and the set size (slope) effects in the visual search task was uncorrelated (Pearson, all n.s.). However, at the 0.3 mg/kg donepezil dose the target-distractor similarity effect (i.e. the search slope change) in the visual search task positively correlated with the difference of the learning speed at high versus low distractor load in the learning task (Pearson, ρ: 0.60; p = .008). This effect signifies that better attentional search of a target among similar distractors is associated with poorer flexible learning of new targets when there are multiple object features to search through (high distractor load).

In contrast to accuracy, choice reaction times in the learning task and visual search were significantly correlated for the 0.1 mg/kg donepezil dose (Pearson, ρ: 0.52; p = .016), the 0.3 mg/kg dose (Pearson, ρ: 0.66; p = .002), and the vehicle control condition (Pearson, ρ: 0.60; p < .001)(**Figure 3.4B**).

3.4.4 Determination of extracellular donepezil and choline levels in the prefrontal cortex and anterior striatum

Visual search and flexible learning are realized by partly independent brain systems, including the PFC and anterior striatum (Cools, 2019). To determine whether extracellular levels of donepezil were increased to a similar magnitude in the PFC and anterior striatum, we measured its concentration after administering doses of either 0.06 and 0.3 mg/kg donepezil IM in the PFC, assumed to be necessary for efficient interference control during visual search (Cohen et al., 2007), and in the head of the caudate nucleus which is necessary for flexible learning of object values (Williams and Eskandar, 2006; Amita and Hikosaka, 2019). We used a recently developed microprobe that samples chemicals in neural tissue based on the principles of solid-phase microextraction (SPME) (Hassani et al., 2019; Lendor et al., 2019b). We found that donepezil was available in both brain areas and its extracellular concentration more than doubled after injecting 0.3 mg/kg than 0.06 mg/kg in both areas ($F(1,16) = 9.69$, p = .007), with no significant difference between PFC and caudate ($F(1,16) = 1.44$, n.s.)(**Figure 3.5A**). Donepezil should cause a depletion of the ACh metabolite choline (Parikh et al., 2004). Using HPLC/MS analysis of the SPME

samples we found in the PFC that 0.06 and 0.3 mg/kg donepezil reduced choline concentrations by 74.2% ±14.9 ($p = .005$) and 85.7% ± 26.9 ($p = .007$) of their baseline concentrations, and in the caudate, it reduced choline by 68.4% ±13.8 ($p = .022$) and 81.0% ±12.9 ($p = .009$) of respective baseline concentrations (**Figure 3.5B**). The 11.5% and 12.6% stronger reduction of choline at the 0.3 versus 0.06 mg/kg dose in PFC or caudate was not significant (n.s.).

To obtain an independent physiological marker of dose-dependent effects we quantified during actual task performance how donepezil changed the heart rate (HR) before versus after drug administration (**Appendix B**). HR showed a transient peak ~20 min after donepezil injection relative to baseline, which was significant for the 0.3 mg/kg dose (pre-injection 102.3 ±7.1 to post-injection 121.6 ±2.6; $p = .021$), but not for the 0.06 mg/kg dose (pre-injection: 90.3 ±4.2 to post-injection: 94.8 ±5.4; n.s.). The 0.3 mg/kg dose caused a significantly higher HR peak than the 0.06 mg/kg dose ($p = .006$) (**Figure 3.5C**).

3.5 Discussion

Here, we dissociated donepezil's improvement of attentional control of interference during visual search from improvements of cognitive flexibility during feature reward learning. At the highest dose tested donepezil reduced interference during visual search particularly when there were many distractors and high similarity of distractors to the target, while concomitantly slowing down overall reaction times and inducing temporary peripheral side effects. In contrast, the lowest dose donepezil did not affect target detection times during visual search, but improved adapting to new feature-reward rules and reduced perseverative responding. These findings document a dose-dependent dissociation of the best dose of donepezil for improving attention and for improving cognitive flexibility.

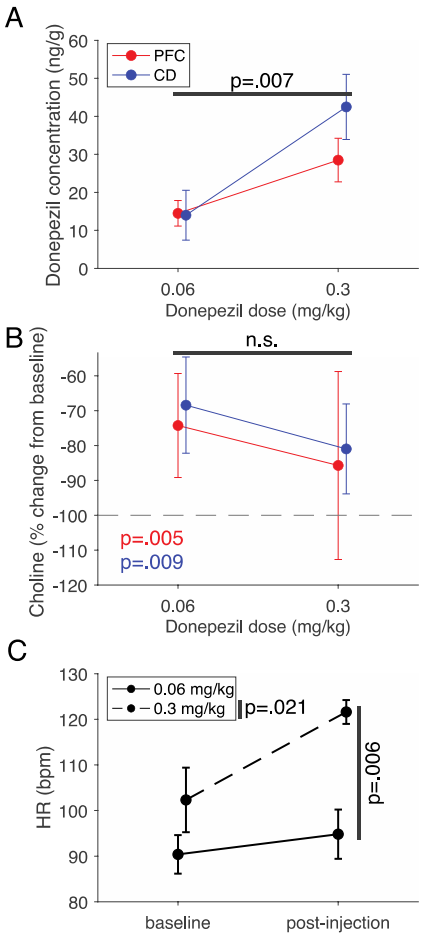

Fig 3.5 In-vivo extracellular measurements of choline, donepezil as well as donepezil's effect on heart rate. (**A**) Quantified concentration of extracellular unbound donepezil with 0.06 and 0.3 mg/kg donepezil administration in the PFC and CD. We are able to reliably detect higher donepezil concentrations with 0.3 mg/kg dosing relative to 0.06 mg/kg dosing (Condition $F(1,16) = 9.69$, $p = .007$) with SPME. We also see a trend towards higher detectable donepezil in the caudate relative to the PFC at the 0.3 mg/kg dose tested, however, we found neither significant group or interaction effects. (**B**) We used choline concentrations as a metric for donepezil bio-activity as it de-activates AChE and prevents acetylcholine's degradation into choline. We extracted average session-wise change in choline from baseline with 0.06 and 0.3 mg/kg donepezil doses within the PFC and CD. Although we find significant decreases in choline by up to >80% of baseline concentrations, we found no significant effect of dosing in either the PFC or CD. (**C**) The heart rate of our fourth monkey was monitored during the neurochemical experiments. This revealed a sharp and transient increase in HR post administration of donepezil at 0.3 mg/kg dose (**Appendix B**) which lead to a higher average bpm. We found that we can significantly distinguish 0.06 and 0.3 donepezil administration via HR ($p = .006$).

3.5.1 Different donepezil dose-ranges for improving interference control and flexible learning

Using a behavioral assessment paradigm with two tasks allowed us to discern differences of the donepezil dose that maximally improved interference control (in the visual search task) versus the dose that maximally improved flexible learning (in the reward learning task). In both

tasks, donepezil modulated performance early within the session (first of two VS blocks and first third of learning blocks) consistent with its short half-life and rapid time to peak concentration with IM delivery (Shiraishi et al., 2005; Lange et al., 2015b). Our results focused therefore on these early time windows. We do not expect different conclusions if we had altered the task sequence (see **Appendix B.3**). At the 0.06 mg/kg dose donepezil facilitated flexible learning of a new feature reward rule and reduced the length of perseverative errors (**Figure 3.3C,F**). These behavioral effects are indicators of improved cognitive flexibility across reward learning and set-shifting tasks (Clarke et al., 2008; Passingham and Wise, 2015; Mansouri et al., 2020). At the same 0.06 mg/kg dose visual search response times were unaffected (**Appendix B, Figure B1**) and visual search accuracy was overall improved but independent of the number of distractors, i.e. independent of the degree of interference (**Figure 3.1E,F**). In contrast, at the higher donepezil doses flexible learning behavior was indistinguishable from the no-drug vehicle control condition showing that improving flexibility required donepezil at a lower dose.

This conclusion is opposite to the drug effects on visual search performance, which was maximally improved at the 0.3 mg/kg dose. At this dose, subjects not only showed improved resistance to interference when there were more distracting objects (**Figure 3.1E,F**), but also improved resistance to distracting objects that were visually similar to the searched-for target (**Figure 3.2B-D**). These findings document that donepezil enhances the robustness to distraction (Womelsdorf and Everling, 2015; Noonan et al., 2018), which critically extends insights from existing primate studies with donepezil that mostly used simpler tasks to infer pro-cognitive effects on working memory or arousal (*see* **Appendix B, Table B1**). The process of attentional control of interference also goes beyond a short-term memory effect measured with delayed match-to-sample tasks. In the visual search paradigm we used, short-term memory of the target object is already necessary for performing the easier trials with 3 or 6 distractors, while an attention specific effect can be inferred when there is greater improvement in performance with increased attentional demands in trials with 9 or 12 distractors. Thus, our study provides strong evidence that donepezil causes specific attentional improvement at higher doses, which supports the neuro-genetic model of cholinergic modulation of attention (Sarter et al., 2016) that has received recently functional support in studies reporting enhanced distractor suppression in nonhuman primates with nicotine receptor specific ACh modulation (Hahn, 2015; Hassani et al., 2017; Azimi et al., 2019), and

improved suppression of perceptually distracting flankers in human subjects tested with a single dose (Gratton et al., 2017). We should note, however, that donepezil caused at the high dose already a non-selective slowing of reaction times indicative of peripheral side effects (see **Appendix B.3**).

The finding that different dose ranges improved flexible learning and visual search distractor filtering suggests that these processes have partially independent Yerkes-Dodson style inverted-U dose-response curves (**Figure 3.6**). One reason supporting this suggestion is that flexible learning and distractor filtering are supported by partially different brain networks, which likely have differential sensitivity to cholinergic modulation. Lesion studies in nonhuman primates have shown that flexible reward learning is closely associated with the medial and orbito-frontal prefrontal cortex and the striatum where lesions impair learning visual reward associations (Clarke et al., 2008; Rothenhoefe et al., 2017). In contrast, visual search distractor filtering in primates depend on the dorsolateral prefrontal cortex (dlPFC) and its connections with posterior parietal cortices, with bilateral dlPFC lesions impairing filtering distraction (Rossi et al., 2007). Brain areas within these partly segregated networks for learning and distractor filtering might be differently sensitive to cholinergic modulation. For example, primate dlPFC has been documented to be uniquely sensitive to neuromodulation by catecholamines and ACh for spatial working memory and switching between distracting features (Arnsten et al., 2010; Cools and Arnsten, 2022), with ACh depletion in PFC causing deficits in attention, but not learning (Voytko et al., 1994). During cognitive processes ACh modulates synaptic efficacy, post-synaptically, in an inverted-U manner through both alpha 7 nicotinic receptors (Yang et al., 2013) and M1 muscarinic receptors (Galvin et al., 2020b). Such inverted-U curves for different receptors are not likely to be homogenous or fully overlapping when taking into consideration variable task demands within a cognitive domain or when considering different cognitive domains entirely (Floresco, 2013). This is supported by studies showing the disruption of rule-selective activity with iontophoretic M1 overstimulation of dlPFC neurons (Vijayraghavan et al., 2018), while at lower doses, delay-cell firing and spatial tuning were enhanced (Galvin et al., 2020b). Our results may thus reflect different inverted-U curves along a construct of flexible attention shifting, required for optimal performance in our feature learning task, and stable filtering of distractors required for optimal performance in our visual search task (**Figure 6**).

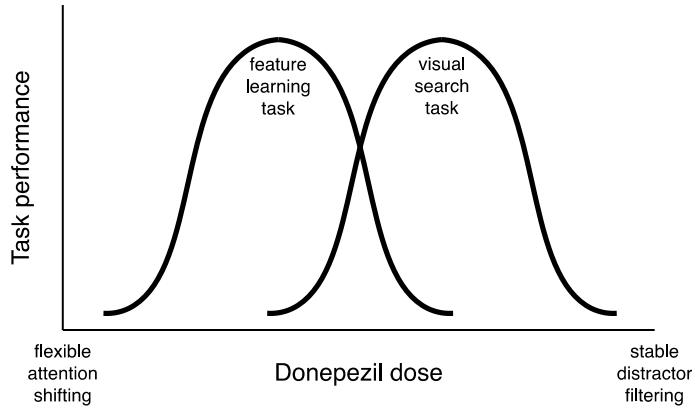

Fig 3.6 Theoretic curves.
Each task will have its own specific demands based on the cognitive domain(s) involved that may be best met with some cholinergic tone which may be endogenously, or in this case pharmacologically, shifted to reach optimal performance. Here, the 'feature learning task' and 'visual search task' have varying demands in terms of attentional flexibility and therefore different inverted-U curves for optimal performance. These curves may be shifted by changing the attentional flexibility or a given subject may travel along the x-axis due to pharmacological intervention, aging-related changes and other mechanisms that may change their effective cholinergic tone

3.5.2 Quantifying extracellular levels of donepezil and choline in prefrontal cortex and striatum

We confirmed the presence of extracellular donepezil in the PFC and the anterior striatum at the doses tested (**Figure 3.5A**) and that it prevented ACh metabolism as evident in 68-86% reduced choline levels (**Figure 3.5B**). To our knowledge this is the first quantification of donepezil's action on the breakdown of ACh in two major brain regions in the primate. The observed reduction of choline is higher than reductions of AChE activity (of ~25- 70%) reported with positron emission tomography or in brain homogenate (Kaasinen et al., 2002; Geerts et al., 2005). Previous studies suggest that evaluating blood plasma levels or cerebrospinal concentrations may not predict how effectively AChE drugs influence behavioral outcomes (Imbimbo, 2001). One likely reason is that intracerebral concentrations can be multifold higher than extracerebral concentration levels (Geerts et al., 2005; Karasova et al., 2020) and do not reflect the actual bioactive concentration available in target neural circuits. By confirming that donepezil prevented ACh breakdown in the PFC and striatum, we thus established a direct link of behavioral outcomes and local drug bioavailability in two brain structures that causally contributes to attention and learning (*see* above) (Voytko et al., 1994; Rossi et al., 2007; Clarke et al., 2008;

Rothenhoefe et al., 2017; Hikosaka et al., 2019). While our study showed that donepezil has a similar effect on ACh breakdown in both areas, it leaves open whether or how choline concentrations in either brain area relate to finer performance variations across tasks as we measured choline only during one task and with insufficient statistical power to establish such a link at this stage.

The neurochemical measurements of donepezil in PFC and striatum were achieved with a recently developed microprobe that samples neurochemicals through principles of solid phase microextraction (SPME) (Pawliszyn, 2000; Cudjoe et al., 2013; Hassani et al., 2019; Lendor et al., 2019b; Reyes-Garcés et al., 2019), and so far was used for testing the consequence of drugs only in rodents (Cudjoe et al., 2013; Cuthbert and Insel, 2013; Cudjoe and Pawliszyn, 2014). We believe that leveraging this technique in primate drug studies will be important for clarifying whether systemically administered drugs reach the desired target brain systems in which they are supposed to exert their pro-cognitive effects.

In our study, confirming donepezil's action in PFC and striatum critically constrains the interpretation of the behavioral results, suggesting that different behavioral outcome profiles are not due an uneven drug availability. Rather, the different '*Best Doses*' for visual search and flexible learning performance will likely be due to brain area specific pharmacokinetic profiles of receptor densities, drug clearance profiles, or auto-receptor mechanisms that intrinsically downregulate local drug actions (de Boer et al., 1990; Coppola et al., 2016; Venkatesan et al., 2020). One prediction from the specific distribution and kinetics of nicotinic or muscarinic receptors in PFC and striatum is that donepezil might at lower doses act predominantly in the striatum via activation of muscarinic sub-receptors as they have a particularly high binding potential (Tsukada et al., 2004b) and respond stronger to muscarinic ACh receptor activation compared with the PFC (Thorn et al., 2019) (*see* **Appendix B.3**). However, it might also be possible that donepezil recruits nicotinic receptors which are upregulated with chronic donepezil use (Kume et al., 2005). It will be important to disentangle in future studies the role of nicotinic and muscarinic sub-receptors in PFC and striatum to optimize the clinical potential to improve learning and attention functions in conditions with cognitive impairment and particularly in dementia (see **Appendix B.3**).

In summary, our results provide rare quantitative evidence that a prominent ACh enhancing drug exerts domain specific cognitive improvements of attentional control and cognitive flexibility at a distinct dose range. A major implication of this finding is that for understanding the strength and limitations of pro-cognitive drug compounds it will be essential to test their dose-response efficacy at multiple cognitive domains.

3.6 Acknowledgements

We thank Dr. Carrie K Jones and Jason Russel for helpful feedback throughout the study and about the manuscript. Research reported in this publication was supported by the National Institute of Mental Health of the National Institutes of Health under grants MH123687 (T.W.) The content is solely the responsibility of the authors and does not necessarily represent the official views of the National Institutes of Health. A prior version of this article has been posted on the bioRxiv preprint server as doi: https://doi.org/10.1101/2021.08.09.455743.

All authors report no biomedical financial interests or potential conflicts of interest.

Chapter 4 M_1 selective muscarinic allosteric modulation enhances cognitive flexibility and effective salience in nonhuman primates

4.1 Abstract

Acetylcholine (ACh) in cortical neural circuits mediates how selective attention is sustained in the presence of distractors and how flexible cognition adjusts to changing task demands. The cognitive domains of attention and cognitive flexibility might be differentially supported by the M_1 muscarinic cholinergic sub-receptor. Understanding how M_1 mechanisms support these cognitive subdomains is of highest importance for advancing novel drug treatments for conditions with altered attention and reduced cognitive control including Alzheimer's disease or schizophrenia. Here, we tested this question by assessing how the subtype selective M_1-receptor specific positive allosteric modulator (M_1 PAM VU0453595) affects visual search and flexible reward-learning in nonhuman primates. We found that allosteric potentiation of the M_1 receptor enhanced flexible learning performance by improving extra-dimensional set shifting, by reducing latent inhibition from previously experienced distractors, and by reducing response perseveration in the absence of adverse side effects. These pro-cognitive effects occurred in the absence of apparent changes of attentional performance during visual search. In contrast, non-selective ACh modulation using the acetylcholinesterase inhibitor donepezil improved attention during visual search at doses that did not alter cognitive flexibility and that already triggered gastrointestinal cholinergic side effects. These findings illustrate that M_1 positive allosteric modulation enhances cognitive flexibility without affecting attentional filtering of distraction, consistent with M_1 activity boosting the effective salience of relevant over irrelevant objects. These results suggest that M_1 PAMs are versatile compounds for enhancing cognitive flexibility in disorders spanning schizophrenia and Alzheimer's diseases.

4.1.1 Statement of significance

Muscarinic receptors mediate the pro-cognitive effects of acetylcholine, but it has remained unclear whether they differentially affect the cognitive subfunctions of attentional filtering, set shifting, and learning. To clarify the functional specificity of M_1 receptors, we assessed these

diverse functions using a recently developed, highly selective M_1 PAM. This M_1 PAM caused domain-specific cognitive improvement of flexible learning and extra-dimensional set shifting, reduced perseverations and enhanced target recognition during learning without altering attentional filtering functions. These domain-specific improvement contrasted to effects of a non-selective acetylcholinesterase inhibitor that primarily enhanced attention and caused dose limiting adverse side effects. These results demonstrate domain-specific improvements of cognitive flexibility suggesting M_1 PAMs are versatile compounds for treating cognitive deficits in schizophrenia and Alzheimer's disease.

4.2 Introduction

Cholinergic activity has far reaching consequences on attention and attentional control functions (Levin et al., 2011; Sarter and Lustig, 2019) with long-standing suggestions that cholinergic modulation is involved in faster updating of expectations during learning (Doya, 2002; Hirayama et al., 2004; Vossel et al., 2014). Depleting cholinergic innervation to the prefrontal cortex compromises while stimulation of cholinergic activity can enhance attentional control functions (Turchi and Sarter, 1997, 2000; Botly and de Rosa, 2009; Ljubojevic et al., 2014; Sarter et al., 2016). These cholinergic effects have been suggested to be supported differently by nicotinic versus muscarinic receptors (Bertrand and Terry, 2018; Thiele and Bellgrove, 2018). Antagonizing muscarinic cholinergic action with scopolamine in healthy humans and nonhuman primates (NHPs) increases false alarm rates and impairs sustained attention by slowing response times and impairing signal detection in two-alternative choice tasks (Bushnell et al., 1997; Davidson et al., 1999; Davidson and Marrocco, 2000; Ellis et al., 2006; Furey et al., 2008). Consistent with these behavioral effects, neuronal recordings in the prefrontal cortex of NHPs has shown that attentional signaling depends on muscarinic receptor activation (Dasilva et al., 2019b). One key open question from these insights is to what extent are attentional subcomponent processes supported by muscarinic signaling and whether there are sub-receptors of the muscarinic receptor family that differentially support separable subcomponent processes underlying attention, such as filtering of distracting information, enhancing the flexible updating and shifting of attention sets, or supporting robust goal representations during goal-directed behavior. Each of these diverse subcomponent processes has been associated in prior studies with the muscarinic M_1 muscarinic

receptor, which is widely expressed in the cortex, striatum and hippocampus (Levey, 1996; Rapan et al., 2022) and may thus mediate some of these muscarinic pro-cognitive effects (Jones et al., 2012; Sarter and Lustig, 2019).

One set of prior studies has implicated the M_1 receptor to memory processes because M_1 selective drugs can restore deficits in novel object recognition (Rook et al., 2017; Moran et al., 2018), and can partially reverse scopolamine induced deficits in contextual fear conditioning consistent with M_1 selective compounds enhancing the salience of the (aversive) outcomes during learning (Ma et al., 2009; Chambon et al., 2011; Moran et al., 2018). But it has remained unclear whether the effects described in these studies are best accounted for by an improvement of memory, or whether enhanced cognitive control processes contribute to more effective encoding of stimuli as opposed to enhancing learning processes. A similar question about the specific cognitive process that are modulated arises when considering the M_1 effects on different forms of attentional performance. While some studies have shown that M_1 receptor modulation is important for attentional modulation of neural firing (Herrero et al., 2008; Dasilva et al., 2019b), behavioral studies using M_1 selective ago PAMs (positive allosteric modulators with partial agonistic properties) in NHPs (Lange et al., 2015a) and rodents (Kucinski et al., 2020) have not found primary improvements of sustained attention performance. Rather than modulating attention, the M_1 receptor actions improved behavior only in more demanding task conditions in which M_1 modulation enhanced the adjustment of performance when task requirements changed (Kucinski et al., 2020). These results are consistent with findings showing that M_1 specific drugs can enhance the likelihood of subjects to apply complex sensorimotor transformations to reach a goal (as in Object Retrieval Detour Tasks) (Uslaner et al., 2018), and to facilitate odor-based reversal learning of objects (Shirey et al., 2009). These cognitive enhancing effects suggest that M_1 receptors may be particularly important for higher cognitive control processes that go beyond attentional focusing or the filtering of distraction (Sarter and Lustig, 2019). However, it is not apparent which particular control processes might be supported by M_1 receptors as the existing studies used widely varying tasks and a study using one of the classical cognitive control task (the anti-saccade task) was not successful in identifying neural correlates of M_1 receptor specific effects in the prefrontal cortex of NHPs (Vijayraghavan et al., 2018).

The current study set out to address these questions about the specific pro-cognitive role of the M_1 receptor in supporting cognition. Firstly, to distinguish cognitive subcomponent processes we devised two tasks. A visual search task allowed for distinguishing attentional subcomponent processes by varying distractor load and perceptual interference. And a intra-/extra-dimensional set shifting learning task distinguishing cognitive control processes and cognitive flexibility. Secondly, we assessed NHP performance in these tasks using VU0453595, which is a recently developed subtype selective positive allosteric modulator (PAM) for the M_1 muscarinic receptor that has exceptional specificity and effectivity to potentiate cholinergic signaling without exerting direct agonistic effects (Ghoshal et al., 2016; Moran et al., 2018; Rook et al., 2018a). This M_1 selective PAM is from a family of advanced drug compounds that avoid dose limiting side effects which are prevalent with existing orthosteric compounds (Korczyn, 2000; Li et al., 2019), and which has the potential to treat deficits in attention control and cognitive rigidity prevalent in schizophrenia, Alzheimer's disease and substance use disorders (Perry and Hodges, 1999; Woicik et al., 2011; Rohlf et al., 2012; Waltz, 2017; Tobin, 2018). Assessing the pro-cognitive profile of VU0453595 for these higher cognitive functions is therefore pivotal to advance therapeutic solutions for these widespread neuropsychiatric conditions (H. Ferreira-Vieira et al., 2016; Moran et al., 2018; Foster et al., 2021).

We found that the M_1 PAM VU0453595 exerts an inverted-U shaped improvement of cognitive flexibility, causing faster learning, extra-dimensional set shifting, and reduced perseverations (i.e. enhanced flexibility), while leaving attentional filtering during visual search unaffected. These results are contrasted to the non-selective acetylcholine esterase (AChE) inhibitor donepezil which improved attentional filtering with only marginal effects on cognitive flexibility (Hassani et al., 2021).

4.3 Results

Each of the four monkeys completed 60 sessions composed of 40 vehicle days and 7 days for each of the three tested doses of VU0453595 (0.03, 0.1, and 0.3 mg/kg). No adverse effects were observed in any of the 21 drug dosing days in any of the monkeys.

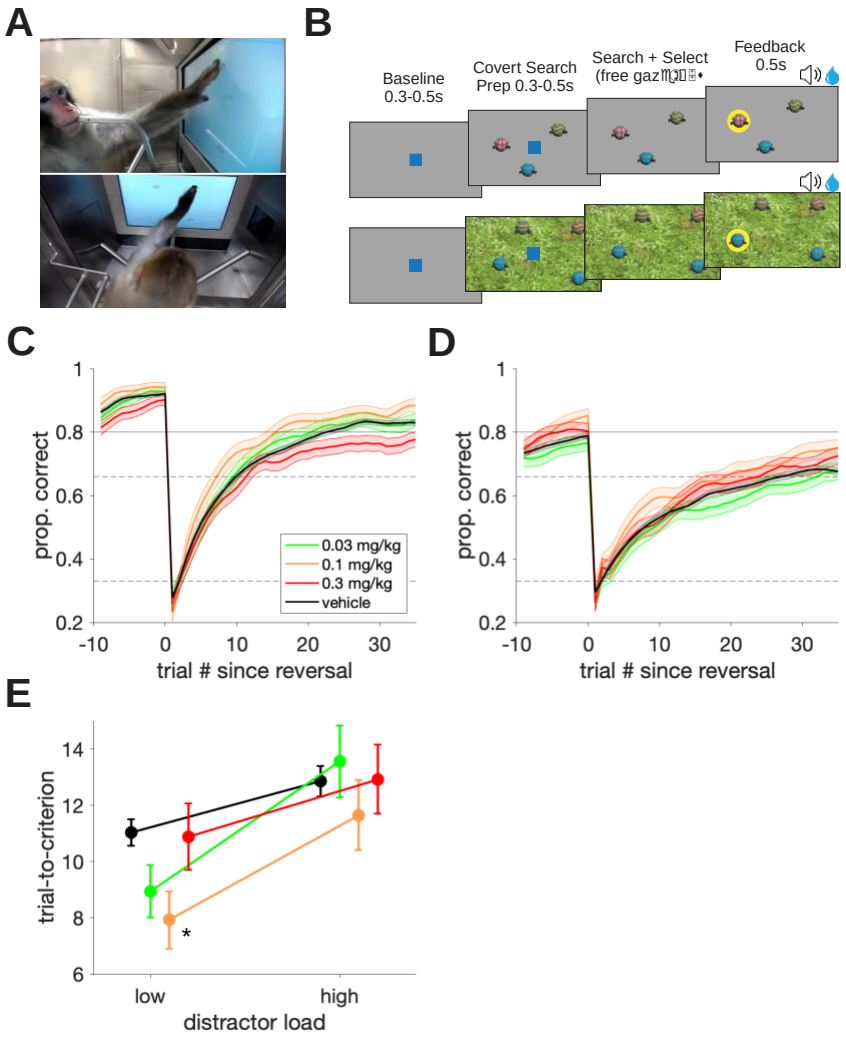

Fig 4.1 Task design and feature-reward learning task performance enhancement by VU0453595
(**A**) Images of cage-mounted kiosk and monkey Ba utilizing the touch screen to perform the feature-reward learning (FRL) task taken via the video monitoring system. Both images are taken from the same time point from different angles. (**B**) Trial progression of the FRL task (top) and the VS task (bottom). The example FRL task here is a high distractor load block where objects vary in both color and pattern. Although the red checkered object was correctly chosen in this trial, the animal would need to learn through trial-and-error if future red or checkered objects will be rewarded. The example VS block here shows a 3 distractor trial with the target object consisting of the features: blue, striped and straight arms. The red distractor has zero features in common with the target, the yellow distractor has one feature in common with the target (striped pattern) and the blue distractor has two features in common with the target (blue color and straight arms). Trials in either task were initiated by a 0.3-0.5s touch and hold of a central blue square (3° visual radius wide) after which the square disappears (for 0.3-0.5s) and task objects (2.5° visual radius wide) are presented on screen. For the VS task, the background changes to one of 5 images cuing the animal to the task rule while the background remains neutral (gray) in the FRL task. In either task, subjects have 5s to select one of the objects with a 0.2s touch and hold. Failure to choose an object resulted in an aborted trial which was ignored. Feedback for choice selection was provided 0.2s after object selection for 0.5s via both a visual halo around the chosen object as well as a auditory cue alongside any earned fluid. Both the frequency of the audio feedback and color of the feedback halo differed based on outcome. (**C**) Block-wise average learning curves for the low distractor load blocks of the FRL task aligned to block start for vehicle, 0.03, 0.1 and 0.3 mg/kg VU0453595, smoothed after the first 3 trials with a sliding window (shaded area: SE). Dotted horizontal lines signify 0.33 and 0.66 probabilities with the solid horizontal line at 0.8 signifying the block learning criterion. (**D**) The same as C but for the high distractor load blocks. (**E**) Median trials-to-criterion for the low and high distractor

load blocks of the FRL task. For the low distractor load blocks, trials to criterion were 11.03 (SE: 0.38), 8.94 (SE: 0.75), 7.93 (SE: 0.81) and 10.88 (SE: 0.94) for vehicle, 0.03, 0.1 and 0.3 mg/kg doses of VU0453595 respectively. Only the 0.1 mg/kg dose was significantly different from vehicle ($F(3,691) = 3.54$, $p = .01$; $\eta^2 = .015$; Tukey's, $p = .028$; Cohen's $d = -.352$). For the high distractor load blocks, trials to criterion were 12.85 (SE: 0.43), 13.56 (SE: 1.03), 11.65 (SE: 1.00), and 12.92 (SE: 0.98) for vehicle, 0.03, 0.1 and 0.3 mg/kg doses of VU0453595 respectively with no significant effect ($F(3,565) = .40$, n.s.).

4.3.1 M_1 PAM VU0453595 enhances learning

Animals performed and consistently completed all 21 blocks of the feature learning task per session in all experimental conditions and expectedly showed faster learning in the easier low distractor load condition versus the more difficult high distractor load condition (**Fig. 4.1C**,**D**). Administration of VU0453595 improved multiple measures of the learning performance compared to the vehicle control condition. In order to reveal any temporally specific effects on learning, we implemented a linear mixed effects model on the median trials-to-criterion for the feature-reward learning (FRL) task (see **Appendix C.1**). Faster learning with 0.1 mg/kg dosing was evident in the early, middle, and last thirds of the 21 learning blocks per session with the first third of blocks showing the strongest effects (0.1 mg/kg fixed effect: $t(3674) = -2.67$, $p = .008$; first third Cohen's $d = -.228$; overall Cohen's $d = -.061$) (**Appendix C, Fig. C1A**). For this reason, all future analyses of the FRL task use the first third of blocks. Faster learning was particularly evident at low distractor load for which animals reached the trials-to-criterion at 7.93 (SE: 0.81) trials after a block switch with 0.1 mg/kg, compared to 11.03 (SE: 0.38) trials with vehicle ($F(3,691) = 3.54$, $p = .01$; $\eta^2 = .015$; Tukey's, $p = .028$; Cohen's $d = -.352$) (**Fig. 4.1E**). After the performance criterion was reached, VU0453595 also enhanced plateau performance (**Appendix C, Fig. C1B**) and increased the proportion of blocks in which the animals reached the learning criterion at the 0.1 mg/kg dose (**Appendix C, Fig. C1C**).

Faster learning and improved performance accuracy in the 0.1 mg/kg dose condition was accompanied by faster response times (RTs). Over the course of a learning block, subjects showed a characteristic change of RTs with fast RTs early in the block that slowed down and plateaued around the trial within the block when animals started learning the rewarded target feature (**Fig. 4.2A**,**B**). Notably, administering the middle (0.1 mg/kg) dose of VU0453595 led to significantly faster RTs of 870 ms (SE: 23 ms; low load) and 960 ms (SE: 23 ms; high load) relative to vehicle

RTs of 960 ms (SE: 11 ms; low load) and 984 ms (SE: 11 ms; high load) ($F(3,1672) = 2.97$, $p = .03$; $\eta^2 = .005$; Tukey's, $p = .04$; Cohen's $d = -.350$) (**Fig. 4.2C**). Moreover, the number of trials needed for the RTs to plateau was significantly fewer with the 0.1 mg/kg dose taking until trial 6.5 (SE: 0.5) relative to vehicle until trial 8.7 (SE: 0.3) ($F(3,193) = 2.67$, $p < .05$; $\eta^2 = .040$; Tukey's, $p = .03$; Cohen's $d = -.674$) (**Fig. 4.2D**).

4.3.2 Improved cognitive control with M_1 PAM VU0453595

Learning a new feature-reward rule following a block switch entailed either identifying a target feature that was new or from a different feature dimension as in the previous block (extra-dimensional switches, ED), or from the same feature dimension as the previous target (intra-dimensional switches, ID). We found that the 0.1 mg/kg dose with VU0453595 significantly improved learning for both, ED and ID switches (**Fig. 4.2E,F**) but not switches where the current target was from a novel feature dimension (data not shown). A large improvement was evident for ED switches with the average trials-to-criterion of 4.0 (SE: 0.7) after 0.1 mg/kg dose administration being significantly lower than the average 12.2 (SE: 1.0) trials-to-criterion of the vehicle condition ($F(3,122) = 3.15$, $p = .03$; $\eta^2 = .072$; Tukey's, $p = .02$; Cohen's $d = -.868$) (**Fig. 4.2E**). Please note that ED switches reported in our task were to a target of the previous distractor feature dimension and thus required disengaging from that dimension in addition to identifying the newly rewarded dimension. ID switches had a more moderate but still significant advantage after administration of 0.1 mg/kg dose of VU0453595 with a trials-to-criterion of 9.3 (SE: 0.7) relative to 12.6 (SE: 0.5) with vehicle ($F(3,518) = 3.26$, $p = .02$; $\eta^2 = .019$; Tukey's, $p = .04$; Cohen's $d = -.349$) (**Fig. 4.2F**).

A learning advantage after ED and ID switches indicates that VU0453595 at the 0.1 mg/kg dose enhanced cognitive control. Cognitive control processes also entail the ability to avoid erroneous perseverative responding. We quantified the perseverative responses as the proportion of repeated unrewarded choices to a feature in the target-feature dimension or in distractor-feature dimensions. We found that VU0453595 reduced perseverative responding to other features in the target feature dimension at 0.1 mg/kg from the 10.7% (SE: 0.2) of vehicle down to 8.5% (SE: 0.6) ($F(3,1679) = 3.74$, $p = .01$; $\eta^2 = .007$; post-hoc analysis of 0.1 mg/kg condition Tukey's, $p = .01$;

Cohen's d = -.243) (**Fig. 4.2G**). Perseverative responding to objects with features of the distractor dimension was moderately, but non-significantly reduced with VU0453595 ($F(3,844) = 2.36$, $p = .07$; $\eta^2 = .008$) (**Fig. 4.2H**).

4.3.3 M_1 PAM VU0453595 has no consistent effect on interference control

Cholinergic compounds modulate attention and interference control (Thiele and Bellgrove, 2018; Azimi et al., 2019; Hassani et al., 2021). We evaluated these functions using a visual search (VS) task that varied the requirements to control interference from increasing numbers of distractor objects during search, and from increasing the number of features that were shared between target and distractors (target-distractor similarity, see **Methods**).

Animals showed prominent slowing of target detection times with increasing number of distractors from 3, 6, 9 to 12. VU0453595 did not consistently modulate this slowing with increasing distractor set size (defined as slope of the linear fit) (**Fig. 4.3A**,**B**). Similar to target detection times, accuracy was not consistently affected by VU0453595 with no modulation of set size effects. For both the raw values of target detection times and accuracy, some significant changes were observed (see **Appendix C.2**) but no systematic pattern could be extracted (**Fig. 4.3C,D**). Similarly, VU0453595 did not consistently alter perceptual interference operationalized as changes in performance with increasing similarity between the target and distractors (**Fig. 4.3E,F**). We did not observe significant changes in the set size effect for target detection times (first block: $F(3,236) = 0.54$, n.s.; second block: $F(3,236) = 1.81$, n.s.; **Fig. 4.3E**) or performance accuracy (first block: $F(3,236) = 0.53$, n.s.; second block: $F(3,236) = 0.51$, n.s.; **Fig. 4.3F**). Similar to the distractor effect, the comparisons of how perceptual interference impacted raw target detection times and performance showed no systematic improvements (see **Appendix C.2**). No changes to speed of processing, operationalized as the time to response during familiarization trials (see **methods**) were observed with VU0453595 at any dose for neither the first VS block ($F(3,236) = .56$, n.s.) nor the second block ($F(3,236) = .35$, n.s.) (**Appendix C, Fig. C2**).

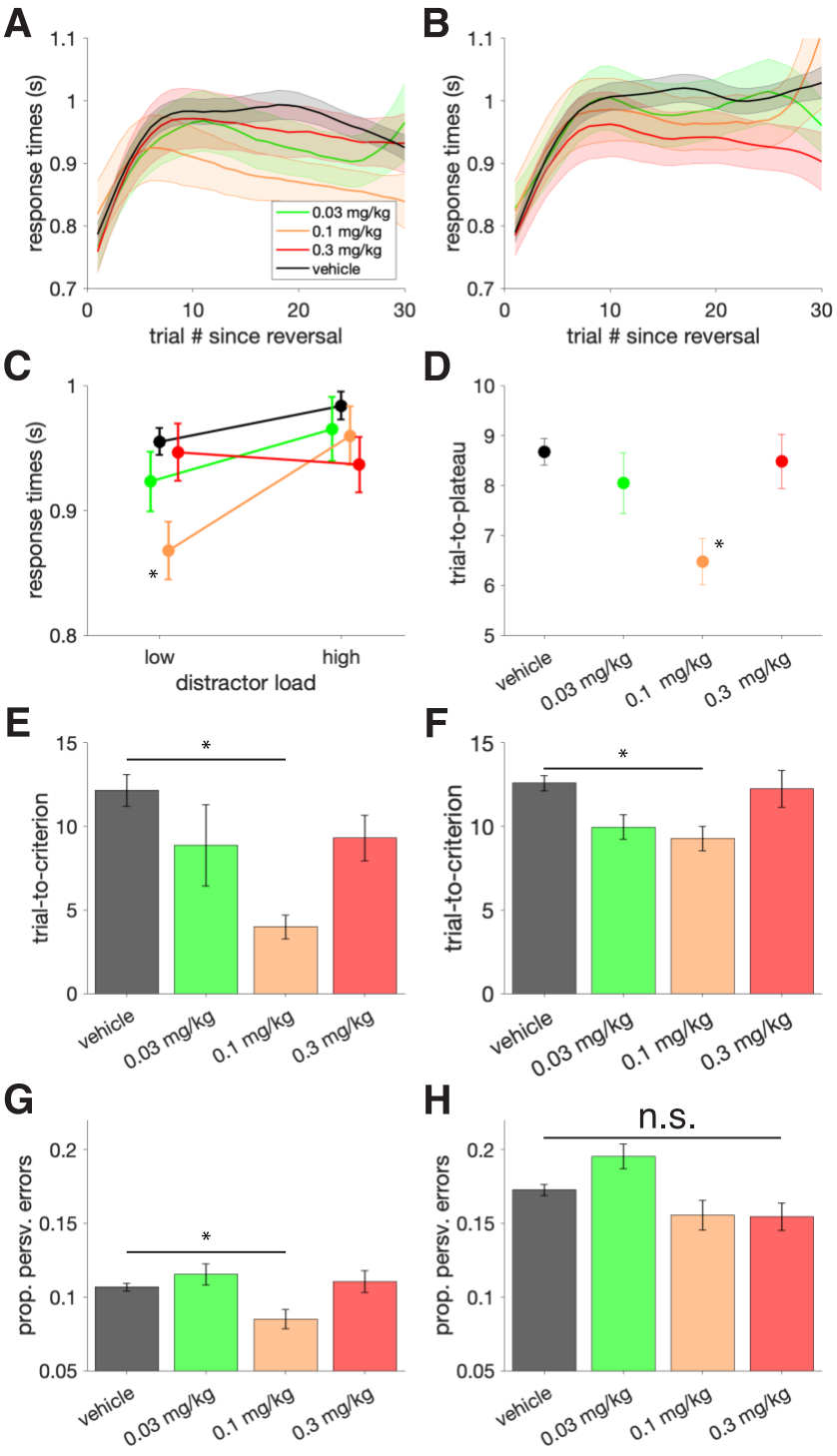

Fig 4.2 Feature-reward learning task efficiency and cognitive flexibility improvements with VU0453595
(**A**) The average RT curve of each session (correct trials only) aligned to block start for the low distractor load blocks of the FRL task for vehicle, 0.03, 0.1 and 0.3 mg/kg doses of VU0453595 (shaded area: SE) (**B**) The same as A but for high distractor load blocks of the FRL task. (**C**) Block-wise averages of the traces plotted in A and B visualized to compare RTs between distractor load conditions. Low distractor load blocks had RTs of 960 ms (SE: 11), 923 ms (SE: 24), 870 ms (SE: 23) and 974 ms (SE: 23) for vehicle, 0.03, 0.1 and 0.3 mg/kg doses of VU0453595 respectively. High distractor load blocks had RTs of 984 ms (SE: 11), 965 ms (SE: 26), 960 ms (SE: 23) and 937 ms (SE: 22). Only the 0.1 mg/kg dose of VU0453595 was significantly different from vehicle

($F(3,1672) = 2.97$, $p = .03$; $\eta^2 = .005$; Tukey's, $p = .04$; Cohen's $d = -.350$) (**D**) Trials-to-plateau for RTs in the low distractor load blocks defined as the first trial per block (excluding trial 2) that RTs become faster (error bars: SE). Trials-to-plateau was 8.7 (SE: 0.3), 8.0 (SE: 0.6), 6.5 (SE: 0.5) and 8.5 (SE: 0.5) for vehicle, 0.03, 0.1 and 0.3 mg/kg doses of VU0453595 respectively. Only the 0.1 mg/kg dose was significantly different from vehicle ($F(3,193) = 2.68$, $p < .05$; $\eta^2 = .040$; Tukey's, $p = .017$; Cohen's $d = -.674$). (**E**) Block-wise average trials-to-criterion after extra-dimensional shifts were 12.2 (SE:1.0), 8.9 (SE: 2.4), 4.0 (SE: 0.7) and 9.3 (SE: 1.4) for vehicle, 0.03, 0.1, and 0.3 mg/kg doses of VU0453595 respectively. Only the 0.1 mg/kg dose showed a significant difference from vehicle ($F(3,122) = 3.15$, $p = .03$; $\eta^2 = .072$; Tukey's, $p = .02$; Cohen's $d = -.868$). (**F**) Block-wise average trials-to-criterion after intra-dimensional shifts were 12.6 (SE: 0.5), 10.0 (SE: 0.7), 9.3 (SE: 0.7) and 12.3 (SE: 1.1) for vehicle, 0.03, 0.1, and 0.3 mg/kg doses of VU0453595 respectively. Only the 0.1 mg/kg dose showed a significant difference from vehicle ($F(3,518) = 3.26$, $p = .02$; $\eta^2 = .019$; Tukey's, $p = .04$; Cohen's $d = -.349$). (**G**) The proportion of errors that were perseverative in nature with the feature that was perseverated being from the same feature dimension as the target feature. The proportion of perseverative errors from the target feature dimension were 10.7% (SE: 0.2), 11.5% (SE: 0.7), 8.5% (SE: 0.6) and 11.0% (SE: 0.7) for vehicle, 0.03, 0.1, and 0.3 mg/kg doses of VU0453595 respectively with only the 0.1 mg/kg dose being significantly different from vehicle ($F(3,1679) = 3.74$, $p = .01$; $\eta^2 = .007$; Tukey's, $p = .01$; Cohen's $d = -.243$). (**H**) The same as G but with the feature that was perseverated being from the distracting feature dimension (different from the target feature dimension). The proportion of perseverative errors from the distracting feature dimension were 17.3% (SE: 0.3), 19.6% (SE: 0.8), 15.6% (SE: 1.0) and 15.6% (SE: 1.0) for vehicle, 0.03, 0.1, and 0.3 mg/kg doses of VU0453595 respectively. There was a non-significant trend for a main effect of experimental condition ($F(3,844) = 2.36$, $p = .07$; $\eta^2 = .008$).

4.3.4 Double dissociation of VU0453595 and Donepezil for cognitive flexibility and interference control

VU0453595 improved learning and reduced perseveration, but without reducing interference from distracting objects and features. This pattern of results contrasts to the effects of non-selective acetylcholine esterase inhibitor donepezil for which a prior study using the same tasks as in the current study found that an optimal dose range improved VS performance but without affecting reward learning and perseveration (Hassani et al., 2021). To quantify this difference, we re-analyzed the performance of reward learning and visual search with donepezil in the prior study using the best-dose for VS improvements (0.3 mg/kg) (Hassani et al., 2021). This comparative approach revealed a double dissociation (**Table 4.1**). VU0453595 enhanced metrics of learning efficiency and cognitive flexibility but not metrics of interference control during VS, while donepezil made the animals more robust against distraction (improved interference control) during visual search but did so without improving feature-reward learning performance. Furthermore, at this dose, donepezil slowed down response times in the FRL task as well as search times in the VS task and even slowed the speed of processing early, partially as a consequence of dose-limiting side effects that accompanied donepezil. In contrast, VU0453595 at 0.1 mg/kg sped up response times in the FRL task without slowing down VS search times or the speed of processing and without any observable side effects (**Table 4.1**).

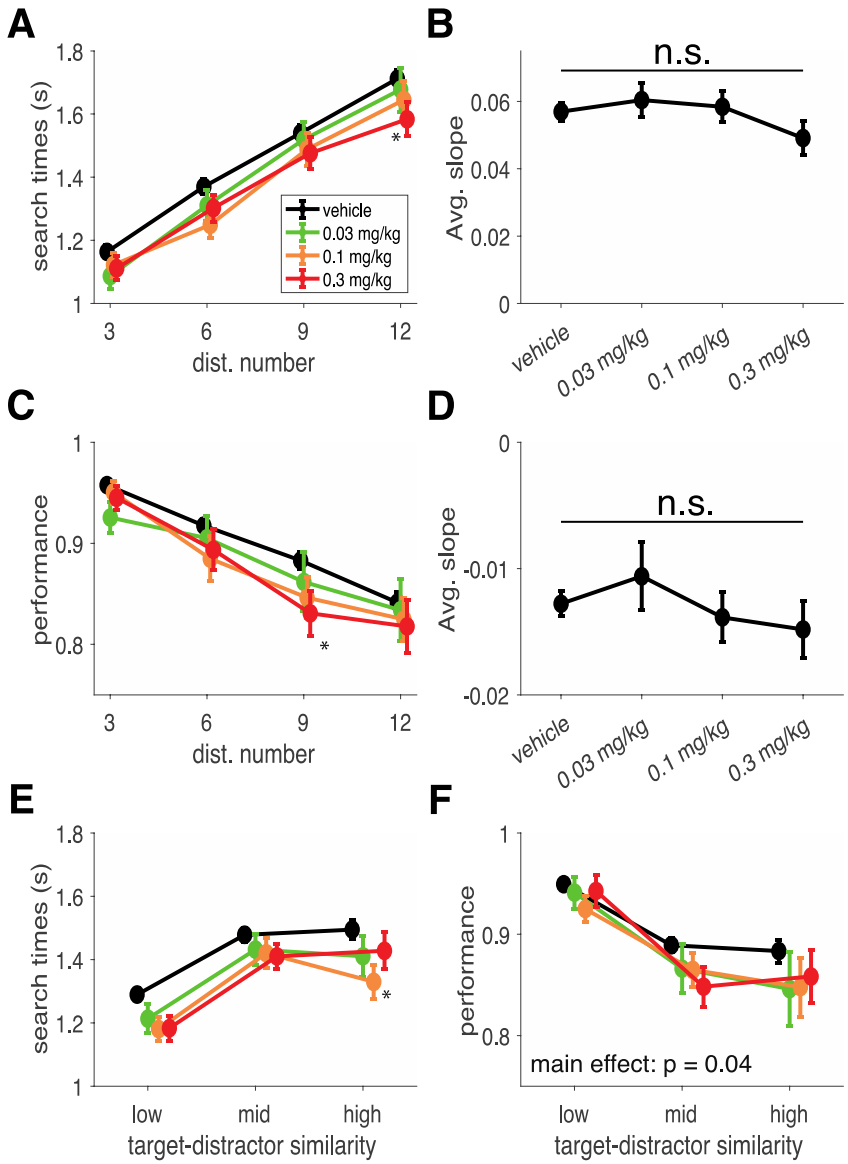

Fig 4.3 Distractor effect and interference control are not consistently impacted by VU0453595
(**A**) Target detection durations (reaction times) as a function of distractor number for the second VS block. There was a significant main effect of experimental condition with a significant different between the 0.3 mg/kg dose of VU0453595 compared with vehicle ($F(3,944) = 3.67$, $p = .01$; $\eta^2 = .008$; Tukey's, $p < .05$). The 0.3 mg/kg dose improved search times from 1.16 s (SE: 0.02), 1.37 s (SE: 0.02), 1.54 s (SE: 0.03) and 1.72 (SE: 0.03) with vehicle to 1.11 s (SE: 0.04), 1.30 s (SE: 0.04), 1.48 s (SE: 0.05) and 1.58 s (SE: 0.05) for 3, 6, 9 and 12 distractors respectively. There was no significant change in the first VS block (data not shown). (**B**) The set size effect, operationalized as the slope of the linear fit of search times as a function of distractor numbers for the second VS block (0.057 (SE: 0.003), 0.060 (SE: 0.005), 0.058 (SE: 0.005) and 0.049 (SE: 0.005) for vehicle, 0.03, 0.1 and 0.3 mg/kg doses of VU0453595) was not significant ($F(3,236) = .67$, n.s.). There was also no significant set size effect in the first VS block (data not shown). (**C**) VS task performance as a function of distractor number for the first VS block. There was a significant main effect of experimental condition with a significant different between the 0.3 mg/kg dose of VU0453595 compared with vehicle ($F(3,944) = 3.80$, $p = .01$; $\eta^2 = .010$; Tukey's, $p = .04$). The 0.3 mg/kg dose reduced performance from 95.8% (SE: 0.4), 91.8% (SE: 0.7), 88.3% (SE: 0.8) and 84.1% (SE: 1.0) with vehicle to 94.5% (SE: 1.2), 89.4% (SE: 2.0), 83.1% (SE: 2.2) and 81.8% (SE: 2.7) for 3, 6, 9 and 12 distractors respectively. There was no significant change in the second VS block (data not shown). (**D**) The set size effect, operationalized as the slope of the linear fit of performance as a function of distractor numbers for the first VS block (-0.013 (SE: 0.001), -0.011 (SE: 0.003), -

0.014 (SE: 0.002) and -0.015 (SE: 0.002) for vehicle, 0.03, 0.1 and 0.3 mg/kg doses of VU0453595) was not significant ($F(3,236) = .60$, n.s.). There was also no significant set size effect in the second VS block (data not shown). (**E**) VS task search times as a function of target-distractor similarity for the second VS block. There was a significant main effect of experimental condition with a significant different between the 0.1 mg/kg dose of VU0453595 compared with vehicle ($F(3,708) = 4.67$, $p = .003$; $\eta^2 = .018$; Tukey's, $p = .02$) but no significant set size effect ($F(3,236) = 1.81$, n.s.). Search times were faster from 1.29 s (SE: 0.02), 1.48 s (SE: 0.02) and 1.49 (SE: 0.03) with vehicle to 1.18 s (SE: 0.04), 1.42 s (SE: 0.05) and 1.33 s (0.05) for low, medium and high average target-distractor similarity respectively. (**F**) VS task performance as a function of target-distractor similarity for the second VS block. There was a significant main effect of experimental condition but no significant post-hoc comparison was found ($F(3,708) = 2.84$, $p = 0.04$; $\eta^2 = 0.011$; Tukey's, n.s.). We also failed to find a significant set size effect ($F(3,236) = .53$, n.s.).

4.4 Discussion

Here, we found that healthy adult rhesus monkeys show M_1-receptor specific improvements of cognitive flexibility in a feature-reward learning task, while leaving attentional filtering unaffected. In particular, the middle of three doses of the M_1 PAM VU0453595 increased the speed of learning a new feature-reward rule, particularly with extra-dimensional rule changes. At the same dose animals showed less perseveration on unrewarded features. These pro-cognitive effects contrasted to the absence of distractor dependent changes in accuracy or search times during VS. At the dose range tested no adverse side effects were noted. This result pattern contrasts to the effects of donepezil which improved attentional filtering during VS at a dose at which it did not affect cognitive flexibility, but already resulted in dose-limiting side effects. Taken together, these findings document a functional dissociation of the role of M_1 receptor modulation with highly selective M_1 receptor potentiation, suggesting it is a versatile treatment target for disorders suffering from inflexible, rigid cognition and behavior including schizophrenia, Alzheimer's disease and addiction.

4.4.1 M_1 PAM enhances learning and extra-dimensional shifts

We found that the medium dose of VU0453595 improved learning of feature values. Compared to the vehicle control, the medium dose allowed subjects to reach the performance criterion 3.10 trials earlier at the low distractor load condition (**Fig. 4.1E**) and the number of trials to reach plateau RT decreased by 2.20 trials for low distractor load blocks (**Fig. 4.2D**) (see **Appendix C.3** with regard to dose specificity of the effects). The learning improvement was particularly apparent with extra-dimensional (ED) switches, i.e. when the target feature in a block was from a different feature dimension as the target in the preceding block (**Fig. 4.2E**). Typically,

ED switches take longer and are more difficult than intra-dimensional switches by requiring the recognition of a new dimension and integrating it in a new attentional set (Izquierdo et al., 2016), suggesting that VU0453595 particularly benefits the flexible updating and switching of attention sets. This finding in NHPs extends the insights that the M_1 selective ago PAM BQCA (benzylquinolone carboxylic acid) can restore odor-based reversal learning of objects in transgenic mice (Shirey et al., 2009).

Computationally, human and animal studies support the suggestion that the M_1 PAM might enhance the updating of attention sets. Enhanced learning following ED switches in our task paradigm suggests that the M_1 PAM allowed the animals to more effectively recognize that previously unrewarded, distracting, features became rewarded. The M_1 PAM effect is therefore akin to increasing the effective salience of those targets that were 'learned distractors' from the previous block while suppressing the salience of current distractor features (**Fig. 4.1**). Recent modeling suggests that increasing effective salience is achieved with an attention-augmentation mechanism that enhances learning from attended features by actively un-learning (forgetting) unattended features (Womelsdorf et al., 2021b). Various studies have documented that such an attention-augmentation mechanism is important for fast learning in complex tasks like the one used here (Wilson and Niv, 2012; Niv et al., 2015; Radulescu et al., 2016; Hassani et al., 2017; Oemisch et al., 2019; Womelsdorf et al., 2021b). The M_1 PAM effect may thus enhance the effective salience of target features, consistent with neuronal recordings that show M_1 receptor activation in the prefrontal cortex is necessary during the early processing of targets (Howe et al., 2017). Support for this suggestion comes from an elegant multi-task study in NHPs that found compromising muscarinic activity with scopolamine increased the pro-active interference of prior spatial information onto current performance in a self-ordered search task (Taffe et al., 1999). The current findings suggest that potentiating M_1 receptor activity reduces pro-active interference with the net effect of enhanced effective salience.

Recent human studies found that the learning of stimulus-response reward probabilities is enhanced with the AChE inhibitor galantamine (Vossel et al., 2014) and impaired when antagonizing muscarinic receptors with biperiden (Marshall et al., 2016a). In a Bayesian framework, these performance improvements were linked specifically to enhanced versus reduced

weighting of top-down expectancies and prediction errors during learning (Vossel et al., 2014; Marshall et al., 2016a). In this framework, muscarinic receptor activity determined how fast prediction errors led to belief updating about how stimuli are linked to reward. The results of the current study therefore suggest that enhanced belief updating and effective salience is mediated specifically through the potentiation of the M_1 receptor. Supporting this conclusion, in rodents, the M_1 selective ago PAM BQCA reverses scopolamine induced deficits in a contextual fear conditioning consistent with M_1 enhancing the salience of the (aversive) outcomes during learning (Ma et al., 2009; Chambon et al., 2011; Moran et al., 2018).

These functions of the M_1 receptor may be realized in the prefrontal cortex. In primates, reversal learning and the extra-dimensional updating of attentional sets depend on dissociable subareas of the prefrontal cortex with ED shifting and the recognition of attention sets depending particularly on the ventrolateral prefrontal cortex (Rudebeck et al., 2017; Friedman and Robbins, 2022). Support for such a prefrontal mechanisms comes from a rodent study that found the M_1 selective PAM TAK-701 can partially reverse a deficit of target detection selectively on signal trials that followed no-signal trials when the deficit was induced by partially (~60%) depleting ACh afferents to the prefrontal cortex (Kucinski et al., 2020). These considerations support the notion that M_1 receptors in prefrontal cortex are pivotal for the improved updating of attentional sets (Sarter and Lustig, 2019).

In previous work, faster learners of feature-reward associations were shown to have improved working memory capacity (Womelsdorf et al., 2021b), which raises the possibility that M_1 allosteric modulation may have affected learning through enhanced short-term memory of targets. We believe this is unlikely. While the non-selective muscarinic antagonist scopolamine impairs short term memory retention and non-selective AChE inhibitors partially reverse the deficit (Bartus and Johnson, 1976; Aigner and Mishkin, 1986; Buccafusco and Terry, 2004; Buccafusco et al., 2008; Knakker et al., 2021), the short-term deficits can be independent of the delay and more prominent for short or intermediate delays, making it unlikely that muscarinic receptors have primary effects on recurrent persistent delay representations (Glick and Jarvik, 1970; Aigner et al., 1991; Taffe et al., 1999; Knakker et al., 2021).

4.4.2 M_1 PAM reduces perseverative responding

A second main result of the current study is VU0453595 reduced response perseveration, allowing animals to avoid repeating erroneous responses to objects with the same non-rewarded features (**Fig. 4.2E**). This finding supports early insights into the effects of the muscarinic antagonist scopolamine in the prefrontal cortex to increase omissions (ROBBINS et al., 1998), suggesting that it is the M_1 muscarinic receptor that is particularly important for minimizing error rates. Support for the M_1 specificity of these effects also comes from a study treating transgenic mice with an M_1 selective ago PAM which resulted in reduced erroneous choices of compound object discrimination in the trials after reversing object-reward associations (Shirey et al., 2009).

Perseverative responding is the key characteristic of inflexible, habitual responding because it reflects that performance feedback is not utilized for adjusting behavior. It has been shown that performance feedback triggers transient activation of cholinergic neurons in the basal forebrain in mice (Hangya et al., 2015) and activates the basal forebrain in humans (Iglesias et al., 2021). In the prefrontal cortex, cholinergic transients trigger gamma activity (Lin et al., 2006) that depends specifically on local M_1 receptors (Howe et al., 2017).

Taken together, the reduction of perseverative responding with VU0453595 implicates the M_1 receptors also in the effective processing of feedback to adjust future performance. Perseverative, habitual responding is a hallmark of multiple psychiatric disorders including schizophrenia, obsessive compulsive disorder and substance use disorders (Floresco et al., 2009; Moritz et al., 2009). The current result therefore bears particular relevance by suggesting that potentiating the M_1 receptor critically reduces perseverative response tendencies (Lustig and Sarter, 2015).

4.4.3 M_1 PAM has no consistent effect on interference control over distractors

We found that VU0453595 did not affect VS performance differently with few or many distractors. Target detection response times were moderately faster and accuracy was moderately lower to a similar extent for 3, 6, 9, or 12 distractors (**Fig. 4.3A-D**). This finding shows that the

M_1 PAM dose range that improved cognitive flexibility did not alter attentional filtering of distracting information. This finding adds clarity to diverse results in previous studies. Firstly, the absence of M_1 specific distractor effects resonates with a recent finding in rodents that the M_1 selective PAM, TAK-071, did not modulate the distracting effects of light on/off switches during a sustained attention task, but started to improve performance in the second half of testing when distraction ended and the animals adjusted to a no-distractor regime (Kucinski et al., 2020). This result pattern is congruent with our result pattern. Allosteric modulation of the M_1 receptor improved adjusting behavior to challenges, but without improving interference control from distraction. A similar lack of effects of muscarinic modulation on distractor interference control were found in other task contexts. Scopolamine-induced deficits of continuous recognition performance can be partially reversed with an M_1 selective agonist (O'Neill et al., 2003) or the non-selective muscarinic agonist milameline (Callahan, 1999; Schwarz et al., 1999), but this deficit reversal is independent of the similarity between distracting and target objects (Lange et al., 2015a). Similarly, scopolamine does not alter distractor effects in an attentional flanker task, but rather causes an overall slowing and selective impairment of learning reminiscent of the reward learning effect we found (Thienel et al., 2009).

The observed result pattern with the M_1 PAM contrasts to apparent effects to reduce distraction with nicotinic modulation (Parikh et al., 2010; Terry et al., 2016; Thiele and Bellgrove, 2018; Azimi et al., 2019), with non-selective cholinergic increases using donepezil (Hassani et al., 2021) (see **Table 4.1**), or with the improvement of target detection accuracy and visuo-spatial attentional orienting when enhancing cholinergic transmission from the basal forebrain (Voytko et al., 1994; Chiba et al., 1999; Phillips et al., 2000; Levin et al., 2011). Particularly relevant in this context is a prior NHP study that found the nicotinic alpha-4/beta-2 receptor agonist selectively enhanced distractor filtering when two stimuli underwent salient changes but had no effect on reversal learning speed (Azimi et al., 2019).

One caveat when interpreting the absence of a drug effect is that we cannot know whether higher VU0453595 doses than were used here would have affected distractor filtering during VS performance. The highest dose used in this study (0.3mg/kg, oral) is a magnitude lower than the ≥3mg/kg doses that previous studies found to be safe and void of adverse side effects (Gould et

al., 2020), suggesting that future studies will need to identify possible dose specific effects on attention functions.

Table 4.1 Comparison of performance metrics with the best-doses of VU0453595 and Donepezil.

	Extracted Measure	Donepezil (0.3 mg/kg)	VU0453595 (0.1 mg/kg)
Learning Task	Learning efficiency & performance	↓	↑↑↑
	Cognitive control & flexibility		↑↑↑
Attention Task	Speed of processing	↓	
	Distractor interference	↑↑↓	↑ †
	Perceptual interference	↑↓	

†: no systematic effect of 0.1 mg/kg of VU0453595 was found in the VS attention task.

Table 4.1 From the FRL task and VS task, we extracted 5 different performance metrics. Learning efficiency and performance entails the number of trials-to-criterion, plateau performance, proportion of learned blocks, response times and trials-to-response-time-plateau. Cognitive control and flexibility entails perseverative error measures and the role of block switches (e.g. ED and ID) on learning efficiency (trials-to-criterion). Speed of processing is a single measure extracted from familiarization trials. Distractor interference entails search time and performance changes as a function of the number of distractors. Perceptual interference entails search time and performance changes as a function of target-distractor similarity.

4.4.4 Limitations

While our study already tested multiple markers of cognitive flexibility and attention, it was not yet incorporating tests of other domains that M_1-modulating drugs might affect and which are compromised in psychiatric patient populations such as long-term memory and motivation (Broks et al., 1988; Edginton and Rusted, 2003; Ellis et al., 2006; Millan et al., 2012). Further tasks, where we can extract measures of longer-term memory processes and motivation for example would be important additions for a more comprehensive characterization of possible M_1-dependent behaviors (see **Appendix C.3**). Such an expansion of extracted measures would align

well with efforts to develop multi-task batteries for NHPs covering a wide range of cognitive domains (Taffe et al., 1999; Weed et al., 1999; Wither et al., 2020; Palmer et al., 2021; Womelsdorf et al., 2021a).

4.5 Conclusion

In summary, the M_1 positive allosteric modulator VU0453595 produced selective improvements in cognitive flexibility in the absence of adverse side effects. The results were obtained with cognitive tasks that tap into real-world cognitive demands for adjusting to the changing relevance of visual objects. This result pattern suggests that M_1 PAMs will be powerful targets for drug discovery efforts to augment cognitive flexibility.

4.6 Methods and Materials

4.6.1 Subjects

Four adult male rhesus macaques (*Macaca mulatta*) were separately given access to a cage-mounted Kiosk Station attached to their housing unit where they performed a visual search attention task and a feature-reward learning task via a touchscreen interface (Womelsdorf et al., 2021a) (**Fig. 4.1A**) (see **Appendix C** for more details).

4.6.2 Compounds and Procedures

VU0453595 was synthesized in house (Shirey et al., 2009; Ghoshal et al., 2016) and mixed with a vehicle of 18g of strawberry yogurt and 2g of honey provided to the monkeys in a small paper cup (oral administration). All monkeys received vehicle or drug 2h prior to the start of behavioral performance and were observed to ensure full consumption of vehicle or drug. VU0453595 was administered once per week to allow appropriate washout. Based on the weight of each animal, drug volume was calculated for 0.03, 0.1 and 0.3 mg/kg doses. Drug side effects were assessed 15 min following drug administration and after completion of the behavioral performance with a modified Irwin Scale for rating autonomic nervous system functioning (salivation, etc.) and somato-motor system functioning (posture, unrest, etc.) (Irwin, 1968; Patel

et al., 1997; Andersen et al., 2003; Hassani et al., 2021). Furthermore, monkeys' behavioral status was video-monitored throughout task performance.

4.6.3 Behavioral Paradigms

Monkeys performed a sequence of two tasks in a single behavioral session including a VS task block, 21 reward learning task blocks and finally, another visual task block. Rewarded and unrewarded objects in the VS task and FRL task were multidimensional, 3D rendered Quaddle objects (Watson et al., 2019a) that shared few or many features of different features dimensions (colors, shapes, arms, body patterns). The VS task varied the perceptual target-distractor similarity by changing the average number of common features between distractors and the target object. The FRL task varied the complexity of the feature space by varying features of objects in only one or of two feature dimensions from trial to trial.

Animals first performed a VS task block consisting of ten familiarization trials that showed the same object on a screen without distracting objects, followed by a set of 100 trials that contained the previously shown object amongst 3, 6, 9, or 12 distracting objects (**Fig. 4.1B**). Animals received fluid reward for touching the previously shown target object. Following the VS task, the animals performed a FRL task that required learning, by trial-and-error, which feature was associated with reward for each block of 35-60 trials. Trials in this task always contained 3 objects that each contained one or two features, depending on the block, with only one instance of each feature presented per trial (**Fig. 4.1B**).

The FRL task indexes cognitive flexibility by testing how fast subjects learn which feature is rewarded when the feature-reward rule switched between blocks. Block switches were un-cued and could involve switching the newly rewarded feature to the same or different feature dimensions, which makes the task similar to conceptual set shifting tasks, but different by using a larger set of features that varied within and across sessions in order to vary task difficulty. In each trial three objects were shown that varied either in features of one feature dimension (e.g. having different colors *or* body shapes), or that varied in features of two feature dimensions (e.g. having different colors *and* body shapes). Choosing the object with the correct feature was rewarded with

a probability of 0.85. Blocks where only 1 feature dimension varied (low distractor load) were easier as there were less distracting features than in blocks with 2 varying feature dimensions (high distractor load).

4.6.4 Statistical Analysis

Data were analyzed with standard nonparametric and parametric tests with test statistics, p values and effect sizes reported where appropriate in text. For detailed statistical methods, please see **Appendix C**.

4.7 Financial Disclosures

The authors declare no competing financial interests.

4.8 Acknowledgements

This work was supported by the National Institute of Mental Health of the National Institutes of Health under Award Number R01MH129641 (TW). The content is solely the responsibility of the authors and does not necessarily represent the official views of the National Institutes of Health.

4.9 Author Contributions

S.A.H., J.R., C.J. and T.W. conceived the experiments. A.N. and S.A.H. performed the experiment. J.R. and C.J. contributed the drug compounds. S.A.H analyzed and visualized the data. S.A.H. and T.W. wrote the first paper draft. All authors contributed writing the paper.

Chapter 5 A computational psychiatry approach identifies how alpha-2A noradrenergic agonist Guanfacine affects feature-based reinforcement learning in the macaque

5.1 Abstract

Noradrenaline is believed to support cognitive flexibility through the alpha 2A noradrenergic receptor (a2A-NAR) acting in prefrontal cortex. Enhanced flexibility has been inferred from improved working memory with the a2A-NA agonist Guanfacine. But it has been unclear whether Guanfacine improves specific attention and learning mechanisms beyond working memory, and whether the drug effects can be formalized computationally to allow single subject predictions. We tested and confirmed these suggestions in a case study with a healthy nonhuman primate performing a feature-based reversal learning task evaluating performance using Bayesian and Reinforcement learning models.

In an initial dose-testing phase we found a Guanfacine dose that increased performance accuracy, decreased distractibility and improved learning. In a second experimental phase using only that dose we examined the faster feature-based reversal learning with Guanfacine with single-subject computational modeling. Parameter estimation suggested that improved learning is not accounted for by varying a single reinforcement learning mechanism, but by changing the set of parameter values to higher learning rates and stronger suppression of non-chosen over chosen feature information.

These findings provide an important starting point for developing nonhuman primate models to discern the synaptic mechanisms of attention and learning functions within the context of a computational neuropsychiatry framework.

5.2 Introduction

Attentional flexibility is compromised in many neuropsychiatric diseases and becomes manifest in perseverative behaviours, impulsivity, poor set-shifting abilities, or higher

distractibility. These cognitive effects can be experimentally dissociated in reversal learning tasks, providing a rich test-bed to identify the neuromodulatory and synaptic mechanisms that support flexible attention during reversal learning. Previous studies have implicated, in particular, dopaminergic and noradrenergic signaling in prefrontal-striatal loops to support cognitive flexibility (Arnsten and Dudley, 2005; Arnsten et al., 2012; Clark and Noudoost, 2014). One prominent receptor subtype involved is the alpha 2A noradrenergic receptor (a2A-NAR) whose activation at optimal concentrations enhances working memory representations in prefrontal cortex (PFC) by increasing neuronal firing of memorized target locations (Wang et al., 2007, 2011). Such an enhanced delay firing during a2A-NAR activation could be the correlate for enhanced flexibility during goal-directed behaviour.

However, how improved working memory representations relate to otherwise dissociable measures of behavioural flexibility, such as reduced impulsivity, reduced distractibility from irrelevant salient events, enhanced attentiveness/vigilance, improved sensitivity to salient events, or heightened sensitivity to behavioural outcomes to adjust behaviour in the light of errors has remained elusive. All these cognitive subfunctions render behaviour flexible and have also been linked to catecholaminergic action in the PFC. For example, noradrenergic activation has been implicated to balance the relative weighting of explorative tendencies over exploitative tendencies during periods of uncertainty (Aston-Jones and Cohen, 2005a; Yu and Dayan, 2005), and to enhance the focusing on relevant sensory information (Amemiya and Redish, 2016; Mather et al., 2016). Such influences of noradrenergic action could act in addition to changes in working memory and could have complex behavioural effects that have not only benefits, but also costs to behavioural performance. For example, favoring exploratory choices can enhance performance and reduces perseverative tendencies in uncertain situations, but it can also introduce noise and thereby reduce performance when the environment does not change akin to enhanced distractibility (Doya, 2002).

To understand the specific cognitive consequences of noradrenergic action on goal-directed behaviour it seems therefore pivotal to study selective receptor systems in a variety of tasks. Guanfacine is a selective a2A-NAR agonist with low affinity for the receptor subtypes alpha 2B and 2C (Uhlen et al., 1995). For the selective a2A-NAR system, studies in rodents and

nonhuman primates suggest that certain doses improve working memory (e.g. Arnsten and Goldman-Rakic, 1990; Franowicz and Arnsten, 1998; Mao et al., 1999), as well as decrease impulsivity, reduce distractibility and possibly facilitate faster, more consistent learning (Seu et al., 2009; Caetano et al., 2012; Kim et al., 2012). At the molecular level, Guanfacine preferentially binds to post-synaptic alpha 2A receptors (Kawaura et al., 2014). Pyramidal cells in prefrontal regions richly express post-synaptic alpha 2A receptors (Aoki et al., 1994), and stimulation of these receptors is thought to inhibit cyclic adenosine monophosphate (cAMP) production, which leads to closing of nearby HCN channels, which in turn leads to increased excitability in prefrontal pyramidal cells and increased connectivity within prefrontal microcircuits (Wang et al., 2007; Barth et al., 2008). Guanfacine is suggested to exert its positive effects on cognitive functions via these actions on post-synaptic a2A-NAR receptors in the dorsolateral PFC (Wang et al., 2007). Guanfacine is also suggested to suppress glutamatergic synaptic transmission and thereby neural excitability at deeper layers (V/VI) in PFC, potentially governed by similar intra-cellular mechanisms as those controlling HCN channels (Ji et al., 2008; Yi et al., 2013). It has been proposed that at low concentrations, Guanfacine's actions on HCN channels may predominate, while only at high concentrations glutamate transmission is affected, potentially explaining an inverted-U type function of Guanfacine (Wang et al., 2007; Yi et al., 2013). Guanfacine also binds to pre-synaptic alpha 2A receptors on locus coeruleus terminals that act as inhibitory auto-receptors, thereby decreasing NE release (Engberg and Eriksson, 1991), which may again suggest that high doses of Guanfacine could impair cognitive functions.

The evidence of positive effects seen with Guanfacine in rodents and non-human primates is not easily reconciled with results from healthy human subjects, where the influence of single doses of Guanfacine on behavioural flexibility is inconclusive. Some studies report improved planning performance, improved working memory, and improved paired-associates learning (Jäkälä et al., 1999a, 1999b), while other studies did not see changes with Guanfacine on a broad range of executive function tests including spatial working memory, problem solving, intra-/extra-dimensional attentional shift and behavioural inhibition tasks (Müller et al., 2005). This mixture of results in healthy humans following administration of a single dose contrasts to those from ADHD diagnosed subject groups in which Guanfacine has been found at the group level to improve interference control (Stroop task), and to enhance sustained attention in the continuous

performance task (e.g. Scahill, 2001; Huys et al., 2016). These task improvements in clinical populations reflect enhanced attentiveness (i.e. detecting more target stimuli, showing less omission errors) and reduced impulsiveness (i.e. higher capability to correctly withhold responding to non-target stimuli, less commission errors)(Scahill et al., 2001).

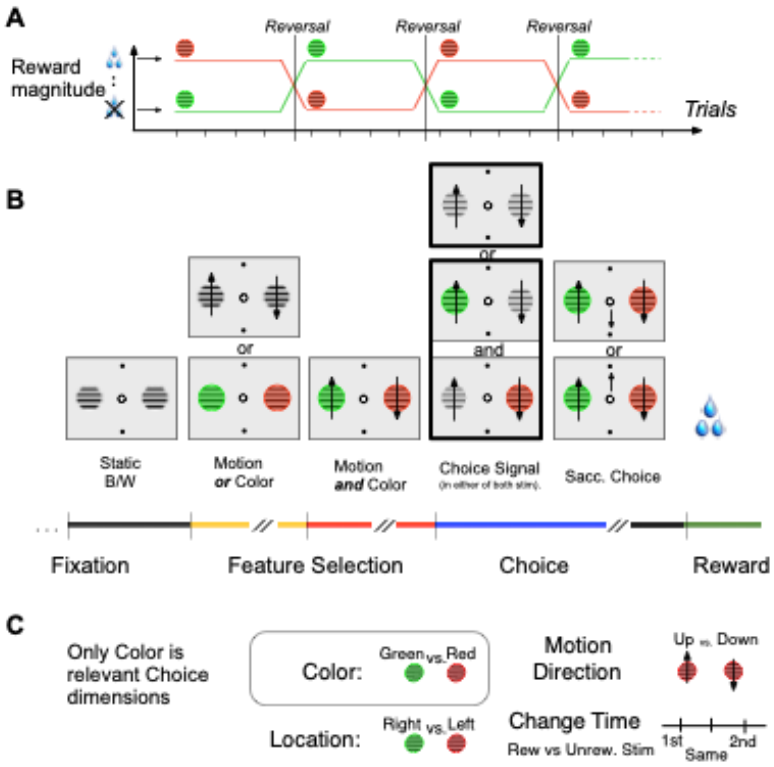

Fig 5.1 Feature-based reversal learning task.
(**A**) Sketch of the reversal of colour-reward association with stimuli coloured in red (green) being associated with reward in successive blocks of trials. Colour-reward reversals were un-cued and triggered when the monkey reached a learning criterion or 50 trials. (**B**) Single trials started with fixation on a central fixation point. Two peripheral grating stimuli were shown for 0.4 sec. and either began to show movement in opposite directions, or they were coloured red/green. Following up to 0.9 sec. the feature (colour or motion) that was not present was added to the stimulus. The animal had to respond to the dimming of the stimulus with the rewarded colour. The dimming occurred either in both stimuli at the same time, or in the rewarded or the unrewarded stimulus first. Reward was provided when the animal made a saccade within 0.5 sec. after the dimming of the reward associated stimulus in the direction of motion of that stimulus. (**C**) Illustration that only colour was systematically associated with reward, while the location, motion direction or time of dimming were dimensions of the stimulus not linked to reward.

Table 5.1 Meta-survey of cognitive effects from systemic Guanfacine administration in non-human primates.

	Task	Processing Demands						Dose Effects and References		
		Stimulus Encoding	Working Memory	Attention Control / Interference Control	Choice / Stim- Resp. Mapping	Learning Requirements	Formalized decision variable		Beh. Effect of Guanfacine	Reference
1	Delayed 2 well spatial response task	Stim. location	Location of reach goal		Location- to reach	Increasing delays	-	✓ ✗	0.1-0.7 mg/kg 0.01-0.001 mg/kg	Franowicz and Arnsten, 1998
								(aged) ✓ ✗	0.0001 mg/kg 0.00001 mg/kg	Rämä et al., 1996
								(aged) ✓	0.00001-0.1 mg/kg	Arnsten et al., 1988
2	Delayed 2 well spatial response task with distractor interference	Stim. location	Location of reach goal	Visual distraction during delay (30% of trials)	Location- to reach	-	-	(aged) ✓	0.0001-0.001 mg/kg	Arnsten and Contant, 1992
3	Delayed non-match to sample object	Object identity	Object type	Select new over old object	Select new object	Increasing delays + increasing object lists	-	✓	0.001 mg/kg	Arnsten and Goldman-Rakic, 1990
4	Delayed match-to-sample	Object shape	Object shape 4-32 sec.	-	Touch Object	Increasing delays	-	(aged) ✓	0.05 mg/kg	O'Neill et al., 2000
5	Visuospatial focused attention	1 moving worm like shape	-	Visually tracks target versus distractor worm	Touch when target reaches center	-	-	(aged) ✓[1]	0.001 mg/kg	
6	Visuospatial divided attention	2 moving worm like shapes	-	Visually tracks two target worms	Touch targets when center is reached	-	-			
7	Acquisition of object-reward association	Object identity	-	Select one of three objects	Reach to object	Increasing to criterion	-	(aged) ✗	0.001 and 0.1 mg/kg	Streere and Arnsten, 1997
8	Reversal of object-reward association	Object identity	-	Select one of three objects	Reach to object	Reversing object reward association (1 reversal/week)	-	(aged) ✓ ✗	0.1 and 0.5 mg/kg 0.001 mg/kg	
9	Acquisition of shape-response direction associat.	Object shape	-	Touch one of two objects	Touch Object	Daily novel pair of visual patterns	-	✗	0.1 mg/kg	Wang et al., 2004
10	Acquisition of stim.-response associations	Object shape	-	-	Turn handle left / right for shape A / B	Daily a new shape	-	✓ ✗	0.001 and 0.1mg/kg 0.0001 mg/kg	
11	Posner cueing paradigm	Peripheral cue location	-	Spatial readiness to make saccade	Stim. location to saccade	-	-	✓[2] ✗	0.0001 mg/kg 0.00001 mg/kg	Witte and Marrocco, 1997
12	Continuous perform. task (sustained attn.)	Single colored squares	-	(vigilance)	Touch stimulus	-	-	(aged) ✓[3] ✗	0.0015 mg/kg 0.5 mg/kg	Decamp et al., 2011
13	Self-ordered, sequential non-match to sample with 2 sec. delay	2-4 col. squares	Previ. Touched location (2s delay)	(select 1 of 2-4 stimuli)	Touch objects in sequence	Increasing number of objects (2-4)	-	(aged) ✗	0.0015 and 0.5 mg/kg	
14	Reward gambling with changing uncertainty and reward delays	Color and number of stimuli	-	Select one of two stimuli	Stimulus location to saccade	-	Temporal discounting risk preference	✓ ✗	0.2 mg/kg	Kim et al., 2012
15	Feature-based reversal learning	2 stimuli color, motion, location	-	Select one of two stimuli based on color	Motion-direction to saccade direction mapping	Reversing color-reward association (~8 times per day)	Reinf. Learning[4] parameters	✓ ✗	0.075 mg/kg 0.15 and 0.3 mg/kg	Our study

1 Low dose improved accuracy in one of two animals.
2 No effects on accuracy and cue validity, and opposite signs of altering effect with increased and decreased reaction times in each monkey.
3 Performance improvement evident in less omission errors, but accuracy (commission erros) was unaffected.
4 Reinforcement learning parameters (learning rate, inverse temperature selection parameter) were not individually significant, but contributed to improved learning

Table 5.1 Columns indicate the cognitive subfunctions, the dosages, and the obtained effect (tick mark indicates statistical significance, cross indicates lack of significance), and the study reporting the effect. Rows indicate the experimental manipulation tested during systemic drug administration. Note that some studies use different tasks and different dosages of Guanfacine.

Here, we apply a computational psychiatry approach to understanding a2A-NA drug action on higher cognitive functions, examining how a formal framework can add clarity to the complex empirical state of a2A-NA effects. Computational psychiatry includes as one branch quantitative Bayesian and Reinforcement learning (RL) modeling of drug actions on higher cognitive functioning (Huys et al., 2016). Testing formal Bayes and RL models of drug action promises critical benefits over non-formal approaches. Firstly, they come with statistical tools of model selection and validation, thereby making it possible to quantitatively test different theoretical constructs. Secondly, common model parameters provide a common language that facilitates comparisons between different studies, task paradigms, and subject groups. Thirdly, quantitative model selection enables single subject predictions of behavioral drug effects (Stephan et al., 2015). We utilize these benefits of a computational framework to identify which model and model parameters best account for alpha 2A influences on the performance of a healthy macaque monkey in a feature-based reversal learning task.

5.3 Results

We reviewed the literature in order to identify non-human primate studies where systemically delivered Guanfacine improved cognitive performance (**Table 5.1**). The literature showed no consensus in the concentration of Guanfacine that produced observable improvement in a number of various behavioral paradigms. Furthermore, between the tasks used to test the efficacy of Guanfacine, there seemed to be considerable variation amongst the cognitive demands required for the performance of each task. This leads us to conclude that there is a lack of clarity revolving the specific cognitive change brought about by Guanfacine that leads to behavioral improvement. Across the 11 studies we found we broke down the (n = 14) behavioral paradigms used to evaluate Guanfacine into six temporally sequenced processing demands: stimulus encoding, working memory, attentional or interference control, choice/stimulus response mapping, learning requirement and formalized decision variable. Not all processing demands were present in every behavioral paradigm, of the 14 tasks in the 11 studies, 5 tasks had a demand on working memory, 11 tasks explicitly required attention or interference control, 8 defined a learning requirement and only 1 study quantified the influence of a formal decision variable using a computational model (see **Table 5.1**). Notably, of the 9 tasks that did not contain an explicit

working memory component, 7 reported improvements using Guanfacine with at least one concentration tested. This survey result suggests that there are likely multiple routes through which Guanfacine affects goal directed behavior in addition to working memory.

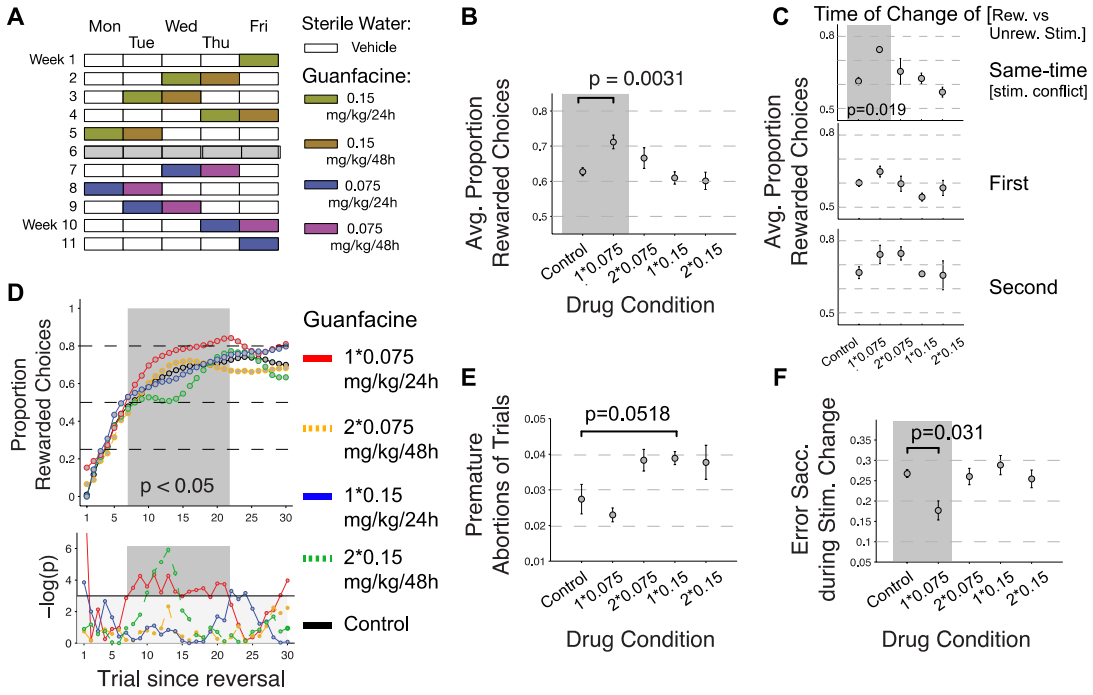

Fig 5.2 Dose-dependent improvement of reversal learning performance.
(**A**) Illustration of the dose-identification protocol with blinded application of sterile water (control condition) or 0.15 mg/kg Guanfacine on two successive days in the first 5 weeks, and 0.075 mg/kg on two successive days in the last 5 weeks. No drug or vehicle was administered in week 6. (**B**) Average proportion of rewarded choices for the control and drug conditions. The bracket connects those points with statistically significant differences (Wilcoxon rank sum test). The grey background additionally highlights the significantly different pair. **(C)** Average proportion of rewarded choices separated by the time of change (top: simultaneous dimming; middle: rewarded stimulus dims first; bottom: rewarded stimulus dims second) of the rewarded versus the unrewarded stimulus for the Control and Guanfacine conditions. A significant difference was only found in the simultaneous dimming condition (top) between the control and 0.075 mg/kg/24h condition (grey background, Wilcoxon rank sum test). (**D**) Proportion of rewarded choices across trials since the colour-reward reversal (top panel) and the evolution of p-values (as -log(p)) (bottom panels). Dark grey box highlights the trials with significantly better performance in the Guanfacine 0.075 mg/kg/24h condition compared to the control condition (Wilcoxon rank sum test). (**E**) Proportion of trials with a premature abortion (fixation breaks) prior to onset of the stimulus colour. There were statistical trends for increased premature trial abortions with higher Guanfacine dosages. (**F**) Significant reduction of erroneous fixation breaks (e.g. toward the peripheral stimuli and without reaching the response targets) during the dimming of the stimuli with Guanfacine 0.075 mg/kg/24h compared to the control conditions (Wilcoxon rank sum test).

We also noted the concentration used by each study, whether the study involved aged primates, and noted if an effect was or was not found using that concentration (**Table 5.1**). The concentrations with which task-related improvement was observed ranged from 0.00001mg/kg to 0.2mg/kg. The concentration range was broad for studies that used both aged and non-aged

primates. Studies suggest that higher concentrations of Guanfacine shift its locus of action from post-synaptic to pre-synaptic a2A-NAR (Arnsten et al., 1988). Pre-synaptic a2A-NAR's are present in the locus coeruleus (LC) and act as inhibitory auto-receptors reducing NE release throughout the cortex (Callado and Stamford, 1999). This suggests that depending on the concentration of Guanfacine used, different adjustments to behavior may result from pre-synaptic a2A-NAR driven shifts of NE concentrations (Wang et al., 2007), which may help explain the variability seen in **Table 5.1**. From a general perspective this survey illustrates that Guanfacine can improve performance for healthy monkeys at different age groups, for tasks requiring multiple different processing components, and for concentration ranges benefitting behavior that are highly variable and presumably subject specific. We believe that this lends power to single subject studies in which careful analysis of the cognitive change from Guanfacine borne improvement can help inform us of its mechanism of action.

For this purpose, we report the influence of systemic Guanfacine injections on behavioural performance in a single case of a macaque monkey performing a feature-based reversal learning task (**Fig 5.1**), in an initial 11-week dose-identifying test protocol and a subsequent 19-week behavioural testing protocol using the best working dose (for details, see **Appendix D.2**).

During the initial 11-week drug testing protocol four doses were tested with a two doses per week schedule (see **Fig. 5.2A**), yielding for the lowest to highest dose 4, 4, 4, and 3 test sessions with 45, 31, 41, and 21 reversal blocks and 3049, 2091, 2068, 1418 trials for analysis of task performance, respectively. No drug dose had a systematic effect on the overall number of learned reversal blocks, but we found a dose-dependent effect in more fine-grained performance metrics. Firstly, the overall accuracy indexed as the overall proportion of rewarded over unrewarded choices was significantly enhanced with the 0.075mg/kg/24h dose compared to the control condition (Wilcoxon rank sum test, $p = 0.0031$), with no differences between control condition and 0.075mg/kg/48h, 0.15mg/kg/24h, and 0.15mg/kg/48h dose condition (all n.s.) (**Fig. 5.2B**). This enhanced overall performance improvement in the 0.075mg/kg/24h dose was particularly evident when calculated for the one third of trials in which the rewarded and unrewarded stimulus changed (dimmed) at the same time (Wilcoxon rank sum test, $p = 0.019$ for the difference of 0.075mg/kg/24h to control), compared to the other two third of trials in which the rewarded

stimulus dimmed either before or after the unrewarded stimulus (**Fig. 5.2C**). The stimulus change (dimming) acted as go cue to elicit the choice if it occurred in the attended stimulus (see **Methods**). We next tested whether Guanfacine affected performance at different stages of reversal learning and found that 0.075mg/kg/24h of Guanfacine significantly increased performance over the control condition at trials 7 to 21 after the reversal event, i.e. during the learning period of the task and prior to asymptotic performance (see **Fig. 5.2D**, Wilcoxon rank sum test p values of $p < 0.05$ are shown on grey shaded area as -log(p)). In addition to this improved performance during learning with the 0.075mg/kg/24h dose of Guanfacine, we found reduced performance at trials 10 to 14 after colour-reward reversal for the highest dose (0.15mg/kg/48h) compared to the control condition (see **Fig. 5.2D**, Wilcoxon rank sum test p values of $p < 0.05$ are shown on grey shaded area as -log(p)). The improved performance at low dose and decreased performance at high dose are thus occurring during overlapping time periods during the learning of reversed colour-reward associations.

Analysis of the pattern of errors showed that there were similar amounts of premature fixation break errors prior to any stimulus change event with 0.075mg/kg/24h compared to control days, while higher doses were loosely linked with a statistical trend to higher proportions of premature fixation break errors (Wilcoxon rank sum test, $p = 0.0518$) (**Fig. 5.2E**). Moreover, 0.075mg/kg/24h Guanfacine, but no other dose, significantly reduced erroneous fixation breaks during the 0.5 sec. time period of the actual stimulus change (dimming) compared to the control condition (Wilcoxon rank sum test, $p = 0.031$). Further analysis of other subtypes of errors and their relation to the learning improvement were hampered by the low number of errors and the low number of testing days during the dose-testing protocol.

The previous results identified 0.075mg/kg/24h Guanfacine as beneficial for reversal learning performance. Higher dosages caused either no change, or were detrimental for performance and learning relative to control days. This may be due to shifts along the theoretical inverted-U plot of concentration for optimal behavioral performance that many endogenous compounds and exogenous drugs share where concentrations that are relatively too low or too high are detrimental (Millan et al., 2012). In our study, our subject benefited from 0.075mg/kg/24h Guanfacine suggesting that this dose placed them closer to the peak of this inverted-U curve of optimal behavior relative to the higher dose. We tested this behaviourally beneficial dose for an

extended 19-week testing protocol to test which of the behavioural performance effects would predominate and remain evident in a larger, statistically more robust dataset, and are independent of possible influences from additional injections of the drug in the same week. During this optimal dose testing protocol, the animal performed on average a similar number of reversal blocks per session in Control sessions (n: 7.96, SE: 0.38) and in Guanfacine sessions (n: 7.79, SE: 0.55) (Wilcoxon rank sum test, p = 0.4938). This provided a similar total number of reversal learning blocks for analysis in Control (n: 151 blocks) sessions and Guanfacine (n: 148 blocks) sessions with a total of 19632 trials for analysis. Across sessions, the average number of performed choices was similar for Control days (n=332.37, SE: 14.63) and Guanfacine days (n=334.21, SE: 18.27) (Wilcoxon rank sum test, p=0.12). Similarly, analysis of the pattern of erroneous choices, fixation breaks indicative of distractibility, or perseverative errors indicative of inflexibility showed no prominent effect of Guanfacine compared to Control day performance during the 19-week testing period (**Appendix D.1.1***).*

These results illustrate that Guanfacine administered once a week for 19 weeks does not simply improve overall accuracy and reduce distractibility when administered at the dose (0.075mg/kg) that has proven to improve accuracy and reduce distractibility during the multi-dose test protocol. However, the prolonged 19-week testing could entail more specific effects on subsets of trials during reversal learning, similar to the specific improvement of behaviour during trials 7-21 since reward reversal reported above (see **Fig. 5.2D**). To test for such effects of learning we used an ideal observer approach to quantify when the succession of monkey choices indicates the actual learning of a colour-reward association since the time of colour-reward reversal (see **Methods**). We first verified across multiple examples that the ideal observer estimate of learning success reliably indexed reversal learning (**Appendix D, Fig. D1**). Using the ideal observer statistics for extracting the learning trials across sessions showed that the median learning was two trials earlier on Guanfacine days (median learning: trial 10) than on Control days (median learning: trial 12) (**Fig. 5.3A**). Directly comparing the distribution of learning trials across sessions between conditions illustrates that the proportion of blocks with relatively fast learning, within 10 trials after reward reversal, was enhanced with Guanfacine, while there were less blocks with slower learning in trials 11 to 18 after reward reversal (**Fig. 5.3B**). To test statistically whether the difference between Guanfacine and Control conditions is evident at specific trials since reversal

we directly compared the ideal observer confidence (which is the probability of making rewarded choices) between conditions on a trial-by-trial basis (**Fig. 5.3C,D**). We found that the probability of rewarded choices was significantly larger during 0.075mg/kg Guanfacine than during Control days on trials 8-10 after reversal ($p < 0.05$, randomization test with multiple comparison correction, individual p values for trials 8-10 were: $p = 0.0432$, $p = 0.0343$, and $p = 0.0359$, respectively) (**Fig. 5.3C,D**). We next looked at the consistency of the behavioral enhancement of Guanfacine over all blocks in each recording day and found reliable enhancement early in the block but not late, and on average learning effects did not fluctuate across experimental sessions (see **Appendix D, Fig. D2** and **Appendix D.1.2 and D.1.3**). In order to discern possible long-term effects of drug administration that may have an influence on overall performance we tested control session performance during the 19 week drug testing and found that learning performance remained similar for early and later control sessions (**Appendix D.1.4**).

5.3.1 Reinforcement learning mechanisms underlying faster versus slower learning

The above results provide quantitative evidence that Guanfacine increases the proportion of blocks in which learning happens fast, i.e. within ~10 trials after reversal, relative to those blocks in which learning is slower. Such faster learning could be achieved by various underlying mechanisms that learn the reward value of stimulus features through trial-and-error (**Fig. 5.4A)**. To discern which mechanism could underlie faster learning with Guanfacine we devised various learning models using either reinforcement learning (RL) of value predictions, Bayesian learning of reward probabilities, or hybrid approaches combining Bayesian learning and RL learning mechanisms (Niv et al., 2015; Balcarras et al., 2016) (*see* **Methods**).

Evaluating the different models using log-likelihood based optimization and cross-validation showed that both, drug and control performance, was best predicted by the same model (**Fig. 5.4 B, C**) and **Appendix D, Fig. D3**). This *feature-weighting plus decay (FW+Decay) RL model* combined Bayesian- and RL- mechanisms using four parameters (*see* **Fig. 5.4A**): (1) An α parameter weights the relevance of stimulus features (color, location, and motion direction) in predicting high reward probabilities; (2) An η *parameter* implements the learning rate (scales the prediction error signal); (3) A β parameter sets the noise level of a softmax selection process for

choosing one versus the other stimulus (i.e. it translates differences in value predictions into choice probabilities); (4) A decay parameter (ω) scales how much the reward-value predictions of non-chosen stimulus features decay over time. With these four parameters the choice patterns on both, drug and control days were predicted with highest accuracy (**Fig. 5.4A, B**). Alternative models with either the same number or fewer parameters (e.g. without the α, or ω parameter) were less accurate in predicting choices as was evident in larger model log likelihoods for the training cross validation set (**Fig. 5.4B**), worse log likelihoods for the test cross validation set (**Fig. 5.4C**), and larger deviations (Sum of Squared Errors) of the model generated choice probabilities relative to monkey proportion of choices (**Appendix D, Fig. D3**).

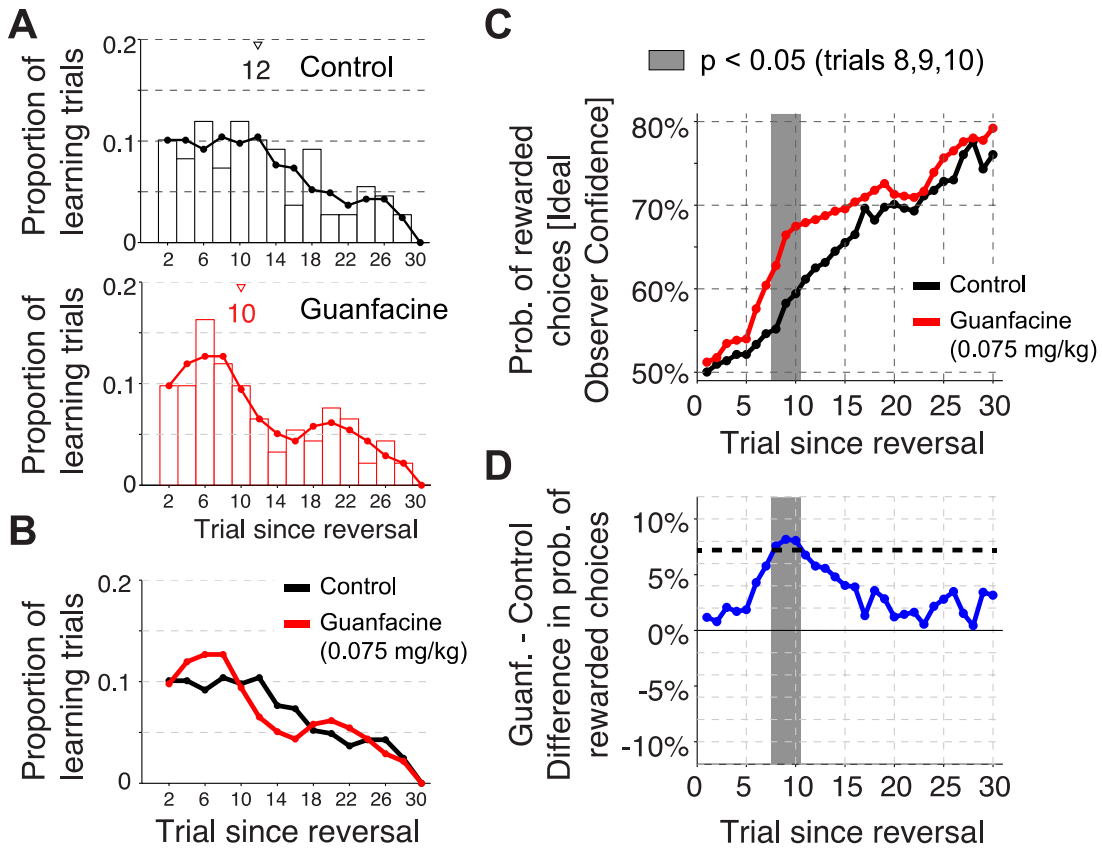

Fig 5.3 Comparison of reversal learning on Guanfacine days versus Control days.
(**A**) Distribution of the proportion of trials at which learning was statistically identified across blocks in control sessions (upper panel) and in Guanfacine sessions (bottom panel). Open triangles denote the median learning trial (trial 12 for control, and trial 10 for Guanfacine sessions). (**B**) Overlay of the smoothed distribution lines from (*A*) illustrating a shift to faster learning blocks relative to slower learning blocks in the Guanfacine condition. (**C**) Median probability of rewarded choices since the reversal across all blocks that showed learning in control (black) and Guanfacine (red) sessions. The dark grey bar denotes the trial with a difference between conditions significant at p <0.05 (dark grey), or only approaching significance at p <0.1. (**D**) Difference of the average probability of rewarded choices in control and Guanfacine condition. Grey bars as in (*C*).

To ensure that the performance of the *FW+Decay RL* model was not spurious due to using four parameters instead of three or two, we calculated the Akaike Information Criterion (AIC). The AIC penalizes model performance by the number of free parameters and show lowest AIC values for the model that conveys most information after considering the number of free parameters. We found that the *FW+Decay* RL model had the lowest AIC score (AIC: 3023.0) compared to all other models tested including a *FW* (*feature-weighting)* model with only three parameters lacking the decay parameter (AIC: 3331.1), and a *Feature Value Decay* RL model (*see* model 2 in methods) that included the value decay parameter, but lacked the relevance weighting of feature dimensions (AIC: 3394.6).

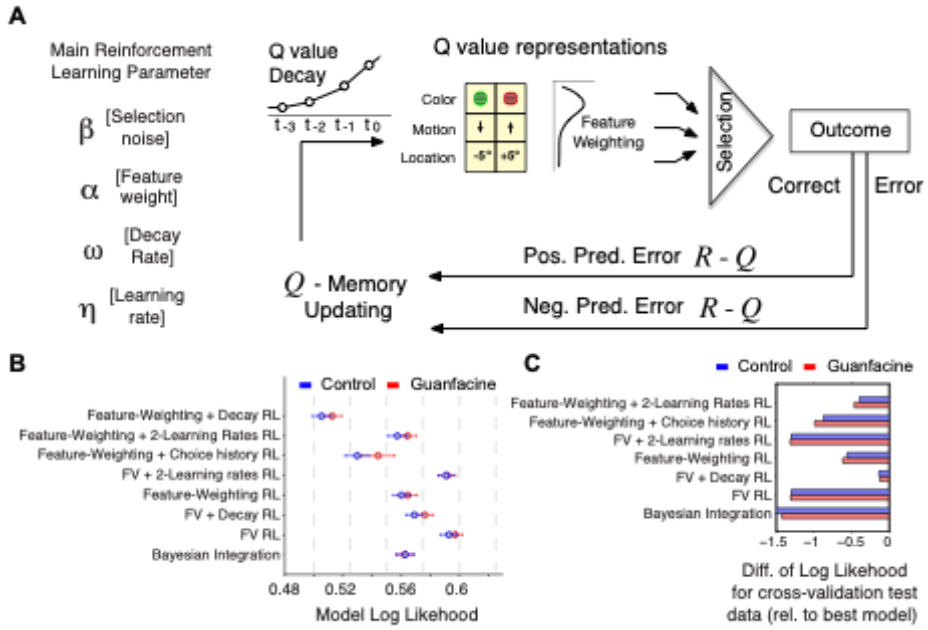

Fig 5.4 Reinforcement learning (RL) modeling of reversal learning during drug and control sessions.
(**A**) Conceptual overview of the basic RL parameters (*left*) and RL mechanisms (*right*) used to account for feature based reversal learning. In the RL framework the selection of a stimulus depends on the (Q-) value prediction for the features of that stimulus (colour, location, and motion direction). Value representations can be weighted to enhance the influence of relevant features. Experiencing the outcome of stimulus selection and the saccadic choice results in a prediction error (PE), which is used to update the value prediction for future trials scaled according to a learning rate. In addition, previous studies suggest that values of non-chosen features decay according to a decay rate. (**B)** The log likelihoods for eight models described in the main text. Lower LL's indicate better trial-by-trial prediction of the rewarded target stimulus. Error bars are STDs across 100 cross-validation training datasets. (**C**) The Feature-Weighting + Decay model provided the best LL prediction not only for the cross validation training datasets (see *B*), but also for independently predicting the 20% of reversal blocks of the test dataset. The panels show the difference in LL for the cross validation test data for all models relative to the best model. More negative values denote worse test data prediction. Red and blue points (*B*) and bars (*C*) denote LLs for the Guanfacine and control sessions, respectively.

We next quantified whether the drug and the control performance was supported by different parameter values of the best fitting *FW+Decay* RL model. To this end we used the parameter values of the 80/20 cross-validation training sets as estimate for the variability of the parameter values across subsamples of the reversal blocks (**Fig. 5.5C)**. We found that Guanfacine performance showed a higher learning rate (η drug: 0.648 STD:0.118, η control: 0.561 STD:0.081, t-value: 6.1, $p < 0.001$, after Bonferroni correction) and a stronger value-decay (ω drug: 1.179 STD:0.108, ω control: 1.043 STD:0.092, t-value: 9.529, $p < 0.001$, after Bonferroni correction). Notably, the beta parameter value was significantly lower for the drug condition than the control condition (β drug 2.12 STD:0.048 vs. β control 2.18 STD:0.053, t-test, t-value -7.59, $p < 0.001$, after Bonferroni correction). Alpha values of the optimal model for Guanfacine performance (α = 0.41, STD 0.126) and control performance (α = 0.44, STD 0.084) were not significantly different (**Fig. 5.5D**, t-test, t-value -2.18, $p > 0.05$, after Bonferroni correction).

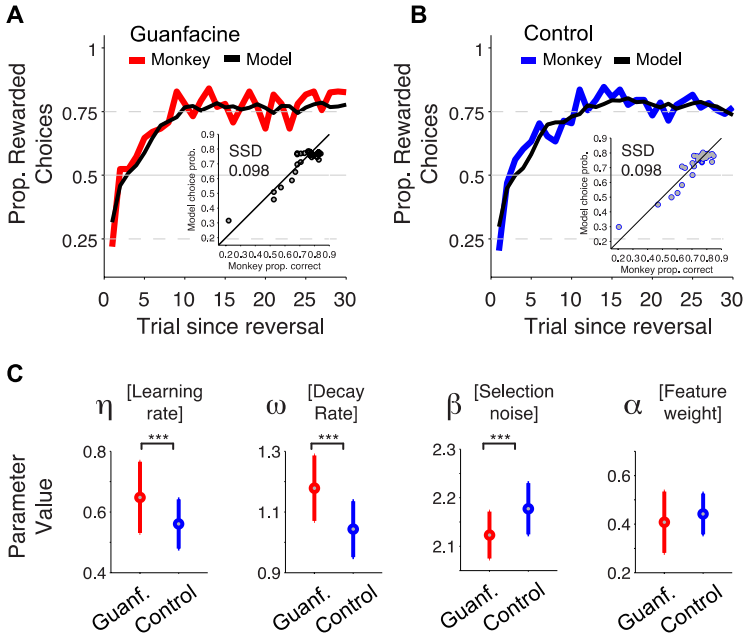

Fig 5.5 Performance and parameter values for the most-predictive RL model
(**A,B**) Proportion of rewarded choices for the monkey and model across trials since reversal in Guanfacine (*A*) and control (*B*) sessions. The model simulations are based on the best predicting *Feature-Weighting + Decay RL model* (see Fig. 4). The inset shows the sum of squared errors (SSD) between the proportion of correct monkey choices (*x-axis*) and the choice probability of the model across trials since reversal. (**C**) The average parameter values for n=100 models fitted to subsets of 80% (cross-validation) reversal blocks for the Guanfacine (*red*) and control (*blue*) sessions. Errors bars denote STD. Three stars denote significance at $p < 0.001$ after Bonferroni correction). Guanfacine reversal performance was based on models with higher learning rate, higher decay rate and lower beta (softmax selection noise).

We next validated that the observed parameter value space of the RL model for Guanfacine does indeed relate to the main behavioral analysis results showing faster learning with Guanfacine (*see* **Fig. 5.3**). To this end we fit the *FW+Decay* RL model to subsets of reversal blocks showing fast, intermediate and slow learning. This approach allows identifying the set of model parameter values that best explains the different reversal learning speeds using the actual choices of the monkey. Blocks were split into five bins according to whether the ideal observer statistics used in the behavioral analysis (*see* **Fig. 5.3**) identified learning to have occurred within trials 1-10, 5-15, 10-20, 15-25, or >20). Data from both, drug and control conditions were combined for this analysis to retain maximal number of blocks in each bin when optimizing for minimal negative log-likelihood of the model fit. We found that faster reversal learning speed is characterized by a model with higher learning rate (η) (**Fig. 5.6C**) and relatively larger feature-value decay (**Fig. 5.6A**). The beta parameter value remains high (β values >1.95) for the first three bins with relatively fast learning (with mean learning occurring at trials 6 (SE 2.6), 9.9 SE 2.8, and 14.8 (SE 3.0)) and is relatively lower in the slowest two sets of learning blocks (with mean learning occurring at trials 20.3 (SE 2.7) and 27.3 (SE 5.5)) (**Fig. 5.6B**). The α parameter value varies non-monotonically across the sets of learning speed (**Fig. 5.6D**). This pattern of learning speed dependent changes in parameter value space closely corresponds to the overall effect of Guanfacine on RL parameter values showing enhanced learning rate and enhanced value decay for non-chosen values (above). In summary, this analysis establishes a link between the behavioral analysis showing faster learning with Guanfacine and the RL model fitting approach showing variations of parameter values best explaining the learning behavior under Guanfacine.

The modeling results showed that Guanfacine performance is linked to changes of more than one RL parameter raising the question on whether the model parameters are affected independently, or whether they co-vary to account for the faster learning performance. We tested this question by correlating the values of pairs of parameters from the optimal *FW+Decay* RL model of the n = 100 subsampled datasets (from the 80/20 training cross validation runs). This analysis showed significant correlations among all parameter pairs (**Fig. 5.7**). Larger learning rates were associated with larger value decay (ω) and larger β values (**Fig. 5.7 A, B, D**), while larger feature-weighting (α) was associated with lower learning rate, β, and feature value decay (ω) (**Fig. 5.7 C, E, F**). These findings corroborate the suggestion that compared to control performance

Guanfacine modulates the values of more than one parameter and hence acts on multiple RL mechanisms.

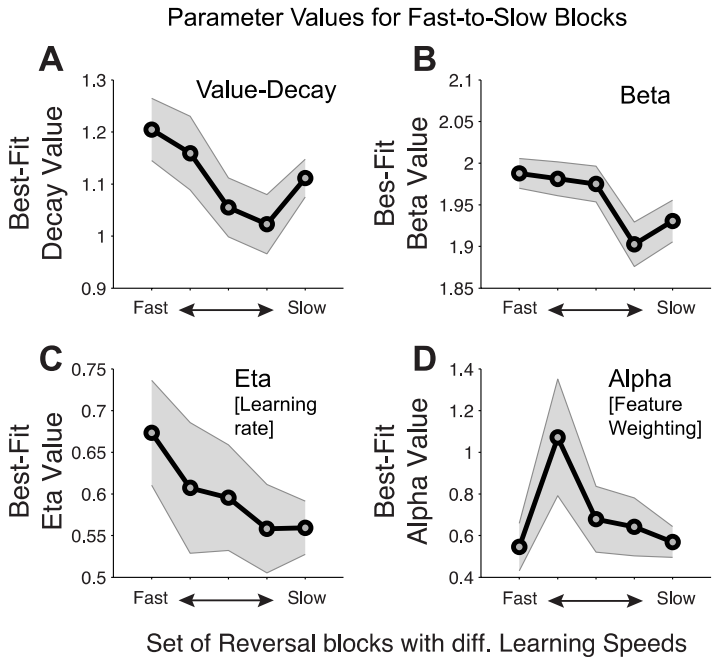

Fig 5.6 Parameter values for the Feature-Weighting + Decay RL model applied to different sets of reversal blocks showing slow and fast learning.
(**A-D**) The value decay parameter values (*y-axis*) of the feature value decay model optimized for different sets of reversal learning blocks (*x-axis*). Bins with fast to slow reversal learning contained blocks selected according to the learning trial identified by the ideal observer statistics applied for results in Fig. 3 (*see* Methods). The five bins were 10 trials wide and slid over the data every 5 trials. The mean learning trial for each of the five bins was 6 (SE 2.6), 9.9 (SE 2.8), 14.8 (SE 3.0), 20.3 (SE 2.7), and 27.3 (SE 5.5). The panels show the optimal values for the parameters value decay (*A*), beta (*B*), eta (*C*), alpha (*D*). The error shading denote 95% confidence intervals.

5.4 Discussion

Using behavioral analysis and computational modeling of a single subject's performance, we found that Guanfacine can enhance specific reinforcement learning mechanisms supporting reversal learning. Initial dose testing over a short time period showed that this concentration was capable of enhancing overall performance and reducing distractibility from simultaneous luminance changes occurring in non-relevant and relevant stimuli (**Fig. 5.2**). Higher doses of Guanfacine did not improve performance and, when given for two successive days, significantly reduced performance. The second, longer experimental phase similarly showed improved learning effects with the best Guanfacine concentration, becoming evident in reliably faster reversal blocks

with increased learning success within the first 10 trials in the drug condition compared to the control condition. This enhancement in reversal learning was evident in the absence of changes in other performance measures such as (1) overall motivation to perform the task (number and length of performed trials), (2) attentional interference control (influences of distractors on accuracy), (3) impulsivity (proportion of premature responses), or (4) perseveration tendencies (repetitions of unrewarded responses). Analysis of the reinforcement learning mechanisms identified one model that best accounted for both, drug and control performance. The model parameter values suggested that the Guanfacine effect on fast learning is not achieved by modifying a single learning parameter. Rather, our findings suggest that Guanfacine may shift values in the parameter space of the reinforcement learning towards higher learning rates and more pronounced decaying of the value of non-chosen stimulus features. Both of these parameters showed higher values for faster as opposed to slower learning blocks validating that the Guanfacine effect on learning improvement could originate from larger learning rates and stronger decay of feature values of non-chosen stimuli. In summary, these findings indicate that Guanfacine facilitated behavioural flexibility at the subject-specific drug concentration in a task requiring selective attention to the value of stimulus features and their reward outcomes over multiple reversals of stimulus relevance per daily session. These results may have implications for the clinical usage of Guanfacine for treating ADHD and multiple other conditions characterized by learning disabilities, attention deficits, or impaired behavioural flexibility (Arnsten et al., 2012; Millan et al., 2012).

5.4.1 Alpha 2A noradrenergic action supports multiple routes to behavioural flexibility

The primary behavioural signature of Guanfacine in our task is an enhanced reliability to learn from trial-and-error during the first ten trials after reversal. This reversal was un-cued and hence became apparent to the subject by experiencing unexpected erroneous outcomes after attending a now non-rewarded (in the current block), but previously rewarded (in previous block) stimulus colour. Guanfacine enhanced the likelihood to use these erroneous outcomes and to increase more quickly the ideal observer confidence that a new colour has become rewarded. This behavioural pattern parsimoniously can be described to reflect enhanced flexibility to adjust to changing reward contingencies in the task environment, e.g. by identifying how a current task situation (or ‘state’) differs to a previous situation (Redish et al., 2007) and by updating the internal

beliefs about feature-reward contingencies (Nassar et al., 2012; O'Reilly et al., 2013). Such update-specific action of noreprinephrine has been inferred in previous human studies from putatively norepinephrine mediated pupil dilation changes specifically during task epochs that required an update of beliefs to better predict future events (Nassar et al., 2012) and to better predict future saccade target locations (O'Reilly et al., 2013). These studies support the interpretation that the main effect of Guanfacine in our task was to facilitate the updating of color-reward contingencies during the learning process. According to this interpretation, Guanfacine increases endogenous control over stimulus selection during periods when changing environmental reward contingencies call for adjusting beliefs and behavior (Shenhav et al., 2013; Womelsdorf and Everling, 2015). There are multiple routes how such a higher level effect could be implemented and supported by Guanfacine action. For example, to improve flexibility in responding to environmental changes can be achieved by (1) enhanced attentiveness and control of interference from distractors, (2) from preventing perseverations and habitual responding, (3) from increased vigilance and arousal, (4) from increasing the representations about which features are relevant in a working memory that persist across trials, or (5) from lowering impulsive response tendencies.

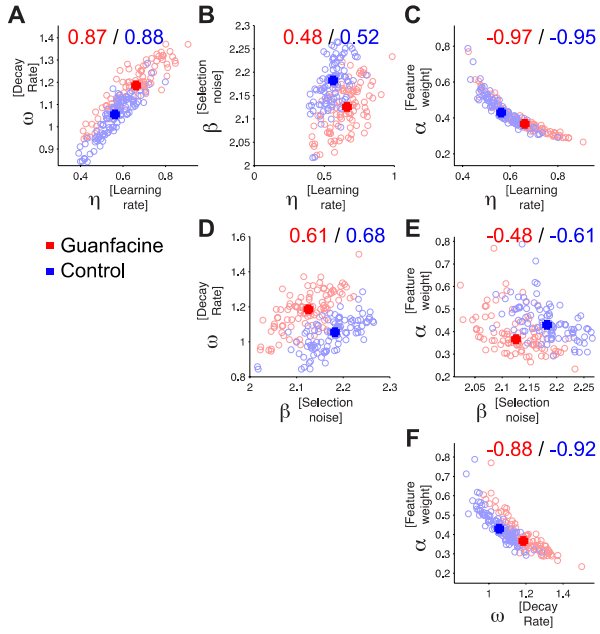

Fig 5.7 Relation of model parameters underlying reversal performance.
(**A-C**) Changes in learning rate (*x-axis*) across n=100 cross validation training models are positively correlated with value decay (*A*) and beta selection noise (*B*), and negatively correlated with feature weighting (*C*). Red and blue numbers denote the correlation coefficient for Guanfacine (*red*) and control (*blue*) data points. (D-F) Same format as A-C but showing scatterplots of the correlation between beta selection noise, decay rate and feature weighting.

Among these many possibilities of Guanfacine action, the best understood effect is enhanced working memory. Previous nonhuman primate studies have documented improved working memory performance in delayed response, delayed match-to-sample, and delayed non-match-to-sample tasks, requiring short-term maintenance of stimulus locations and object identities (Arnsten et al., 2012). Young and aged nonhuman primates tolerate increased delays at subject specific Guanfacine doses ranging from as low as 0.00015 to 0.5mg/kg (see **Table 5.1**). This working memory benefit has been traced back to Guanfacine induced increases in spatially specific delay firing in lateral PFC (Wang et al., 2007, 2011). This prefrontal effect of a2A-NAR activation is well explained by blocking cAMP signaling and concomitant increases in NMDA conductance at the spines of pyramidal cells (Wang et al., 2007, 2011; Yang et al., 2013).

These insights reveal that a2A-NAR activation specifically increases task relevant representations in the PFC, making it likely that such an effect contributes to the behavioural improvements that we report. This contribution would be plausible if Guanfacine would not only increase the representation of stimulus location or prospective saccade location that would explain previous studies' effects, but if it would enhance the representation of colour-reward conjunctions irrespective of the location or saccadic action plan. An enhanced working memory of which stimulus features are currently task relevant (rewarded) could reduce the need for explorative choices and increase the confidence in trial-by-trial selections (Amemiya and Redish, 2016). These effects could indirectly become visible in the enhanced decay, i.e. active suppression, of values from non-chosen stimuli, and thus could culminate in faster learning rates as we observed in the RL model. However, this account predicts that Guanfacine should not only improve the initial reversal learning, but should increase overall performance accuracy. We did not find this effect, suggesting that Guanfacine's primary behavioral effects are on alternate mechanisms.

One alternate mechanism that has been associated with phasic noradrenergic activation is enhanced control of interference, a main pre-requisite for flexible behaviour that strives towards achieving a goal irrespective of distractions (Cole and Robbins, 1992; Aston-Jones et al., 1999; Mather et al., 2016). Evidence for this suggestion derives from rodent studies (Dalley et al., 2004) (see also Devauges and Sara, 1990) and from human studies describing reduced scores of distractibility in ADHD patients treated with Guanfacine (Scahill et al., 2001). Intriguingly, we

observed enhanced focusing in our task during the three sessions of drug testing at the optimal 0.075mg/kg dose with enhanced performance during trials with an enhanced stimulus conflict, i.e. when targets and distractors dimmed simultaneously rather than at separate times (**Fig. 5.2D**). However, this effect did not retain across the nineteen-week behavioural testing sessions that commenced after the dose testing at the same concentration (0.075mg/kg), which notably is in the same range (0.05-0.12mg/kg) proposed to be effective for extended release medication in ADHD (Sallee et al., 2009; Connor et al., 2014). This suggests that the influence of a2A-NAR activation on interference control at the dose tested is not a primary effect in healthy brains and may only appear when the attention system is compromised. This conclusion resonates with the difficulty to observe Guanfacine effects in healthy humans on attentional set shifting tasks (Aoki et al., 1994), and with a previous Guanfacine study in aged monkeys showing an improved performance to select rewarded over non-rewarded objects that were reversed once over the course of a week (Steere and Arnsten, 1997). Taken these lines of evidence together suggests that Guanfacine's influences on interference control do not explain our main findings in this study, but rather may be unmasked in aging or disease states when the strength of target representations is compromised.

Another contribution to improved learning in our task could be an increase in vigilance, or so-called 'scanning attentiveness' that has been hypothesized to be a main route for noradrenergic action (Arnsten et al., 1988). This aspect is particularly important for our task, because it required repeated reward reversals in a single experimental session that continued for an extended duration (≥55min) until the subject self-terminated working. We can rule out that Guanfacine simply prolonged vigilance, as we did neither observe longer performance, nor a change in the average number of learning blocks per session, and learning speed at the end of experimental sessions was similar for control and Guanfacine days (**Appendix D, Fig. D3**).

5.4.2 Reinforcement learning modeling of behavioural drug effects advances computational psychiatry.

Our study tested eight reinforcement learning models to recover the possible learning mechanisms underlying the observed behavioural drug effect on reversal learning and arrived at the same model, the *feature-weighting + decay* (*FW+decay*) RL model, to account for both, drug

and control reversal learning. We found that this model provided the best independent prediction for test-data during cross-validation (**Fig. 5.4C**), and allowed the generation of choices that closely resembled the subject's choice patterns (**Fig. 5.5A, B**). Moreover, we found that the two model parameters that characterized faster learning during Guanfacine than control sessions, were directly linked to the results from the model-free behavioral analysis results that showed faster learning with Guanfacine. This observation provides evidence that the model captures some fundamental learning principles underlying task performance, supporting the notion that such modeling will be pivotal to understand the working mechanisms of behavioural neuromodulation (Doya, 2008) and, more generally, to approach better testable theories of cognitive dysfunction in the new field of computational psychiatry (Wang and Krystal, 2014). We see our RL modeling as an early starting point to approach individualized, subject-specific characterization of cognitive profiles that are called upon in currently developed neuropsychiatric research frameworks (e.g. Wiecki et al., 2016). This framework accepts that there will be individual differences in learning and choice behaviors that call upon the characterization of what could be called a subject-specific drug effect on the parameter space of the underlying learning and attention systems. We embrace this approach with this single-case monkey study, but note the necessity that large samples of subjects are needed to arrive at conclusions that hold at the population level. We expect that future studies will extend this modeling endeavor, for example, by separating learning rates from sensitivity to reward per se (Huys et al., 2013), dissociating value-based prediction processes from value-independent biases of subjects (e.g. Balcarras et al., 2016), and estimating the type of state representation that best explains value predictions and choices in various tasks employed (Gershman and Niv, 2010; Niv et al., 2015; Voon et al., 2015).

In conclusion, the results presented here illustrate how a computational approach links the influence of alpha 2AR activation to variations of formally defined reinforcement learning mechanisms. We expect that such a linkage will be pivotal to advance our understanding of higher-order cognitive phenomena such as distractibility and flexible adjustments of attentional sets following feedback (Stephan et al., 2015). Firstly, these phenomena closely relate to fundamental RL mechanisms and thus can be captured with a common terminology in a unifying theoretical framework (Maia and Frank, 2011; Adams et al., 2015; Huys et al., 2016). Such common terminology will facilitate comparison of results between studies, task paradigms, study subjects

and between species. Secondly, the power to predict single-subject drug effects on behavior bears enormous potential for individualizing treatments in psychiatry. For example, recent studies have shown that knowledge of the formal model and parameter values best describing individual subjects, provide hints to the underlying cognitive weaknesses that can be targeted with drugs affecting those specific weaknesses (e.g. Schlagenhauf et al., 2014; Harlé et al., 2015). Thirdly, we believe that a computational framework as we applied here may prove to be essential to identifying the neuronal mechanisms underlying the neurochemistry of higher cognitive functions. A main reason for this potential is that formal Bayesian and RL models provide essential information about hidden variables that account for variations in behaviour not captured by raw performance data (e.g. Frank et al., 2015; Zhang et al., 2016).

5.5 Methods

5.5.1 Subject and apparatus

Data was collected from a 9 year-old male rhesus macaque (*Macaca mulatta*). All animal care and experimental protocols were approved by the York University Animal Care Committee and were in accordance with the Canadian Council on Animal Care guidelines. Eye positions were monitored using a video-based eye-tracking system (Eyelink 1000 Osgoode, Ontario, Canada, 500Hz sampling rate), and calibrated prior to each experiment to a 9-point fixation pattern. During the experiments, stimulus presentation, eye position monitoring, and reward delivery were controlled via MonkeyLogic (open-source software http://www.monkeylogic.net). Reward was delivered as liquid drops from a sipper tube in front of the monkey's mouth and controlled from an air-pressured mechanical valve system (Neuronitek, London, Ontario, Canada). To ensure the monkey's motivation, fluid intake was controlled during training and experimental sessions; unrestricted access to monkey chow was available. The experiments proceeded in a dark experimental booth with the animal sitting in a custom made primate chair with the eyes 65cm away from a 21' LCD monitor refreshed at 85Hz.

5.5.2 Behavioural paradigm

The monkey performed a variant of a feature-based reversal learning task (Steere and Arnsten, 1997) that required covert spatial attention to one of the two stimuli, the identity of which depended on the current colour-reward association. To obtain reward, an up-/downward saccade had to be performed to the motion direction of the attended stimulus, which was varied independently from the colour of the stimuli. The colour-reward associations were reversed in an un-cued manner between blocks of trials with constant colour-reward association (**Fig. 5.1A**). By separating the location of attention from the location of the saccadic response, this task allowed studying visual attention functions independent of motor intention related processes during reversal learning. Each trial started with the appearance of a grey central fixation point, which the monkey had to fixate. After 0.5 - 0.9s, two black/white drifting gratings appeared to the left and right of the central fixation point (**Fig. 5.1B**). Following another 0.4s the two stimulus gratings either changed colour to black/green and black/red, or started moving in opposite directions up and down, followed after 0.5 - 0.9s by the onset of the second stimulus feature that had not been presented so far, i.e. if after 0.4s the stimulus gratings changed colour then after another 0.5 - 0.9s they started moving in opposite directions or vice versa. After 0.4 - 1s either the red and green stimulus dimmed simultaneously for 0.3s or they dimmed separated by 0.55s, whereby either the red or green stimulus could dim first. The dimming represented the go-cue to make a saccade to one of two response targets displayed above and below the central fixation point (**Fig 5.1B**). Please note that the monkey needed to keep central fixation until this dimming event occurred. A saccadic response following the dimming was only rewarded if it was made to the response target that corresponded to the movement direction of the stimulus with the colour that was associated with reward in the current block of trials, i.e. if the red stimulus was the currently rewarded target and was moving upward, a saccade had to be made to the upper response target at the time the red stimulus dimmed. A saccadic response was not rewarded if it was made to the response target that corresponded to the movement direction of the stimulus with the non-reward associated colour. A correct response was followed by 0.33ml of water delivered to the monkey's mouth. Across trials within a block, the colour-reward association remained constant for 30 to a maximum of 50 trials. Performance of 90% rewarded trials (calculated as running average over the last 12 trials) automatically induced a block change. The block change was un-cued, requiring the subject to use

the reward outcome they received to learn when the colour-reward association was reversed in order to covertly select the stimulus with the rewarded colour. In contrast to colour, other stimulus features (motion direction or stimulus location) were only randomly related to reward outcome (**Fig. 5.1C**).

To ensure the deployment of covert attentional stimulus selection we dimmed the rewarded stimulus only after the dimming of the unrewarded stimulus in one third of the trials (requiring the attentional filtering of the unrewarded stimulus). In another third of trials the rewarded and unrewarded stimulus dimmed at the same time, which probed the animal to focus attention prior to the dimming to resolve the stimulus conflict from the simultaneous dimming. In the remaining third of trials the rewarded stimulus dimmed prior to the un-rewarded stimulus. This timing regime ensured that first, second and same-time dimming of the rewarded versus unrewarded stimulus occurred unpredictably for the monkey. Saccadic responses had to be initialized within 0.5 s after dimming onset to be considered a choice (rewarded or non-rewarded). All other saccadic responses, e.g. towards the peripheral stimuli, were considered non-choice errors.

5.5.3 Experimental procedures for dose identification testing protocol

In each experimental session the monkey was given the opportunity to perform the task for a minimum of 55 minutes after which, if he chose to continue, he could do so indefinitely. However, if he chose to stop working, he was given an additional 5 minutes before the session was stopped by the experimenter. If a trial was successfully completed within these 5 minutes, the timer would re-set and allow him another 5 minutes before the daily behavioural session was ended. This procedure led to an average working duration of 68.7 minutes (SE 0.21).

For treatment sessions, the monkey received an intramuscular (IM) administration of Guanfacine (Guanfacine hydrochloride, Sigma-Aldrich, St. Louis, MO), or an IM injection of sterile water at about 2.5 h before the first trial of the experimental session (across sessions the average time was 150.8 minutes (SE: 0.88)). This time frame is similar to previous studies that have shown significant effects of Guanfacine on cognition in young and aged monkeys (Arnsten et al., 1988; Franowicz and Arnsten, 1998). Immediately prior to IM administration, Guanfacine

was mixed with sterile water as vehicle; the total injection volume was 0.1 ml. Doses of Guanfacine investigated were 0.3, 0.15 and 0.075 mg/kg. 0.3 mg/kg was used in only two sessions and was discarded because it caused increased fixation breaks of the animal during the trial, which ruled out overall positive effects at that dose. Doses were chosen as previous studies have found significant enhancements in cognition with similar doses of Guanfacine (e.g. Franowicz and Arnsten, 1998). We performed a meta-survey of all available nonhuman primate studies that used Guanfacine to evaluate the dose range and expected cognitive effects in our study (please see **Table 5.1**).

To identify the dose of Guanfacine that is behaviourally beneficial we applied an efficient 11-week dose identification testing protocol that allowed us to discern drug effects of the same dosage given on two consecutive days (**Fig. 5.2A**). All other days prior or following treatment days were control days with control injections. Treatment days were shifted randomly weekly and could occur on any two consecutive days during the week, thereby balancing the drug injection weekdays across the testing period. During the entire dose identifying protocol, drug administration was blinded, hence the experimenter did not know whether a given day was a treatment or control day. All experimental sessions were conducted at the same time of day. Prior to this experiment, the monkey had not received any Guanfacine, or any other catecholaminergic drugs, in an experimental setting.

5.5.4 Experimental procedures for optimal dose testing protocol

Following the 11-week dose testing protocol and a 4-week washout period we tested the influence of the dose that resulted in improved behavioural learning during the dose identifying test protocol. To this end we applied control injections on one day a week and Guanfacine (0.075mg/kg) injections on another day of the week 75-120 min prior to commencing behavioural testing of the animal. Injection procedures were identical to those described above. This optimal-dose testing protocol provided 19 control sessions and 19 sessions with Guanfacine 0.075mg/kg. Behavioural task, fluid control regimes for the animal, and reward schedules were identical to the previous testing protocol.

5.5.5 Behavioural analysis of learning trials

Analysis was performed with custom MATLAB code (Mathworks, Natick, MA), utilizing functionality from the open-source fieldtrip toolbox (http://www.ru.nl/fcdonders/fieldtrip/). To identify at which trial during a block the monkey showed statistically reliable learning we analyzed the monkeys' trial-by-trial choice dynamics using the state–space framework introduced by Smith and Brown (Smith and Brown, 2003) (see Millan et al., 2012, **Appendix D.2** and **Appendix D, Fig. D1** for examples).

5.5.6 Testing for trial-by-trial differences of the probability of rewarded choices.

To test whether the probability of rewarded choices differed between drug and control conditions in specific trials following the first trial after the reversal we applied permutation statistics. In particular, we tested the null hypothesis that the probability of rewarded choices at individual trials since reversal is the same in drug and control conditions. To test this hypothesis we extracted the average (median) probability of rewarded choices for each trial since the reversal until trial 30 across blocks of the Guanfacine condition and across blocks of the control condition. We used the difference in the average probability of rewarded choices between conditions for each trial since reversal as test statistics in a randomization test that corrected for multiple comparisons across trials. For the randomization procedure, we extracted the difference in the average probability of rewarded choices for each trial since reversal n = 1000 times with randomly assigned condition labels. To correct for multiple comparisons, we pooled the random distributions across trials and calculated the 95% threshold value (the 28.500's of 30.000 values) of the difference in the probability of rewarded choices that would be obtained when the condition labels were unknown. We then compared the observed differences between Guanfacine and Control conditions in trials 1 to 30 to the 95% threshold value. If the observed difference at any trial in the block exceeds the threshold value it can be inferred that reward probability is significantly higher in the Guanfacine compared to the control condition at $p < 0.05$. This randomization procedure prevents multiple comparison correction by calculating a single threshold value across trials.

5.5.7 Testing for the consistency of learning differences across blocks within sessions.

The effect of Guanfacine on learning could be consistent within an experimental session, or it could increase or decrease across blocks within a session. We tested for the consistency of learning effects by first extracting the learning trials for all blocks performed during behavioural test sessions using the ideal observer estimate of learning described above (Wilson and Niv, 2012). We then calculated the average (median) learning trial across four successive blocks starting with the first four blocks since reversal and stepping from the first to the eights block of a session. For each set of blocks we calculated the median learning trial in the Guanfacine sessions and in the control sessions. This procedure provided the average learning trial for each block relative to the first block in a session. We then repeated the procedure, but starting from the last block in a session and going backwards, averaging the learning trials in the last four blocks, the second to last four blocks, etc. until the seventh to last block. This procedure provided an estimate of the change in median learning trials relative to the end of the session. This was done to account for the variability in the number of blocks completed in any given experimental session.

To test whether the average learning trials were consistently earlier or later in the Guanfacine condition relative to the control condition we used a randomization procedure. For this purpose we used as test statistics the proportion of blocks with an average learning trial that was earlier in the Guanfacine condition than in the control condition. This test statistics included eight average learning trials since reversal and seven average learning trials since the last block in a session (see above and **Fig. 5.5**). We then tested the null hypothesis that the drug condition label (Guanfacine or Control) has no effect on the proportion of earlier learning trials. To this end we computed n=1000 times the proportion of blocks with an earlier learning trial in a random condition A relative to condition B with random assignment of Guanfacine and Control blocks to conditions A and B. We then calculated the p-value as 1 minus the proportion within which the truly observed proportion of blocks with earlier learning trials in the Guanfacine condition relative to the control condition exceeded the proportion of earlier learning in the n=1000 random distribution. Guanfacine would consistently have resulted in earlier learning trials across blocks when the true observed learning trial was earlier than in control conditions in >95% of the random distribution that was blind to the condition label.

5.5.8 Reinforcement learning modeling

In order to infer possible learning mechanisms underlying the behavioral drug effects we tested various computational models using reinforcement learning and Bayesian learning principles following an approach and terminology from Niv and Wilson and colleagues (Wilson and Niv, 2012; Niv et al., 2015). These models aim to find the potential variables that can predict which of the two stimuli the subject picks on a given trial given the history of stimuli, rewards, and choices on past trials up to trial t, which will be denoted by $\mathcal{D}_{1:t}$. We assume that the subject represents the past trials' data as a set of values, rather than keep the entire past in memory, that is, there are quantities that can act as so called sufficient statistics. Models are comprised of specifying whether features (color, motion, location), feature values (colour A, colour B, downward motion, upward motion, left, right), or stimuli (combinations of feature values) are assigned a value, and how this value is updated following a new choice and its outcome (i.e. whether a reward was received or not).

The *first* model, Feature-Value Reinforcement Learning (*FV RL*), assigns values to feature values that define each stimulus. There are three features in each of the two stimuli, the location (left (L) versus right (R)), the direction of motion (up (U) or down (D)) and the color (1 or 2). Across the whole experiment there are only two different colors in each presented stimulus configuration, hence we indicate them just as 1 and 2. This yields six different feature values: L, R, U, D, 1, 2, which we will label with the indices 1 to 6, the corresponding value is thus V_i. A presented stimulus has a value for each of three features, and thus possesses 3 feature value combinations (FVCs), the other stimulus has the remainder of the FVCs. All the FVCs corresponding to the chosen stimulus are updated, because each of them in principle could be a target that was rewarded, which of the three FVCs is the target can only be disambiguated across the presentation of multiple informative stimulus configurations. After receiving an outcome *R* (1 if rewarded, 0 if non rewarded) the value update is done according to

$$V_{i,t+1} = V_{i,t} + \eta(R_t - V_{i,t}) \,, \qquad \text{(eq. 1)}$$

for all FVCs *i* that belong to the stimulus. This equation ensures that when there is a difference between the received reward and the expected (predicted) reward, the value gets updated to get closer to the received reward – implementing the delta rule of classical prediction error learning, with η representing the learning rate. When η=1, the new value is set to R_t, when η exceeds 2, the update becomes unstable, as it can grow without bound.

The choice C_t (which stimulus) is made by a softmax rule according to the sum of values of each FVC that belongs to the stimulus. We indicate the stimulus by the index j and the set of feature values that belong to it by s_j.

$$P(C_{t+1} = j) = \frac{\exp(\beta \sum_{i \in s_j} V_{i,t})}{\sum_j \exp(\beta \sum_{i \in s_j} V_{i,t})} \quad \text{(eq. 2)}$$

The *second* model, Feature-Value plus Decay Reinforcement Learning (*FV+Decay RL*), is an extension of the first model, and includes in addition a decay constant, which reduces the value of the FVCs of the stimuli that were not chosen. The feature values belonging to the chosen stimulus are updated according to eq. 1. The feature values *i* of the non-chosen stimulus decay according to

$$V_{i,t+1} = (1 - \omega)V_{i,t} \text{ ,} \quad \text{(eq. 3)}$$

The decay parameter is denoted by ω. The choice is made as before (eq. 2).

The *third* model, Feature-Value with 2-Learning Rate Reinforcement Learning (*FV+2 Eta RL*), is also an extension of the first model, in that it includes two different learning rates, one for when the choice is rewarded (η_1) and the other (η_0) for when it is not. The value update proceeds according to

$$V_{i,t+1} = V_{i,t} + (\eta_0(1 - R_t) + \eta_1 R_t)(R_t - V_{i,t}) \quad \text{(eq. 4)}$$

The choice again is made as described before (eq. 2).

5.5.9 Bayesian learning modeling

The remaining models have a Bayesian component, which we introduce here and which has been described in detail elsewhere (Niv et al., 2015). The learning goal is to choose the stimulus that gives a reward, hence the one that has the target feature value (color 1 or 2). The information provided in each trial can be accumulated across trials by using Bayes' rule. This starts from the probability of obtaining a reward R_t as a function of the presented stimulus S_t and the choice C_t made assuming the target feature value combination is f: $p(R_t|C_t, f) = p_r R_t + (1 - p_r)(1 - R_t)$ and thus that the chosen stimulus S_{Ct} contains f. The expression tells us that the probability for getting reward (R_t=1) is p_r and for getting no reward (R_t=0) is (1-p_r). When the chosen stimulus S_{Ct} does not contain f, $p(R_t|C_t, f) = p_n R_t + (1 - p_n)(1 - R_t)$. We can combine these two expressions into one by defining $S_{Ct}(f)$=1, when it contains feature f, and zero otherwise yielding

$$p(R_t|C_t, f) = S_{C_t}(f)[p_r R_t + (1 - p_r)(1 - R_t)] + (1 - S_{C_t}(f))[p_n R_t + (1 - p_n)(1 - R_t)]. \quad \text{(eq. 5)}$$

The calculations simplify further when choosing $p_n = 1 - p_r$. What we are interested in is $p(f|\mathcal{D}_{1:t})$, and aim to express it iteratively in terms of $p(f|\mathcal{D}_{1:t-1})$. We start the iteration from a uniform initial distribution representing the lack of knowledge about the target. Each trial gives independent information, hence we can write

$$p(f|\mathcal{D}_{1:t}) = p(f|R_t, C_t)p(f|\mathcal{D}_{1:t-1}) = \frac{p(R_t|C_t,f)p(f)}{p(R_t)} p(f|\mathcal{D}_{1:t-1}) \quad \text{(eq. 6).}$$

The expression depends only on f and factors that do not depend on f, such as $p(R_t)$, will be taken into account as a consequence of normalization of this probability distribution across f. On trial t, when ignoring the past, target f could be anything, hence p(f) is constant, we thus obtain:

$$p(f|\mathcal{D}_{1:t}) \propto p(R_t|C_t, f)p(f|\mathcal{D}_{1:t-1}), \quad \text{(eq. 7)}$$

where after each update we need to normalize this distribution again.

The *fourth* model BI (*Bayesian integration*), adapted from previous reports (Wilson and Niv, 2012; Niv et al., 2015), uses as a value the probability of reward on a new trial, as a function of the choice (still to be made), given the past data:

$V_{i,t} = p(R_{t+1}|C_{t+1}, \mathcal{D}_{1:t}) = \sum_f p(R_{t+1}|C_{t+1} = i, f)p(f|\mathcal{D}_{1:t})$ (eq. 8)

The choice is then made in the same way as before using a Boltzman function with parameter β:

$P(C_{t+1} = i) = \frac{\exp(\beta V_{i,t})}{\sum_j \exp(\beta V_{j,t})}$ (eq. 9)

We noticed that Bayesian updates are much faster than expected from the subjects' choices (see e.g. **Appendix D, Fig. D3A**), hence we kept p_r as a parameter. In the experimental setup the subject will receive a reward when it makes the correct choice, hence p_r=1, but here we take p_r=0.99<1 in which case the Bayesian integration is slower.

5.5.10 Hybrid Bayesian-Reinforcement learning modeling

The *fifth* model, Bayesian Feature-Weighting Reinforcement Learning (*FW RL*) combines the Bayesian inference of the target f via $p(f|\mathcal{D}_{1:t})$, with values for all feature value combinations. We introduce a new notation to properly specify the model: f normally takes 6 values, now we use f_d, where d represents the dimension or feature (1: location; 2: direction of motion, 3: color) and for each d, f_d, takes two values 1 and 2. For instance, f_3=1 indicates the first color. We can then calculate the probability for the target to have feature d, $p_d = p(d|\mathcal{D}_{1:t}) = \sum_{f_d=1,2} p(f_d|\mathcal{D}_{1:t})$. This defines a feature dimension weight $\phi_d = \frac{p_d^\alpha}{\sum_{d'} p_{d'}^\alpha}$, with exponent α and normalized to yield a sum across dimensions equal to one. The predicted reward value of a feature value is then denoted by W_{f_d} and the value of stimulus i is given by the sum across all feature values that are part of the stimulus

$V_i = \sum_d \phi_d W_{f_d}$ (eq. 10)

The choice is then again given by a Boltzmann function

$P(C_{t+1} = i) = \frac{\exp(\beta V_{i,t})}{\sum_j \exp(\beta V_{j,t})}$ (eq. 11)

In addition to the Bayesian update of the feature weights, the values of each Feature value of the chosen stimulus is updated as well, with a prediction error that is the difference between the rewarded and the calculated value of the chosen object, rather than the value of the feature value:

$$W_{f_d,t+1} = W_{f_d,t} + \eta\phi_d(R_t - V_{i,t}) \quad \text{(eq. 12)}$$

The ***sixth*** model, Bayesian Feature Weighting plus Choice History Reinforcement Learning (*FW+Choice History RL*), extends the fifth model by an influence of choice history that is independent of reward history and was found in a previous experiment to be a superior model[34]. Choice history is included in a two-step selection process. First, it calculates the values V_i and choice probabilities $P_j = P(C_{t+1} = j)$ as before and makes a stochastic choice j. It then compares whether the so chosen stimulus has the same color as the previous choice. If this is the case the choice is accepted, otherwise it will be accepted with probability

$$p = \frac{P_j}{P_j + (\exp(\gamma) - 1)}. \quad \text{(eq. 13)}$$

If it is not accepted the other stimulus will be chosen instead, which is the one that matches the previously chosen color.

The ***seventh*** model, Bayesian Feature Weighting + 2 Learning Rates Reinforcement Learning (*FW+2 Eta RL*), combines feature weighting (model 5) with the updating with two different η-values (model 3). The only change with respect to the procedure outlined for model 5 is the update of the values for each feature value:

$$W_{f_d,t+1} = W_{f_d,t} + (\eta_0(1 - R_t) + \eta_1 R_t)\phi_d(R_t - V_{i,t}) \quad \text{(eq. 14)}$$

The ***eight*** model, Bayesian Feature Weighting + Decay Reinforcement Learning (*FW+Decay RL*) combines feature weighting (model 5) with the update with decay (model 2). The feature value belonging to the chosen stimulus are updated according to $W_{f_d,t+1} = W_{f_d,t} + \eta\phi_d(R_t - V_{i,t})$, whereas those belonging to the non-chosen object are updated according to $W_{f_d,t+1} = (1 - \omega\phi_d)W_{f_d,t}$.

5.5.11 Model optimization, evaluation and comparison

The RL models were optimized by minimizing the negative log likelihood over all trials using up to 20 iterations of the simplex optimization method (matlab function fminsearch) followed by fminunc which constructs derivative information. We used a 80% / 20% (training dataset / test dataset) cross-validation procedure repeated for n=100 times for each of the eight models. Each of the hundred cross-validations per model optimizes the model parameters on the training dataset. We then quantified the log-likelihood of the independent test dataset given the training datasets optimal parameter values (see **Fig. 5.4C**). We used the variability of the training datasets' optimal parameter values to evaluate their standard deviation (see **Fig. 5.4B**), and to evaluate how the values of different model parameters co-vary (see **Fig. 5.7**).

To compare RL models with different numbers of free parameters we calculated the Akaike Information Criterion (AIC) for each best-fit model as [$2k - 2ln(L)$] with k reflecting the number of free parameters and L the maximum likelihood value of the model. Lower AIC values indicate a better model fit after penalizing for the number of free parameters used for fitting the respective model.

5.6 Acknowledgments

This research was supported by grants from the Canadian Institutes of Health Research (CIHR), the Natural Sciences and Engineering Research Council of Canada (NSERC) and the Ontario Ministry of Economic Development and Innovation (MEDI). We thank Dr. Hongying Wang for invaluable help with drug administration and animal care.

5.7 Author Contributions

S. A. Hassani and M. Oemisch conducted the experiments and collected data, and also helped analyze the data and write the paper.
P. Tiesinga assisted with analyses and contributed writing the paper
S. Ardid, M. Balcarras, and M.A. van der Meer assisted with analyses.

S. Westendorff helped with the experiments conducted.

T. Womelsdorf was involved in designing the research, analyzing the data and writing of the manuscript.

Chapter 6 α2A adrenoceptor stimulation in primates supports fronto-striatal functions by enhancing reward prediction error encoding

6.1 Abstract

The noradrenergic system and its receptors, including the α2A adrenoceptor, is implicated to critically support cognitive processes such as attention, working memory, and cognitive flexibility. Previous studies suggest that the α2A adrenoceptor improves spatial working memory likely through enhancing neural signaling in the dorsolateral prefrontal cortex (dlPFC), but it is unknown whether the dlPFC is the major site for modulating attention or flexible learning processes. We addressed this question by tracking how guanfacine, a selective α2A selective agonist, modulates neural activity in the anterior cingulate cortex (ACC), the caudate nucleus (CD), and the dlPFC while nonhuman primates performed a reversal learning task.

We found that guanfacine enhanced reversal learning and post-error behavioral adjustments. This behavioral improvement was reflected in enhanced neuronal encoding of reward prediction errors in the ACC and CD, but not the dlPFC during the reversal learning period. Guanfacine selectively increased the encoding of feedback of narrow spiking putative interneurons in dlPFC and ACC and in putative fast spiking interneurons in the CD. These findings suggest that the noradrenergic system, driven by α2A adrenoceptor stimulation, enhances cognitive flexibility by scaling feedback processes and RPE signals across medial and lateral fronto-striatal networks.

6.2 Introduction

Noradrenergic fibers from the locus coeruleus (LC), the primary source of norepinephrine (NE), innervate most of the forebrain (Foote et al., 1983; Nomura et al., 2014). NE is thought to take part in gain modulation in sensory processes (Aston-Jones and Cohen, 2005b), modulation of the signal-to-noise ratio (SNR) of sensory representations (Kolta et al., 1987; Kossl and Vater, 1989; Waterhouse et al., 1990; Ciombor et al., 1999; Devilbiss and Waterhouse, 2004; Decamp et al., 2011; Ghosh and Maunsell, 2022), triggering network resets (Bouret and Sara, 2005; Yu and Dayan, 2005; Dayan and Yu, 2006) and supporting attention enhancement (Mather et al., 2016;

Ghosh and Maunsell, 2022) through the β, α1 and α2 adrenoceptors. At the behavioral level, noradrenergic activity modulation has been implicated to critically contribute to a number of cognitive functions such as attention, working memory (WM) and cognitive flexibility (Berridge and Waterhouse, 2003; Aston-Jones and Cohen, 2005a; Bouret and Sara, 2005; Doya, 2008; Sara, 2009; Bouret and Richmond, 2015; Bornert and Bouret, 2021).

Among the NE receptors, the α2 adrenoceptors have the greatest affinity for NE and act as auto-receptors for the noradrenergic system pre-synaptically as well as being expressed post-synaptically where they disrupt cAMP-PKA signaling (Arnsten, 2000; Wang et al., 2007; Arnsten and Pliszka, 2011). Several α2 adrenoceptor agonists are available including guanfacine which has 15-60x higher affinity for the α2A, over the α2B and α2C subtypes (Uhlen and Wikberg, 1991; Uhlen et al., 1994). Guanfacine is known to enhance performance in a variety of tasks utilizing cognitive processes such as spatial WM, associative learning, attention, distractor filtering and cognitive flexibility (O'Neill et al., 2000; Wang et al., 2004, 2007; Hassani et al., 2017). It is also FDA approved for the treatment of ADHD and explored as a therapeutic option for other disorders (Arnsten, 2020). While the mechanisms of α2A mediated enhancement of WM in neurons in the dlPFC is well documented (Arnsten and Goldman-Rakic, 1985; Li and Mei, 1994; Mao et al., 1999; Wang et al., 2007), it has remained unknown how the α2A adrenoceptor enhances other cognitive processes, like cognitive flexibility.

A recent study has shown that systemic guanfacine injections enhance cognitive flexibility and performance in a feature-based reversal learning task primarily by increasing the learning rates after reversal events (Hassani et al., 2017). This conclusion was based on guanfacine modulating selectively the learning rates estimated using a hybrid Bayesian-reinforcement learning model. One possibility of how guanfacine may improve cognitive flexibility could thus be an increased neuronal signaling of reward prediction errors (RPEs) which reflect how feedback signals are scaled to update expected values during reversal learning. Moreover, RPE signals have been shown to be relevant for the ability of the fronto-striatal network, namely the dorsolateral prefrontal cortex (dlPFC), anterior cingulate cortex (ACC) and the head of the caudate nucleus (CD), to support performance within this feature-based reversal learning task (Oemisch et al., 2019). Functions critical to the performance of the feature-based reversal learning task are known to be supported

by these areas, such as the maintenance of abstract rules, conflict monitoring, search and attention by the dlPFC (Buckley et al., 2009; Kaping et al., 2011; Gläscher et al., 2012; Passingham, 2021), the shifting of behavioral strategies and tracking of reward history by the ACC (Kennerley et al., 2006; Buckley et al., 2009; Kaping et al., 2011; Gläscher et al., 2012; Heilbronner and Hayden, 2016), and feature-value learning and error detection in the CD (Cromwell and Schultz, 2003; Williams and Eskandar, 2006; Kim and Hikosaka, 2013, 2015; Vo et al., 2014), with all three areas known to have RPE signals (Asaad and Eskandar, 2011; Glimcher, 2011; Heilbronner et al., 2011; Wallis and Kennerley, 2011).

Here, we set out to test if or how guanfacine's modulation of learning rates during reversal learning (Hassani et al., 2017) may change neural activity in any or all of these brain regions. We recorded single units from the dlPFC, ACC and CD simultaneously as two rhesus macaques performed a feature-based reversal learning task. We find that within the task's feedback period, trial outcomes are better encoded across all recorded regions, particularly in narrow spiking putative inhibitory interneurons. Furthermore, we found empirical evidence for the model-predicted increased learning rate with ACC and CD neurons having stronger representations of negative and positive RPEs respectively. We observed these changes in encoding strength without overall changes of the proportion of neurons encoding outcomes of RPE suggesting that guanfacine gain modulates the intrinsic learning related activity without recruiting additional neurons.

6.3 Materials and Methods

6.3.1 Subjects and apparatus

Data was recorded from two male rhesus macaques (*Macaca mulatta*) age 7 and 9 years old. Both subjects were fluid restricted during the length of the experiment with unrestricted access to chow. All animal care and experimental protocols were approved by the York University Council on Animal Care and were in accordance with the Canadian Council on Animal Care guidelines.

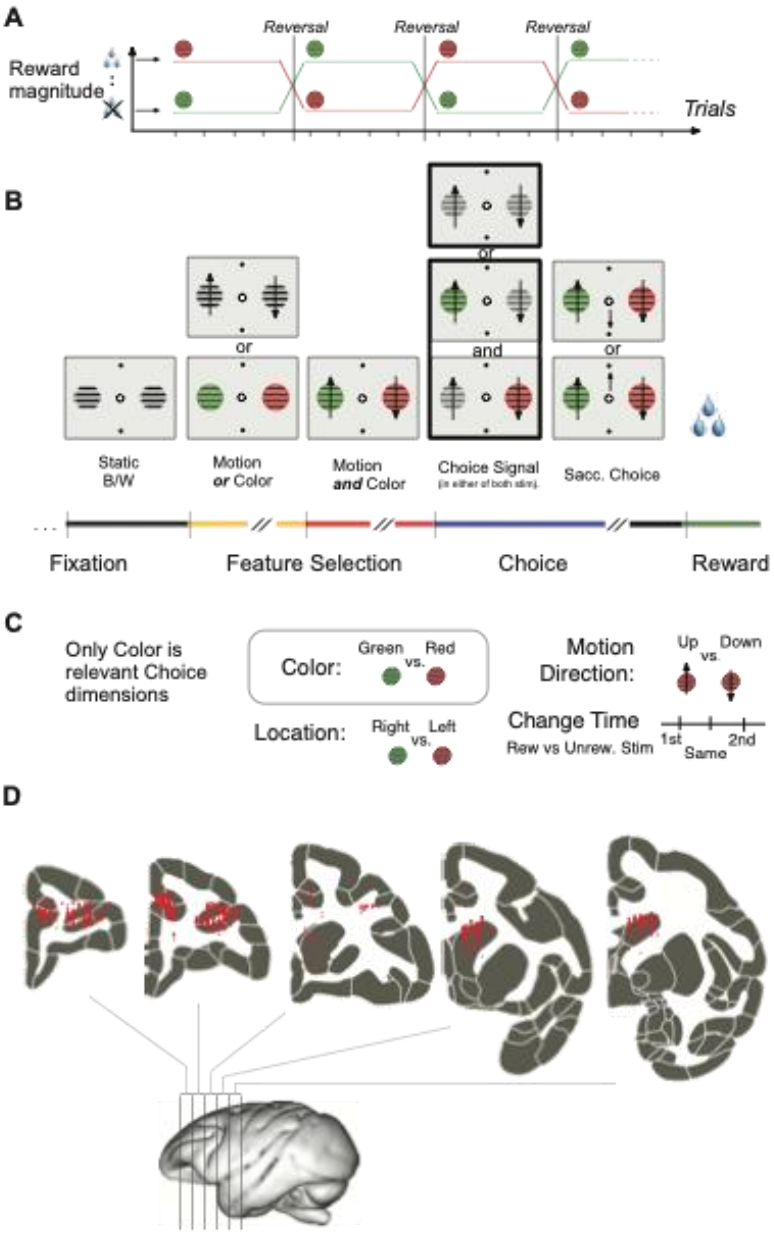

Fig 6.1 Feature-based reversal learning task with simultaneous electrophysiological recordings.
(**A**) During each block, one of two colored stimuli (monkey Ha: green or red; monkey Ke: cyan or yellow) was deterministically rewarded (~0.33 ml of water). Each block was a minimum of 30 to a maximum of 100 trials long. Block switches occurred in an un-cued manner after the minimum 30 trials were completed if the subject reached a performance criterion of 90% correct over the last 12 trials. (**B**) Each trial started with the appearance of a gray central fixation point, which the subjects had to fixate. After 0.5–0.9 s, two black/white gratings appeared to the left and right of the central fixation point. Following another 0.4 s, the two stimulus gratings gained a color or had their gratings drift in opposite directions (up or down), followed after 0.5–0.9 s by the onset of the second stimulus feature such that both stimuli eventually had both color and motion. After 0.4–1 s, the two stimuli dimmed simultaneously for 0.3 s or one stimulus dimmed first followed by the other separated by 0.55 s. The dimming represented a go-cue to make a saccade from the central fixation point to one of two response targets displayed above and below the central fixation point. Since breaking fixation from the central fixation point up to the dimming event terminated the trial, both stimuli had to be covertly attended. In order to acquire reward, subjects had to make either an upward or downward saccade matching the motion of the stimulus grating with the rewarded color, and this saccade had to occur no later than 0.55 s after the dimming of the stimulus with the rewarded color. Therefore,

a saccade in the correct direction would be unrewarded if the saccade occurred after the go cue (dimming) of the incorrect stimulus if the correct stimulus did not also dim. (**C**) Each stimulus varied across three features: color, location and motion. Only color was associated with reward while the other features were only randomly associated with reward. Each trial also varied in the temporal sequence of the go cue (dimming), with one third of trials having both stimuli dim simultaneously, a second third of trials having the rewarded stimulus dim first followed by the unrewarded stimulus, and a final third of trials having the unrewarded stimulus dim first followed by the rewarded stimulus. (**D**) Reconstructed locations of the tungsten electrode contact points yielding single units in the dlPFC, the ACC and CD. Each coronal slice represents the ~middle 0.5 mm of each 5 mm window, from -2 to +23 mm anterior to the anterior commissure. Recording sites from the entire 5mm window are plotted on each coronal section, hence why some data points seem to be in white matter.

Animals were seated in a custom-made primate chair and placed in a dark, sound attenuated booth such that their eyes were 65 cm away from a 21' LCD monitor with a 85 Hz refresh rate. Experimental control, including stimulus presentation, eye positioning monitoring and reward delivery was done through MonkeyLogic (open-source software https://www.brown.edu/Research/monkeylogic/). Eye positions were calibrated and tracked monocularly using a video-based eye tracking system (Eyelink 1000 Osgoode, Ontario, Canada; 500 Hz sampling). Eye calibration occurred daily using a 9-point fixation pattern and was monitored throughout each session. Liquid reward, controlled from an air-pressure mechanical valve system (Neuronitek, London, Ontario, Canada) was delivered via a sipper tube.

6.3.2 Behavioral task

The animals performed a feature-based reversal learning task as previously described (Hassani et al., 2017; Oemisch et al., 2019). Briefly, subjects learned through trial-and-error which one of two grating stimuli was deterministically rewarded in any given block. Each grating stimulus was defined in any given trial by a combination of three features: location (left vs right), color (monkey Ha: red vs green; monkey Ke: cyan vs yellow), and motion direction of the stimulus grating (up vs down). The two stimuli always contained opposite values for each of these three dimensions. Only color was indicative of reward value and thus is referred to as the attention cue in text, while location and motion were randomly associated with reward (see **Figure 6.1A-C** for details).

6.3.3 Statistical measure of learning

To identify learned blocks and an individual trial where statistically reliable learning could be said to have occurred in each block, we used an ideal observer estimation maximization (EM) algorithm (Smith and Brown, 2003; Smith et al., 2004). Briefly, this framework utilized a state equation to represent the internal learning process as a hidden Markov or latent process which was updated with each trial. This provided an estimate of the probability of a correct choice taking into account all trials within the block (**Figure 6.2A** *bottom*). The learning trial was then defined as the trial during which the lower 95% confidence bound exceeded chance ($p = 0.5$) and did not drop back down below chance for the rest of the block.

6.3.4 Drug dosing

Guanfacine was purchased (Guanfacine hydrochloride; Sigma-Aldrich, St. Louis, MO) and prepared with sterile water vehicle (0.1 mL volume) immediately before blinded IM injections. Subjects received Guanfacine (0.075 mg/kg) or sterile water vehicle injections close to 2 hours before the start of the first trial (mean: 135 ± SE 2 min). Each week contained at most a single Guanfacine administration day which was always either on Thursday or Friday while vehicle data was collected on either Tuesdays or Wednesdays; animals still trained every day. In total, we recorded 17 and 12 guanfacine days for monkey Ha and monkey Ke respectively. The selected dose of Guanfacine has previously been shown to enhance performance in this task (Hassani et al., 2017).

6.3.5 Electrophysiological recordings and unit isolation

Single contact tungsten electrodes (FHC, Bowdoinham, ME; 1.2-2.2 MOhm impedance electrodes) were used for extracellular recordings. They were loaded into up to 4 software-controlled precision micro-drives (NAN Instruments Ltd., Israel) and lowered into the brain through a 20x25 mm rectangular recording chamber guided by MR images. Single units were recorded in the dlPFC (area 46), the ACC (area 24), and the head of the caudate nucleus (Calabrese et al., 2015) (**Figure 6.1D**). Data amplification, filtering and acquisition were done with a multi-

channel acquisition processor (Neuralynx). Spiking activity was obtained following a 300-8000 Hz passband filter and further amplification and digitization at 40 kHz sampling rate. After the initial acquisition of highly isolated waveforms in the regions of interest, electrodes were left to stabilize for 30-60 minutes before the start of the task. Sorting and isolation of single unit activity was performed manually offline with the Plexon Offline Sorter, based on principal component analysis of the spike waveforms. In order to maximize statistical power in neural analyses, an extended dataset previously recorded from monkey Ha without any injections was also considered and pooled with the vehicle data and referred to as 'non-drug data'. Although behavioral performance in these sessions was superior to the vehicle sessions, virtually all relevant behavioral trends and results remained consistent (data not shown).

6.3.6 Putative cell type classification

Highly isolated single units were classified based on the properties of their actin potential waveforms using previously published methods (Lansink et al., 2010; Ardid et al., 2015; Oemisch et al., 2019). Briefly, all waveforms were normalized and aligned to their peak and classified by clustering the first PCA of different metrics based on if they were cortical or striatal in origin (**Figure 6.6C-D**). Cortical neurons (from dlPFC or ACC) were classified based on peak-to-trough duration and time to repolarization with broad spiking neurons being putative pyramidal neurons and narrow spiking neurons being putative interneurons. Striatal neurons (from CD) were classified based on peak width and the initial slope of the valley decay with broad spiking neurons being putative medium spiny neurons (MSNs) and narrow spiking neurons being putative fast spiking interneurons (FSIs).

6.3.7 Multi-linear regression

Spike trains were transformed into spike-density functions smoothed with a Gaussian kernel with a standard deviation of 50 ms. Only correct (rewarded) and incorrect choice trials were analyzed; incorrect trials were defined as unrewarded trials where either the unrewarded object was chosen or any choice was made during the dimming (go signal) of the unrewarded object (either before or after the dimming of the rewarded object). The average trial-wise activity during

the epoch of interest (0.05-1s during the feedback epoch and 0.05-0.7s during the attention cue onset epoch) of each neuron was regressed to 18 variables that were classified as either stimulus variables, outcome variables or latent model variables. The 6 binary stimulus variables were the color (color 1 vs color 2), motion (up vs down) and location (left vs right) of the chosen stimulus and the color, motion and location of the rewarded stimulus. The outcome variables were trial outcomes (binary: rewarded or unrewarded), trial outcomes during learning only (see **Statistical measure of learning** above), trial outcomes after learning, prior trial outcome for correct trials (binary: rewarded trial preceded by a rewarded trial or an error trial), prior trial outcome for error trials (binary: error trial preceded by a rewarded trial or an error trial) and error trial order during learning (non-binary: ranking errors in descending order until the statistically defined learning trial). The latent model variables were all non-binary but different depending on the epoch in question. During the feedback epoch, the latent model variables were signed RPEs, positive RPEs, negative RPEs, and the same three variables for trials during learning only. During the attention cue onset epoch, the latent model variables were the choice probability of the chosen stimulus, value of the chosen rewarded stimulus, value of the chosen unrewarded stimulus and the same three variables but for trials during learning only.

A single neuron may have multiple significant regressions and for each significant regression (neurons had to be isolated for at least 30 trials), a correlation coefficient was computed. These coefficients were then averaged for guanfacine and non-drug neurons and their difference plotted separated between unsigned, positive and negative correlation coefficients for each brain region and also split by putative cell types. Statistical comparison between guanfacine and non-drug neurons was done through bootstrapping with shuffled condition labels (5000 permutations). Only comparisons with at least 3 neurons in both guanfacine and non-drug categories were statistically tested.

For each neuron, the strongest regression (significant regression with the highest R^2) was also identified. Then the variables that best explained activity in each brain region were ranked based on the proportion of neurons that had the highest R^2 value per variable (Padoa-Schioppa and Assad, 2006). This ranking was done separately for guanfacine and non-drug days which were then compared using Kendall's tau correlation.

6.3.8 Model variables

We estimated latent variables underlying learning performance including the reward prediction error and the expected stimulus values using a hybrid Bayesian-reinforcement learning model as validated and described in previous studies (Niv et al., 2015; Hassani et al., 2017; Oemisch et al., 2019; Womelsdorf et al., 2021b). This model was the best performing model among a number of different reinforcement learning, Bayesian and hybrid models (see Hassani et al., 2017 for detailed model description and comparisons). Briefly, the model describes each object's value as a weighted combination of its features (color, location, motion). For each trial, a single object is then selected through a softmax selection process with a RPE being computed based on the outcome. This RPE signal is then scaled by a learning rate to adjust the values of the chosen object's features while the feature values of the unchosen object decay.

6.4 Results

The two monkeys performed a feature-based reversal-learning task (**Figure 6.1A-C**) for 42 (17 with guanfacine injections) and 66 (12 with guanfacine injections) electrophysiological recording sessions respectively. A total of 1281 single units were collected across the dlPFC, ACC and CD (**Figure 6.1D**).

6.4.1 Guanfacine enhances reversal learning and post-error adjustment

The performance in the feature-based reversal-learning task was compared between days with vehicle and drug administration. To capture changes in learning speed, we used an ideal observer statistic to identify a trial for each block at which performance exceeded the learning criterion (see **Methods**). The monkeys learned 59.0% of blocks with a median learning trial of 16. With Guanfacine, monkeys reached the learning criterion in a similar proportion of blocks (1.2% more blocks learned on vehicle days; n.s.), but faster with a median reduction of 4 trials to reach the learning criterion (mean: 3.2 trials; $p = .002$). Subjects learned faster and more rewards with guanfacine. The summed difference in reward probability after reversals differed significantly between vehicle and guanfacine administrations ($p = .003$; **Figure 6.2A**) as did the summed

difference in the EM derived reward probabilities ($p < .001$; **Figure 6.2A**). Fatser learning was evident only from the second block onwards. The summed difference in reward probability for just the first block only was not significantly different between guanfacine and vehicle (**Appendix E, Figure E1B**).

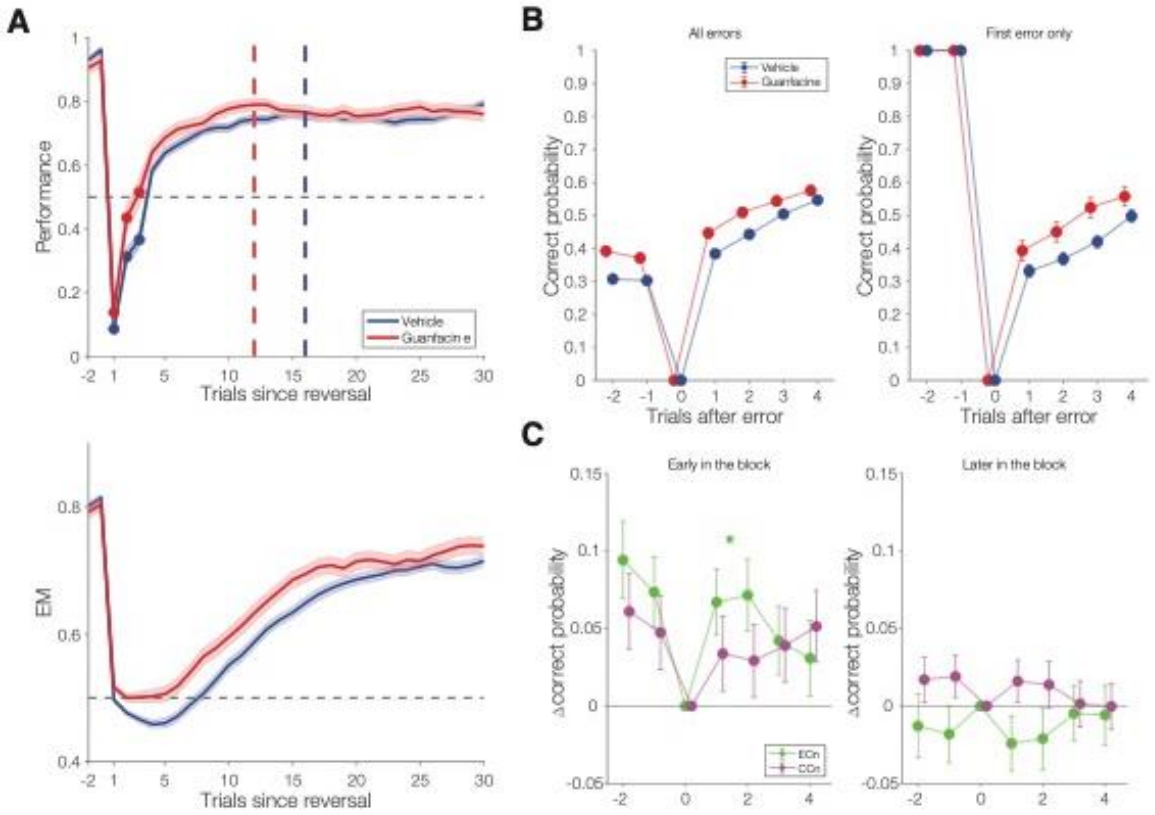

Fig 6.2 Enhanced learning speed and improved post-error behavioral adjustment with guanfacine.
(**A**) *Top*: Average learning curves of learned blocks (first block excluded) for guanfacine and vehicle sessions (shaded area: SE of the mean). Learning curves were smoothed by a 4 trial moving average, shifted every trial. The first 3 trials are marked to indicate the lack of smoothing. The horizontal dashed line represents chance probability. The vertical dashed lines represent the median learning trial for guanfacine (12) and vehicle (16). *Bottom*: average estimate of the probability of a correct choice based on the estimation maximization algorithm (**see methods**). (**B**) ECn plots showing the average performance with guanfacine or vehicle injections after an error trial (*left*) or after only the first error in each block (*right*). (**C**) ECn (proportion correct after an error trial) and CCn (proportion correct after a correct trial) analysis plots. The difference between the guanfacine and vehicle ECn (green) and CCn (purple) performance for early in the block (first 9 trials; *left*) and later in the block (trial 10 onwards; *right*).

Next, we evaluated whether guanfacine changed how performance adjusted in the trials following errors or correct trials early or later in the block (**Figure 6.2C**). We found a significant main effect for drug condition ($F(1,412) = 4.89$; $p = .028$), block timing ($F(1,412) = 62.54$; $p < .001$) and post error vs post correct trials ($F(1,412) = 266.48$; $p < .001$) with a significant interaction between drug condition and timing in the block ($F(1,412) = 6.63$; $p = .010$). Specifically, during

the learning period early in the block (first 9 trials), guanfacine significant improved performance for the 2 trials after an error trial (6.9%; p = .022) but not correct trials (3.2%; p = .809). Later in the block (trials 10 onwards), guanfacine had no significant effect in performance after error (2.3%; p = .963) or correct trials (1.5%; p = .997). The post-error enhancement of performance with guanfacine was already observable after the very first error trial in a new reversal block (**Figure 6.2B** *right*).

6.4.2 Pupils constrict with guanfacine

To infer a possible effect of guanfacine on noradrenergic neuron activity in the LC we analyzed the pupil diameter of the monkeys (see **Appendix D.1** and **D.2**). During the first three blocks of each session, when guanfacine concentrations would be highest, monkeys had a significantly more constricted pupil diameter compared to vehicle (monkey Ha: p < .001; monkey Ke: p = .010; **Appendix E, Figure E1C**), suggesting a reduction in LC activity (see **discussion**).

6.4.3 Guanfacine reduces pairwise firing correlations in ACC

We next evaluated whether guanfacine modulated the firing rate, firing variability or inter-neuronal correlations during the attention cue onset epoch and during the feedback epoch of the task. We found no overall change in the average firing rate of neurons in either epoch (**Appendix E, Figure E2A**; see **Appendix E.2**), but when analyzing narrow spiking neurons separately from broad spiking neurons, firing rates of broad spiking (putative pyramidal) neurons in the dlPFC were significantly reduced (p = .034) and as were firing rates of broad spiking neurons (putative MSNs) in the CD (p = .008) during the feedback epoch (see **Appendix E.2**). We also found no significant changes in two different measure of spike train regularity: coefficient of variation (CV) and local variability (LV) in either the feedback or the attention cue onset epoch (**Appendix E, Figure E2B**). This result remained consistent when looking at narrow and broad spiking neurons separately (see **Appendix E.2**).

Next, we investigated whether guanfacine induced changes in the pair-wise correlation between single unit spike counts (Rsc) within brain region (see **Appendix E**). We found that the

average Rsc in the ACC, but not the dlPFC or CD, was reduced with guanfacine during both the feedback epoch ($p < .001$) and after attention cue onset ($p < .001$) (**Appendix E, Figure E2C**). We also investigated if there was a change in the signal-to-noise ratio, operationalized as d', for the encoding of color during the attention cue onset epoch. We found no significant change in d' between guanfacine and non-drug neurons (not shown).

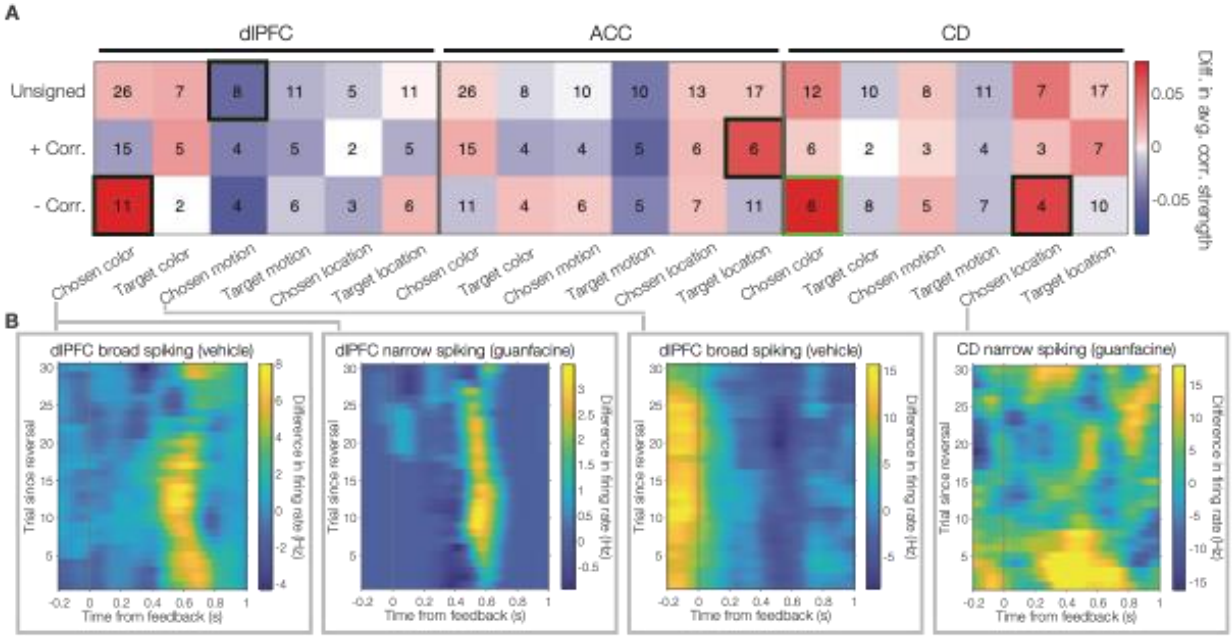

Fig 6.3 Guanfacine-mediated changes in neural activity correlations to stimulus variables during the feedback epoch.
(**A**) Difference in average correlation strength (unsigned, positive and negative) of neurons in the dlPFC, ACC and CD for 6 stimulus variables. The hotness of the color bar signified the magnitude of difference with hotter colors meaning higher (more positive or more negative) correlation coefficients with guanfacine while cooler colors signifying the magnitude of how much lower the guanfacine correlation coefficients were. Solid black outlines around a cell signifies statistical significance, while a solid green outline signifies a trend (< 0.075). The number within each cell denotes the number of guanfacine neurons which was almost always lower than the number of non-drug neurons. (**B**) The difference in the firing rate (Hz) of example neurons between the two chosen colors (left two examples), chosen motion directions (middle right example) and chosen locations (far right). Firing rate was smoothed over 100 ms centered windows shifted every ms and over 6 trials (2 trials backward looking and 4 trials forward looking) shifted every trial.

6.4.4 Guanfacine enhances encoding of reward prediction errors during learning

We next analyzed whether guanfacine impacts neuronal encoding of task and model variables of the reinforcement model, especially early in the block where it enhanced behavior. Single unit activity, averaged for the feedback or attention cue onset epoch, was regressed to

stimulus variables, trial outcome variables, and latent model variables (RPEs during the feedback epoch and the value of the chosen stimulus during the attention cue onset epoch) using multi-linear regression (see **Methods**).

During the feedback epoch, we found that the proportion of neurons significantly correlating with task variables was unchanged between the guanfacine and non-drug condition (**Appendix E, Figure E3**). However, the strength of encoding varied with guanfacine in the feedback epoch with increased encoding of the chosen stimulus color in the dlPFC (p = .003), the chosen location in the CD (p = .019) and the target location in the ACC (p = .024). We also saw reduced encoding of the chosen motion with guanfacine in the dlPFC (p = .032) (**Figure 6.3A**). Outcome variables also showed significant guanfacine-induced enhancement, with stronger encoding of trial outcomes in the dlPFC (p = .005), of the trial outcome in the preceding trial prior to a correct trial in the CD (p = .014), and for trial outcomes after the learning criterion was reached (dlPFC: p = .002), ACC: p = .030; CD: overall: p = .010; for positive correlations only: p = .014) (**Figure 6.4A**). Example neurons for the significant effects are shown in **Figure 6.4B**.

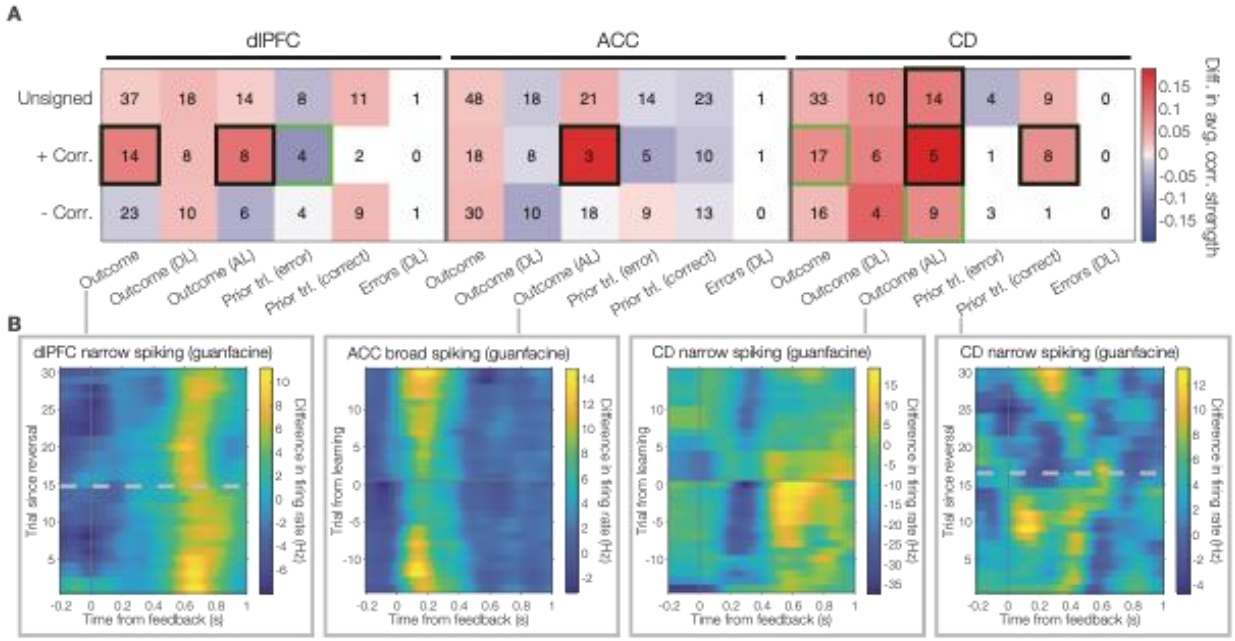

Fig 6.4 Guanfacine-mediated changes in neural activity correlations to outcome variables during the feedback epoch.
(**A**) The same as figure 6.3A but for outcome variables. (**B**) Example neurons with significant correlations to outcome (far left; difference between rewarded and unrewarded trials aligned to block reversal), outcome after learning (middle two; difference between rewarded and unrewarded trials), and prior trial outcome for correct trials (far right; difference between the prior trial being rewarded or unrewarded). The dashed line represents the average learning trial if aligned to block reversal.

Reversal learning of stimulus colors is closely linked to the encoding of reward prediction errors (RPEs) (Oemisch et al., 2019).We correlated neural firing with the model derived RPEs during drug and non-drug conditions and found significantly enhanced [RPE x firing] correlations with guanfacine in the CD ($p = .024$; unsigned correlations: $p = .014$; negative correlations: $p < .001$; positive RPEs: $p = .049$; positive RPEs prior to reaching learning criterion: $p = .016$) and in the ACC (negative RPEs: $p = .039$; negative RPEs prior to reaching learning criterion, unsigned correlations: $p = .029$; negative correlations: $p = .016$) (**Figure 6.5A**).

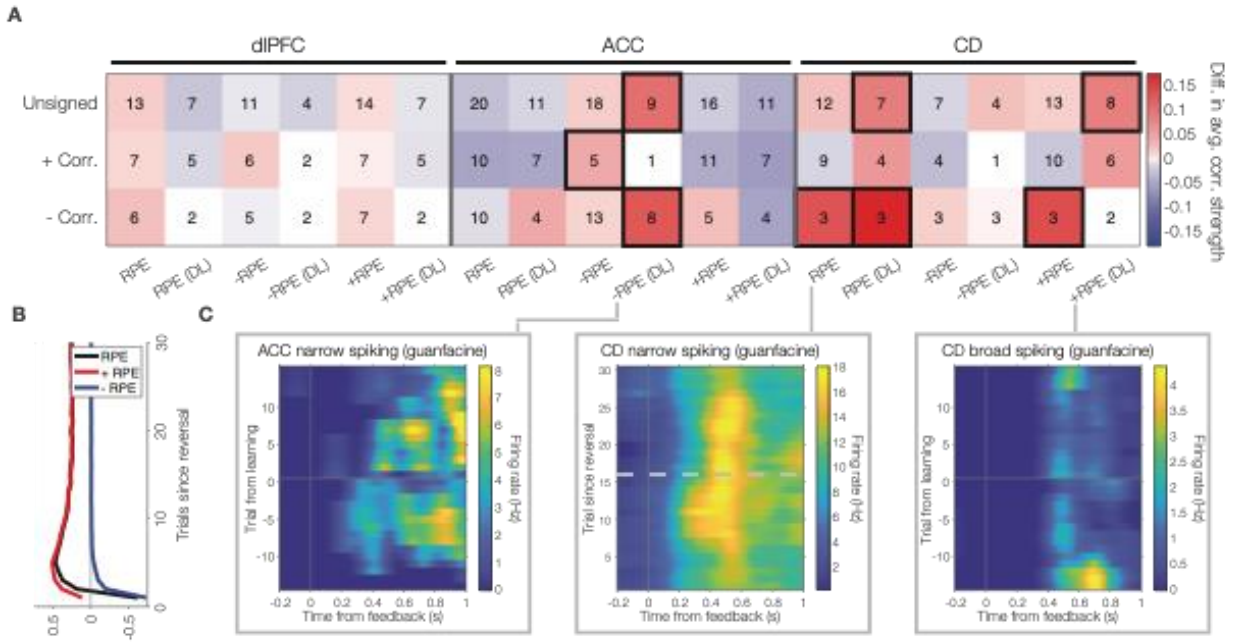

Fig 6.5 Guanfacine-mediated changes in neural activity correlations to RPEs during the feedback epoch. (**A**) The same as figure 6.3A and 4A, but for RPEs. (**B**) Average RPE, positive RPE and negative RPE signals aligned to block reversal. (**C**) Example neurons with significant correlations to negative RPEs during learning (far left; firing rate during unrewarded trials only), signed RPEs (middle; firing rate during all trials), and positive RPEs during learning (far right; firing rate during rewarded trials only). The dashed line represents the average learning trial if aligned to block reversal.

The observed effects with guanfacine occurred without apparent changes in the relative ranking of which task or model variables were encoded in the front-striatal network. We tested whis by identifying for each neuron the best explaining variable through the regression R^2 values and compiling area-specific rankings of the number of cells best explained by each of the 18 observed and model derived task variables. This approach showed that the guanfacine and non-drug best-fit variable rankings were significantly correlated and therefore comparable during the feedback epoch in the dlPFC ($p = .006$; Tau = .477), ACC ($p = .014$; Tau = .425), and CD ($p = .014$; Tau = .425; **Appendix E, Figure E5A**).

6.4.5 Guanfacine modulates signaling which stimulus will be chosen after the attention cue onset

During the onset of the attentional cue, we found that with guanfacine, the proportion of significantly correlating neurons encoding the value of stimulus that will be chosen, i.e. the chosen stimulus, varied across areas. The proportion of significantly correlating neurons was higher in the dlPFC for signaling the value of the stimulus that will be chosen in that trial (the 'chosen unrewarded stimulus') during learning ($p = .044$), in the CD for signaling the choice probability of the stimulus that will be chosen in that trial during learning ($p = .033$) and the previous trial outcome prior to correct trials ($p = .032$). Additionally, we found that with guanfacine, the dlPFC showed a decreased proportion of significantly correlating neurons signaling the value of the chosen rewarded stimulus during learning ($p = .011$) as did the ACC for outcome after learning ($p = .049$; **Appendix E, Figure E4**).

In the attention cue epoch guanfacine did not result in changes of firing correlations with RPE or other model variables. However, guanfacine enhanced correlation strength of the previous trial outcome during error trials in the CD (unsigned correlations: $p = .025$; positive correlations: $p = .005$). In contrast to the feedback epoch, in the attention cue onset epoch, we found that the rankings for the best-fit parameter with guanfacine versus non-drug condition differed (no significant correlation of ranking; dlPFC: n.s.; Tau = -.007; ACC: n.s.; Tau = -.281; CD: n.s.; Tau = .242), which reflects that in the non-drug condition the best-ranked (most) encoded variable was the target color and that trial outcomes were encoded more strongly after learning than in the guanfacine condition (for details see: **Appendix E, Figure E5B**).

6.4.6 Guanfacine enhances outcome encoding particularly for putative interneurons

In order to explore whether guanfacine disproportionally affects the encoding of task relevant variables in excitatory or inhibitory neurons, we separately analyzed neurons with narrow versus broad action potential waveforms (see **Methods**). Within the cortical regions of dlPFC and ACC, narrow spiking neurons were considered putative interneurons and broad spiking neurons

were considered putative pyramidal neurons (**Figure 6.6C**) while in the striatal region of the CD, narrow spiking neurons were considered putative FSIs and broad spiking neurons were considered putative MSNs (**Figure 6.6D**).

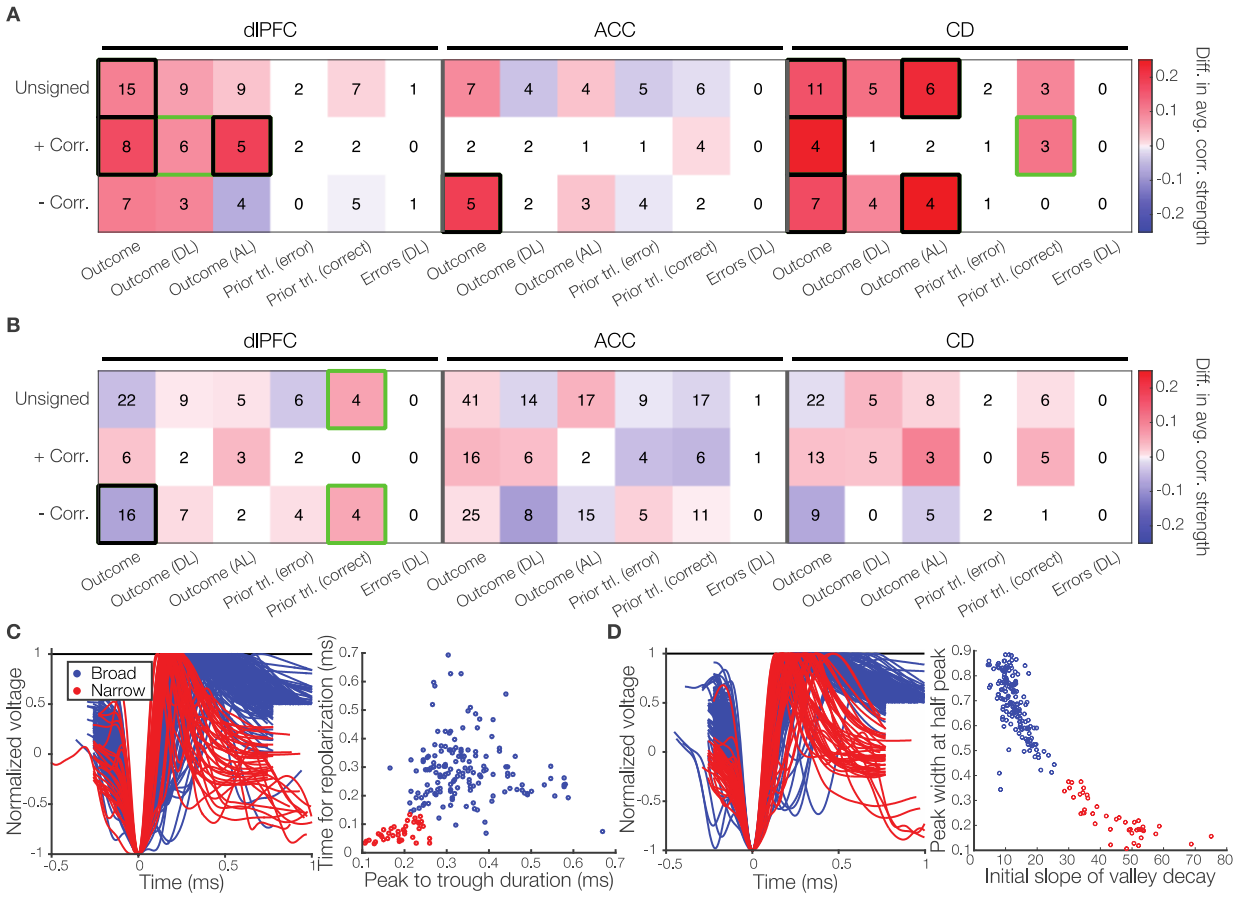

Fig 6.6 Guanfacine-mediated changes in neural activity correlations to outcome variables during the feedback epoch for broad and narrow spiking neurons.
(**A**) The same as figure 6.4A but including only narrow spiking neurons. (**B**) Same as A but including only broad spiking neurons. (**C**) Normalized voltage of cortical (dlPFC and ACC) waveforms (left) and the scatter plot of the used classification criteria: time to repolarization and peak-to-trough duration (right). Broad spiking putative pyramidal neurons in blue and narrow spiking putative interneurons in red. (**D**) The same as C but for striatal (CD) neurons. Normalized voltage of waveforms (left) and the scatter plot of the used classification criteria: peak width at half peak and initial slope of valley decay (right). Broad spiking putative MSNs in blue and narrow spiking putative FSIs in red.

During the feedback epoch of the task, we found that narrow spiking neurons drive the enhanced trial outcome encoding with guanfacine in all brain regions. Guanfacine enhanced narrow spiking neuron encoding of outcome (unsigned correlations: $p = .016$; positive correlations: $p = .004$) and outcome after learning ($p < .001$) in the dlPFC, outcome after learning ($p = .027$) in the ACC, and outcome (unsigned correlations: $p = .001$; positive correlations: $p < .001$; negative

correlations: p = .006) as well as outcome after learning (unsigned correlations: p = < .001; negative correlations: p < .001) in the CD (**Figure 6.6A**). In contrast, the broad spiking neuron population showed with guanfacine significantly reduced encoding of trial outcomes in the dlPFC (p = .016) (**Figure 6.6B**). There was no clear putative cell type driving observed results for either the stimulus or model variables (data not shown).

In the attention cue onset epoch, due to a smaller population of neurons with significant regressions, we could not reasonably compare narrow and broad spiking neurons for most variables. However, we found a significant enhancement of the encoding of target color in the ACC with guanfacine that was specific to putative interneurons (unsigned correlations: p = .006; positive correlations: p < .001; negative correlations: p = .021; **Appendix E, Figure E6**). Moreover, narrow spiking neurons in the CD, putative FSIs, showed with guanfacine an enhanced encoding of previous trial outcomes during error trials (p = .043; **Figure 6.7B**) and during correct trials (p = .030; **Figure 6.7B**) which was not evident for broad spiking CD neurons (not shown).

6.5 Discussion

Here, we found that systemic guanfacine administration enhances cognitive flexibility evident in faster learning after reward reversals and enhanced post-error behavioral improvement. This improved cognitive flexibility was accompanied by the enhanced representation of outcomes and model-derived RPEs in the spiking activity of single neurons within the fronto-striatal network during the feedback epoch. Outcome representations were stronger with systemic guanfacine administration in the dlPFC, ACC and CD while the enhanced RPE signaling was specific to the ACC and CD. These enhancements were observed in the absence of overall changes in firing rate or firing variability at a global level (coefficient of variation) or local level (local variability) and without overall changing the proportion of neurons encoding the tested variables. Cell type classification revealed that putative interneurons and putative fast spiking interneurons were driving the cortical (dlPFC and ACC) and subcortical (CD) enhancement of outcome encoding, respectively. These results suggest a mechanism regarding the role of α2A adrenoceptors in enhancing cognitive flexibility, complimentary to their involvement in spatial WM. Although the nature of systemic administrations make it difficult to ascertain the adrenoceptors or even

neuromodulators that are causally involved, the results illustrate that systemic α2A stimulation is *sufficient* for enhancing both outcome and RPE encoding in the fronto-striatal network which we could link with faster reversal learning and post-error behavioral adjustments.

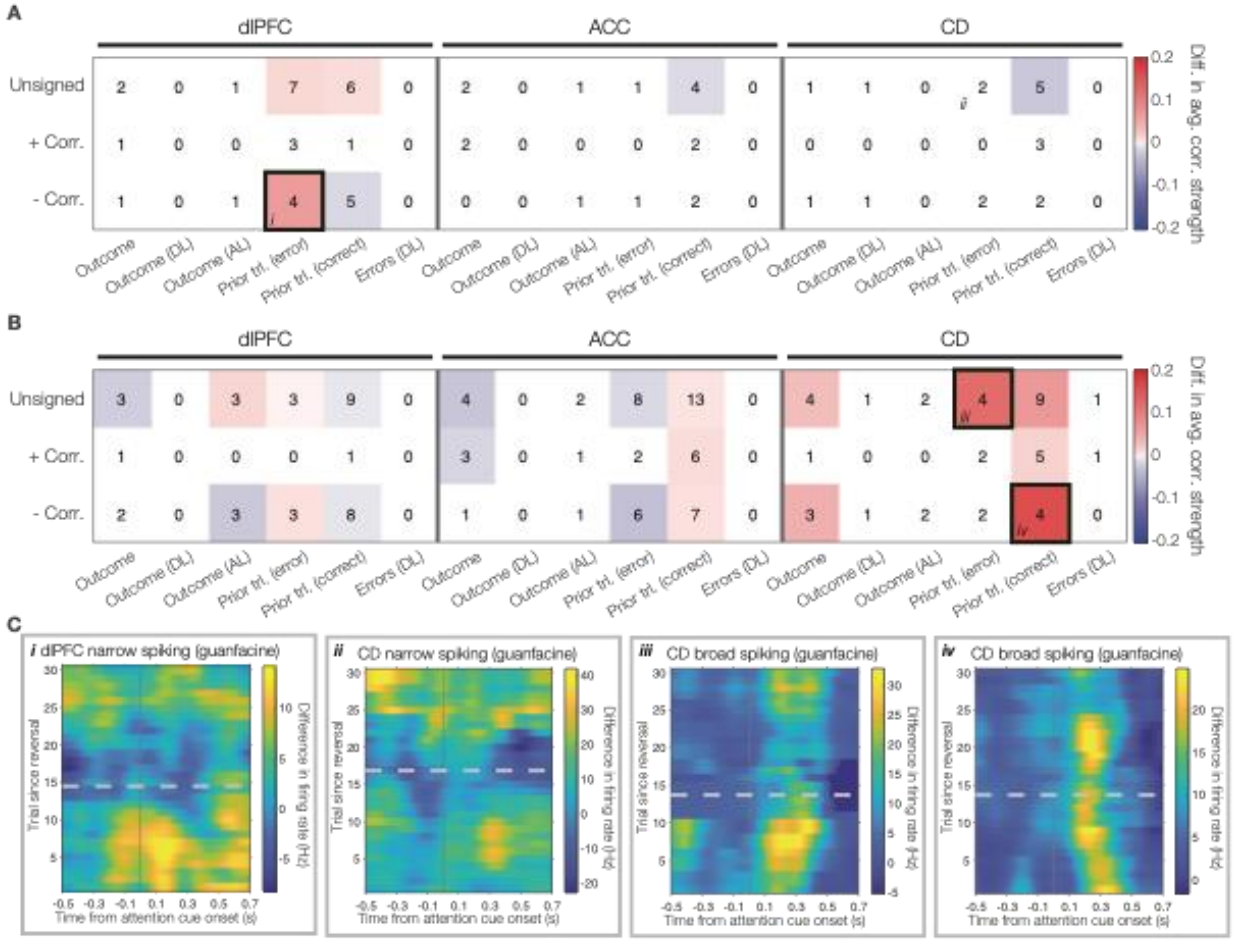

Fig 6.7 Guanfacine-mediated changes in neural activity correlations to outcome variables during the attention cue onset epoch for broad and narrow spiking neurons.
(**A**) The same as figure 6.6A but for the attention cue onset epoch. Roman numerals correspond with example neurons in C. (**B**) The same as figure 6.6B but for the attention cue onset epoch. Roman numerals correspond with example neurons in C. (**C**) Example narrow (two left most examples) and broad (two right most examples) spiking neurons with significant correlations for prior trial outcome for (to be) error trials (three left most examples) and prior trial outcome for (to be) correct trials (far right). Roman numerals map onto figures A and B to indicate where the example neuron was pulled from. The dashed line represents the average learning trial if aligned to block reversal.

6.5.1 The α2A adrenoceptor and cognitive flexibility.

Our findings suggest that α2A adrenoceptor activation supports cognitive flexibility by modulating three core brain areas of the anterior fronto-striatal loops, which goes beyond previous studies that demonstrated how α2AR activation modulates neuronal activity and behavioral

performance for spatial working memory tasks in the dlPFC. Molecular and iontophoretic experiments have described post-synaptic α2A receptors on unique dendritic spines exclusive to the dlPFC (Arnsten et al., 2010; Cools and Arnsten, 2022), and stimulation of these post-synaptic α2A receptors disrupts intracellular cAMP signaling leading to enhanced delay firing (activity persisting through WM delay) for the preferred spatial location of these dlPFC pyramidal neurons (Wang et al., 2007). However, this mechanism of α2A receptor action does not account for the enhanced cognitive flexibility observed here. First, the feature-based reversal learning task used here does not contain any explicit working memory 'delay' period (**Figure 6.1B**). Second, the improved learning performance was specifically dependent on the requirement to reverse a learned reward association, because we did not observe better performance with guanfacine during the first block prior to the first reversal (**Appendix E, Figure E1B**). This finding resonates well with a recent study where optogenetic activation of LC enhanced performance after a rule switch but not in the first block of a given session (McBurney-Lin et al., 2022). Taken together, the behavioral improvement with guanfacine in our study is likely reflecting an increased efficiency to learn from trial outcomes and to utilize error signals for improving future performance.

6.5.2 Enhanced outcome and RPE encoding without increased proportion of encoding neurons.

We found that guanfacine increased the strength of neuronal encoding of trial outcomes in dlPFC, ACC, and CD (**Figure 6.4**) and of RPEs in ACC and CD (**Figure 6.5**) during the feedback epoch. These changes could be the neural substrate for the enhanced post-error adjustment and the faster adjustment to reversed color-reward associations after a block reversal (**Figure 6.2C**). The enhanced neural encoding is consistent with α2A adrenoceptors enhancing the gain of neuronal responses in each of the three recorded brain areas. Gain modulation has been proposed to be a primary effect of increased NE activity, capable of potentiating responses of neurons and also capable of making neural responses to previously sub-threshold inputs supra-threshold (Berridge and Waterhouse, 2003; Aston-Jones and Cohen, 2005a).

While we did observe enhanced encoding strength with guanfacine, consistent with potentiating existing responses, we did not find proportionally more neurons encoding for

outcomes or RPEs (**Appendix E, Figure E3**). This finding shows that the putative gain modulation process induced by guanfacine in dlPFC, ACC, and CD primarily affects neurons that are already functionally recruited without switching on previously non-active neurons. Consistent with this suggestion, we found that guanfacine had a moderately suppressive effect on the overall average firing of neurons during in the feedback epoch with significantly reduced firing rates of putative pyramidal neurons in the dlPFC and putative MSNs in the CD (see **Appendix E.2**). Moreover, the NE mediated switching of sub-threshold to supra-threshold responses has largely been described in sensory cortices, which differs in composition and α2A receptor densities from fronto-striatal circuits (Ciombor et al., 1999; Devilbiss and Waterhouse, 2004; Waterhouse and Navarra, 2018). However, we cannot rule out that higher concentration of guanfacine, or the direct increase of NE would have recruited additional neurons encoding outcomes and RPEs during the task.

6.5.3 Spatial and cell-type specificity.

We found that the significantly stronger outcome encoding with guanfacine during the feedback epoch was driven by narrow spiking putative interneurons in the dlPFC and ACC, and putative FSIs in the CD (**Figure 6.6A**). This finding is consistent with studies have shown that adrenoceptor expression and modulation is stronger for interneurons than pyramidal cells with α2 and β adrenoceptors enhancing their inhibitory actions while α1 adrenoceptors decrease their inhibitory actions in prefrontal cortex (Kawaguchi and Shindou, 1998; Wang et al., 2013; Liu et al., 2014; Xing et al., 2016; Lee et al., 2020), as well as in sensory and sensorimotor cortices (Bennett et al., 1998; Nai et al., 2009; Salgado et al., 2011, 2012; Ohshima et al., 2017). This suggests guanfacine may enhance the inhibitory activity of interneurons which is consistent with the decreased firing we observed in putative pyramidal neurons in the dlPFC and with the decreased firing of putative MSN spiking in the CD (see **Appendix E.2**).

A prominent role of interneurons in learning from outcomes and reward predictions errors has recently been demonstrated for putative fast spiking interneurons in the lateral PFC of macaques (Boroujeni et al., 2021), as well as for fast spiking interneurons in the head of the caudate (Boroujeni et al., 2020). In these studies, narrow spiking neurons encoded reward prediction errors particularly during the learning period of reward reversal. Our results of guanfacine enhancing the

encoding of outcomes and reward prediction errors may thus directly support the interneuron-mediated learning and behavioral adjustment. Systemic guanfacine may thus have gain modulated the intrinsic neuronal dynamics underlying cognitive flexibility during color-based reversal learning.

While we found that trial outcomes were enhanced with guanfacine in all three areas, stronger RPE encoding was only observed in the ACC and CD (**Figure 6.5**). We unfortunately did not have enough data for a reasonable comparison of putative cell types that significantly encoded RPE signals. However, we did observe enhanced negative, but not positive or signed RPE signaling in the ACC. Negative RPEs are only computed for unrewarded trials and are critical signals for the adjustment of behavioral strategy upon failing to acquire reward, a major function of the ACC (Kennerley et al., 2006; Buckley et al., 2009; Kaping et al., 2011; Gläscher et al., 2012; Heilbronner and Hayden, 2016). Furthermore, a previous study demonstrated that switches in behavioral strategy may be triggered by LC input to the ACC (Tervo et al., 2014). Similarly, we only observed enhanced positive and signed, but not enhanced negative RPE signaling in the CD during the feedback epoch with guanfacine. This, too, matches known functions of the striatum and the head of the caudate for value updating (Cromwell and Schultz, 2003; Williams and Eskandar, 2006; Kim and Hikosaka, 2013, 2015; Vo et al., 2014; Rothenhoefe et al., 2017). The systemic administration of guanfacine is thus helping inch the functions of the ACC and CD, which support behavioral flexibility (shifting behavioral strategies and value updating respectively), towards greater flexibility.

A recent study describes two distinct populations of LC neurons distinguishable by their waveforms which are excited by positive RPEs and a lack of reward respectively (Su and Cohen, 2022) suggesting that distinct noradrenergic neuronal populations in the LC (Chandler et al., 2014; Totah et al., 2018; Breton-Provencher et al., 2022) may be responsible for the observed RPE enhancement we see in the ACC and CD. The same study (Su and Cohen, 2022) has posited that noradrenergic signaling from the LC may serve to communicate RPE information to the cortex while dopaminergic signaling communicates RPEs to the basal ganglia. This proposed dichotomy is consistent with our findings. Future studies may thus test more directly whether distinct neuromodulatory systems mediate prediction error signaling in ACC and striatum.

6.5.4 Insights from α2A stimulation: norepinephrine and behavior.

Pre-synaptic α2A adrenoceptors act as noradrenergic auto-receptors, reducing the further release of NE. It has been previously shown that systemic guanfacine administration reduces LC activity (Engberg and Eriksson, 1991; Okada et al., 2018). Consistent with reduced LC firing we observed reduced pupil diameter in the blocks temporally closest to the inject time (**Appendix E, Figure E1C**). However, guanfacine also resulted in on average reduced pair-wise spike count correlations in the ACC relative to the non-drug condition, which a recent study have shown to be indicative of higher LC activity (Joshi and Gold, 2022). This discrepancy might be resolved by distinguishing tonic from phasic LC activity modulations. The increases of pairwise firing correlations in Joshi and Gold (2022) likely reflect reduced tonic LC firing, while the reduction of firing correlation that we found indicates enhanced phasic LC firing in the presence of reduced tonic LC firing. This proposal is consistent with findings showing that noradrenergic auto-receptor activation can increase LC neuron sensitivity to glutamatergic and cholinergic stimulation thus emulating an increase in phasic LC firing (Aston-Jones et al., 1991a; Aston-Jones and Cohen, 2005a). This suggests that systemic guanfacine administration may reduce tonic LC activity while simultaneously boosting phasic LC activity.

This α2A stimulation resulted in enhanced cognitive flexibility in our feature-based reversal learning task with faster behavioral adjustments after unexpected outcomes. It is possible that this enhanced flexibility comes at a behavioral cost. Although guanfacine lead to better immediate post-reversal performance as can be seen in the raw performance average of the first three post-reversal trials, it does not improve overall plateau performance at the end of the reversal block and may even reduce it as visible in the subtly (non-significantly) lower end-of-block performance plateaus (**Figure 6.2A** & **Appendix E, Figure E1A**). This observation suggests that the systemic guanfacine administration promoted exploratory behavior facilitating the learning but hampering the exploitative behavioral after an initial learning criterion was achieved. Our results are therefore consistent with a role of the α2A adrenoreceptor in re-balance the exploration-exploitation trade-off towards a higher weighting of explorative behavior, mediated potentially by an overall increase of learning rates from performance feedback (Hassani et al., 2017).

6.6 Conclusions

Based on our results, we believe that noradrenergic mechanisms determine learning rates for stimulus value updating based on a running measure of environmental volatility. The action of NE at its various metabotropic adrenoceptors may adjust the parameters of local computations to better meet the demands of the subject's currently perceived environmental statistics. This suggestion is congruent with current theories of NE that emphasize requirements of uncertainty and salience for LC activity resulting in alterations to neural functions and behavior based on unexpected events or surprising information (Berridge and Waterhouse, 2003; Bouret and Sara, 2005; Yu and Dayan, 2005; Dayan and Yu, 2006; Doya, 2008; Silvetti et al., 2013; Bornert and Bouret, 2021). Our conclusion also resonates well with a number of human psychopharmacological studies that associate the action of NE/dopamine reuptake inhibitors with the modulation of learning rates based on environmental uncertainty (Jepma et al., 2016; Howlett et al., 2017; Cook et al., 2019).

Increases in environmental volatility can be addressed by increasing learning rates resulting in increased flexibility for adjusting behavior and faster updating of object values which would lead to enhanced attentional focusing onto sensory stimuli which biases credit assignment processes towards the attended stimuli (Oemisch et al., 2019). At the extreme, a highly volatile environment may benefit from a 'fight or flight' type response with hyper-focused attention, one-shot learning and rapid switching between behavioral strategies. While low environmental volatility allows for diffuse attention and low learning rates for slower value updating in order to avoid switching away from successful strategies and over-correcting object value representations from singular unexpected outcomes.

Our data suggests that the stimulation of the α2A adrenoceptor is sufficient for enhancing RPE encoding in the fronto-striatal network and more flexible learning. It is important to note, however, that due to the nature of systemic administration we cannot be certain about the direct involvement of α2A adrenoceptors as opposed to the involvement of other adrenoceptors due to α2A's auto-receptor activity. Furthermore, other neuromodulatory systems interact heavily with

NE, including strong interactions between dopamine and NE, particularly in the PFC (Devoto et al., 2005; Jentsch et al., 2008; Xing et al., 2016; Cools and Arnsten, 2022), and interactions with 5-HT and acetylcholine (Aston-Jones et al., 1991a; Berridge and Foote, 1991; Berridge and Wifler, 2000). Such interactions bring into question the involvement of dopamine in our results for example (Marshall et al., 2016b; Xing et al., 2016; Wang et al., 2018), with evidence that prefrontal dopamine is in part provided by LC noradrenergic terminals (Devoto et al., 2005, 2019, 2020). However, to understand which other neuromodulatory systems might support cognitive flexibility beyond the α2A adrenoceptors will be an important venue for future research.

6.7 Acknowledgements

The authors would like to thank Mariann Oemisch and Marzyeh Azimi for their help with animal training and data collection and Hongying Wang for help with drug administration and animal care. This research was supported by grants from the Canadian Institutes of Health Research (CIHR), the Natural Sciences and Engineering Research Council of Canada (NSERC), the Ontario Ministry of Economic Development and Innovation (MEDI), and the National Institute of Mental Health of the National Institutes of Health under Award Number R01MH129641 (TW). The content is solely the responsibility of the authors and does not necessarily represent the official views of the National Institutes of Health.

Chapter 7 General discussion

In order to better understand the role of neuromodulatory systems on the function of the fronto-striatal network, we utilized multiple pharmacological agents to enhance primate behavior in tasks dependent on the functions of the dlPFC, ACC and striatum. We utilized an FDA approved AChE inhibitor (chapter 3), an FDA approved α2A specific agonist (chapters 5 and 6), as well as an M_1 positive allosteric modulator (chapter 4), part of a newer family of drugs showing great clinical potential for the treatment of AD and schizophrenia (Korczyn, 2000; Conn et al., 2009; Jones et al., 2012; Tobin, 2018). We explored behavioral changes during the performance of a reversal learning task (chapters 5 and 6), set shifting task (chapters 3 and 4) and visual search task (chapters 3 and 4) to identify the cognitive domains impacted by these pharmacological agents. In chapter 5 we utilized computational modelling to explore a potential mechanism underlying guanfacine's enhancement of selective attention and cognitive flexibility in a reversal learning task. And in chapter 6 we found empirical evidence for this model-predicted mechanism in the activity of neurons in the fronto-striatal network. Lastly, in chapter 2 we discuss development efforts for an *in vivo* neurochemical sampling method for multiple endogenous neuromodulators that we show in chapter 3 is also capable of measuring exogenous pharmacological agents. Throughout these 5 chapters, we examined the neuromodulatory influence on higher order cognitive processes in the fronto-striatal network by utilizing behavioral, computational, electrophysiological and neurochemical perspectives.

Here, I will only discuss the cross-relevance between the chapters and avoid repeating discussion points from individual chapters.

7.1 Evaluating pharmacological influence on multiple cognitive domains

As described in chapters 3 and 4, we utilize a cage-mounted touch-screen testing platform capable of executing a variety of tasks and collecting behavioral data from monkeys (Womelsdorf et al., 2021a). We utilized a feature-reward learning task (akin to a set-shifting task) and a visual search task allowing us to extract multiple measures of several cognitive domains such as speed of processing, distractor filtering, perceptual filtering, learning efficiency and cognitive flexibility.

We were then able to compare and contrast the cognitive enhancement that resulted from systemic donepezil vs systemic M_1 PAM (VU0453595) administration.

Such a framework is necessary for testing multiple cognitive domains with increasingly selective compounds in order to dissociate receptor-specific contributions towards cognition and reveal the receptors underlying the behavioral consequences of a given pharmacological compound. For example, as discussed during chapter 6, it is unclear if the guanfacine-mediated enhanced outcome and RPE encoding observed across the fronto-striatal network is due to α2A specific actions, or involves other noradrenergic or even dopaminergic receptors. This is true despite its α2A specificity (Uhlen and Wikberg, 1991; Uhlen et al., 1994) due to the role of α2A as an auto receptor (Engberg and Eriksson, 1991), the unclear source of prefrontal dopamine (Devoto et al., 2005, 2019, 2020), and the prevalence of dopamine for RPE signaling, especially in the striatum (Schultz et al., 1997; Glimcher, 2011). Even drugs that target the same receptors may vary in behavioral outcomes and would benefit from characterization in such a framework.

Outside of direct multi-modulator measurements from multiple candidate brain regions, it is conceivable that by mapping the cognitive impact of receptor specific compounds (such as PAMs) using the same behavioral tasks as a baseline, we could infer the mechanism of action for less specific drugs or those with unclear *in vivo* mechanisms. Allosteric modulators are the most likely compounds to be free of off-target effects and are thus best suited for such an endeavor as they simply modulate receptor responses to endogenous compounds (Moran et al., 2018). Such an understanding would allow for the design and testing of drug 'cocktails' targeting multiple neuromodulatory receptors simultaneously. By mapping a patient's baselines for various cognitive domains, an individualized cocktail of neuromodulatory compounds could be planned to best address their personal deficits.

7.2 Broader frameworks for neuromodulatory actions

Due to their virtually global influence and capacity to organize neural activity to support broad behavioral states, it has been proposed that the neuromodulatory systems operate in a meta-learning framework (Doya, 2002). It has been proposed that essentially, each major

neuromodulator represents a meta-learning parameter: dopamine signals RPEs, 5-HT controls the time scale of RPEs, NE controls stochasticity of action while ACh controls the speed of memory updating. Thus, it is posited that changes in the activity of the nuclei responsible for these neuromodulators adjusts these parameters and shifts behavioral strategies and behaviors. Although studies find general support for shifts in meta-learning parameters though pharmacological manipulation of neuromodulators (Jepma et al., 2016; Howlett et al., 2017; Cook et al., 2019), the specificity of the neuromodulators and the exact measure of 'neuromodulation' in such a framework is not clear. There is recent data suggesting that the activity of noradrenergic neurons in the LC (Su and Cohen, 2022), serotonergic neurons in the dorsal raphe (Grossman et al., 2022) and cholinergic neurons in the basal forebrain (Hegedüs et al., 2023) encode RPEs or learning rates. Although RPE signaling could still be predominantly carried out and propagated by one neuromodulator, it is possible that individual neuromodulators do not directly map onto single parameters in a meta-learning framework. However, the exact same line of evidence strongly suggests that neuromodulators are somehow involved in adjusting meta-learning parameters, perhaps by their extra-cellular concentrations.

The optimization of meta-learning parameters will differ between tasks based on the environmental statistics and internal goals. Furthermore, the strength of externally driven shifts in meta-learning parameters through, e.g. pharmacological intervention, will vary based on the individual's baseline neuromodulatory tone. Such task specific modulation of neuromodulatory effects would explain different optimal doses for individuals engaged in tasks with different cognitive demands as described in chapter 3 and is consistent with the general premise of inverted-U curves describing dose – performance relationships. Furthermore, shifts of cholinergic tone has been implicated in other trade-offs such as speed-accuracy (Turchi and Sarter, 1997). Similarly, as described in chapter 6, guanfacine administration enhances post-reversal learning, already in the first 3 post-reversal trials, but this may reflect enhanced tendencies for exploratory behavior at the expense of exploitative behaviors as evident in somewhat reduced plateau performance and a slightly reduced likelihood to finish blocks learned. Optimization of meta-learning parameters through neuromodulatory action will thus likely come at a cost, at the very least a metabolic one, otherwise they would evolutionarily be pushed towards being static, instead of dynamic. Lastly, a variable baseline of neuromodulatory tone may help explain the heterogeneity of optimal doses

for the clinical population. It can be predicted that depending on the neuromodulator in question, an individual's baseline may be significantly different for some clinical populations. The extent of the loss of cholinergic synapses in the cortex and hippocampus has been linked to symptom progression in AD (Fahnestock and Shekari, 2019) and pharmacological strategies have been proposed utilizing different drug cocktails at different stages of AD to account for the progression in cholinergic loss (Tobin, 2018). Ultimately, based on an individual's baseline neuromodulatory tone, optimal performance may require more or less neuromodulatory activation depending on the particular demands of a given task.

7.3 Multi-modulator measurements

Based on the discussion so far, in a meta-learning framework, we may predict that the pattern of neuromodulatory tone could be informative of an individual's cognitive state as defined by the current values of meta-learning parameters. Furthermore, shifts in behavioral needs may require shifting multiple meta-learning parameters and thus be reflected in multi-modulatory changes. Unpublished data from our lab using the SPME method described in chapter 2 shows that we do indeed see such multi-modulatory changes. During the same feature-learning task used in chapters 3 and 4, we find that low attentional load blocks contain higher concentrations of dopamine, and lower concentrations of ACh and 5-HT in the striatum. Furthermore, some changes seem to be area specific. For example, before and after the start of the task, we find that prefrontal ACh increases while striatal ACh decreases. This suggests that despite overlap in stimuli and events that may trigger neuromodulatory release (see section 1.4.1), they are differentially modulated in time scales measurable by SPME.

This data supports the role of neuromodulators in adjusting meta-learning parameters to meet different environmental demands through multi-modulatory shifts. However, the differences we find between brain regions brings up another question: in which brain region do multi-modulatory tones best reflect the current meta-learning parameters? It is possible that multi-modulatory shifts observable in the PFC correspond to different changes in meta-learning variables than the multi-modulatory shifts observable in the striatum. A study utilizing human neuroanatomy and receptor density maps suggests that areas with similar functions have similar receptor

fingerprints (Zilles et al., 2002) consistent with later findings utilizing similar methods in primates (Rapan et al., 2022) as well as the actual area-specific volume of available neuromodulators in the macaque brain (Ward et al., 2018). Although, this does not yet reveal if the neuromodulatory changes in the striatum, for example, do indeed provide additional information to the neuromodulatory changes in prefrontal cortices for understanding meta-learning parameters.

7.4 Perspective on neuromodulation

Neuromodulatory action at metabotropic receptors can never hyper- or de-polarize neurons at the same temporal precision as ionotropic receptors. This means that with the exceptions of the ionotropic nicotinic receptors (ACh) and 5-HT_3 receptors (5-HT), the function of major neuromodulatory systems involves layering on top of electrophysiological circuits and networks in order to 'modulate' their activity. This positions them well for adjusting meta-learning parameters by optimally tuning local circuit properties in order to modulate their on-going computations.

Our findings in chapter 6 strongly support such a notion. We found that through the collective neuromodulatory changes elicited by systematic guanfacine administration, encoding strength for stimulus, outcome and task parameters relevant for the known functions of each brain region and the task demands were enhanced. The encoding of a handful of parameters were also reduced with the notable case of a non-relevant stimulus feature representation. This aligns with deafferentation studies discussed in section 1.2.1 where performance of animals for a given task becomes sub-optimal (Muir et al., 1992; Voytko et al., 1994; Turchi and Sarter, 1997; Dalley et al., 2001; Botly and de Rosa, 2009; Leo et al., 2023). Thus, it is likely that neuromodulation tunes meta-parameters for area-specific functions as suggested in chapter 6 and is supported by studies utilizing area specific deafferentations (McGaughy et al., 2008; Croxson et al., 2011) and selective activation (Tervo et al., 2014). This conclusion predicts that such area specific or global deafferentation studies would cause more severe deficits for animals when they must rapidly shift behavior and meta-learning parameters to meet vastly different task and environmental demands. Such a hypothesis is well suited to be addressed in the testing environment utilized in chapters 3 and 4. Another extension of this conclusion focuses on the different innervation and receptor

expression patterns seen between brain regions. If we are to assume that neuromodulators indeed shift local computational parameters, their role is then to gate synaptic activity resulting in more or less efficient computations. Their global innervation and influence may then orchestrate such gating in multiple circuits to broadly support some general behavioral state.

A final extension from such a conclusion pertains to potential clinical strategies in addressing psychiatric symptoms. Inappropriate tuning of meta-learning parameters arising from the loss of neuromodulatory neurons may indeed result in the cognitive deficits observed in psychiatric disorders (Whitehouse et al., 1981; Mesulam et al., 1983; Delaville et al., 2011; Schmitz and Nathan Spreng, 2016; Fahnestock and Shekari, 2019). However, if we conclude that these neuromodulators are simply layering onto and adjusting the electrophysiological circuits, with advances in non-invasive technologies, we could potentially directly modulate these circuits in a therapeutic manner. Increasing our understanding of the neuromodulator-driven changes in local electrophysiology may allow methods such as focused ultrasound, transcranial magnetic stimulation and others to be better utilized in targeted ways.

7.5 Conclusion

In summary, my work has demonstrated the crucial role of neuromodulators on the higher cognitive functions supported by the fronto-striatal network in the primate brain. By utilizing pharmacological agents with high clinical relevance, we have demonstrated that we can modulate local computations to optimize behavioral performance and that such an optimization is contingent on the environmental statistics and internal state of the animal. My work here demonstrates a framework for the future investigations of pharmacological agents to advance our understanding of the multi-modulator brain such that we may better the cognitive deficits found in psychiatric disorders.

Appendix A: Supplemental information for Chapter 2

A.1 Supplementary Methods Chemicals, Reagents and Materials

The LC-MS-grade solvents methanol (MeOH), acetonitrile (ACN), isopropanol (IPA) and water, as well as the acetylcholinesterase inhibitor phenylmethylsulfonyl fluoride (PMSF) were purchased from Fisher Scientifc. Formic acid, polyacrylonitrile (PAN), N,N-dimethylformamide (DMF) and the standards of neurotransmitters: γ-aminobutyric acid (GABA), glutamic acid (Glu), acetylcholine (ACh), histamine (Hist), serotonin (5-HT), dopamine (DA) and choline (Cho) as well as their deuterated analogues were purchased from Millipore Sigma (Oakville, ON, Canada). Epinephrine (Epi), norepinephrine (NE) and their deuterated analogues were obtained from Cerilliant Corporation (Round Rock, TX, USA). Choline-D9, was purchased from Cambridge Isotope Laboratories (Tewksbury, MA, USA). The reagents used for synthesis of hydrophilic-lipophilic balance polymer particles functionalized with strong cation exchange groups, as well as compounds for preparation of PBS were purchased from Millipore-Sigma. The stainless steel wire (stainless steel grade AISI 304, 150 μm diameter) used for manufacturing of SPME probes was purchased from Unimed S.A. (Lausanne, Switzerland). The stainless steel tubing used as guiding cannulas (270 μm O.D.; 200±5 μm I.D.) was obtained from Vita Needle (Needham, MA, USA).

A.1.1 LC-MS/MS Analysis

On the day of analysis, the SPME probes were defrosted and desorbed into 40 μL of water/ACN/MeOH 40:30:30 (v/v/v) mixture containing 1 % of formic acid and a mixture of deuterated isotopologues of targeted neuromodulators (used as internal standards, IS) at 20 ng/mL. The desorption was carried out for 1 h with agitation at 1500 rpm. The extracts were injected into the LC-MS system for targeted neurotransmitter analysis within a few hours after desorption. All experiments were carried out using an Ultimate 3000RS HPLC system coupled to TSQ Quantiva triple quadrupole mass spectrometer (Thermo Fisher Scientific, San Jose, California, USA). Data processing was performed using Thermo software Xcalibur 4.0 and Trace Finder 4.1. For chromatographic separation of the target compounds, a modified method of what is previously reported (Cudjoe and Pawliszyn 2014) was used, adjusted to include more targeted

neuromodulators and their corresponding IS. A Kinetex® PFP LC column (100 x 2.1 mm, 1.7 μm; Phenomenex, Torrance, CA, USA) was held at 30°C with the mobile phase flow rate at 400 μL/min. The mobile phase A consisted of water/MeOH/ACN 90:5:5 (v/v/v) with 0.1 % formic acid, and mobile phase B was ACN/water 90:10 (v/v) with 0.1% of formic acid. The chromatographic gradient was applied starting from 100% B for 1 min and increasing the aqueous mobile phase A to 100% for 3 min with convex gradient function, held for 0.5 min and subsequent linear return to initial conditions and re-equilibration for 1 min, yielding total time of 6.5 min. The injection volume was 10 μL. MS/MS analysis was performed with electrospray ionization in positive mode under selected reaction monitoring conditions, with two MS/MS transitions for each neuromodulator (quantifier and qualifier) and one for each IS.

A.1.2 Quantitation of neuromodulators

Individual stock standard solutions of all targeted neuromodulators were prepared in methanol or water with 0.1% formic acid at a concentration of 1 mg/mL and stored at −80 °C for maximum of one month. In order to calculate the amounts of neuromodulators extracted by each probe, calibrator standards prepared in the same desorption solvent as real samples were analyzed in the same batch. This instrumental calibration curve was prepared in the range of 0.1-200 ng/mL by a serial dilution of the stock standard mixture of all compounds at 1μg/mL. The IS concentration was kept constant at 20 ng/mL in all calibrators, identically as in the real samples. The amounts extracted were calculated based on linear regression equation obtained from the analytical signal (the ratio of chromatographic peak areas of analytes and their corresponding IS) plotted against the concentration.

In order to calculate the concentrations of neuromodulators in brain, matrix-matched external calibration approach was used. The surrogate matrix consisted of 2% agar gel mixed with brain homogenate in the ratio 1:1 (*v/w)*. The homogenized brain tissue was earlier incubated with 1 mM PMSF for 1 h at 37°C to prevent enzymatic digestion of acetylcholine in the calibrator samples. Due to several target compounds being present in brain homogenate at high concentrations (e.g. for glutamate and choline the “blank” brain homogenate matrix doesn’t exist), their quantitation was based on signals of their deuterated isotopologues. The calibrator samples

were prepared in the surrogate matrix with concentrations of neuromodulators ranging from 5 to 3000 μg/mL for the isotopically labelled compounds or from 10 to 2000 ng/mL for the remaining compounds.

The extractions were carried out with SPME probes manufactured and pre-treated identically to the probes used for *in vivo* sampling and using the same 20 min extraction time and desorption conditions as for the real samples. The amounts of neuromodulators extracted from the calibrator samples were determined in the same way as described above and plotted against concentrations of calibrators. The resulting weighted linear regression equations were applied to the amounts of neuromodulators extracted from the *in vivo* samples, yielding values of concentrations of the compounds of interest in brain.

The limits of detection (LOD) were estimated as the levels corresponding to the signal to noise ratio of 3 and were calculated based on the signal of blank calibrator sample (considered as the noise).

A.2 Figures

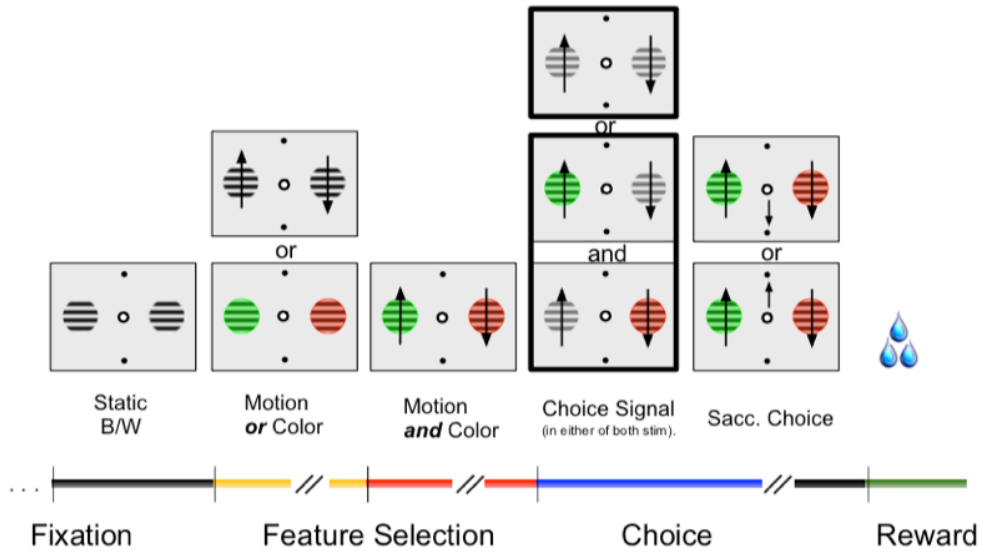

Fig A1 Behavioral task that the monkeys were engaged in.
Briefly, the monkey was expected to fixate a central fixation point until criterion when two graded stimuli appeared. The graded stimuli acquired color and motion, of the graded stripes, features in either order. The two stimuli then either simultaneously dimmed (go-signal), or dimmed one at a time in either order. The monkey, through trial and error, identified the rewarded stimulus via its color feature which was the sole identifying feature informative of reward. The monkey was then expected to wait until the dimming of the selected stimulus and respond in the same direction as the motion of the graded stripes on the chosen stimulus. If the monkey correctly accomplished this, it would receive deterministic reward in the form of liquid juice. Monkey As was engaged in a variation of this task with reduced complexity in order to match monkey Ke in performance and reward acquisition over the sampling period. Figure reproduced from Hassani et al., 2017.

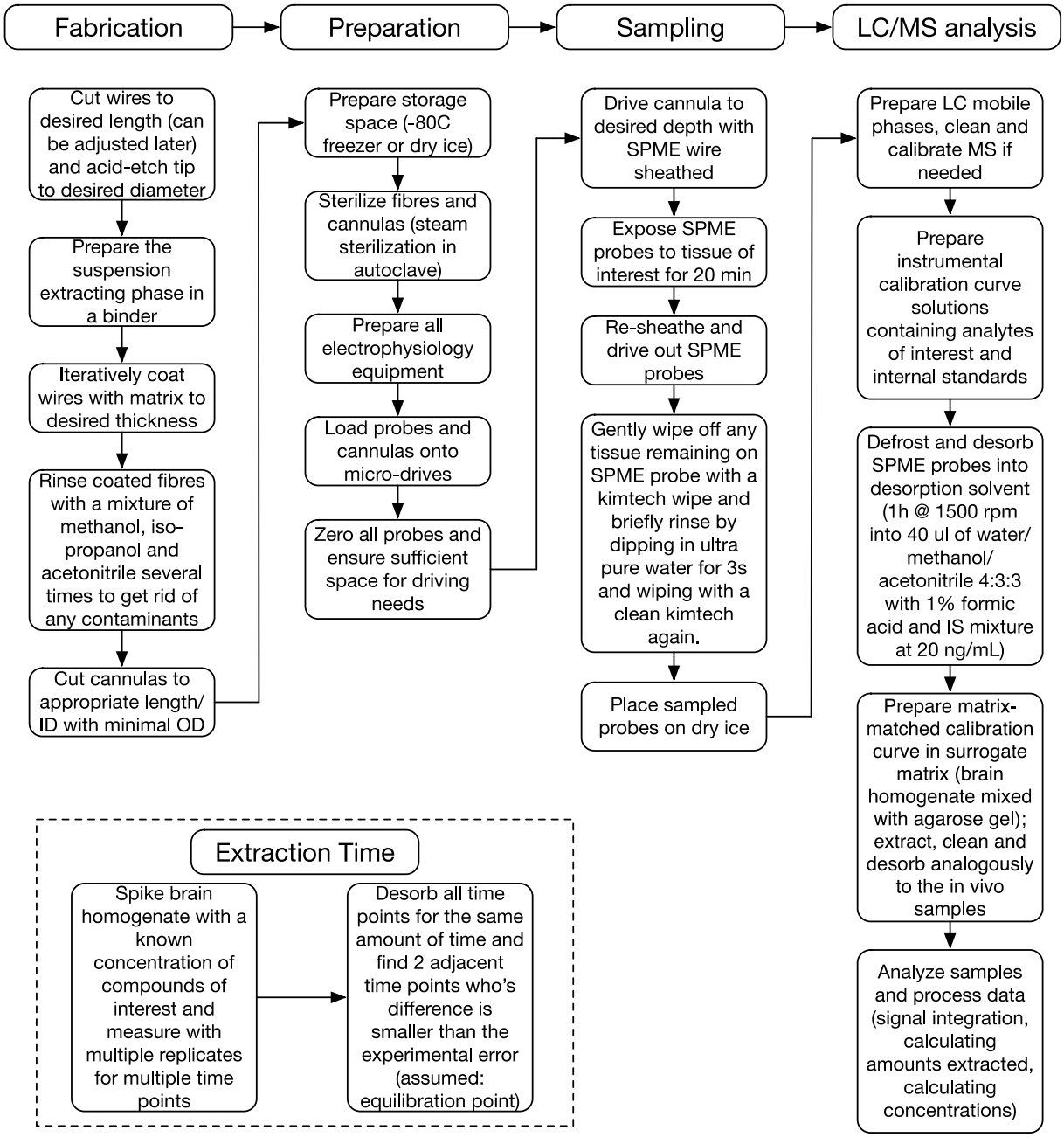

Fig A2 Experimental procedure from SPME probe fabrication to quantitation.
Fabrication described the in-house procedure to prepare SPME probes. Preparation describes experimental set- up. Sampling describes the actual data collection process. LC/MS analysis describes the chemical quantitation of collected data samples.

A.3 Tables

Table A1 A comparison of methods capable of measuring single or multiple neurochemicals in vivo.

	PET imaging	**Electro-chemistry**	**Micro-dialysis**	**Solid phase micro-extraction**
Temporal Resolution	Minutes	Highest (millisecond range)	1-30 minutes; dependent on MS sensitivity, target etc.	<5-30 minutes; dependent on MS sensitivity, coating thickness, target etc.
Spatial Resolution	Voxel	High; surface area may vary (relevant for enzyme based methods)	Diffusion based; surface area may vary	Diffusion based; surface area may vary
Sensitivity	Indirect measurement via competitive radiolabeled species	High	Depending on post-hoc methods (i.e. MS)	Depending on post-hoc methods (i.e. MS)
Neuro-active targets	A few at most	A few at most	Many	Many
Non-neuro-active targets	No	No	Yes, greater efficacy for hydrophilic compounds	Yes, greater potential efficacy for hydrophobic compounds
In vivo feasibility	Difficult in awake, behaving animal models; movement highly restricted	Good (low reliability in NHPs)	Good, often requires chronic implant of cannula for repeated measurements	Very good; robust placement of multiple simultaneous probes and repeatable acute measurements
Cost	High	Requires special equipment	Requires special equipment	Easy to port to an acute micro-electrode setup; requires a chemistry core

Table A1 Temporal resolution, spatial resolution, sensitivity, capability to measure neuro-active and non-neuro-active compounds, in vivo feasibility and cost. PET: positron emission tomography; NHP: non-human primate; MS: mass spectrometer.

Appendix B: Supplemental information for Chapter 3

B.1 Supplemental methods

B.1.1 Ethics Statement

All animal related experimental procedures were in accordance with the National Institutes of Health Guide for the Care and Use of Laboratory Animals, the Society for Neuroscience Guidelines and Policies, and approved by Vanderbilt University Institutional Animal Care and Use Committee.

B.1.2 Animals

Three adult male rhesus macaques (*Macaca mulatta*; ~8-15 kg, 6-9 years old) were used for this experiment. They were cognitive cognitively assessed at the same time of day for ~20ml/kg fluid reward. All of the monkeys were pair-housed, except for monkey Si, who was individually housed with protected contact. This allowed all monkeys to have grooming access and social bonding with a compatible partner. An Institutional Animal Care and Use Committee-approved enrichment plan was used for the monkeys involved in this experiment. Four categories of enrichment were utilized: social, structural, sensory and feeding. Both the macro- and microenvironments are involved in the enrichment plan. Prior to this experiment, monkeys Ig and Wo had been exposed to an experimental positive allosteric modulator. Otherwise, subjects were naïve to donepezil and other neurological or psychiatric medications.

B.1.3 Drug Procedures

For the double blinded drug administration, one experimenter prepared drug doses while another handled injections and observations for potential side effects using a modified Irwin-rating scale. Ratings were assigned on a scale of 0, 1, or 2 per monkey reflecting no change, a slight change or a significant change respectively. Donepezil volumes were separated into vials for storage, and were sonicated and vortexed with sterile saline immediately before injection.

Depending on the weight of the animals, the appropriate volume (0.1-0.7 ml) of donepezil was then drawn for the planned injection dose; all daily injections were thus prepared together.

B.1.4 Visual Stimuli

The behavioral tasks used 3-dimensionally rendered visual objects, so called quaddles, which varied in four visual feature dimensions (shape, color, pattern, and arms of a 3D rendered object) described in detail elsewhere (Watson et al., 2019b). Each visual feature dimension can be parametrically changed which we then used to generate a number of variants, feature values, of each of the mentioned visual features (e.g. up-, and downward bended arms with blunt pointy or flared shape). From here on out, we will refer to the used visual feature spaces as 'feature dimensions' and any specific variant of each visual feature as 'feature values'. During training, all monkeys were exposed to a so-called 'neutral' quaddle object composed of a spherical shape, grey color, uniform pattern, and straight arms, which were features values that were never rewarded and served as a null feature value for each dimension. Therefore, to practically achieve objects with only color and pattern feature dimensions, and therefore without shape and arms, we kept the shape and arm dimension constant at the neutral quaddle's value for shape and arms while having color and pattern feature values that were different from the neutral quaddle's color and pattern.

B.1.5 Behavioral Tasks

Monkeys performed a visual search (VS) task and a feature-reward learning (FL) task in each experimental session. For each experimental session and for the VS task, we selected randomly 3 feature dimensions from the pool of 4 possible dimensions (shape, color, pattern, arms) and we chose randomly 3 feature values per dimension (e.g. the 3 shape feature values pyramidal, oblong and cubical) (**Figure 3.1Bi**). Stimuli, task protocols, and Matlab analysis procedures and the USE software are available online at
http://accl.psy.vanderbilt.edu/resources/analysis-tools/unifiedsuiteforexperiments/.

Visual search with different target-distractor similarity. The VS task quantified how much visual distractors slow down the detection of a target object and how the distraction varied with

the feature similarity of targets and distractors. The task required finding a cued object amongst distractors on the screen by touching it for a minimum of 0.2s. At the beginning of each VS block, the monkey learned which object is the target object in 10 familiarization trials that presented the target object without any distractors. Touching the object triggered fluid reward. The target was always an object that varied in three feature dimensions from the feature values of the neutral object, i.e. a so called 3-D target. This is proceeded by 100 trials, each with a random counterbalanced distribution of 3/6/9/12 distractors. Distractors were also 3-D objects with feature values selected at random and thus could share 0/1/2 features with the rewarded object and could be identical to other distractors within the same trial. If the distractors were dis-similar from the target, independent of the number of distractors, trials may have a pop out effect with the target being easily distinguishable while if distractors were similar to the target, trials may resemble a conjunction search more closely (**Figure 3.2A**). Objects are presented at random within the intersections of a 4x5 grid (example trials in **Figure 3.1Bii**).

Individual VS trials are initiated via a 0.3-0.5s long touch to a centrally presented blue square that is 3° radius wide with a side-length of 3.5 cm (baseline). This was then followed a 0.3-0.5s period where the blue square disappears and there are no objects on screen except for the background image. The task objects are then presented allowing the animal to freely explore for a maximum of 5s (search + selection). During this 5s window, the animal could at any point touch and hold for 0.2s an object in order to select it. The selected object would then prompt both visual and auditory feedback 0.2s after the selection lasting 0.5s. The color of the visual feedback and the pitch of the auditory feedback correspond to the valence of the selected object's value either signaling a correct or incorrect choice. Correct choices were followed by fluid reward (water) (**Figure 3.1C**).

The VS task at the beginning and end of the experimental session utilized targets and distractors that were composed of features from the same 3x3 feature space. Targets were never identical between these two blocks but may appear as distractors in the other VS block. Similarly, all distractors were created at random from the same 3x3 feature space as well and therefore would be similar between the two blocks. The background image of the two VS blocks always differed and acted as a cue for the VS rule set but are different in order to prevent the association of the

rewarded target object with a particular background image. Thus, the first and second VS search block varied in the target object pulled from the same 3x3 feature space, the background image, as well as the timing of their occurrence being at the start or the end of the daily session (**Figure 3.1Aii**).

Feature-reward learning at different distractor load. The FL task quantifies how fast and accurate subjects adjust to changing reward rules, indexing cognitive flexibility. The task required monkey to learn by trial-and-error which object feature is associated with reward. The same feature remained rewarded within blocks of 35-60 trials. Monkeys had to choose one amongst three objects (1 target and 2 distractors) where a single feature value in a single feature dimension is linked to reward with a p = 0.85 reward probability. Distractors contain the same dimensions as the target but have different, non-repeated feature values. All objects are presented in 1 of 8 possible locations randomly, all with 17 degrees eccentricity from the central touch location (example trials in **Figure 3.1Bii**). With one experimental session we ran 21 FL blocks. The feature-reward association must be learned through trial and error and may switch after 35, 40, or 45 trials from the start of the block if the learning criterion is reached (80% over 10 trials) or in 60 trials otherwise (uniform max FL block trial number). Block changes are un-cued but can be inferred if there is a change in the object feature dimensions presented and the newly rewarded feature value may be in the same dimension or a different dimension relative to the previously rewarded feature value; the two types of shifts are semi-randomly determined to occur in similar frequencies. The temporal structure and sequence of epochs in the FL task is the same as the VS task.

The structure of the trials within the FL task was very similar to that of the VS task. Trials are initiated in a similar manner via a 0.3-0.5s touch on a central blue square. This is followed by a 0.3-0.5s period where the blue square is not present and task objects have not yet been made visible yet. Three task objects are then presented for up to 5 sec during which at any point the subject is allowed to make a 0.2s touch and hold on an object to select it. Following a 0.2s delay after the selection of an object, auditory and visual feedback as well as potentially fluid reward are presented for 0.5 s. The pitch of the auditory feedback and the color of the visual feedback vary depending on the presence of reward and not on making a high reward probability choice (**Figure 3.1C**).

B.1.6 Neurochemical Quantification of Drug Effect

To confirm the bioactivity of donepezil in the brain we measured the neurochemistry in the prefrontal cortex and the head of the caudate nucleus after intramuscular administering a low (0.06 mg/kg) and high (0.3 mg/kg) dose of donepezil. We used biocompatible microprobes that sampled the local neurochemical milieu with the principles of solid phase micro-extraction (SPME) probes (Pawliszyn, 2000) previously shown to provide comparable and complimentary outcomes to micro-dialysis (Cudjoe et al., 2013; Cudjoe and Pawliszyn, 2014). These probes sampled the drug and metabolites of the neurotransmitters (e.g. choline) via diffusion until an equilibrium is reached with the extracellular concentrations with minimal damage and disturbance to the studied biochemical environment. The detailed procedures used here are described in (Hassani et al., 2019). In brief, for each brain area a microdrive was prepared holding a cannula and SPME probe inside it, as well as a microdrive with an electrode to record activity prior to SPME sampling. The electrode was driven to the target location in prefrontal cortex / striatum. The target location was confirmed by measuring spiking activity of neurons from the electrode. The cannula shielded SPME was then lowered to just above the target area and the SPME probe was then exposed to gray matter of the target area for 20 minutes before being retracted into their respective cannula and drive back out of the brain. Samples were then stored in a -80°C freezer, stored for less than 2 weeks and shipped overnight in dry ice to Waterloo, Ontario (Canada) where they were desorbed and underwent liquid chromatography separation and mass spectrometry quantification.

The SPME probes were desorbed into 50 µL of acetonitrile/methanol/water 40:30:30 solution containing 0.1% formic acid and internal standard citalopram-D_6 at 20 ng/mL for 1 h with agitation at 1500 rpm. The liquid chromatography with tandem mass spectrometry analysis was carried out using an Ultimate 3000RS high-performance liquid chromatography system coupled to a TSQ Quantiva triple quadrupole mass spectrometer (Thermo Fisher Scientific, San Jose, CA, USA). Data acquisition and processing were performed using Xcalibur 4.0 and Trace Finder 3.3 software (Thermo Fisher Scientific, San Jose, CA, USA). The chromatographic separation employed Hypersil Gold C18 column, 50 x 2.1 mm, 1.9 µm particle size (Thermo Scientific, Ashville, NC, United States) held at 35°C. The aqueous mobile phase (A) consisted of water/acetonitrile/methanol 90:5:5 with 0.1 % formic acid, while the organic mobile phase (B)

consisted of acetonitrile/water 90:10 with 0.1% formic acid. The following chromatographic gradient at a flow rate of 400 µL/min was applied (%B): 0-0.5 min 0 %; 0.5-3 min linear gradient to 100 %; 3-3.65 min held at 100 %; 3.65-3.7 min linear gradient to 0 %; re-equilibration at 0 % until 4.5 min. The injection volume was 5 µL. The mass spectrometry analysis was performed in positive ionization mode under selected reaction monitoring conditions; for the analyte donepezil the quantifier transition monitored was m/z 380.3 -> 243.2 and the qualifier transition was 380.3 -> 91.1, while one transition at m/z 331.1 -> 109.1 was monitored for internal standard citalopram-D_6. The capillary voltage was set at 3.5 kV, with the remaining electrospray source conditions set to the following values: vaporizer temperature 358 °C, ion transfer tube temperature 342 °C, sheath gas pressure 45, auxiliary gas pressure 13, and sweep gas pressure 1 (arbitrary units). The instrumental stability throughout the sequence was monitored by analysis of an instrumental quality control sample consisting of the target analyte and internal standards spiked into a neat desorption solvent at 20 ng/mL.

The concentration of donepezil in brain tissue was determined using a modified external surrogate matrix-matched calibration approach developed in previous work (Hassani et al., 2019; Lendor et al., 2019a, 2019b). The surrogate matrix consisted of agarose gel (1% agarose in PBS solution, *w/v*) mixed with lamb brain homogenate in the ratio 1:1 (*v/w)*. Prior to combining the agarose gel with the brain homogenate, the latter was spiked with donepezil in the concentration range 5-750 ng/g. Extractions were carried out in static mode from 1g of the matrix with extraction time matching the *in vivo* experiments. The probes were subsequently rinsed with water and desorbed into 50 µL of the desorption solvent containing internal standard citalopram-D_6 at 20 ng/mL. The analytical response in the form of relative peak area ratios (analyte to internal standard) was converted to amounts extracted by employing an instrumental calibration curve consisting of donepezil in neat desorption solvent in the range 0.1-100 ng/mL. The resulting matrix-matched calibration curve was expressed as amounts extracted in the function of concentration in tissue. A weighted linear regression equation was fitted to the analytical response in the function of concentration. Limits of quantitation were determined as the lowest concentration of analyte producing a signal to noise ratio ≥ 5, with a relative standard deviation of 4 replicate measurements below 20%, and accuracy within 20%. Accuracy was calculated as the relative percent error of concentrations of analytes in the calibrator samples determined experimentally with the use of

calibration curves versus theoretical (spiked) concentrations (Food and Drug Administration (FDA), 2001).

A single, fourth, *Macaca mulatta* (male, 8 years old) with an implanted recording chamber above the left hemisphere was chaired, head-fixed and performed the VS task (data not included in analysis) to emulate performance by the other 3 subjects. Details about the surgical implantation of the recording chamber and headpost are reported in (Hassani et al., 2019). Performance of the VS, virtually identical to the VS task reported above, was done with eye saccades using a Tobii Spectrum eye tracker instead of touch screen. Subject underwent 6 instances of both 0.06 and 0.3 mg/kg donepezil dosing in the primate chair at the same time of day as the other 3 non-human primates received donepezil. Injections were done after the animal had been performing one VS block for roughly 20min, followed by a 15min period of quiet wakefulness after which they proceeded to do a second VS block. SPME sampling events took place once at the beginning of each VS block with probes being exposed to tissue for 20min in both instances.

During each SPME sampling event heart rate was monitored using a pulse oximeter (PalmSAT 2500, Nonin Inc, MN), with the sensor clipped at the ear lobe of the subject and a sampling rate of 0.25 Hz. Heart rate data was collected 20 min before task start both before and after donepezil injection. The data was smoothed with a centered 8 sample window (40 sec) with 1 sample shifts (4 sec) and normalized to the average heart rate 5 min before task start.

B.1.7 Literature Surveys

In order to place our results within the broader published work, we identified nine papers involving donepezil and non-human primates (Rupniak et al., 1997; Buccafusco et al., 2003, 2008; Buccafusco and Terry, 2004; Tsukada et al., 2004b; Callahan et al., 2013; Uslaner et al., 2013; Lange et al., 2015b; Vardigan et al., 2015) and summarize the papers' main results, tasks used, donepezil dosages and administration methods in **Table B1**. Notably, six of the identified papers provided donepezil in conjunction with other pharmaceutical agents such as scopolamine. The papers were found by conducting an online search of the NIH (PubMed) database, as well as google scholar. The keyword search terms of 'Donepezil', 'Aricept' and 'E2020' were used with

the terms ‘NHP’, ‘monkey’, ‘primate’, ‘cognition’, and ‘brain’ or some combination of them. We did not consider eight studies that utilized donepezil in primates but lacked a cognitive component. They did however provide insight in dosing ranges for different dosing routes, dose-limiting side effects and donepezil’s kinetics (Tsukada et al., 1997, 2000, 2001; Nishiyama et al., 2001; Shiraishi et al., 2005; Asai et al., 2009; Kikuchi et al., 2010; Gould et al., 2020).

In order to make explicit the larger variety of tasks and results in donepezil studies in rodents we conducted a similar literature survey as for the nonhuman primate and summarize the results for nine studies in **Table B2** in the same format as **Table B1** (Luine et al., 2002; Csernansky et al., 2005; Prickaerts et al., 2005; Spowart-Manning and van der Staay, 2005; Bartko et al., 2011; Romberg et al., 2011; Podkowa et al., 2015; Shin et al., 2018). These papers were chosen to showcase the variety of tasks used in the rodent field to quantify donepezil’s effect on behavioral and cognitive variables. The literature survey also illustrates a variety of tools utilized to model dementia including genetic lines, bilateral-lesions and scopolamine. These papers were found by conducting a similar online search as described above but with key words of ‘rodent’, ‘mouse’ and ‘rat’ to replace ‘NHP’, ‘monkey’ and ‘primate’.

B.1.8 Data Analysis

All behavioral analysis was completed using MATLAB (Mathworks Inc., MA).

Analysis of Visual Search. The set size effect of the VS performance was either defined as proportion of correct trials by the distractor number or by the average target-distractor (T-D) similarity of trials. The set-size effect was estimated by a linear regression which is specified as either utilizing distractor number or T-D similarity. The average T-D similarity of a trial was calculated by averaging the number of shared feature values (0/1/2) of all distractors in said trial to the target. Reaction times, referred to as choice RTs for the VS task, were defined as the time from the initiation of a trial by pressing and holding the central blue square to the initiation of touch to the selected object leading to feedback. Reaction time data only takes into consideration rewarded trials. Descriptive statistics are provided as means with ±SEMean unless specified otherwise. Similarly, error bars in figures are either mean ±SEMean or median ±SEMedian unless

specified otherwise. After pooling data from all three subjects, the measure of interest is averaged across appropriate trials or blocks to get a per session value.

Analysis of Feature-Reward Learning. FL blocks were either labeled as 'low distractor load' if no distracting feature dimension was present, or as 'high distractor load' if a single distracting feature dimension was presented alongside the feature dimension to which the rewarded feature value belonged to. We calculated learning curves by averaging smoothed trial-wise performance aligned to block reversals. We defined learning speed by calculating at which trial, since block start, the subjects started performing at ≥80% over 10 trials, the maximally rewarded object. This trial was termed the 'learning point' (LP). For analysis, blocks were excluded if the monkey took a break of at least several minutes. Furthermore, blocks were excluded where the LP was calculated to be trial 1 (reflecting ≥80% performance in the first 10 trials since reversal) as well as if the LP occurred beyond the 40^{th} trial. Reaction times, referred to as choice RTs for the FL task, were temporally defined the same as for the VS task and also only include rewarded trials.

Perseverative errors were defined as two or more consecutive choices of low probability rewarded objects with at least 1 shared feature value. Analysis of perseverative errors for feature values in the same feature dimension as the target feature are separated from those where the perseverated feature value was in the distracting dimension. For perseverative errors to occur in the distractor dimension, the block is required to contain a distracting dimension to begin with and is therefore necessarily a high distractor load block. Perseverative errors in the target feature dimension could occur in both low and high distractor load blocks.

B.1.9 Statistical Analysis of Drug Effects

Comparisons between vehicle and donepezil doses (0.06, 0.1 and 0.3 mg/kg) were done for all doses combined followed by post-hoc pair-wise statistics with multiple comparisons corrections unless specified otherwise. Probability level of less than 5% ($p < 0.05$) was considered statistically significant.

Descriptive statistics for individual performance measures is reported and significant tests for individual differences stated where appropriate. The data is pooled between all 3 monkeys for analyses. For comparing visual search task performance as a function of distractors per trial, data was averaged and pooled across blocks, a comparison of donepezil and vehicle for each block number was done by ANOVA (**Figure 3.1D**). Performance at specific donepezil doses were compared to vehicle performance in the first of the two visual search blocks only using ANOVA with corrected (Tukey's) post-hoc tests (**Figure 3.1E**). The slopes of the linear fits (Pearson coefficients) for each session's first block for each donepezil dose and vehicle were compared by a Kruskal-Wallis test with a corrected (Tukey's) post-hoc test (**Figure 3.1F**). Similarly for comparing visual search performance as a function of target-distractor similarity, first block performance at specific donepezil doses were compared to vehicle via ANOVA with a corrected (Tukey's) post-hoc test (**Figure 3.2B**). The same process was used for evaluating reactions times (**Figure B4A**). The separation of trials from the first block by both distractor number and target-distractor similarity also utilized ANOVAs to evaluate change in performance (**Figure 3.2D**) as well as reaction times (**Figure B4B**). Similar to distractor number, slopes of the linear fits (Pearson coefficients) for each session's first visual search block performance as a function of target-distractor similarity for each donepezil dose and vehicle were compared using a Kruskal-Wallis test (**Figure 3.2C**). For speed of processing, block average data was pooled and an ANOVA was applied (**Figure B1A**). Similarly, for reaction times measures in the visual search task, block average data was pooled and an ANOVA was applied (**Figure B1B**), with dose specific comparisons in the first visual search block only being done via ANOVA as well (**Figure B1C**). Linear fits (Pearson coefficients) for reaction times as a function of distractor numbers were computed on a per-session basis and compared via a Kruskal-Wallis test (**Figure B1D**). All reported correlations values are Pearson coefficients, with correlations being done on a per session basis (**Figure B2, B3)**.

For the feature-reward learning task, LP were pooled in temporally separated thirds of blocks and compared to vehicle via ANOVA with pairwise comparisons done via corrected (Bonferroni) Wilcoxon rank sum tests taking into consideration either only low distractor load blocks (**Figure 3.3C**) or only the first third of feature-reward learning blocks (**Figure 3.3D**). Similarly for the reaction times in the feature-reward learning task, the first third of blocks were

pooled and the effects of donepezil at its tested doses relative to vehicle was evaluated via ANOVA followed by a corrected (Tukey's) post-hoc test (**Figure 3.3E**). Perseverative errors were pooled across sessions, only taking into account the first third of blocks, and compared in a pair-wise fashion using Wilcoxon rank sum tests. Correlations between the visual search and feature-reward learning tasks reported as Pearson coefficients (**Figure 3.4**). The collected donepezil concentrations per area per dose were compared via ANOVA (**Figure 3.5A**). The choline concentrations, relative to vehicle for each tested brain region utilized Wilcoxon rank sum tests and then again when comparing different doses within each area (**Figure 3.5B**). Heart rate data utilized t-tests to compare baseline to post-injection values as well as comparing the post-injection values between doses (**Figure 3.5C**).

B.2 Supplemental results

B.2.1 Overall Visual Search Performance

We performed and report here the results of various analysis to evaluate the overall performance of the animals on the tasks, or to test specific performance metrics that provide a more comprehensive overview of how the drug conditions did or did not affect task performance.

For the visual search task, 10 familiarization trials with no distractors were presented prior to each of the two visual search blocks. The reaction times to detect these single objects on the screen will be referred to as speed of processing (SoP). They were completed in 628 ms ±133 (Ig: 616 ms ±8.5; Wo: 693 ms ±6.6; Si: 588 ms ±5.3) with the first block having faster SoP at 611 ms ±7.7 relative to the second block with 646 ms ±4.8 ($p < .001$)(**Figure B1A**).

On average, monkeys performed the VS task with 84.4% (± 0.54) accuracy (Monkey Ig: 85.2% ±0.81; Wo: 88.3% ±0.94; Si: 79.8% ±0.97) and with 1158 ms ±9.7 search times (Ig: 1281 ms ±18.3; Wo: 1171 ms ±15.9; Si: 1020 ms ±13.3). Increasing numbers of distractors slowed search RTs, with 3/6/9/12 distractors having 1019 ms, 1216 ms, 1409 ms, and 1552 ms search times respectively (Distractor Number $F(3,1240) = 241.32$, $p < .001$) as well as decreasing accuracy, with 3/6/9/12 distractors having 91.7% ±0.6, 87.1% ±0.6, 82.9% ±0.8, and 80.0% ± 0.9

accuracy respectively (all pair-wise comparisons were significant using Tukey's HSD multiple comparisons test among proportions at an alpha of 0.05, except for 0.1 mg/kg donepezil dose and vehicle). Search RTs did not vary significantly with regards to VS block number (Block Number $F(1,1240) = 3.18$, n.s.) (**Figure B1B**) while trial outcomes did vary significantly with VS block number ($F(1,1722) = 22.19$, $p < .001$) (**Figure 3.1D**). This difference in performance between the two VS blocks may be due to fatigue, as reflected by the significantly reduced SoP, or otherwise satiation.

Both the change in search time and performance by distractor number were fit by a linear regression, revealing that each additional distractor increased search duration on average by 60 ± 1.6 ms (Ig: 72 ± 2.7 ms/distractor; Wo: 57 ± 2.8 ms/distractor; Si: 49 ± 2.1 ms/distractor) as well as decreasing performance by 1.3% ± 0.1 per additional distractor (Ig: 1.2% ± 0.1; Wo: 0.9% ± 0.1; Si: 1.8% ± 0.1) (inlets in **Figures 3.1D and B1B** show individual monkey fits for vehicle). The set size effect on search RT was on average larger in the first than the second VS block (first VS block: 63 ms/distractor; second VS block: 56 ms/distractor; $p = .0254$; Ig: $p = .0604$; Wo: $p = .0401$; Si: $p = .7199$). The set size effect on performance was on average the same in the first and the second VS block (first VS block: -1.3% change in performance per distractor; second VS block: -1.3% change in performance per distractor; p = n.s.; Ig: p = n.s.; Wo: p = n.s.; Si: p = n.s.).

We analyzed how the similarity of distractors with the target influenced search RT and performance. Distracting stimuli could have 0, 1 or 2 shared feature values with the target and the thus some trials could provide a greater challenge for the monkeys given the average target-distractor similarity (T-D similarity)(**Figure 3.2A**). We found that search RT increased with average T-D similarity from 1227 ms ±9 to 1410 ms ±7 and 1334 ms ±17 for low, medium and high T-D similarity respectively (T-D similarity $F(2,14467) = 107.1$, $p < .001$)(**Figure B4A**). VS performance decreased with T-D similarity from 92.9% ±0.4 to 85.5% ±0.3 and 81.6% ±1.0 for low, medium and high T-D similarity respectively (T-D similarity $F(2,672) = 16.17$, $p < .001$) (**Figure 3.2B**). Both distractor number, and T-D similarity impact VS performance significantly (Distractor number $F(3, 2615) = 28.85$, $p < .001$; T-D similarity $F(2, 2615) = 64.59$, $p < 0.001$) but no significant interaction was found between the two variables (T-D similarity x Distractor number $F(6,2615) = 0.69$, n.s.)(**Figure 3.2D**) with VS RT showing a similar relationship with significant

main effects (Distractor number $F(3, 2530) = 242.2$, $p < 0.001$; T-D similarity $F(2,2530) = 18.75$, $p < .001$) but not interaction ($F(6,2530) = 0.85$, n.s.)(**Figure B4B**). Individual sessions also showed no strong correlation between the set size effect of performance by distractor number relative to the set size effect of performance by T-D similarity (Pearson, n.s.)(**Figure B3**).

B.2.2 Overall Feature Reward Learning Performance

For the feature reward learning (FL) task, monkeys reached learning criterion on average in 63 ±1% of the 21 daily learning blocks (Ig: 71 ±1%; Wo: 61 ±2%; Si: 56 ±1%) once exclusion criteria were applied (see methods). Learning criterion was reached more often in the low distractor load than high distractor load blocks with proportion of learned blocks being 70% and 56% respectively (Ig: 80 vs 62% of blocks; Wo: 66 vs 56%; Si: 63 vs 49%). Average learning curves for low and high distractor load blocks of each individual monkey, as well as the average across monkeys is provided in **Figure 3.3A**. Monkeys reached the learning criterion on average within 12.5±0.2 and 15.6±0.2 trials in the low and high distractor load condition (Ig: 9.9±0.2 and 14.9±0.3; Wo: 13.5±0.4 and 17.0±0.4; Si: 14.9±0.4 and 15.0±0.4). The average choice reaction time of a correct FL trial was 986 ±2 ms with faster reaction times in the low than high distractor load blocks ($p < .001$; 965 ±3 ms and 1013 ±3 ms respectively).

B.2.3 Visual Search Performance with Donepezil

The SoP (reaction time to a single object during familiarization trials) showed a significant main effect of block number ($F(1,424) = 6.29$, $p < .001$), as well as a significant main effect of drug condition ($F(3,424) = 15.16$, $p < .001$)(**Figure B1A**). Pair-wise statistics comparing the first block SoPs of the control condition and 0.06, 0.1 and 0.3 mg/kg doses (Tukey's, n.s, n.s, and $p < .001$ respectively) suggests that the main effect of condition is driven by the 0.3 mg/kg dose SoP.

B.2.4 Feature-Reward Learning Performance With Donepezil

For the low distractor load condition the proportion of learned blocks were on average 72.3% ±1.4, 75.2% ±2.4, 78.0% ±3.9 and 75.9% ±3.2 in the vehicle, and 0.06 / 0.1 / 0.3 mg/kg)

days, which was not significant (n.s.). Similarly, for the high distractor load condition the proportion of learned blocks was 60.0% ±1.5, 74% ±4.0, 62.3% ±3.8 and 65.0% ±4.2 in the vehicle, and 0.06 / 0.1 / 0.3 mg/kg) days (n.s.). Comparisons between the proportion of blocks learned in low and high distractor load conditions revealed a significant difference for vehicle and drug conditions with more blocks learned in the low distractor load condition than in the high distractor load condition (X^2 values contrast 1D vs 2D learning blocks for vehicle, 0.06, 0.1, and 0.3 mg/kg conditions: $X^2(1, N_1 = 1757, N_2 = 1750) = 58.6$, $p < .001$; $X^2(1, N_1 = 222, N_2 = 219) = 8.2$, $p = .004$; $X^2(1, N_1 = 219, N_2 = 222) = 12.6$, $p < .001$; $X^2(1, N_1 = 209, N_2 = 190) = 5.6$, $p = .018$ for vehicle, 0.06, 0.1 and 0.3 mg/kg doses respectively). Monkey Ig had a higher overall proportion of blocks learned than both Monkey Wo and Si with vehicle ($p < .001$), however, there were no statistically significant differences between monkeys between low and high distractor loads in vehicle or any drug conditions (n.s.).

In addition to learning speed we also analyzed in detail the choice reaction times across drug conditions. Relative to the low distractor load condition, in the high distractor load condition, FL choice RTs slowed from 993 ±11 to 1060 ±14, from 964 ± 31 to 1048 ±33, from 988 ±27 to 1015 ±36, and from 1126 ±29 to 1167 ±31 ms for the vehicle, 0.06, 0.1 and 0.3 mg/kg donepezil doses respectively (**Figure 3.3E**).

There was also significant inter-subject variability in choice RTs with monkey Si having significant faster choice RTs in the FL task (Subject $F(2,1052) = 183.53$, $p < .001$)(**Figure B2C**) as well as a significant monkey-drug interaction ($F(6,1052) = 3.5$, $p = .002$). Alongside the general slowing with the 0.3 mg/kg donepezil dose (see main text), we found in a pair-wise analysis a significant slowing of search RTs with the 0.3 mg/kg donepezil dose for monkey Si (Tukey's, $p < .001$), and a significant faster search RTs with the 0.1 mg/kg donepezil dose for monkey Wo (Tukey's, $p = .003$).

The main text reports the length of consecutive, perseverative errors. Perseverative errors may occur in the same dimension as the target feature value (12% of all errors), possible in low and high attentional load blocks, or they may occur in the distracting dimension (26% of all errors) only possible in high attentional load blocks. The proportions of perseverative errors within the

target dimension were 12% ±1, 11% ±2, 12% ±2 and 11% ±2 for vehicle, 0.06, 0.1 and 0.3 mg/kg donepezil doses (n.s.), while within the distracting dimension they were 26% ±0, 23% ±6, 22% ±2, and 24% ±2 for vehicle, 0.06, 0.1 and 0.3 mg/kg donepezil doses (n.s.).

We next analyzed whether donepezil modified how flexible subjects learned a new target feature depending on whether the target feature was from a novel feature dimension and whether the target was a previous distractor. First, we asked whether donepezil modulates learning differently depending on whether a newly rewarded (target) feature values belonged to the same feature dimension as the target feature in the previous block, or to a new target feature dimension. If the target belonged to a new target feature dimension, we may suspect some enhancement based on previously shown scopolamine-induced deficits (Chen et al., 2004). This analysis quantifies whether learning a new feature set was easier or more difficult than re-assigning a reward association within the previously relevant feature set. In our task a shift to a new target feature of a new dimension should be easier because it occurred by presenting new objects that were not shown in the previous block. We thus compared learning speed for blocks where the rewarded feature dimension was not presented in the previous block and blocks where the rewarded feature value was from the same dimension as the previously rewarded feature. We found that donepezil did not alter learning for block transitions to 'new target feature dimensions' versus 'another feature of the same dimension' (Condition $F(3,2708) = 0.55$, n.s.; Block Switch $F(1,2708) = 2.7$, n.s.; Condition x Block Switch $F(3,2708) = 1.15$, n.s.).

Secondly, we quantified whether donepezil modulated how subjects learned a new target feature value when that target feature was a distractor in the previous block which has been previously shown to be impaired with scopolamine (Chen et al., 2004). Difficulties in attending a previous distractor is sometimes referred to as latent inhibition. There were only few learning blocks available in which the target feature dimension was a distracting feature dimension in the previous block which we contrasted to blocks where the rewarded feature dimension was not presented in the previous block. We found that donepezil did not alter learning speed for blocks where the 'target was a previous distractor', versus when the 'target was a new feature' (Condition $F(3,1450) = 0.31$, n.s.; Block Switch $F(1,1450) = 0.02$, n.s.; Condition x Block Switch $F(3,1450) = 0.2$, n.s.).

B.3 Supplemental Discussion

B.3.1 Non-selective slowing of response times and dose-limiting side effects

We found that 0.3 mg/kg donepezil overall slowed response times of the monkeys during visual search independent of distractor number or target-distractor similarity (**Figure B1A,C**), and during feature-reward learning independent of distractor load (**Figure 3.3E**). The slowing of reaction times was independent of overall accuracy levels (**Figure 3.4A**), which shows it did not reflect trading off speed for accuracy. The observed slowing occurred at a dose that improved attention and was unexpected, because prior donepezil studies using the delayed match-to-sample task did not report changes in reaction times (Buccafusco et al., 2003; Callahan et al., 2013), including studies involving scopolamine challenges (Buccafusco et al., 2008; Lange et al., 2015b) (**Table B1**). Our findings therefore indicate that 0.3 mg/kg of donepezil already induced cholinergic side effects while still improving cognitive processes. This interpretation is supported by our observation of arousal deficits at the 0.3 mg/kg dose that became apparent in vasoconstriction, changes in posture, visible sedation and paleness (**Table B3**). These side effects were strongest within 30 min. after administration of the drug. Although these side effects did not prevent animals from starting and completing the tasks, they limited the dose range we could test. Such dose-limiting side effects are a well known limitation of donepezil and other AChE inhibitors where therapeutically effective doses cause in a subset of patients gastrointestinal issues such as nausea, diarrhea, and arousal deficits (Wilkinson et al., 2002; Courtney et al., 2004; Jones et al., 2004; Li et al., 2019). Our finding complements this literature by showing that arousal deficits occur at a dose range that causes apparent improvements in attentional control of interference while lower doses that were void of side effects failed to improve attention. These observations might have clinical implications as they predict that lower doses of donepezil might not cause improved attention, but primarily improve cognitive flexibility.

Our finding of dose-limiting side effects and reductions in arousal or speed-of-processing emphasizes the importance of developing drugs that avoid nonselective overstimulation of intrinsic cholinergic neurotransmission. Strong candidate compounds include positive allosteric modulators (PAMs) for nicotinic subreceptors (Terry and Callahan, 2019) and for M_1 and M_4 muscarinic

receptor (Conn et al., 2009; Jones et al., 2012; Dean and Scarr, 2020; Foster et al., 2021). Subtype-specific muscarinic PAMs have no intrinsic activity at their respective receptor subtype, but act to boost normal cholinergic signaling thereby conserving the spatial and temporal endogenous ACh signaling and avoiding overstimulation of peripheral ACh receptors and subsequent adverse side effects (Foster and Conn, 2017; Gould et al., 2018; Rook et al., 2018b). Our study thus provides an important benchmark for the development of new drugs that aim to enhance multiple cognitive domains while minimizing side effects.

B.3.2 Cholinergic receptor expression profiles

Interpreting the cognitive-behavioral effects of donepezil is facilitated by considering the distributions of cholinergic subreceptors. Cholinergic receptors are divided into two broad families of metabotropic muscarinic receptors and ionotropic nicotinic receptors. Nicotinic receptors are made up of subunits with relevant ones being alpha4/beta2-containing nicotinic receptors and alpha7-containing nicotinic receptors. The alpha4/beta2 receptors can be found in the cortex and striatum, while the alpha7 receptors are more abundantly found in the cortex than the striatum while both are found at much higher concentrations in the hippocampus (Breese et al., 1997; Quik et al., 2000; Hillmer et al., 2011). The expression of M1, M2 and M4 muscarinic receptors, muscarinic subtypes most commonly found in the brain, is high within the cortex and striatum among other regions (Levey et al., 1991; Hersch et al., 1994). Despite their comparably high expression in the PFC and striatum, studies suggest that the striatum has a particularly high muscarinic binding potential (Tsukada et al., 2004b) and respond stronger to muscarinic ACh receptor activation compared with the PFC (Thorn et al., 2019). We speculate that these brain area specific neuromodulatory profiles underly the observed dose specific improvements of cognitive flexibility and attentional control of interference.

There is evidence that suggests the M5 receptor subtype is expressed on midbrain dopaminergic neurons and regulates dopamine release (Foster et al., 2014) alongside other cholinergic receptors (Zhang and Sulzer, 2012; Cachope and Cheer, 2014). The role that ACh plays in dopaminergic release is thus a potential confound when using systemic, non-specific

cholinergic agonists and AChE inhibitors such as donepezil and may contribute to the behavioral effects we observe.

The widely accepted use of scopolamine to induce cognitive deficits in monkeys (and rodents) in order to model dementia symptoms may suggest that donepezil's mechanism of action is muscarinic in nature (see **Table B1** and **B2**) and thus muscarinic (M1 receptors particularly) are a common target of pharmacological intervention for Alzheimer's disease (Verma et al., 2018). However, Alzheimer's disease is associated with a loss of cortical alpha4 and (to a lesser degree) alpha7 nicotinic receptor subunits (Court et al., 2001) and chronic donepezil administration is associated with nicotinic receptor upregulation, which suggests a role for nicotinic modulation beyond the involvement of muscarinic receptor action (Kume et al., 2005). Studies directly comparing donepezil with nicotinic agonists find some overlapping results and some differences (Luine et al., 2002).

As discussed in the main text, different dosing regimes may exert behavioral effects more strongly through nicotinic or muscarinic mechanisms and although previous studies have attempted to dissociate their relative contributions (Mirza and Stolerman, 2000), this should be expanded through further studies utilizing tasks with different cognitive demands. It is for example possible that each task may be represented by a non-parabolic function resulting from the interaction of the various cholinergic receptors and their dynamics (**Figure B5**). Such an interaction may potentially explain the lack of enhancement observed at our medium (0.1 mg/kg) donepezil dose in our visual search task.

B.3.3 Clinical relevance for aging and aging-related cognitive disorders

With aging and age-related cognitive disorders, several physiological measures are correlated with cognitive decline such as the loss of cholinergic neurons among others (Perry et al., 1978), loss of cholinergic receptors (Court et al., 2001), reduced dendritic density in the PFC (Dumitriu et al., 2010; Arnsten, 2015) and reduced regional cerebral blood flow (Hock et al., 1995). Chronic use of donepezil has been shown to lead to nicotinic receptor upregulation (Kume et al., 2005). Stimulation, within appropriate parameters, of these cholinergic PFC synapses

enhances their efficacy and may protect against age-related loss of these dendrites (Hains et al., 2015). Regional cerebral blood flow is correlated with cognitive deficits in primates (Tsukada et al., 1997, 2000) and has been shown to be rescued in aged but not young monkeys with the use of donepezil (Tsukada et al., 2004b). In general, we believe aging-related changes to the cholinergic system shifts up individuals along their optimal performance curve (as can be visualized in **Figure 2.6** or **Figure B5**) which may require a higher dose of donepezil with increasing age.

Previously, molecular and iontophoretic work has shown that at high doses, certain agonists and compounds may not be beneficial or may even act in a detrimental manner for various cognitive processes (Yang et al., 2013; Vijayraghavan et al., 2018; Galvin et al., 2020b). This is in contrast to studies where often the highest tolerated dose provides the strongest pro-cognitive effects (Cummings et al., 2013). We speculate that the reason deficits are rarely reported in the literature with donepezil is that the dose-limiting side effects prevent the usage of doses far right of the reported inverted-Us where deficits with molecular or iontophoretic methods are observed. Here we report variability in the optimal dose for different cognitive domains within the same subjects. This suggests that depending on the profile and severity of deficits in different cognitive domains, the optimal dose for addressing different types of deficits may not be the same. Our results suggest that finding the best dose for a patient will benefit from assessing multiple cognitive domains to rule out that beneficial effects of a dose for one domain does not go along with compromised functioning of another domain.

B.3.4 Time-of-testing for drug related changes of task performance

Our finding of a different dose range enhancing flexible learning and visual search is based on behavior in the first third of the experimental session in which the search task always preceded the learning task. One question is therefore whether the conclusions of our study would differ if we had alternated the task order by e.g. randomly presenting part of the FL task in the first 25 min and the visual search task in a ~12 min period after such an initial block of the FL task. However, there are reasons why varying the task order would unlikely change the results and conclusions of our study. First, the FL task learning performance at low dose was facilitated in the first ~25 min of the learning blocks (**Figure 2.2C**), which suggests that after that time at this low dose the

bioavailability of donepezil was reduced below a level that would enhance the learning task. The pharmacokinetics of donepezil suggest that the bio-available donepezil would be expected to be somewhat higher earlier in time. However, at such higher doses the FL task performance was not improved at any period tested. It is therefore unlikely that the low dose would have provided different results when tested at an earlier time after drug administration at which donepezil concentrations would be expected to be higher. Consistent with this conclusion, the learning performance in the FL-task was stable at the medium and high dose and with the vehicle over the whole session across all three time periods (**Figure 2.2C**). If the pharmacokinetics would have caused rapid changes at these doses we would have expected an improvement at later time periods of the task at which the administered high dose might have started to wane off. However, we did not see a flexible learning improvement with the medium or high donepezil dose over the ~65 min of FL learning performance. In contrast to the FL task the performance of the visual search was improved at a high dose in the first ~12 min of the session, but less at the low dose. If the search block would be performed around 25 min later (ie.g. after 25 min. of FL performance) the donepezil bioavailability would be expected to be lower. At such lower concentration we would thus expect a somewhat lower visual search improvement. However, we would not have expected an absence of an attentional effect.

In summary, the provided reasoning suggests that our results and conclusions are expected to be similar when we would have alternated the task order, showing task-dependent pro-cognitive donepezil concentrations with a low dose favoring flexible learning improvement and a higher dose improving visual search.

B.4 Figures

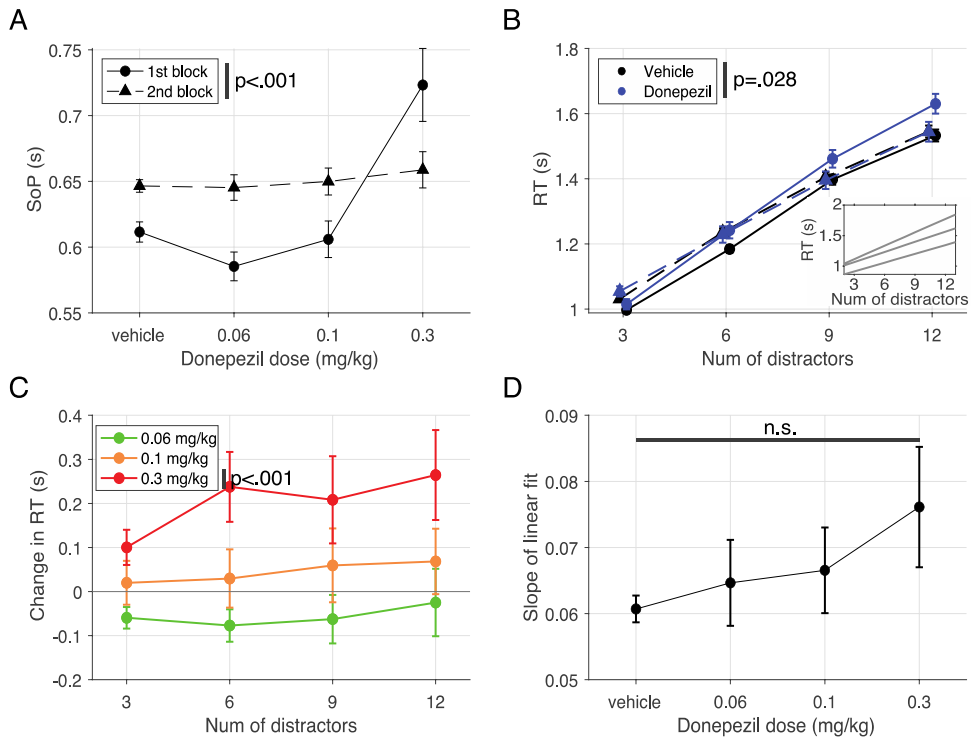

Fig B1 Search reaction time in the visual search task and its relationship with distractor number.
A. The average SoP, for each condition separated by block. The SoP is significantly changed between the first and second VS block (Block Number $F(1,424) = 6.29$, $p < .001$) as well as between conditions (Condition $F(3,424) = 15.16$, $p < .001$; ANOVA). The average SoP in the first VS block is significantly slowed with a 0.3 mg/kg dose of donepezil (Tukey's, $p < 0.001$). **B**. Average search RT per distractor number for vehicle and all donepezil doses combined, both separated by the first vs second VS block. The number of distractors slowed search RTs (Distractor $F(3,1722) = 333.1$, $p < .001$) while the VS block number did not significantly impact search RTs (Block $F(1,1722) = 0.64$, n.s.). Donepezil administration, averaged over all doses, had a significant effect on search RT (Condition $F(1,1722) = 4.83$, $p = .028$), in particular in the first VS block. The inlet shows individual monkey average search RT linear fits. **C**. The difference in search RT by distractor number between donepezil 0.06, 0.1, 0.3 mg/kg doses and vehicle for the first VS block ($F(3,896) = 15.15$, $p < 0.001$) with the 0.3 mg/kg dose having significantly slower search RT than vehicle (Tukey's, $p < .001$). Error bars are standard deviations. **D**. The set size effect of search RT by distractor number for each condition. No significant difference was observed between drug conditions and vehicle. SoP, speed of processing; VS, visual search ; RT, reaction time; n.s., not significant; Num, number.

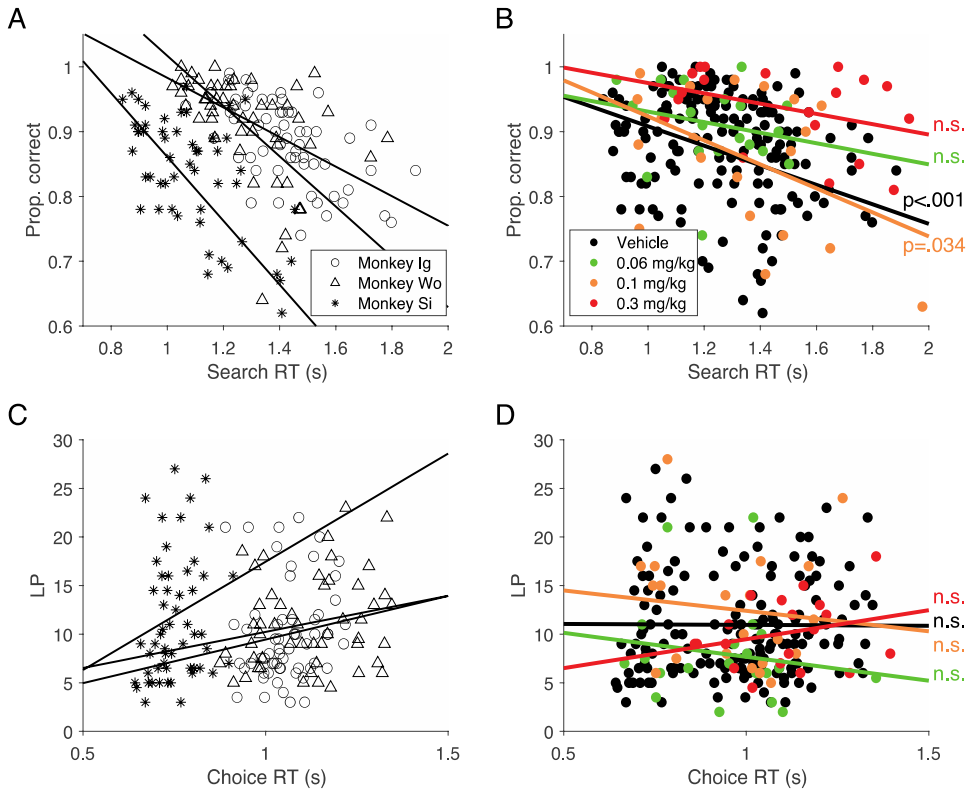

Fig B2 The relationship between performance and reaction times in both the visual search task and FL task. **A**. The session-wise correlation between VS performance and search RT by individual monkey. No difference between monkeys was found. **B**. Same as A but for all monkeys combined and separated by condition. Only vehicle and 0.1 mg/kg doses had a significant correlation, however no significant change in correlation relative to vehicle was found. **C**. Similar to A but looking at the correlation between FL performance (learning speed) and choice RT. Monkey Si was found to have significantly faster choice RTs (Subject $F(2,1052) = 183.53$, $p < .001$). **D**. The same as C but for all monkeys combined and separated by condition. No conditions exhibited significant correlations. FL, feature-reward learning; RT, reaction time; LP, learning speed; Prop., proportion; n.s., not significant.

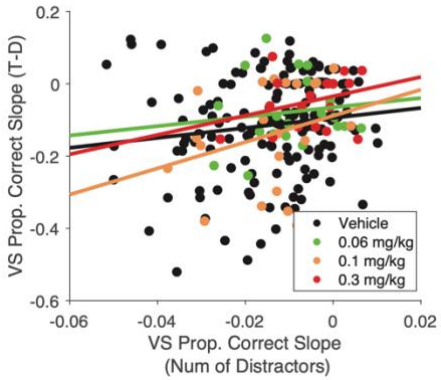

Fig B3 The relationship between the set-size effect of visual search performance as a function of distractor number versus target-distractor similarity.
Session-wise linear fits to performance by distractor number (*x-axis*) and target-distractor similarity (*y-axis*). There was no significant correlation at any condition. VS, visual search; T-D, target-distractor; Prop., proportion; Num, number.

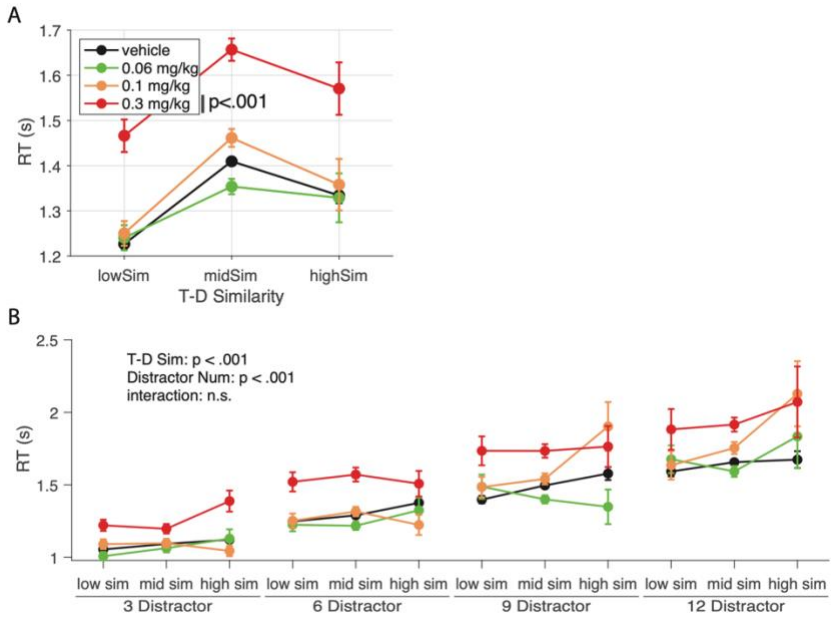

Fig B4 Search reaction times within the visual search task as a function of target-distractor similarity and distractor number.

A. Search reaction time plots as a function of T-D similarity instead of distractor number (as was the case in **Figure B1**) for vehicle and all donepezil doses. There was a significant main effect of condition with the 0.3 mg/kg donepezil dose being significantly different from vehicle ($F(3,267) = 7.75$, $p < .001$; Tukey's, $p < .001$). **B**. Visualization of the combined effect of distractor number and T-D similarity on search RT. From left to right, each cluster of lines represents increasing distractor numbers while data within each line represents low, medium and high T-D similarity from left to right respectively. Both distractor number ($F(3, 2530) = 242.2$, $p < .001$) and T-D similarity ($F(2,2530) = 18.75$, $p < .001$) impact VS performance with no significant interaction ($F(6, 2530) = 0.85$, n.s.). T-D, target-distractor; RT, reaction time; VS, visual search; Sim, similarity; Num, number; n.s., not significant.

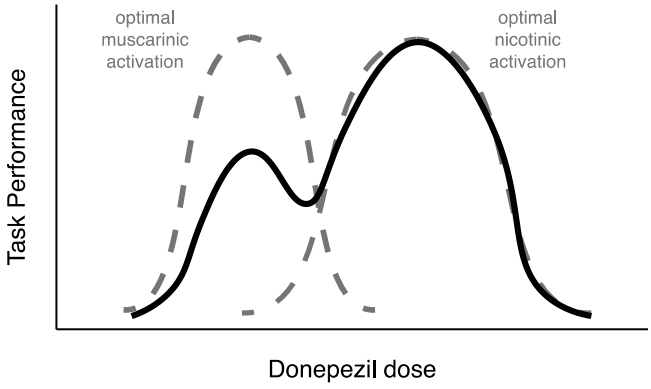

Fig B5 Theoretical curves.

A theoretical, non-parabolic curve (solid line) describing change in performance as a function of ACh concentration derived from theoretical 'optimal' inverted-U curves for specific receptor subtypes (dashed line) based on the specific task demands. These curves may be shifted by changing the task demands or a given subject may travel along the x-axis due to pharmacological intervention, aging-related changes and other mechanisms that may change their downstream receptor stimulation.

B.5 Tables

Table B1 A summary of the literature testing donepezil's cognitive effects in nonhuman primates.

Relevant Task(s)	Subject Details	Dosage & Administration	Cognitive Domain	Relevant Results	Reference
Object retrieval detour (ORD) cognition test	Macaca mulatta (male and female)	0.3, 0.56, 1, 1.8, 3, 5 mg/kg PO*	Reasoning & problem solving (exec function)	Significant interaction of trial type (easy vs difficult) and treatment. Main effect of treatment on the difficult condition	Vardigan et al., 2015
Paired-associates learning (PAL); Continuous-performance task (CPT)	Macaca mulatta (18 males)	0.3-3 mg/kg PO (PAL task); 0.1-0.25 mg/kg IM (CPT task)*	PAL: Working memory; CPT: Attention/vigilance (exec functioning)	Attenuated scopolamine-induced impairments in PAL (at 1.0 and 3.0 mg/kg PO) and CPT (at 0.25 mg/kg IM)	Lange et al., 2015
Delayed matching-to-sample (DMTS) task	Macaca mulatta (4 aged male, 3 aged female)	0.003-0.2 mg/kg PO*	Working memory	Enhanced DMTS accuracy in 'long delay' condition at 0.01, 0.025, 0.05, 0.1 and 0.2 mg/kg doses. No changes in ITI or choice latency	Callahan et al., 2013
Self-ordered spatial search	Macaca fascicularis (6 females; ~15 years old)	3 mg/kg PO*	Working memory, Attention/vigilance	Attenuated the scopolamine-induced impairments in the self-ordered spatial search task	Uslaner et al., 2013
Delayed matching-to-sample (DMTS) task	Macaca mulatta (17 male and 16 female; average ~18 years old)	10, 25, 50, 100 ug/kg IM 50-400 ug/kg PO*	Working memory	Accuracy in long delay condition with IM administration was improved	Buccafusco et al., 2008
Delayed matching-to-sample (DMTS) task	Macaca mulatta (8 male & 9 female; 9-29 years old)	10, 25, 50, 100 ug/kg IM	Working memory	Accuracy increased in medium and long delayed trials (with 25 ug/kg dose being the most efficacious)	Buccafusco & Terry 2004
Oculomotor delay response task (ODR); Visually guided saccade task (VGS)	Macaca mulatta (male; 5 ~5 years old and 5 ~20 years old)	50, 250 ug/kg IV	ODR: Working memory; VGS: attention/vigilance	ODR performance was improved in aged monkeys (not young monkeys). No changes reported in VGS (assay of motor performance, not cognition)	Tsukada et al., 2004
Delayed matching-to-sample (DMTS) task	Macaca mulatta (male & female; >20 years old)	0.01, 0.025, 0.05, 0.1 mg/kg IM	Working memory	Accuracy improved independent of drug dose but dependent on delays (improvement occurred in medium and long delays)	Buccafusco et al., 2003
Spatial delayed response task (SDRT); Visual recognition task (VRT)	Macaca mulatta (9 males)	0.01-1.75 mg/kg IM (SDRT task); 0.003-0.06 mg/kg IM (VRT task)*	SDRT: Working memory; VRT: attention/vigilance	SDRT: Donepezil rescued effects of scopolamine in difficult trials VRT: Performance was enhanced with donepezil pre-treatment (by ~10%)	Rupniak et al., 1997

PO, oral; IM, intramuscular; IV, intravenous
*: Other drugs co-administered at some/all doses.

Table B2 A summary of choice papers testing donepezil's cognitive effects in rodents.

Relevant Task(s)	Subject Details	Dosage & Administration	Cognitive Domain	Relevant Results	Reference
Y-maze	Hairless rats	3-10 mg/kg PO pretreatment*	Learning and memory, working memory	Rescued the reduced spontaneous alternation of arm entries (a measure of exploration and short term spatial memory) with donepezil pre-treatment	Shin et al., 2018
Morris water maze; radial-arm water maze	Male C57BL/6 mice	10 mg/kg IP*	Learning and memory	In the Morris water maze, donepezil did not rescue scopolamaine-induced deficits in escape latency or distance travelled. However, it reduced the number of spatial crossings in the absence of the trained platform rescuing scopolamine-induced deficits. Donepezil administration with scopolamine rescued radial-arm water maze performance early on in learning.	Podkowa et al., 2015
Paired associate learning task	Male C57Bl/6 mice	0.03, 0.1, 0.3 mg/kg IP	Learning and memory	Higher accuracy and reduced correction trials (a measure of perseveration) with 0.3 mg/kg donepezil administration	Bartko et al., 2011
5-choice serial reaction time task	3xTgAD mice	0.03, 0.1, 0.3 mg/kg IP	Attention	Rescued deficits in accuracy in 3xTgAD mice with no benefits to wild type mice. No effects reported for omissions, perseverations, or premature responses.	Romberg et al., 2011
Object recognition task	Male Wistar rats	0.1, 0.3, 1 mg/kg PO	Working memory	Administration of donepezil before, but not after, initial object presentation improved discrimination 24h later with the 1mg/kg dose performing the best.	Prickaerts et al., 2005
T-maze; locomotion; fear conditioning; shock sensitivity	male C57BL/6Hsd mice	0.1, 0.3, 1 mg/kg subcutaneous*	Learning and memory	Faster spatial and reversal learning as well as rescuing the effects of an NMDA antagonist. No effects on locomotion. More freezing as well as frescueing the effects of an NMDA antagonist. No effect on shock sensitivity.	Csernansky et al., 2005
Morris water maze	Male Wistar rats (bilateral entorhinal cortex lesioned)	0.3, 1, 3 mg/kg PO	Learning and memory, attention	Rescue of lesion induced slowing of latency and travel distance to platform in the Morris water maze with 0.3 and 3 mg/kg	Spowart-Manning & van der Staay 2005
Object recognition task; Object placement task	Female Sprague–Dawley rats	1 mg/kg/day subcutaneous	Working memory, learning and memory	Subjects explored novel objects and novel locations more with donepezil.	Luine et al., 2002

*: Other drugs co-administered at some/all doses.

Table B3 A summary of observed dose-limiting side effects.

	Donepezil	0.06 mg/kg		0.1 mg/kg		0.3 mg/kg	
	Observation	Pre-task	Post-task	Pre-task	Post-task	Pre-task	Post-task
Autonomic Nervous System	Salivation	-	-	-	-	-	-
	Lacrimation	-	-	-	-	-	-
	Urination	-	-	-	-	-	-
	Defecation (amount)	-	-	-	-	+	-
	Defecation (consistency)	-	-	-	-	+	-
	Emesis	-	-	-	-	-	-
	Miosis	-	-	-	-	-	-
	Mydriasis	-	-	-	-	-	-
	Ptosis	-	-	-	-	+	-
	Exophtalmos	-	-	-	-	-	-
	Piloerection	-	-	-	-	-	-
	Respiratory Rate	-	-	-	-	-	-
	Yawn	-	-	-	-	+	-
	Vasodilation	-	-	-	-	-	-
	Vasoconstriction	-	-	-	-	+++	-
	Irritability	-	-	-	-	-	-
	Body Temp.	-	-	-	-	-	-
Somatomotor Systems	Physical Appearance	-	-	-	-	+++	-
	Tremor	-	-	-	-	-	-
	Leg Weakness	-	-	-	-	-	-
	Catalepsy	-	-	-	-	-	-
	Visuo-Motor Coordination	-	-	-	-	-	-
	Posture	-	-	-	-	+++	-
	Unrest	-	-	-	-	-	-
	Stereotypies	-	-	-	-	-	-
	Arousal	-	-	-	-	-	-
	Sedation	-	-	-	-	+++	-
	Oral Dyskinesia	-	-	-	-	++	-
	Bradykinesia	-	-	-	-	+	-
	Dystonia	-	-	-	-	-	-

Table B3 The effect of Donepezil (0.06, 0.1 and 0.3 mg/kg IM) on autonomic and somatomotor system function were evaluated. The mean score of 3 monkeys was classified as follows: - no effect; + 0-0.15; ++ 0.16-0.3; +++ 0.31-0.45

Appendix C: Supplemental information for Chapter 4

C.1 Supplemental Materials and Methods

C.1.1 Subjects

All animal related experimental procedures were in accordance with the National Institutes of Health Guide for the Care and Use of Laboratory Animals, the Society for Neuroscience Guidelines and Policies, and approved by Vanderbilt University Institutional Animal Care and Use Committee.

Four pair-housed adult male rhesus macaques (*Macaca mulatta*), 7-11 years old and weighing ~8-15 kg were subjects in this experiment. Monkeys in each pair were separately given access to a cage-mounted Kiosk Station attached to their housing unit uniformly at either 11am (monkeys Ig and Ba) or at 1pm (monkeys Re and Si). Each monkey was overtrained and engaged with and completed a visual search attention task and a flexible feature-reward learning task via a touchscreen interface (Womelsdorf et al., 2021a) with the software being controlled by the Unified Suite for Experiments (USE) (Watson et al., 2019b).

Of the four monkeys, two (monkeys Si and Ig) had previously been involved in a similar study utilizing the acetylcholine esterase inhibitor donepezil (Hassani et al., 2021) with over 6 months between experiments for washout. Prior to the donepezil experiments, monkey Ig had also previously been exposed to a different experimental M_1 PAM. Monkeys Ba and Re were naïve to VU0453595 and other neurological or psychiatric medications.

C.1.2 Comparison table

The comparison table (Table 1) between the best dose of donepezil and VU0453595 was based on the data collected in a previous study (Hassani et al., 2021) but for all measures, identical methods were applied to both datasets consistent to what is described here.

C.1.3 Statistics

Within the feature-reward learning (FRL) task, we use trials-to-criterion to quantify learning efficiency with the criterion being defined as the first trial after at least 1 error which preceded a string of 10 trials with 70% or greater performance. The 70% performance threshold is different from our previous work (Hassani et al., 2021) which was set to 80% performance, which was and still is the criterion for block switches in the FLR task. We found this new threshold to better reflect the occurrence of learning and led to only a mean 0.37 (0 median) trial difference in baseline trials-to-criterion overall. The comparisons between VU0453595 and donepezil were made using the same definition for each measure.

Block switches in the FRL task were labelled based on the status of the target feature relative to the previous block as extra-dimensional, intra-dimensional or as involving a novel target feature dimension. For novel target blocks, the rewarded feature dimension was not present in the previous block, independent of the present or previous block's dimensionality. Similarly, intra-dimensional shift blocks involved the same rewarded feature dimension but a different rewarded feature (e.g. a different color) as the previous block, independent of their dimensionality. However, for extra-dimensional shift blocks, the previous block must have been a high load (objects varying in 2 feature dimensions) block where the current block's target feature was from the previous one's distracting feature dimension. Extra-dimensional shift blocks themselves could be either low or high distractor load.

In the FRL task, for each session, reaction times (RTs) were averaged and smoothed using a 5 trial shifting window for low and high distractor load blocks separately (**Fig. 4.2A,B**). We then defined the time to plateau as the first trial per session, excluding trial two, where the RTs began to decrease.

Perseverative errors were quantified based on the features of the erroneously chosen object. The consecutive errors could be made with objects containing the same feature from the distracting or target feature dimensions. The proportion of perseverative errors are reported as a percentage of all errors (**Fig. 4.2G,H**).

In order to account for temporally specific effects on learning efficiency with VU0453595, as seen with other cholinergic compounds (Hassani et al., 2021), we applied a linear mixed effects model (LMEM) to the trials-to-criterion. The LMEM had three main effects: experimental condition, distractor load and temporal bin (thirds), while individual monkeys were treated as random effects:

$$Trial\ to\ criterion = ExpCond \times DistractorLoad \times TemporalThirds + (1|Monkey) + b + \varepsilon$$

Given the results of the LMEM and the maximal effect size with the first third of blocks in the FRL (**Fig. C1A**), all analyses for the FRL task used only the first third of blocks to capture the period where VU0453595 had its strongest effect on performance.

Effect sizes were reported as either eta squared values when referring to ANOVA results or Cohen's d when appropriate (i.e. when post-hoc analysis showed a significant effect at a single dose). The Cohen's d was computed by directly comparing vehicle to the significant dose using this formula:

$$d = \frac{M_2 - M_1}{\sqrt{\frac{(n_1 - 1)s_1^2 + (n_2 - 1)s_2^2}{n_1 + n_2 - 2}}}$$

C.2 Supplemental Results

C.2.1 Feature-reward learning task

After reaching performance criterion, VU0453595 also resulted in higher plateau accuracy (drug condition main effect: ($F(3,1672) = 3.22$, $p = .02$; $\eta^2 = .005$); low distractor load accuracy: 90.9% (SE: 1.9%); 95.9% (SE: 0.9%); 90.9% (SE: 1.8%); 91.0% (SE: 0.7%) for 0.03. 0.1, 0.3 mg/kg and vehicle respectively; high distractor load accuracy: 74.4% (SE: 3.0%); 80.5% (SE: 2.9%); 84.8% (SE: 2.3%); 77.9% (SE: 1.1%) for 0.03. 0.1, 0.3 mg/kg and vehicle respectively)

(**Fig. C1B**). The middle dose of VU0453595 (0.1 mg/kg) also increased the proportion of blocks in which animals reached the learning criterion ($F(3,1369) = 2.93$, $p = .03$; $\eta^2 = .006$; Tukey's, $p = .02$). Animals reached the learning criterion of 80% accuracy over 10 successive trials in 90.5% (SE: 2.4; low load) and 72.1% (SE: 3.7%; high load) of blocks in the vehicle condition. Tukey's HSD multiple comparisons test among proportions revealed that at the 0.1 mg/kg dose, VU0453595 significantly increased the proportion of learned blocks in the low load condition to 98.7% (SE: 2.6%) ($p = .04$) (**Fig. C1C**).

C.2.2 Visual search task

In the first VS block, target detection times across distractor conditions were not different with VU0453595 relative to vehicle control ($F(3,944) = 1.67$, n.s.; $\eta^2 = .004$), with the exception of faster target detection times in the second VS block at the 0.3 mg/kg dose (experimental condition main effect: $F(3,944) = 3.67$, $p = .01$; $\eta^2 = .008$; Tukey's, $p < .05$). With regards to performance, in the VS block at the end of the session there were no significant effects, while in the first VS block there was a significant main effect of drug condition ($F(3,944) = 3.80$, $p = .01$; $\eta^2 = .010$) with reduced accuracy at 0.3 mg/kg dose (Tukey's, $p = .04$) irrespective of the number of distractors.

Despite the lack of set size effects, the raw target detection times were overall significantly faster with the 0.1 mg/kg dose in the second block ($F(3,708) = 4.67$, $p = .003$; $\eta^2 = .018$; Tukey's, $p = .02$) with more improvement with high target-distractor similarity (cohen's $d = -.447$) than low target-distractor similarity (cohen's $d = -.427$) (**Fig. 4.3E**). There was also a general reduction in performance during the first block ($F(3,708) = 2.84$, $p = 0.04$; $\eta^2 = 0.011$) (**Fig. 4.3F**).

C.3 Supplemental Discussion

C.3.1 Possible M_1 agonism

Although *in vitro* data suggests little to no agonistic properties of VU0453595 (Moran et al., 2018), we cannot completely rule out this possibility in the current study. At high doses, M_1

PAMs may activate M_1 receptors, even with little (sub-threshold) or no endogenous ACh. Especially in cells with high M_1 receptor expression, our macaques may be subject to M_1 agonism with the highest dose of VU0453595 tested. This may explain why the pro-cognitive effects seen at the middle dose of the three tested doses of VU0453595 are not observed at the highest tested dose. This would suggest that the endogenous signaling at the M_1 muscarinic receptor supporting cognitive flexibility is sensitive to exogenous intervention which would predict lower efficacy with orthostatic agonists. The possible agonism of M_1 PAMs such as VU0453595 *in vivo* should be the subject of future studies.

C.3.2 Possible contributions of M_1 potentiation of memory or motivation/effort control

The current study dissociated the relative importance of an M_1 PAM for cognitive flexibility and attentional filtering and contrasted these effects to those of donepezil (**Table 4.1**). The functional dissociation of the drug effects highlights the importance of a multi-task paradigm for understanding drug actions on behavior (Taffe et al., 1999; Weed et al., 1999; Hassani et al., 2021) and supports efforts to develop multi-task batteries covering a wide range of cognitive domains (Taffe et al., 1999; Weed et al., 1999; Wither et al., 2020; Palmer et al., 2021; Womelsdorf et al., 2021a). While our study tested already multiple markers of cognitive flexibility and attention, it was not yet incorporating tests of domains that M_1 modulating drugs might also affect. For example, scopolamine challenges have long suggested that M_1 receptors in the medial temporal lobe support longer-term memory processes (Broks et al., 1988; Edginton and Rusted, 2003; Ellis et al., 2006), making it possible that M_1 receptor modulation might have positive consequences in this domain.

Motivation and the ability to control effort are other domains that we did not test and which some studies have suggested to be modulated my mAChRs. The task we deployed varied cognitive load which inevitably increases difficulty and the amount of effort subjects needed to exert. Although we did not control for motivational factors explicitly, visual inspection suggested it was not modulated by VU0453595 because the learning improvements were somewhat more pronounced at lower than higher load in the learning task and did not vary with increasing distractor difficulty (target-distractor similarity) in the search task. These findings resonate with

the results of a scopolamine challenge study in NHP that found no effects of increasing difficulty in a stimulus-location association learning task (Lange et al., 2015a). However, when testing for a memory load effect with a visuo-spatial paired associate task, Taffe and colleagues (Taffe et al., 2002) found that scopolamine reduced performance particularly when 3 or 4 stimulus-object associations needed to be learned and retrieved but not when 1 or 2 associations were involved. Such a memory load differs from the cognitive load that we imposed by increasing the number of distracting features in the learning task and from the perceptual load that we varied with increasing target distractor similarity. However, it will be important to identify in future studies which motivation or load dependent processes are modulated specifically by M_1 selective mAChR modulation.

C.4 Figures

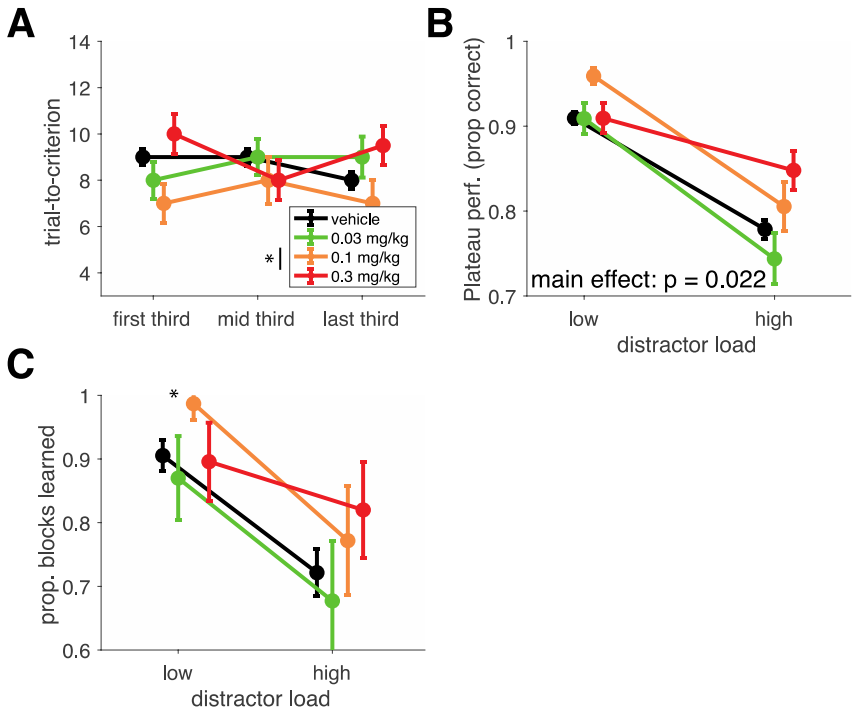

Fig C1 VU0453595 enhances multiple measures of learning performance.
(**A**) The median trial-to-criterion, visually combined for low and high distractor load conditions temporally split by their presentation within a session (7 blocks in each third) for vehicle, 0.03, 0.1 and 0.3 mg/kg doses of VU0453595. The LMEM used the experimental condition, temporal bin (thirds) and distractor load as fixed effects. There was significantly faster learning with 0.1 mg/kg which showed the strongest effect size during the first third of FRL blocks (0.1 mg/kg fixed effect: t(3674) = -2.67, p = .008; first third Cohen's d = -.228; overall Cohen's d = -.061). (**B**) Average performance in the final 10 trials of low and high distractor load blocks of the FRL task. For the low distractor load blocks, plateau performance was 90.95% (SE: 0.73), 90.90% (SE: 1.86), 95.92% (SE: 0.92) and 90.94% (SE: 1.76) for vehicle, 0.03, 0.1 and 0.3 mg/kg doses of VU0453595 respectively. For the high distractor load blocks, plateau performance was 77.86% (SE: 1.12), 74.37% (SE: 3.01), 80.54% (SE: 2.91) and 84.80% (SE: 2.34) for vehicle, 0.03, 0.1 and 0.3 mg/kg doses of VU0453595 respectively. There was a significant main effect of experimental condition ($F(3,1672) = 3.22$, $p = .022$; $\eta^2 = .005$) but post hoc analysis (Tukey's) showed no single dose as significantly different from vehicle. (**C**) Average proportion of learned blocks (defined as blocks that reached the 70% performance over 10 trials) per session in the FRL task. For the low distractor load blocks, the proportion of blocks learned was 90.54% (SE: 2.42), 87.00% (SE: 6.59), 98.68% (SE: 2.56) and 89.58% (SE: 6.11) for vehicle, 0.03, 0.1 and 0.3 mg/kg doses of VU0453595 respectively. For the high distractor load blocks, the proportion of blocks learned was 72.14% (SE: 3.71), 67.71% (SE: 9.35), 77.17% (SE: 8.58) and 82.00% (SE: 7.53) for vehicle, 0.03, 0.1 and 0.3 mg/kg doses of VU0453595 respectively. Pair-wise comparisons between the VU0453595 doses and vehicle revealed a significant improvement at the low distractor load with the 0.1 mg/kg dose (Tukey's multiple comparison test among proportions: $q = 4.082$, $q_{crit} = 3.633$) and no significant changes at the high distractor load (Tukey's multiple comparison test among proportions, n.s.).

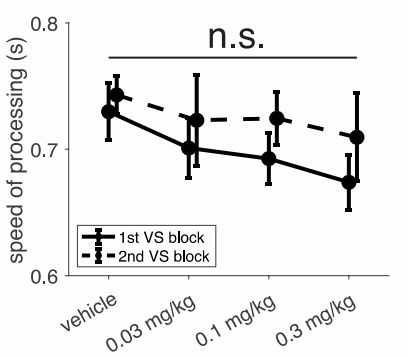

Fig C2 VU0453595 does not impact the speed of processing.
The speed of processing for the first and second VS blocks, defined as the time animals took to touch the only object on screen (during familiarization trials). In the first VS block, speed of processing was 0.730 s (SE: 0.023), 0.701 s (SE: 0.024), 0.693 s (SE: 0.020) and 0.674 s (SE: 0.022) for vehicle, 0.03, 0.1 and 0.3 mg/kg doses of VU0453595 respectively. In the second VS block, speed of processing was 0.743 s (SE: 0.015), 0.723 s (SE: 0.036), 0.725 s (SE: 0.021) and 0.710 s (SE: 0.035) for vehicle, 0.03, 0.1 and 0.3 mg/kg doses of VU0453595 respectively. No significant changes were observed for the first ($F(3,236) = .56$, n.s.) or second VS blocks ($F(3,236) = .35$, n.s.).

Appendix D: Supplemental information for Chapter 5

D.1 Supplementary Results

D.1.1 Early error commissions, attentional lapses and perseverations were unaffected by Guanfacine.

Premature fixation breaks are errors committed during covert attention deployment to one stimulus (i.e. after color onset) and before the change event (the dimming). During the 19 week testing period we found that on average 8.10 % (SE: 0.98) and 13.05 % (SE: 1.35) of trials were premature fixation breaks in the Control and Guanfacine sessions respectively, which is significantly different (Wilcoxon rank sum test, $p < 0.01$), similar to what we had found for higher doses in the dose identification phase of our experiment (see above). We next asked whether erroneous saccadic responses during the time of the stimulus change varied between drug conditions. The task design included trials in which the rewarded stimulus dimmed before, at the same time, and after the unrewarded stimulus. The pilot dose identification testing suggested that Guanfacine reduces these errors which would be a strong indication that Guanfacine acts by reducing interference from salient but irrelevant stimulus events as changes of the unrewarded stimulus when it changed before, or at the same time as the rewarded stimulus. However, we found that outside the pilot dose testing phase, the proportion of errors committed in Control and Guanfacine conditions was on average not different between those trials in which dimming occurred (1) in the unrewarded stimulus before the rewarded stimulus (Control: 0.26 (SE: 0.01); Guanfacine: 0.24 (SE: 0.01)), (2) at the same time in rewarded and unrewarded stimuli (Control: 0.30 (SE: 0.01); Guanfacine: 0.30 (SE: 0.01)), or (3) in the rewarded stimulus before the unrewarded stimulus (Control: 0.17 (SE 0.02); Guanfacine: 0.16 (SE 0.02)). To ensure that we did not miss an effect that occurred only in subsets of trials, we performed this error-saccade analysis also within sliding windows of 5 trials from trial 1 to 30 since the reversal, but did not find differences between Control and Guanfacine conditions for any trial window (data not shown).

We next confirmed the negative results from the error type analysis by comparing the performance accuracy (rather than the proportion of error subtype) in trials when rewarded and

non-rewarded dimming occurred at the same time and found that Control and Guanfacine days were in fact not different (overall accuracy on same-time dimming trials: Control: 64.89% (SE: 1.97); Guanfacine: 62.32% (SE: 1.44), Wilcoxon rank sum test, $p = 0.5019$). Likewise, there was no difference in accuracy on trials when the unrewarded stimulus dimmed before the rewarded stimulus (Control: 71.06% (SE: 1.76); Guanfacine: 69.62% (SE: 2.32), Wilcoxon rank sum test, $p = 0.9302$), and neither when the rewarded stimulus dimmed before the unrewarded stimulus (Control: 60.46% (SE: 01.84); Guanfacine: 58.68% (SE: 01.49), Wilcoxon rank sum test, $p = 0.4137$). We analyzed accuracy also with a sliding window of 5 trials from trial 1 to 30 since the reversal and did not found apparent differences between Control and Guanfacine conditions for any trial window (data not shown).

The 19 week testing period provided sufficient data to test for variations of rare behavioral errors such as perseveration errors. The monkey showed perseveration of unrewarded choices following an unrewarded trial resulting from the wrong color choice in 12.6-14.4% of all unrewarded choices (sequences of successive error trials such as CEE, CEEE, …, CEE_n). These color-based perseveration errors did not differ between Control (12.6%, SE 3.1) and Guanfacine (14.4%, SE 2.9) days (Wilcoxon rank sum test, $p = 0.066$). To test whether the animal persevered on features other than color we calculated the same percent perseverations (successively unrewarded choices) on the motion direction (e.g. successive unrewarded downward saccades to the dimming) and the stimulus location (e.g. successive unrewarded choice on the motion direction of the stimulus in the right visual field), and on combinations of all features (e.g. successive erroneous choice on the stimulus with the same color on the right side moving downward). There was no significant difference in the percentage of perseveration on motion direction (Control: 9.38% (SE: 3.10); Guanfacine: 10.75% (SE: 2.20), Wilcoxon rank sum test, $p = 0.0798$), stimulus location (Control: 10.56% (SE: 03.08); Guanfacine: 11.78% (SE 3.09); Wilcoxon rank sum test, $p = 0.2201$), or conjunctions of stimulus features between Control and Guanfacine sessions (all tests for differences, $p > 0.05$).

D.1.2 Consistency of learning benefit with Guanfacine across blocks in the experimental session.

This result of enhanced learning success during the actual learning period of the task could be robust across all blocks of a session on Guanfacine days. In another scenario, it could emerge particularly at later stages of a training session where sustained attention and motivation may benefit most from enhanced noradrenergic action. Alternatively, it may be evident only during early blocks in which the brain concentration of Guanfacine action will be relatively higher than late in the session (**Supplementary Fig. D2A,** for pharmacokinetic results of Guanfacine, see **Supplementary Results D.1.3**). We tested these alternatives by calculating the average learning trials for sets of 4 adjacent blocks relative to the first block of the day with a sliding window until block eight (which is the average number of performed blocks, see above). We then took the reverse approach and calculated the average learning trials for blocks relative to the last block of the day (see Methods). This procedure ensured that a maximal number of blocks contributed to the estimated learning success across the day. We found that relative to the first block of the day, seven of eight block sets showed an average faster learning on Guanfacine days than on Control days (**Supplementary Fig. D2B**). In contrast, we found that only four of seven block sets since the last block of a day's session showed faster average learning in Guanfacine than Control sessions. To test whether the learning effect is still robust across the behavioral sessions we used permutation statistics) (see **Supplementary Methods**), finding that the likelihood to observe faster learning in Guanfacine versus Control block sets in 11 of 15 possible block sets is significantly larger than chance (permutation statistics, $p < 0.001$) (**Supplementary Fig. D2B**).

D.1.3 Characterization of Guanfacine's pharmacokinetics using High Performance Liquid Chromatography (HPLC) and Mass Spectrometry (MS).

We characterized the pharmacokinetics of Guanfacine at the dose that we identified to be the behaviourally efficient dose (0.75mg/kg) in the dose testing phase of the experiment. In order to quantify Guanfacine's metabolism and degradation rate within the macaque model we devised a protocol in which blood samples were taken every 40 minutes for 4 hours after Guanfacine injection and the blood concentration of Guanfacine was measured using High Performance Liquid

Chromatography (HPLC) and Mass Spectrometry (MS) similar to previous studies in humans[1]. Using this method, we acquired a resolution capable of detecting as little as 30 femtomoles of drug. The procedure started with the placement of a catheder for later blood sample extraction using light anaesthesia (Dexdomitor and Ketamine) reversed with Antisedan. The awake animal was then seated in a custom primate chair and engaged in watching a movie while 300 µl blood samples were taken every 40 minutes for 4 hours (0, 40, 80, 120, 160, 200, and 240min). This time frame was well within the range of all recording sessions relative to injection. The blood samples were left in room temperature until clotting was observed, typically 30-60min, and then transported to a 4 °C fridge. Upon the final sample extraction, all blood samples were transported to a centrifuge where they were spun at 2000 rpm for 40 minutes in order to separate the serum. The serum was then aliquoted and spin filtered (3kDa molecular weight cut off) and had acid added to the sample to help with preservation. The samples were then frozen at -80 °C until the HPLC protocol was applied. Each sample provided triplicate results (technical replicate) and was loaded into the HPLC into a c18 reversed phase column where unbound protein and molecules were washed out for 15 min with 5% aceto-nitrile. Then a quick ramp up to 80% aceto-nitrile (20 min process with a period of 5 min with 80% aceto-nitrile) released the bound compounds in the HPLC column. Then the washed solution was subjected to a multi reaction monitoring protocol using a MS causing the breaking of Guanfacine into two component fragments (control experiments with drug only samples were already done in order to quantify MS peaks expected by Guanfacine) that were used to identify and quantify Guanfacine blood concentrations.

The results of this protocol yielded an expected half life of Guanfacine of 43.23 min with a plateau of Guanfacine concentrations 2 hours after injection at <10µg/kg which is when most of the experimental data collection started (across sessions the average time was 150.8 minutes (SE: 0.88). To our knowledge, Guanfacine concentrations have only been described in humans (Kiechel, 1980; Boellner et al., 2007). And using the orally administered extended release versions with half lives of ~17 hours based off of plasma concentrations. Most macaque papers cite Arnsten et al., (1988) in order to justify their concentration use. Almost all papers with systemic administration do so at a 2h benchmark prior to testing.

D.1.4 Comparing early and late control session performance to discern possible longer-term effects of drug administration

To test whether there were overall changes in behavioral performance over the 19 weeks drug and control period testing, we analyzed early and late control session performance separately. If similar control session performance remained for early and late periods, it would suggest that administering the drug over longer periods does not have adverse effects on overall performance. We found that early (first nine sessions) and late (last 10 sessions) control sessions did not differ with regard to the number of performed reversal blocks (Early / late: 8.1 SE: 0.46 / 7.8 SE: 0.61), the number of blocks with learning within 30 trials (Early / late: 5.3 SE: 0.69 / 5.0 SE: 0.47), the median trial at which the ideal observer procedure detected learning (Early / late: 11 SE: 1.1 / 12 SE: 0.96) (all n.s.). Likewise, early and late sessions did not show differences of the probability of rewarded choices (quantified using the Smith algorithm used for **Fig. 5.3** of the main text) as a function of the trial number since reversal (randomization test with multiple comparison correction for the number of trials).

D.2 Supplementary Methods

D.2.1 Behavioural analysis of learning trials

Analysis was performed with custom MATLAB code (Mathworks, Natick, MA), utilizing functionality from the open-source fieldtrip toolbox (http://www.ru.nl/fcdonders/fieldtrip/). To identify at which trial during a block the monkey showed statistically reliable learning we analyzed the monkeys' trial-by-trial choice dynamics using the state–space framework introduced by Smith and Brown (Smith and Brown, 2003), and implemented by Smith et al. (Smith et al., 2004). This framework entails a state equation that describes the internal learning process as a hidden Markov or latent process and is updated with each trial. The learning state process estimates the probability of a correct (rewarded) choice in each trial and thus provides the learning curve of subjects (see e.g. Balcarras et al., 2016). The algorithm estimates learning from the perspective of an ideal observer that takes into account all trial outcomes of subjects' choices in a block of trials to estimate the probability that the outcome in a single trial is correct or incorrect. The ideal observer

perspective corresponds to smoothing in the Kalman filter context (Rauch et al., 1965). This probability is then used to calculate the confidence range of observing a correct response. We defined the learning trial as the earliest trial in a block at which the lower confidence bound of the probability for a correct response exceeded the $p = 0.5$ chance level.

More specifically, the algorithm defines the learning state process as a random walk whereby each trial's probability of a correct response depends on the previous trials probability, or on the chance level in case there was no previous trial's probability i.e. at the beginning of blocks. According to this formulation, the subject's choices across trials follow a random strategy. The mean of the random process reflects the current probability for a correct response. The variance of the random process determines how fast the learning state process can change from trial to trial and thus, how rapidly learning can take place (see Smith et al., 2004). The Expectation-Maximization (EM) algorithm is used to estimate the mean and variance of the random process by maximum likelihood estimation (Dempster, 1977) to derive the probability to observe a correct response in each trial as a function of the trial number (Smith and Brown, 2003). A forward filter estimates the variance and mean of the value of the Gaussian Random Variable from the first trial to the current trial. This forward process reflects a state estimate from the perspective of the subject performing the task. An additional smoothing algorithm takes the perspective of an ideal observer and estimates the current trials mean and variance of the state process using data from all trials. The estimates of both, the forward filter and the smoothing process are then used to calculate the probability density for the correct response probability at each trial. Please see Smith et al. (2004) equations 2.1 to 2.4 for details. The aforementioned procedure provides the learning curve, i.e. it provides for each trial the probability of a correct response given the sequence of correct and incorrect choices of the monkey. To identify the first trial in a block at which an ideal observer knows with $p \geq 0.95$ confidence that learning has taken place, we calculated the lower confidence bound and identified the first trial where it exceeded the $p=0.5$ chance level, the first 'IO95' learning trial (see Smith et al., 2004). This corresponds to a 0.95 confidence level for an ideal observer to identify learning.

D.3 Figures

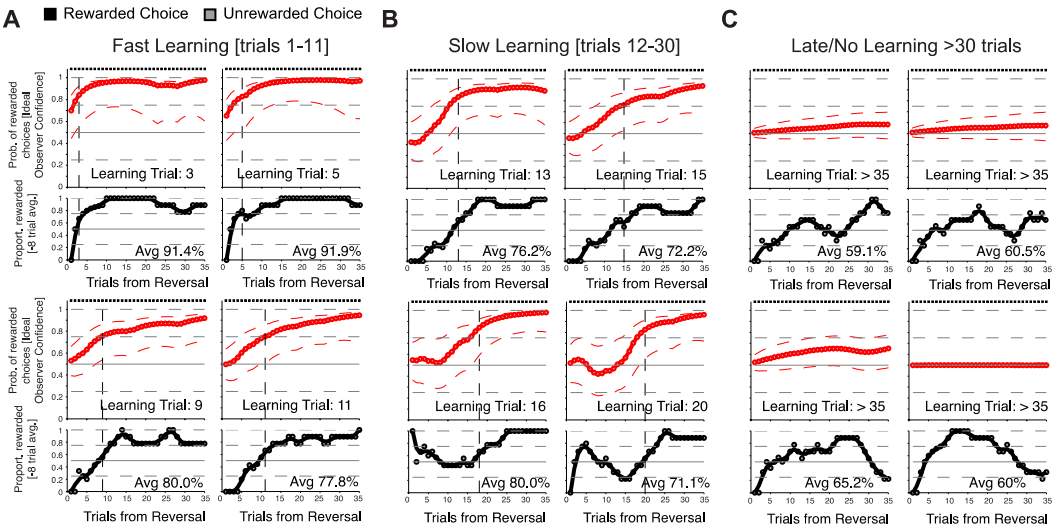

Fig D1 Examples of learning at varying speeds estimated with an ideal observer estimate of choice confidence.

(A) Four example blocks with learning within the first eleven trials, denoted as 'fast learning'. Upper panel show the reward probability (solid red line) estimated with an expectation maximization algorithm and the 95% confidence levels (dashed red line). The learning trial is defined as the first trial at which the lower bound 95% confidence level exceeds and never dips below the 0.5 chance probability with which an ideal observer can estimate that consistent learning has occurred. Squares on top of the panel highlight whether the choice was rewarded (black) or unrewarded (grey). Bottom panel shows for the same block the proportion of rewarded choices calculated with a running average sliding window of up to eight trials in the past. The text denotes overall percent correct (rewarded) performance across all 35 trials. (B) Same format as (A) but for blocks with 'slow learning', defined by learning trials between 12 and 35 within a block. (C) Same format as (A,B) but for blocks with no learning of the new color-reward association evident statistically in the first 35 blocks.

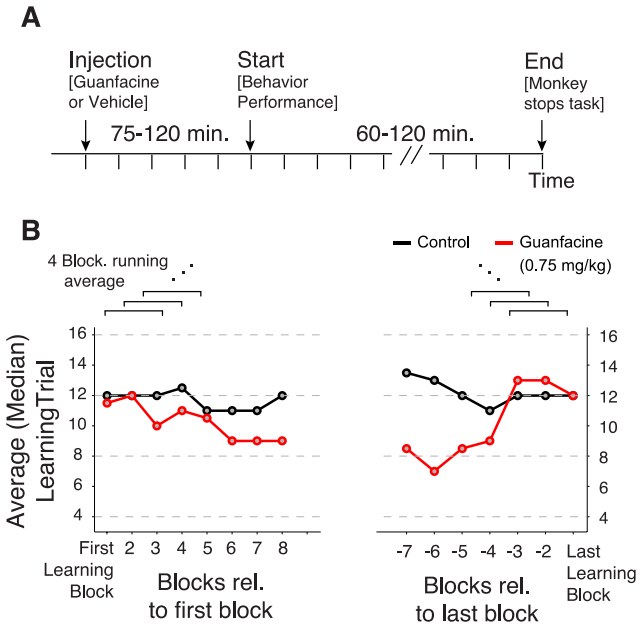

Fig D2 Consistency of reversal learning benefit on Guanfacine days versus Control days.
(A) Illustration of the time of drug/control injection and the time range with behavioural performance. (B) Average learning trials (y-axis) for reversal learning blocks on Control days (black) and Guanfacine days (red) relative to the first block performed in the day (left panel), and relative to the last performed block in the day (right panel). A total of 11 of 15 blocks show on average an earlier learning trial in blocks on Guanfacine days versus Control days, which is a statistically significant difference (randomization test, p = 0.024).

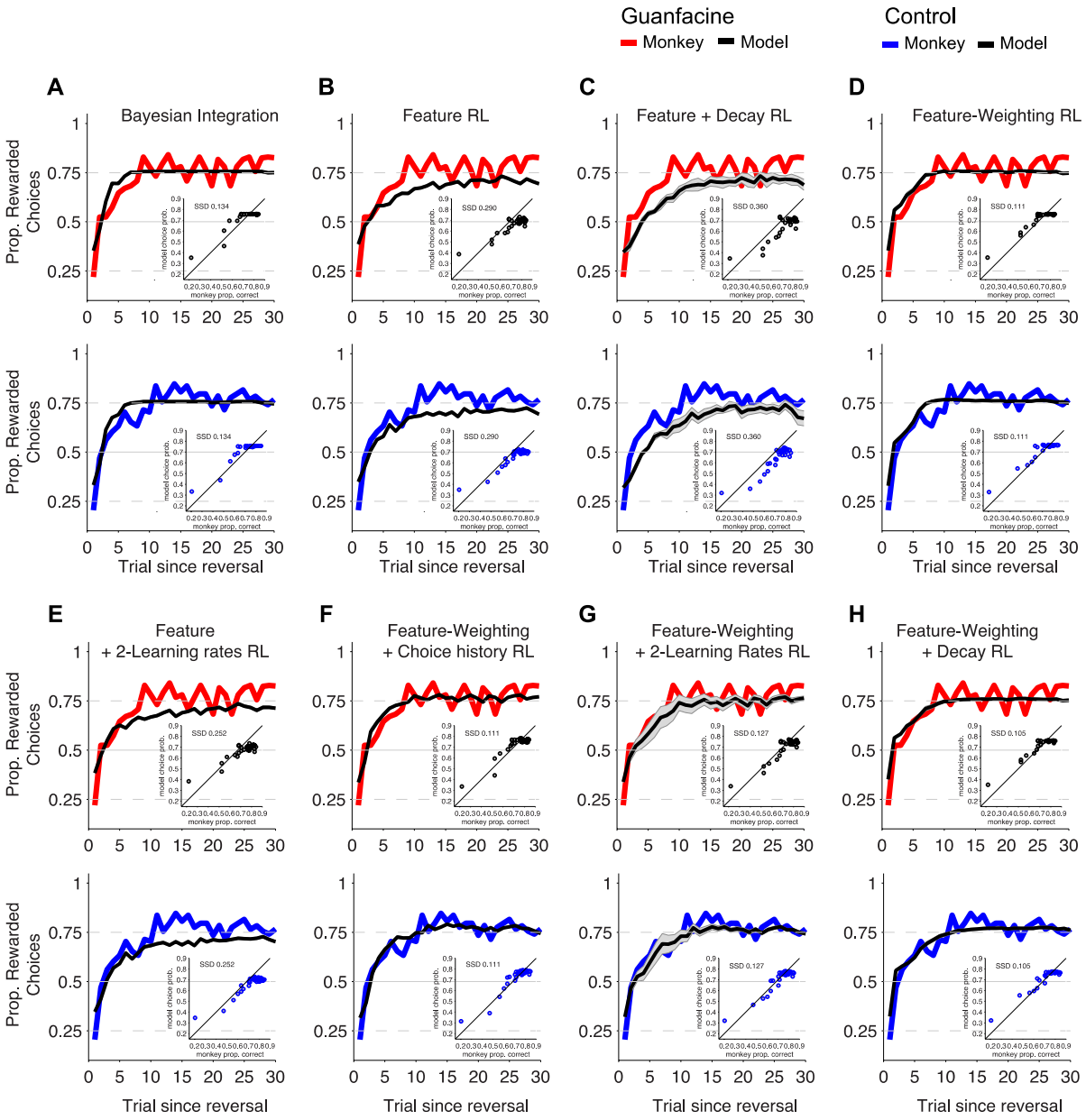

Fig D3 Performance for the seven RL models with worse log likelihood and inferior sum of squared error for the most-predictive RL model

(A,B) Proportion of rewarded choices for the monkey and model across trials since reversal in Guanfacine (A) and control (B) sessions. The model simulations are based on the best model, the Feature-Weighting + Decay RL model (see Fig. 4 and methods). The inset shows the sum of squared errors (SSD) between the proportion of correct monkey choices (x-axis) and the choice probability of the model across trials since reversal. Data on the diagonal in these plots would indicate a perfect match between model choices and subject choices. (C) The average parameter values for n=100 models fitted to subsets of 80% (cross-validation) reversal blocks for the Guanfacine (red) and control (blue) sessions. Error bars denote STD. Three stars denote significance at $p < 0.001$ after Bonferroni correction). See Figure 4 in the main text for a comparison of optimization scores across models.

Appendix E: Supplemental information for Chapter 6

E.1 Supplemental Methods

E.1.1 Pupil diameter

Monocular measurements of pupil diameter were made during experiments by the eye tracker (Eyelink 1000; 500 Hz). The pupil diameter traces were only considered during the 400 ms after stimulus onset and before the onset of either the motion or color features of the object as it was the longest period with the most stable visual stimulation. Only the traces for completed trials in the first three blocks of each session was considered and averaged across the entire 400 ms time bin. These trial averages were then z-normalized by subtracting the grand-averaged pupil diameter of first block trials for each monkey. We then averaged the z-normalized pupil diameter for the first block of sessions with and without guanfacine.

E.1.2 Spiking activity

Spike trains were transformed into spike-density functions smoothed with a Gaussian kernel with a standard deviation of 50 ms. Only correct (rewarded) and incorrect choice trials were analyzed; incorrect trials were defined as trials where the unrewarded object was chosen or any choice being made during the dimming (go signal) of the unrewarded object (either before or after the dimming of the rewarded object). Then the firing rate during the epoch of interest (feedback epoch: 50-1000 ms after feedback; attention cue onset epoch: 50-700 ms after color onset) across all trials was averaged for each neuron and then neurons with or without the administration of guanfacine were then compared with permutation testing where the condition (guanfacine or not) was randomly shuffled.

The regularity of spikes was calculated for each neuron using the measures of coefficient of variation (CV) and local variability (LV) (Shinomoto et al., 2003, 2005). Both CV (formula 1) LV (formula 2) were computed over the entire length of all completed trials using inter-spike intervals (T) where $\bar{T}$ is the mean inter-spike interval.

$$CV = \sqrt{\frac{1}{n-1}\sum_{i=1}^{n}(T_i - \bar{T})^2} \Big/ \bar{T} \tag{1}$$

$$LV = \frac{1}{n-1}\sum_{i=1}^{n-1}\frac{3(T_i - T_{i+1})^2}{(T_i + T_{i+1})^2} \tag{2}$$

The spike count pair-wise correlation (Rsc) was computed by adapting previously described methods (Joshi and Gold, 2022). Spike counts were calculated over the entire epoch of interest (feedback epoch: 50-1000 ms after feedback; attention cue onset epoch: 50-700 ms after

color onset) on every trial. For each neuron pair from the same brain region (dlPFC: dorsolateral prefrontal cortex, ACC: anterior cingulate cortex, and CD: head of the caudate nucleus), only trials where both neurons were stably isolated were considered. The spike count for each neuron was z-scored with trials that were > 3 standard deviations outside of the mean being excluded from both neurons. A Pearson correlation coefficient was then calculated for each neuron pair and separated based on if it were not significant, significant and positive or significant and negative. The correlation coefficients (Rsc) were then split between guanfacine and non-guanfacine days where their median, as well as a 95% confidence interval was extracted through bootstrapping and plotted (**Figure E2C**). Guanfacine and non-guanfacine Rsc was then compared in the feedback epoch and the choice feature onset epoch by a Wilcoxon rank sum test with Bonferroni correction.

E.2 Supplemental Results

E.2.1 Pupil diameter.

Although pupil diameter is often used to infer details about locus coeruleus (LC) activity, it is also highly related to the activity in many other brain regions as well (Murphy et al., 2014; Joshi et al., 2016; Reimer et al., 2016; Joshi and Gold, 2022). Even when only considering the LC however, it can be highly variable especially between sessions (Megemont et al., 2022). Nevertheless, to see if the systemically administered dose of guanfacine (0.075 mg/kg) did reduce LC activity, we looked at changes in pupil diameter during the first three blocks of each session where its concentration would be the highest. Pupil diameter was averaged across the 400 ms window after the onset of the two graded stimuli and before the onset of either the color or motion features. Due to each session's data having either guanfacine administration or not, no direct same-session comparisons could be made. Therefore, pupil diameter trial averages for the first three blocks, where guanfacine concentration is highest, were z-normalized by subtracting the grand-average for each monkey during those trials before comparing guanfacine administration sessions with vehicle. We found a significant reduction in the first three blocks' pupil diameter with guanfacine administration for both monkey Ha (t-test; $p < .001$) and monkey Ke (t-test; $p = .010$) (**Figure E1C**).

E.2.2 Behavioral performance.

Monkey Ha and Ke learned 52.1% and 62.3% of blocks respectively with an average learning trial speed of 15.7 and 18.7 respectively. With Guanfacine, monkey Ha and Ke learned -2.5% and +5.3% more blocks with an average learning speed change of 2.9 and 3.0 trials respectively. The summed difference in reward probability after reversals were significantly different between vehicle and guanfacine administrations (Ha: $p = .042$; Ke: $p = .021$; **Figure E1**) as were the summed difference in the EM derived reward probabilities (Ha: $p = .035$; Ke: $p = .004$; **Figure E1**).

E.2.3 Changes in spiking properties.

We investigated the impact of guanfacine on the firing properties of neurons in the dlPFC, ACC and CD. We looked at both the feedback epoch (50-1000 ms after feedback) and the attention cue onset epoch (50-700 ms after color onset which is the minimum length of this epoch).

Guanfacine did not significantly change the firing rate in the dlPFC, ACC or CD during the feedback epoch (permutation testing: 5000 permutations; all n.s.) or the attention cue onset epoch (permutation testing: 5000 permutations; all n.s.; **Figure E2A**). Separating neurons by their putative cell type revealed a significant reduction in firing rate in broad spiking neurons in the dlPFC and CD during the feedback epoch and no changes in the attention cue onset epoch (permutation testing: 5000 permutations; dlPFC: $p = .034$; ACC: n.s.; CD: $p = .008$; not shown).

We also looked at changes in spiking regularity across the whole trial via the CV and LV in the dlPFC, ACC and CD. Guanfacine administration did not significantly change the CV of neurons in the dlPFC, ACC or CD although a significant main effect of area was found (anova: $F(2,1150) = 13.85$; $p = < .001$) with the caudate having a significantly lower CV than the dlPFC (Tukey's: $p < .001$) and the ACC (Tukey's: $p = .004$) (**Figure E2B** *top*). Results did not change when only considering narrow or broad spiking neurons (data not shown). Similarly, no significant change in LV was observed with guanfacine administration with no significant main effects or interactions (anova: all n.s.). This remained consistent even when only considering narrow or broad spiking neurons (data not shown).

E.3 Figures

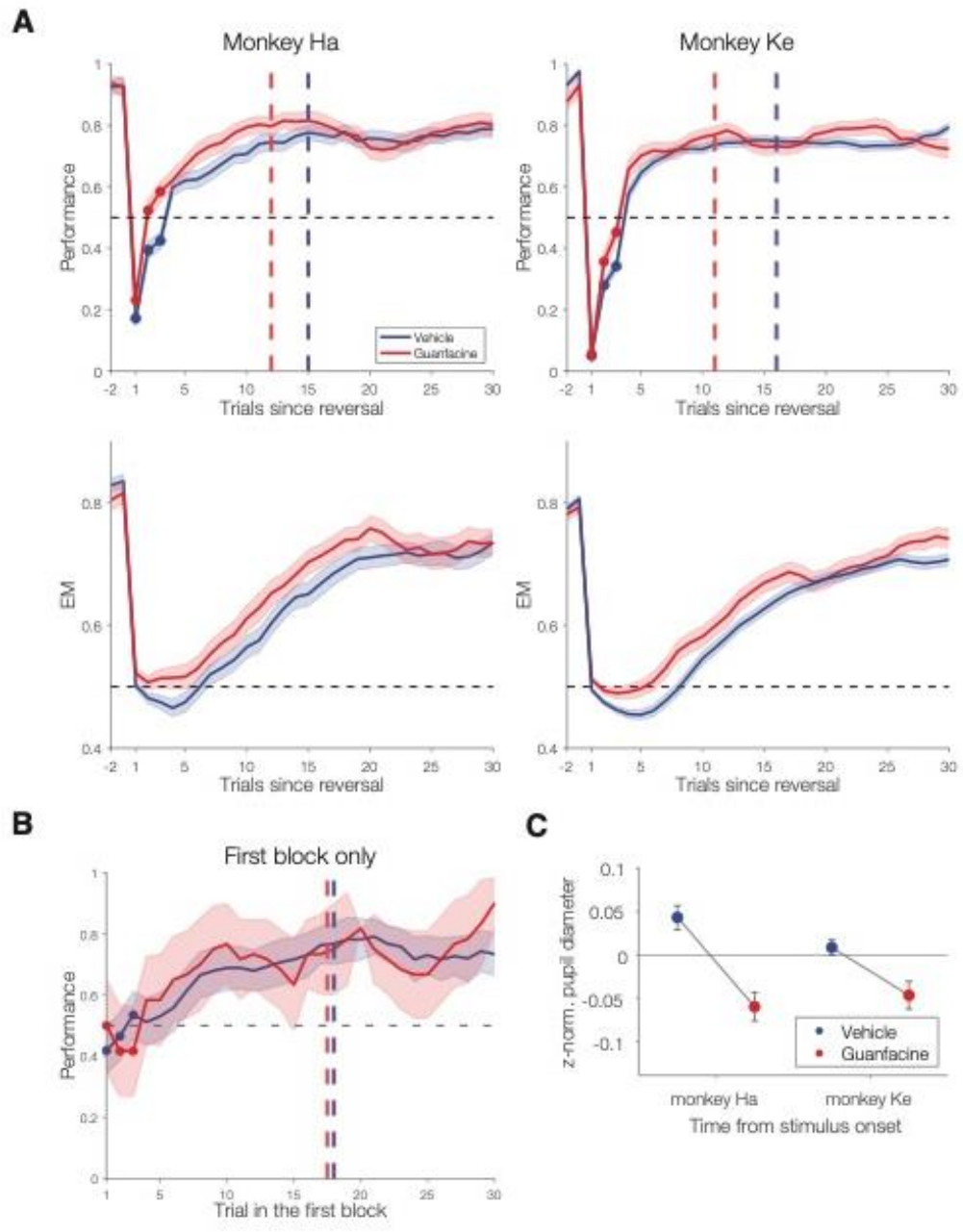

Fig E1 Individual monkey performance curves and pupil diameter.
(**A**) Learning curves (*top*) and probability estimate of correct choices based on the estimation maximization (EM) algorithm (*bottom*) for monkey Ha (*left*) and monkey Ke (*right*). Learning curves were smoothed except for the first 3 trials. The horizontal dashed line represents chance probability. The vertical dashed lines represent the median learning trial for guanfacine (red) and vehicle (blue). (**B**) The same as figure A but combined for both monkeys and only for the first block (if learned) of each session. (**C**) Average normalized pupil diameter in the first 3 blocks of guanfacine and vehicle sessions. Normalization was done per monkey.

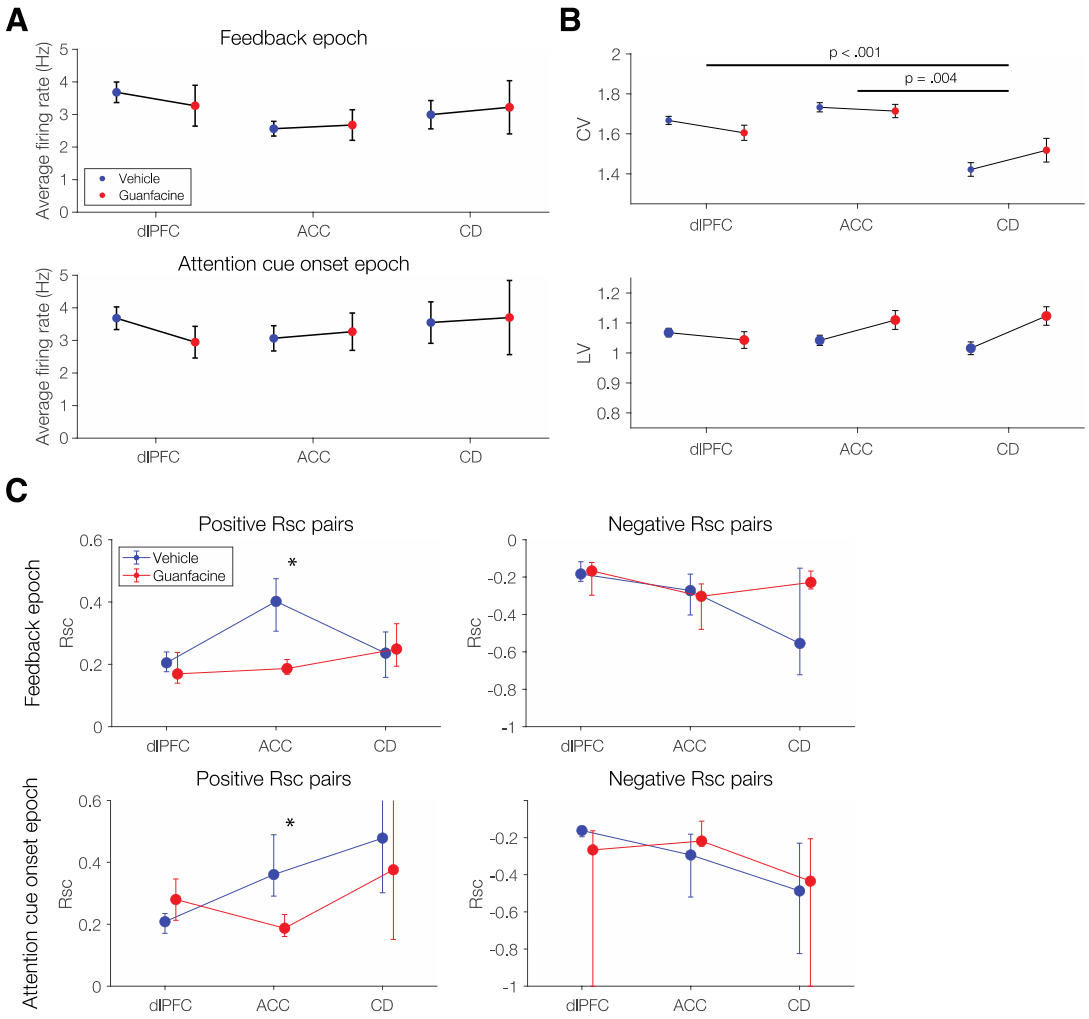

Fig E2 Guanfacine-mediated changes in spiking properties.
(**A**) Average firing rate during the feedback epoch (50-1000 ms after feedback; *top*) and attention cue onset epoch (50-700 ms after attention cue onset; *bottom*). Firing rate was averaged during the epoch of interest during all completed trials for each neuron and then averaged between all neurons for each brain region and condition. (**B**) The coefficient of variation (CV; *top*) and local variability (LV; *bottom*) of recorded neurons. Both CV and LV were calculated using all completed trials over the entire trial length. (**C**) The pair-wise spike count correlation (Rsc) during the feedback epoch (*top*) and attention cue onset epoch (*bottom*) split between positive Rsc pairs (*left*) and negative Rsc pairs (*right*). Values and error bars represent boot strapped averages and 95% confidence intervals. A Wilcoxon rank sum test was used to compare the Rsc of guanfacine and non-drug neuron pairs with Bonferroni correction.

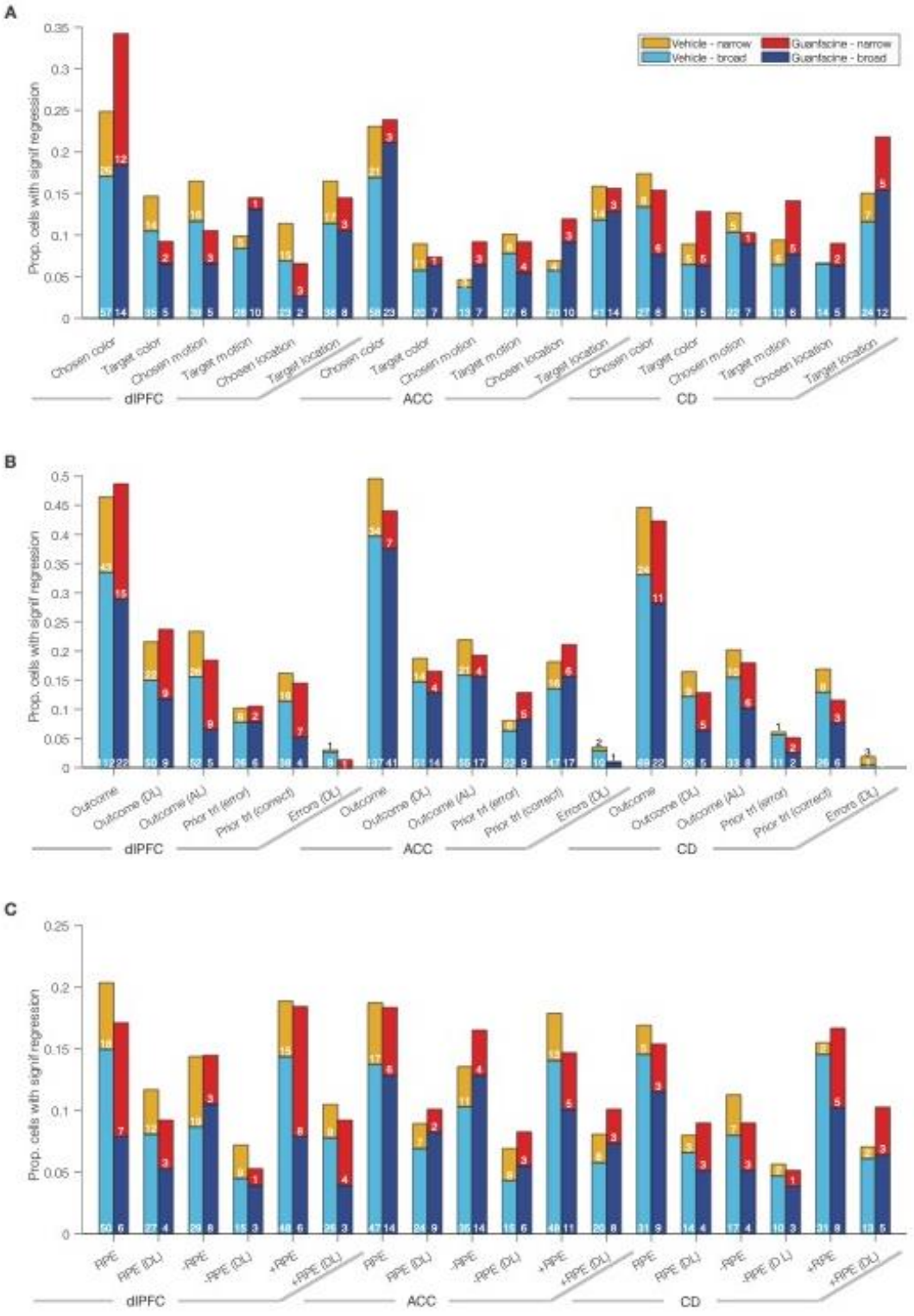

Fig E3 The change in the proportion of neurons that significantly regress to each tested variable during the feedback epoch.

(**A**) The proportion of neurons that significantly regressed to each stimulus variable split into narrow and broad spiking neurons. The small white or black numbers within the bars denote the actual cell counts. (**B**) The same as A but for outcome variables. (**C**) The same as A but for latent model variables.

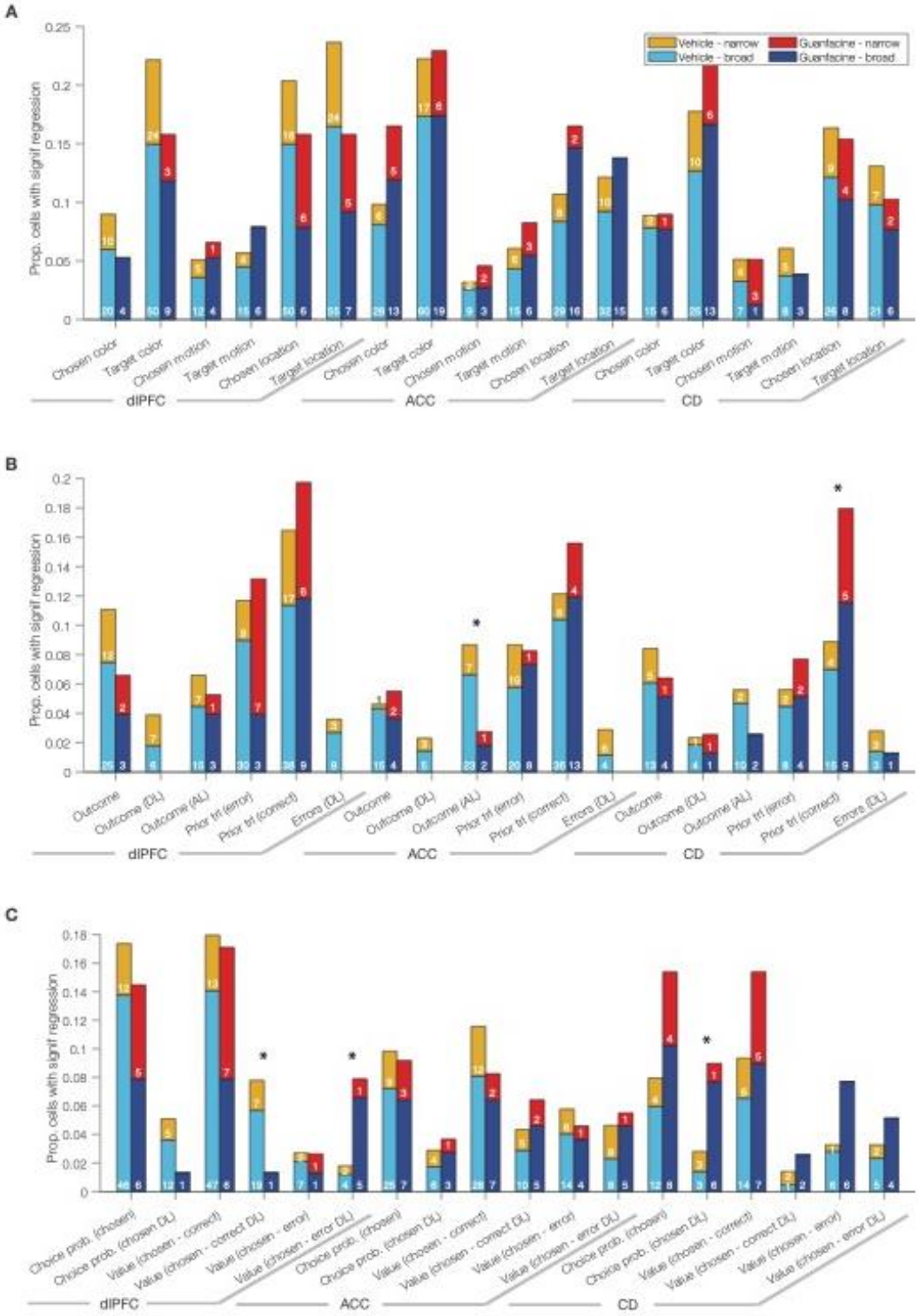

Fig E4 The change in the proportion of neurons that significantly regress to each tested variable during the attention cue onset epoch.

(**A**) The same as figure E3A, but for the cue onset epoch. (**B**) The same as A but for outcome variables. (**C**) The same as A but for latent model variables.

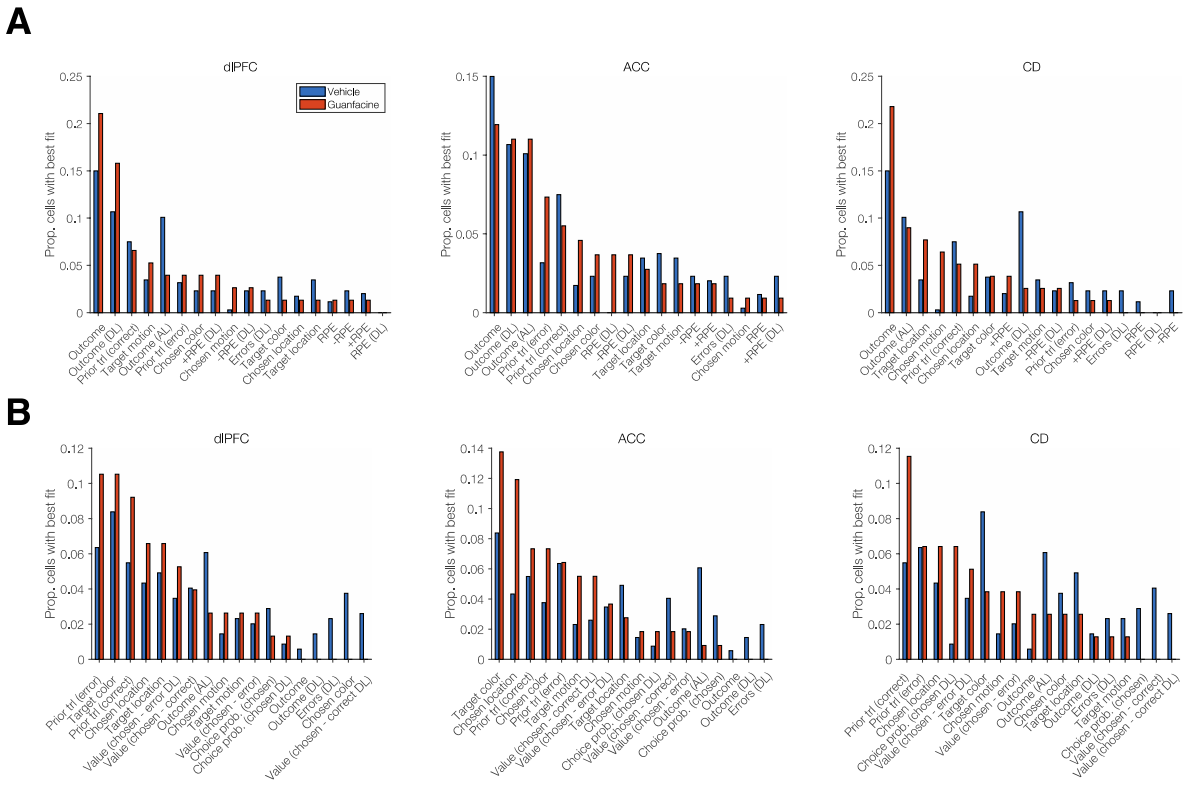

Fig E5 The best fit regressors for explaining the activity of each respective brain region.
(**A**) The number of neurons whose activity during the feedback epoch each regressor best accounts for ranked in descending order for guanfacine neurons and the corresponding ranking for non-drug neurons. The similarity in rankings were tested for via Kendall's tau correlation. From left to right: the dlPFC ($p = .006$; Tau = .477), the ACC ($p = .014$; Tau = .425), and the CD ($p = .014$; Tau = .425). (**B**) The same as A but for the attention cue onset epoch. From left to right: the dlPFC ($p = .970$ n.s.; Tau = -.007), the ACC ($p = .112$ n.s.; Tau = -.281), and the CD ($p = .175$ n.s.; Tau = .242)

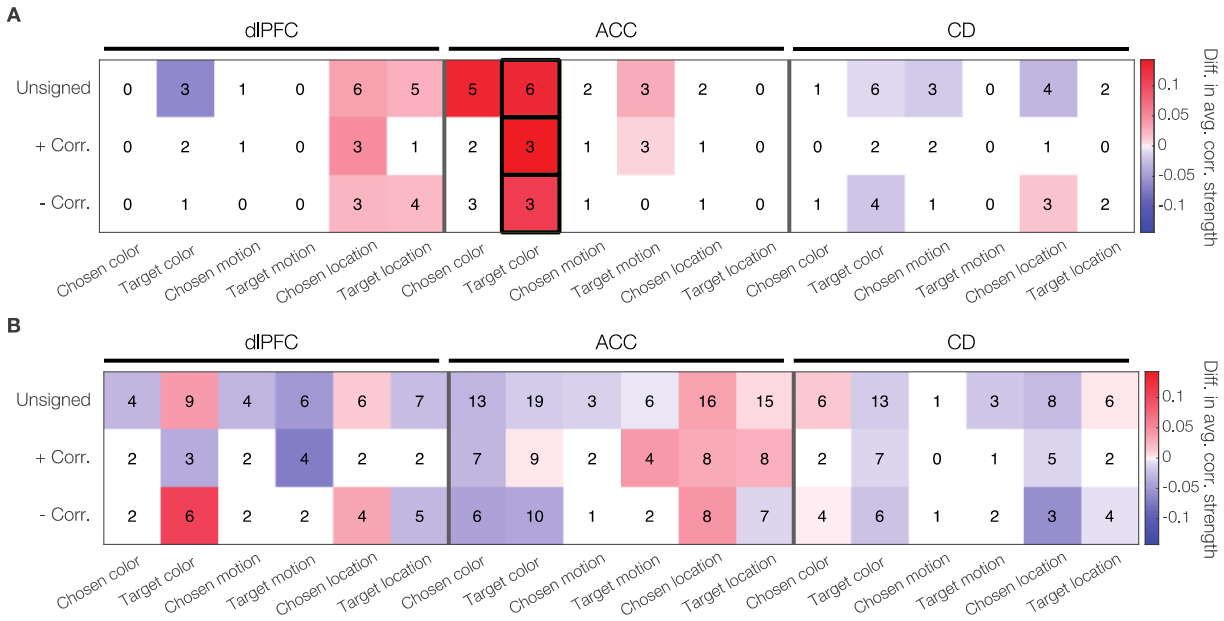

Fig E6 Guanfacine-mediated changes in neural activity correlations to stimulus variables during the attention cue onset epoch separated by putative cell types.
(**A**) The difference in average correlation strength between guanfacine and non-drug narrow spiking neurons for stimulus variables; the same as figure 6.7A in the main text, but for stimulus variables. (**B**) The same as A but for broad spiking neurons.

References:

Adams RA, Huys QJM, Roiser JP (2015) Computational Psychiatry: towards a mathematically informed understanding of mental illness. J Neurol Neurosurg Psychiatry:jnnp-2015-310737- Available at: http://jnnp.bmj.com/content/early/2015/07/08/jnnp-2015-310737.short?rss=1.

Aigner TG, Mishkin M (1986) The effects of physostigmine and scopolamine on recognition memory in monkeys. Behav Neural Biol 45:81–87.

Aigner TG, Walker DL, Mishkin M (1991) Comparison of the effects of scopolamine administered before and after acquisition in a test of visual recognition memory in monkeys. Behav Neural Biol 55:61–67.

Alam N, Pawliszyn J (2016) Numerical Simulation and Experimental Validation of Calibrant-Loaded Extraction Phase Standardization Approach. Anal Chem 88:8632–8639.

Amemiya S, Redish AD (2016) Manipulating decisiveness in decision making: Effects of clonidine on hippocampal search strategies. Journal of Neuroscience 36:814–827.

Amita H, Hikosaka O (2019) Indirect pathway from caudate tail mediates rejection of bad objects in periphery. Sci Adv 5:1–8.

Andersen MB, Fink-Jensen A, Peacock L, Gerlach J, Bymaster F, Lundbæk JA, Werge T (2003) The muscarinic M1/M4receptor agonist xanomeline exhibits antipsychotic-like activity in cebus apella monkeys. Neuropsychopharmacology 28:1168–1175.

Anderzhanova E, Wotjak CT (2013) Brain microdialysis and its applications in experimental neurochemistry. Cell Tissue Res 354:27–39.

Andrews GD, Lavin A (2006) Methylphenidate increases cortical excitability via activation of alpha-2 noradrenergic receptors. Neuropsychopharmacology 31:594–601.

Aoki C, Go CG, Venkatesan C, Kurose H (1994) Perikaryal and synaptic localization of alpha 2A-adrenergic receptor-like immunoreactivity. Brain Res 650:181–204.

Ardid S, Vinck M, Raping D, Marquez S, Everling S, Womelsdorf T (2015) Mapping of functionally characterized cell classes onto canonical circuit operations in primate prefrontal cortex. Journal of Neuroscience 35:2975–2991.

Arikuni T, Sako H, Murata A (1994) Ipsilateral connections of the anterior cingulate cortex with the frontal and medial temporal cortices in the macaque monkey. Neurosci Res 21:19–39.

Arnsten a F, Cai JX, Goldman-Rakic PS (1988) The alpha-2 adrenergic agonist guanfacine improves memory in aged monkeys without sedative or hypotensive side effects: evidence for alpha-2 receptor subtypes. J Neurosci 8:4287–4298.

Arnsten AFT (2000) Through the looking glass: Differential noradenergic modulation of prefrontal cortical function. Neural Plast 7:133–146.

Arnsten AFT (2015) Stress weakens prefrontal networks : molecular insults to higher cognition. Nat Neurosci 18:1376–1385.

Arnsten AFT (2020) Guanfacine's mechanism of action in treating prefrontal cortical disorders: Successful translation across species. Neurobiol Learn Mem 176:107327 Available at: https://doi.org/10.1016/j.nlm.2020.107327.

Arnsten AFT, Dudley AG (2005) Methylphenidate improves prefrontal cortical cognitive function through α2 adrenoceptor and dopamine D1 receptor actions: Relevance to therapeutic effects in Attention Deficit Hyperactivity Disorder. Behavioral and Brain Functions 1:1–9.

Arnsten AFT, Goldman-Rakic PS (1985) α 2 -Adrenergic Mechanisms in Prefrontal Cortex Associated with Cognitive Decline in Aged Nonhuman Primates. Science (1979) 230:1273–1276 Available at: https://www.science.org/doi/10.1126/science.2999977.

Arnsten AFT, Goldman-Rakic PS (1990) Analysis of alpha-2 adrenergic agonist effects on the delayed nonmatch-to-sample performance of aged rhesus monkeys. Neurobiol Aging 11:583–590.

Arnsten AFT, Jin LE (2012) Guanfacine for the treatment of cognitive disorders: A century of discoveries at Yale. Yale Journal of Biology and Medicine 85:45–58.

Arnsten AFT, Paspalas CD, Gamo NJ, Yang Y, Wang M (2010) Dynamic network connectivity: A new form of neuroplasticity. Trends Cogn Sci 14:365–375 Available at: http://dx.doi.org/10.1016/j.tics.2010.05.003.

Arnsten AFT, Pliszka SR (2011) Catecholamine influences on prefrontal cortical function: Relevance to treatment of attention deficit/hyperactivity disorder and related disorders. Pharmacol Biochem Behav 99:211–216 Available at: http://dx.doi.org/10.1016/j.pbb.2011.01.020.

Arnsten AFT, Wang MJ, Paspalas CD (2012) Neuromodulation of Thought: Flexibilities and Vulnerabilities in Prefrontal Cortical Network Synapses. Neuron 76:223–239 Available at: http://dx.doi.org/10.1016/j.neuron.2012.08.038.

Asaad WF, Eskandar EN (2011) Encoding of Both Positive and Negative Reward Prediction Errors by Neurons of the Primate Lateral Prefrontal Cortex and Caudate Nucleus. Journal of Neuroscience 31:17772–17787.

Asaad WF, Lauro PM, Perge JA, Eskandar EN (2017) Prefrontal neurons encode a solution to the credit-assignment problem. Journal of Neuroscience 37:6995–7007.

Asai M, Fujikawa A, Noda A, Miyoshi S, Matsuoka N, Nishimura S (2009) Donepezil- and scopolamine-induced rCMRglu changes assessed by PET in conscious rhesus monkeys. Ann Nucl Med 23:877–882.

Ascenzo MD, Fellin T, Terunuma M, Revilla-sanchez R, Meaney DF, Auberson YP, Moss SJ, Haydon PG (2006) mGluR5 stimulates gliotransmission in the nucleus accumbens. Proceedings of the National Academy of Sciences 104:1995–2000.

Aston-Jones G, Akaoka H, Charlety P, Chouvet G (1991a) Serotonin selectively attenuates glutamate-evoked activation of noradrenergic locus coeruleus neurons. Journal of Neuroscience 11:760–769.

Aston-Jones G, Cohen JD (2005a) An Integrative Theory of Locus Coeruleus-Norepinephrine Function: Adaptive Gain and Optimal Performance. Annu Rev Neurosci 28:403–450 Available at: http://www.annualreviews.org/doi/abs/10.1146/annurev.neuro.28.061604.135709.

Aston-Jones G, Cohen JD (2005b) Adaptive gain and the role of the locus coeruleus-norepinephrine system in optimal performance. Journal of Comparative Neurology 493:99–110.

Aston-Jones G, Rajkowski J, Cohen J (1999) Role of locus coeruleus in attention and behavioral flexibility. Biol Psychiatry 46:1309–1320.

Aston-Jones G, Rajkowski J, Kubiak P, Alexinsky T (1994) Locus coeruleus neurons in monkey are selectively activated by attended cues in a vigilance task. Journal of Neuroscience 14:4467–4480.

Aston-Jones G, Shipley MT, Chouvet G, Ennis M, van Bockstaele E, Pieribone V, Shiekhattar R, Akaoka H, Drolet G, Astier B, Charléty P, Valentino RJ, Williams JT (1991b) Afferent

regulation of locus coeruleus neurons: Anatomy, physiology and pharmacology. Prog Brain Res 88:47–75.
Atallah HE, McCool AD, Howe MW, Graybiel AM (2014) Neurons in the ventral striatum exhibit cell-type-specific representations of outcome during learning. Neuron 82:1145–1156 Available at: http://dx.doi.org/10.1016/j.neuron.2014.04.021.
Avery MC, Krichmar JL (2017) Neuromodulatory Systems and Their Interactions : A Review of Models , Theories , and Experiments. Front Neural Circuits 11:1–18.
Azimi M, Oemisch M, Womelsdorf T (2019) Dissociation of nicotinic α7and α4/β2 sub-receptor agonists for enhancing learning and attentional filtering in nonhuman primates. Psychopharmacology (Berl) 237:997–1010.
Balcarras M, Ardid S, Kaping D, Everling S, Womelsdorf T (2016) Attentional Selection Can Be Predicted by Reinforcement Learning of Task-relevant Stimulus Features Weighted by Value-independent Stickiness. J Cogn Neurosci 28:333–349 Available at: https://www.apa.org/ptsd-guideline/ptsd.pdf%0Ahttps://www.apa.org/about/offices/directorates/guidelines/ptsd.pdf.
Barbas H (2000) Connections underlying the synthesis of cognition, memory, and emotion in primate prefrontal cortices. Brain Res Bull 52:319–330.
Bargmann CI (2012) Beyond the connectome: How neuromodulators shape neural circuits. BioEssays 34:458–465.
Bari A, Xu S, Pignatelli M, Takeuchi D, Feng J, Li Y, Tonegawa S (2020) Differential attentional control mechanisms by two distinct noradrenergic coeruleo-frontal cortical pathways. Proc Natl Acad Sci U S A 117:29080–29089.
Barth AMI, Vizi ES, Zelles T, Lendvai B (2008) α 2 -Adrenergic Receptors Modify Dendritic Spike Generation Via HCN Channels in the Prefrontal Cortex. J Neurophysiol 99:394–401 Available at: http://jn.physiology.org/cgi/doi/10.1152/jn.00943.2007.
Bartko SJ, Vendrell I, Saksida LM, Bussey TJ (2011) A computer-automated touchscreen paired-associates learning (PAL) task for mice: Impairments following administration of scopolamine or dicyclomine and improvements following donepezil. Psychopharmacology (Berl) 214:537–548.
Bartolo R, Averbeck BB (2020) Prefrontal Cortex Predicts State Switches during Reversal Learning. Neuron 106:1044-1054.e4 Available at: https://doi.org/10.1016/j.neuron.2020.03.024.
Bartus RT, Johnson HR (1976) Short-term memory in the rhesus monkey: Disruption from the anti-cholinergic scopolamine. Pharmacol Biochem Behav 5:39–46.
Bennett BD, Huguenard JR, Prince DA (1998) Adrenergic modulation of GABA(A) receptor-mediated inhibition in rat sensorimotor cortex. J Neurophysiol 79:937–946.
Berridge C, Foote S (1991) Effects of locus coeruleus activation on electroencephalographic activity in neocortex and hippocampus. The Journal of Neuroscience 11:3135–3145 Available at: https://www.jneurosci.org/lookup/doi/10.1523/JNEUROSCI.11-10-03135.1991.
Berridge CW, Waterhouse BD (2003) The locus coeruleus-noradrenergic system: Modulation of behavioral state and state-dependent cognitive processes. Brain Res Rev 42:33–84.
Berridge CW, Wifler K (2000) Contrasting effects of noradrenergic β-receptor blockade within the medial septal area on forebrain electroencephalographic and behavioral activity state in anesthetized and unanesthetized rat. Neuroscience 97:543–552.

Bertrand D, Terry A v. (2018) The wonderland of neuronal nicotinic acetylcholine receptors. Biochem Pharmacol 151:214–225 Available at: https://doi.org/10.1016/j.bcp.2017.12.008.
Bichot NP, Heard MT, DeGennaro EM, Desimone R (2015) A Source for Feature-Based Attention in the Prefrontal Cortex. Neuron 88:832–844 Available at: http://dx.doi.org/10.1016/j.neuron.2015.10.001.
Boellner SW, Pennick M, Fiske K, Lyne A, Shojaei A (2007) Pharmacokinetics of a guanfacine extended-release formulation in children and adolescents with attention-deficit-hyperactivity disorder. Pharmacotherapy 27:1253–1262.
Bohnen NB, Albin R, Muller MLTM, Petrou M, Kotagal V, Koeppe RA, Scott PJH, Frey KA (2015) Frequency of Cholinergic and Caudate Nucleus Dopaminergic Deficits Across the Predemented Cognitive Spectrum of Parkinson Disease and Evidence of Interaction Effects. JAMA Neurol 72:194–200.
Bornert P, Bouret S (2021) Locus coeruleus neurons encode the subjective difficulty of triggering and executing actions. PLoS Biol 19:e3001487 Available at: http://dx.doi.org/10.1371/journal.pbio.3001487.
Boroujeni KB, Oemisch M, Hassani SA, Womelsdorf T (2020) Fast spiking interneuron activity in primate striatum tracks learning of attention cues. Proc Natl Acad Sci U S A 117:18049–18058.
Boroujeni KB, Sigona MK, Treuting RL, Manuel TJ, Caskey CF, Womelsdorf T (2022) Anterior cingulate cortex causally supports flexible learning under motivationally challenging and cognitively demanding conditions. PLoS Biol 20:1–24 Available at: http://dx.doi.org/10.1371/journal.pbio.3001785.
Boroujeni KB, Tiesinga P, Womelsdorf T (2021) Interneuron specific gamma synchronization indexes cue uncertainty and prediction errors in lateral prefrontal and anterior cingulate cortex. Elife 10:1–38.
Botly LCP, de Rosa E (2009) Cholinergic deafferentation of the neocortex using 192 IgG-saporin impairs feature binding in rats. Journal of Neuroscience 29:4120–4130.
Bouret S, Richmond BJ (2015) Sensitivity of Locus Ceruleus Neurons to Reward Value for Goal-Directed Actions. Journal of Neuroscience 35:4005–4014 Available at: http://www.jneurosci.org/cgi/doi/10.1523/JNEUROSCI.4553-14.2015.
Bouret S, Sara SJ (2005) Network reset : a simplified overarching theory of locus coeruleus noradrenaline function. 28.
Breese CR, Adams C, Logel J, Drebing C, Rollins Y, Barnhart M, Sullivan B, Demasters BK, Freedman R, Leonard S (1997) Comparison of the regional expression of nicotinic acetylcholine receptor α7 mRNA and [125I]-α-bungarotoxin binding in human postmortem brain. Journal of Comparative Neurology 387:385–398.
Breton-Provencher V, Drummond GT, Feng J, Li Y, Sur M (2022) Spatiotemporal dynamics of noradrenaline during learned behaviour. Nature.
Broks P, Preston GC, Traub M, Poppleton P, Ward C, Stahl SM (1988) Modelling dementia: Effects of scopolamine on memory and attention. Neuropsychologia 26:685–700.
Bromberg-Martin ES, Hikosaka O, Nakamura K (2010) Coding of task reward value in the dorsal raphe nucleus. Journal of Neuroscience 30:6262–6272.
Brown DA (2010) Muscarinic acetylcholine receptors (mAChRs) in the nervous system: Some functions and mechanisms. Journal of Molecular Neuroscience 41:340–346.

Buccafusco JJ, Jackson WJ, Stone JD, Terry A v. (2003) Sex dimorphisms in the cognitive-enhancing action of the Alzheimer's drug donepezil in aged Rhesus monkeys. Neuropharmacology 44:381–389.

Buccafusco JJ, Terry A v. (2004) Donepezil-induced improvement in delayed matching accuracy by young and old rhesus monkeys. Journal of Molecular Neuroscience 24:85–91.

Buccafusco JJ, Terry A v., Webster SJ, Martin D, Hohnadel EJ, Bouchard KA, Warner SE (2008) The scopolamine-reversal paradigm in rats and monkeys: The importance of computer-assisted operant-conditioning memory tasks for screening drug candidates. Psychopharmacology (Berl) 199:481–494.

Buck K, Voehringer P, Ferger B (2009) Rapid analysis of GABA and glutamate in microdialysis samples using high performance liquid chromatography and tandem mass spectrometry. J Neurosci Methods 182:78–84.

Buckley MJ, Mansouri FA, Hoda H, Mahboubi M, Browning PGF, Kwok SC, Phillips A, Tanaka K (2009) Dissociable Components of Rule-Guided Bheavior Depend on Distinct Medial and Prefrontal Regions. Science (1979) 325:52–58.

Bushnell PJ, Oshiro WM, Padnos BK (1997) Detection of visual signals by rats: Effects of chlordiazepoxide and cholinergic and adrenergic drugs on sustained attention. Psychopharmacology (Berl) 134:230–241.

Bymaster FP, Katner JS, Nelson DL, Hemrick-Luecke SK, Threlkeld PG, Heiligenstein JH, Morin SM, Gehlert DR, Perry KW (2002) Atomoxetine increases extracellular levels of norepinephrine and dopamine in prefrontal cortex of rat. Neuropsychopharmacology 27:699–711.

Cachope R, Cheer JF (2014) Local control of striatal dopamine release. Front Behav Neurosci 8:1–7.

Cachope R, Mateo Y, Mathur BN, Irving J, Wang HL, Morales M, Lovinger DM, Cheer JF (2012) Selective activation of cholinergic interneurons enhances accumbal phasic dopamine release: Setting the tone for reward processing. Cell Rep 2:33–41 Available at: http://dx.doi.org/10.1016/j.celrep.2012.05.011.

Caetano MS, Jin LE, Harenberg L, Stachenfeld KL, Arnsten AFT, Laubach M (2012) Noradrenergic control of error perseveration in medial prefrontal cortex. Front Integr Neurosci 6:1–10.

Calabrese E, Badea A, Coe CL, Lubach GR, Shi Y, Styner MA, Johnson GA (2015) A diffusion tensor MRI atlas of the postmortem rhesus macaque brain. Neuroimage 117:408–416 Available at: http://dx.doi.org/10.1016/j.neuroimage.2015.05.072.

Callado LF, Stamford JA (1999) Alpha2A- but not alpha2B/C-adrenoceptors modulate noradrenaline release in rat locus coeruleus: voltammetric data. Eur J Pharmacol 366:35–39 Available at: http://www.ncbi.nlm.nih.gov/pubmed/10064149.

Callahan MJ (1999) Combining tacrine with milameline reverses a scopolamine-induced impairment of continuous performance in rhesus monkeys. Psychopharmacology (Berl) 144:234–238.

Callahan PM, Hutchings EJ, Kille NJ, Chapman JM, Terry A v. (2013) Positive allosteric modulator of alpha 7 nicotinic-acetylcholine receptors, PNU-120596 augments the effects of donepezil on learning and memory in aged rodents and non-human primates. Neuropharmacology 67:201–212 Available at: http://dx.doi.org/10.1016/j.neuropharm.2012.10.019.

Callahan PM, Plagenhoef MR, Blake DT, Terry A v. (2019) Atomoxetine improves memory and other components of executive function in young-adult rats and aged rhesus monkeys. Neuropharmacology 155:65–75 Available at: https://doi.org/10.1016/j.neuropharm.2019.05.016.

Caulfield MP (1993) Muscarinic Receptors-Characterization, coupling and function. Pharmacol Ther 58:319–379.

Chamberlain SR, Müller U, Blackwell AD, Clark L, Robbins TW, Sahakian BJ (2006) Neurochemical Modulation of Response Inhibition and Probabilistic Learning in Humans. Science (1979) 311:861–863 Available at: https://www.science.org/doi/10.1126/science.1121218.

Chambon C, Jatzke C, Wegener N, Gravius A, Danysz W (2012) Using cholinergic M1 receptor positive allosteric modulators to improve memory via enhancement of brain cholinergic communication. Eur J Pharmacol 697:73–80 Available at: http://dx.doi.org/10.1016/j.ejphar.2012.10.011.

Chambon C, Wegener N, Gravius A, Danysz W (2011) A new automated method to assess the rat recognition memory: Validation of the method. Behavioural Brain Research 222:151–157 Available at: http://dx.doi.org/10.1016/j.bbr.2011.03.032.

Chandler DJ, Gao W-J, Waterhouse BD (2014) Heterogeneous organization of the locus coeruleus projections to prefrontal and motor cortices. Proc Natl Acad Sci U S A 111:6816–6821.

Chen KC, Baxter MG, Rodefer JS (2004) Central blockade of muscarinic cholinergic receptors disrupts affective and attentional set-shifting. European Journal of Neuroscience 20:1081–1088.

Chiba AA, Bushnell PJ, Oshiro WM, Gallagher M (1999) Selective removal of cholinergic neurons in the basal forebrain alters cued target detection. Neuroreport 10:3119–3123.

Ciombor KJ, Ennis M, Shipley MT (1999) Norepinephrine increases rat mitral cell excitatory responses to weak olfactory nerve input via alpha-1 receptors in vitro. Neuroscience 90:595–606.

Clark KL, Noudoost B (2014) The role of prefrontal catecholamines in attention and working memory. Front Neural Circuits 8:1–19 Available at: http://www.pubmedcentral.nih.gov/articlerender.fcgi?artid=3986539&tool=pmcentrez&rendertype=abstract%5Cnhttp://dx.doi.org/10.3389/fncir.2014.00033.

Clarke HF, Robbins TW, Roberts AC (2008) Lesions of the medial striatum in monkeys produce perseverative impairments during reversal learning similar to those produced by lesions of the orbitofrontal cortex. Journal of Neuroscience 28:10972–10982.

Cohen JY, Pouget P, Woodman GF, Subraveti CR, Schall JD, Rossi AF (2007) Difficulty of visual search modulates neuronal interactions and response variability in the frontal eye field. J Neurophysiol 98:2580–2587.

Cole BJ, Robbins TW (1992) Forebrain norepinephrine: role in controlled information processing in the rat. Neuropsychopharmacology 7:129–142 Available at: http://www.ncbi.nlm.nih.gov/pubmed/1418302.

Conn PJ, Jones CK, Lindsley CW (2009) Subtype-selective allosteric modulators of muscarinic receptors for the treatment of CNS disorders. Trends Pharmacol Sci 30:148–155.

Connor DF, Arnsten AF, Pearson GS, Greco GF (2014) Guanfacine extended release for the treatment of attention-deficit/hyperactivity disorder in children and adolescents. Expert

Opin Pharmacother 15:1601–1610 Available at: http://www.tandfonline.com/doi/full/10.1517/14656566.2014.930437.
Cook JL, Swart JC, Froböse MI, Diaconescu AO, Geurts DEM, den Ouden HEM, Cools R (2019) Catecholaminergic modulation of meta-learning. Elife 8:1–38.
Cools R (2019) Chemistry of the Adaptive Mind: Lessons from Dopamine. Neuron 104:113–131 Available at: https://doi.org/10.1016/j.neuron.2019.09.035.
Cools R, Arnsten AFT (2022) Neuromodulation of prefrontal cortex cognitive function in primates: the powerful roles of monoamines and acetylcholine. Neuropsychopharmacology 47:309–328 Available at: http://dx.doi.org/10.1038/s41386-021-01100-8.
Coppola JJ, Ward NJ, Jadi MP, Disney AA (2016) Modulatory compartments in cortex and local regulation of cholinergic tone. J Physiol Paris 110:3–9.
Court J, Martin-Ruiz C, Piggott M, Spurden D, Griffiths M, Perry E (2001) Nicotinic receptor abnormalities in Alzheimer's disease. Biol Psychiatry 49:175–184.
Courtney C et al. (2004) Long-term donepezil treatment in 565 patients with Alzheimer's disease (AD2000): randomised double-blind trial. Lancet 363:2105–2115 Available at: http://ovidsp.ovid.com/ovidweb.cgi?T=JS&PAGE=reference&D=medc&NEWS=N&AN=15220031%5Cnhttp://ovidsp.ovid.com/ovidweb.cgi?T=JS&PAGE=reference&D=psyc4&NEWS=N&AN=2004-19061-001%5Cnhttp://ovidsp.ovid.com/ovidweb.cgi?T=JS&PAGE=reference&D=emed9&NEWS=N&AN=3884415.
Cromwell HC, Schultz W (2003) Effects of expectations for different reward magnitudes on neuronal activity in primate striatum. J Neurophysiol 89:2823–2838.
Croxson PL, Kyriazis DA, Baxter MG (2011) Cholinergic modulation of a specific memory function of prefrontal cortex. Nat Neurosci 14:1510–1512.
Cruickshank JW, Brudzynski SM, McLachlan RS (1994) Involvement of M1 muscarinic receptors in the initiation of cholinergically induced epileptic seizures in the rat brain. Brain Res 643:125–129.
Csernansky JG, Martin M, Shah R, Bertchume A, Colvin J, Dong H (2005) Cholinesterase inhibitors ameliorate behavioral deficits induced by MK-801 in mice. Neuropsychopharmacology 30:2135–2143.
Cudjoe E, Bojko B, de Lannoy I, Saldivia V, Pawliszyn J (2013) Solid-Phase Microextraction: A Complementary In Vivo Sampling Method to Microdialysis. Angewandte Chemie International Edition 52:12124–12126 Available at: http://doi.wiley.com/10.1002/anie.201304538.
Cudjoe E, Pawliszyn J (2014) Optimization of solid phase microextraction coatings for liquid chromatography mass spectrometry determination of neurotransmitters. J Chromatogr A 1341:1–7.
Cummings JL, Geldmacher D, Farlow M, Sabbagh M, Christensen D, Betz P (2013) High-Dose Donepezil (23 mg/day) for the Treatment of Moderate and Severe Alzheimer's Disease: Drug Profile and Clinical Guidelines. CNS Neurosci Ther 19:294–301.
Cuthbert BN, Insel TR (2013) Toward the future of psychiatric diagnosis: The seven pillars of RDoC. BMC Med 11.
Dale N, Hatz S, Tian F, Llaudet E (2005) Listening to the brain: Microelectrode biosensors for neurochemicals. Trends Biotechnol 23:420–428.
Dalley JW, Cardinal RN, Robbins TW (2004) Prefrontal executive and cognitive functions in rodents: Neural and neurochemical substrates. Neurosci Biobehav Rev 28:771–784.

Dalley JW, Mcgaughy J, Connell MTO, Cardinal RN, Levita L, Robbins TW (2001) Distinct Changes in Cortical Acetylcholine and Noradrenaline Efflux during Contingent and Noncontingent Performance of a Visual Attentional Task. 21:4908–4914.
Dasilva M, Brandt C, Gotthardt S, Gieselmann MA, Distler C, Thiele A (2019a) Cell class-specific modulation of attentional signals by acetylcholine in macaque frontal eye field. Proc Natl Acad Sci U S A 116:20180–20189.
Dasilva M, Brandt C, Gotthardt S, Gieselmann MA, Distler C, Thiele A (2019b) Cell class-specific modulation of attentional signals by acetylcholine in macaque frontal eye field. Proc Natl Acad Sci U S A 116:20180–20189.
Datta D, Yang ST, Galvin VC, Solder J, Luo F, Morozov YM, Arellano J, Duque A, Rakic P, Arnsten AFT, Wang M (2019) Noradrenergic α1-adrenoceptor actions in the primate dorsolateral prefrontal cortex. Journal of Neuroscience 39:2722–2734.
Davidson MC, Cutrell EB, Marrocco RT (1999) Scopolamine slows the orienting of attention in primates to cued visual targets. Psychopharmacology (Berl) 142:1–8.
Davidson MC, Marrocco RT (2000) Local infusion of scopolamine into intraparietal cortex slows covert orienting in rhesus monkeys. J Neurophysiol 83:1536–1549.
Dayan P, Yu AJ (2006) Phasic norepinephrine: A neural interrupt signal for unexpected events. Network: Computation in Neural Systems 17:335–350.
de Boer P, Westerink BHC, Horn AS (1990) The effect of acetylcholinesterase inhibition on the release of acetylcholine from the striatum in vivo: Interaction with autoreceptor responses. Neurosci Lett 116:357–360.
Dean B, Scarr E (2020) Muscarinic M1 and M4 receptors: Hypothesis driven drug development for schizophrenia. Psychiatry Res 288:112989 Available at: https://doi.org/10.1016/j.psychres.2020.112989.
Decamp E, Clark K, Schneider JS (2011) Effects of the alpha-2 adrenoceptor agonist guanfacine on attention and working memory in aged non-human primates. European Journal of Neuroscience 34:1018–1022.
DeFea K (2008) β-arrestins and heterotrimeric G-proteins: Collaborators and competitors in signal transduction. Br J Pharmacol 153:298–309.
Delaville C, Deurwaerdère P de, Benazzouz A (2011) Noradrenaline and Parkinson's Disease. Front Syst Neurosci 5:1–12 Available at: http://journal.frontiersin.org/article/10.3389/fnsys.2011.00031/abstract.
Dempster A (1977) Maximum likelihood from incomplete data via em algorithm. J Royal Stat Soc B 39:1–38.
Deng J, Yang Y, Wang X, Luan T (2014) Strategies for coupling solid-phase microextraction with mass spectrometry. TrAC - Trends in Analytical Chemistry 55:55–67.
Devauges V, Sara SJ (1990) Activation of the noradrenergic system facilitates an attentional shift in the rat. Behavioural Brain Research 39:19–28.
Devilbiss DM, Waterhouse BD (2004) The effects of tonic locus ceruleus output on sensory-evoked responses of ventral posterior medial thalamic and barrel field cortical neurons in the awake rat. Journal of Neuroscience 24:10773–10785.
Devoto P, Flore G, Saba P, Fà M, Gessa GL (2005) Co-release of noradrenaline and dopamine in the cerebral cortex elicited by single train and repeated train stimulation of the locus coeruleus. BMC Neurosci 6:1–11.
Devoto P, Flore G, Saba P, Scheggi S, Mulas G, Gambarana C, Spiga S, Gessa GL (2019) Noradrenergic terminals are the primary source of α 2 -adrenoceptor mediated dopamine

release in the medial prefrontal cortex. Prog Neuropsychopharmacol Biol Psychiatry 90:97–103 Available at: https://doi.org/10.1016/j.pnpbp.2018.11.015.
Devoto P, Sagheddu C, Santoni M, Flore G, Saba P, Pistis M, Gessa GL (2020) Noradrenergic Source of Dopamine Assessed by Microdialysis in the Medial Prefrontal Cortex. Front Pharmacol 11:1–14.
Disney AA, Higley MJ (2020) Diverse spatiotemporal scales of cholinergic signaling in the neocortex. Journal of Neuroscience 40:720–725.
Disney AA, McKinney C, Grissom L, Lu X, Reynolds JH (2015) A multi-site array for combined local electrochemistry and electrophysiology in the non-human primate brain. J Neurosci Methods 255:29–37.
Doya K (2002) Metalearning and neuromodulation. Neural Networks 15:495–506 Available at: http://www.ncbi.nlm.nih.gov/pubmed/12371507.
Doya K (2008) Modulators of decision making. Nat Neurosci 11:410–416.
Dumitriu D, Hao J, Hara Y, Kaufmann J, Janssen WGM, Lou W, Rapp PR, Morrison JH (2010) Selective changes in thin spine density and morphology in monkey prefrontal cortex correlate with aging-related cognitive impairment. Journal of Neuroscience 30:7507–7515.
Edginton T, Rusted JM (2003) Separate and combined effects of scopolamine and nicotine on retrieval-induced forgetting. Psychopharmacology (Berl) 170:351–357.
Ellis JR, Ellis KA, Bartholomeusz CF, Harrison BJ, Wesnes KA, Erskine FF, Vitetta L, Nathan PJ (2006) Muscarinic and nicotinic receptors synergistically modulate working memory and attention in humans. International Journal of Neuropsychopharmacology 9:175–189.
Engberg G, Eriksson E (1991) Effects of α2-adrenoceptor agonists on locus coeruleus firing rate and brain noradrenaline turnover in N-ethoxycarbonyl-2-ethoxy-1,2-dihydroquinoline (EEDQ)-treated rats. Naunyn Schmiedebergs Arch Pharmacol 343:472–477.
Everitt BJ, Robbins TW (1997) Central cholinergic systems and cognition. Annu Rev Psychol 48:649–684.
Fahnestock M, Shekari A (2019) ProNGF and neurodegeneration in Alzheimer's disease. Front Neurosci 13:1–11.
Fisher RE, Morris ED, Alpert NM, Fischman AJ (1995) In Vivo Imaging of Neuromodulatory Synaptic Transmission Using PET : A Review of Relevant Neurophysiology. Hum Brain Mapp 3:24–34.
Floresco SB (2013) Prefrontal dopamine and behavioral flexibility: Shifting from an "inverted-U" toward a family of functions. Front Neurosci 7:1–12.
Floresco SB, Jentsch JD (2011) Pharmacological enhancement of memory and executive functioning in laboratory animals. Neuropsychopharmacology 36:227–250 Available at: http://dx.doi.org/10.1038/npp.2010.158.
Floresco SB, Zhang Y, Enomoto T (2009) Neural circuits subserving behavioral flexibility and their relevance to schizophrenia. Behavioural Brain Research 204:396–409.
Foldi NS, White REC, Schaefer LA (2005) Detecting effects of donepezil on visual selective attention using signal detection parameters in Alzheimer's disease. Int J Geriatr Psychiatry 20:485–488.
Food and Drug Administration (FDA) (2001) Guidance for Industry Bioanalytical Method Validation. Vet Med:1–25.
Foote SL, Bloom FE, Aston Jones G (1983) Nucleus locus ceruleus: New evidence of anatomical and physiological specificity. Physiol Rev 63:844–914.

Foster DJ (2022) Muscarinic receptors: from clinic to bench to clinic. Trends Pharmacol Sci 43:461–463 Available at: https://doi.org/10.1016/j.tips.2022.01.006.
Foster DJ, Bryant ZK, Conn PJ (2021) Targeting muscarinic receptors to treat schizophrenia. Behavioural Brain Research 405:113201 Available at: https://doi.org/10.1016/j.bbr.2021.113201.
Foster DJ, Conn PJ (2017) Allosteric Modulation of GPCRs: New Insights and Potential Utility for Treatment of Schizophrenia and Other CNS Disorders. Neuron 94:431–446 Available at: http://dx.doi.org/10.1016/j.neuron.2017.03.016.
Foster DJ, Gentry PR, Lizardi-Ortiz JE, Bridges TM, Wood MR, Niswender CM, Sulzer D, Lindsley CW, Xiang Z, Conn PJ (2014) M5 receptor activation produces opposing physiological outcomes in dopamine neurons depending on the receptor's location. Journal of Neuroscience 34:3253–3262.
Frank MJ, Gagne C, Nyhus E, Masters S, Wiecki T v., Cavanagh JF, Badre D (2015) fMRI and EEG Predictors of Dynamic Decision Parameters during Human Reinforcement Learning. Journal of Neuroscience 35:485–494 Available at: http://www.jneurosci.org/content/35/2/485.
Franowicz JS, Arnsten AFT (1998) The alpha-2a noradrenergic agonist, guanfacine, improves delayed response performance in young adult rhesus monkeys. Psychopharmacology (Berl) 136:8–14.
Friedman NP, Robbins TW (2022) The role of prefrontal cortex in cognitive control and executive function. Neuropsychopharmacology 47:72–89.
Froudist-Walsh S, Xu T, Niu M, Rapan L, Margulies DS, Zilles K, Wang X-J, Palomero-Gallagher N (2021) Gradients of receptor expression in the macaque cortex. bioRxiv:2021.02.22.432173 Available at: https://doi.org/10.1101/2021.02.22.432173.
Furey ML, Pietrini P, Haxby J v., Drevets WC (2008) Selective effects of cholinergic modulation on task performance during selective attention. Neuropsychopharmacology 33:913–923.
Galvin VC, Arnsten AFT, Wang M (2018) Evolution in Neuromodulation—The Differential Roles of Acetylcholine in Higher Order Association vs. Primary Visual Cortices. Front Neural Circuits 12:1–14 Available at: https://www.frontiersin.org/article/10.3389/fncir.2018.00067/full.
Galvin VC, Yang ST, Paspalas CD, Yang Y, Jin LE, Datta D, Morozov YM, Lightbourne TC, Lowet AS, Rakic P, Arnsten AFT, Wang M (2020a) Muscarinic M1 Receptors Modulate Working Memory Performance and Activity via KCNQ Potassium Channels in the Primate Prefrontal Cortex. Neuron 106:649-661.e4 Available at: https://doi.org/10.1016/j.neuron.2020.02.030.
Galvin VC, Yang ST, Paspalas CD, Yang Y, Jin LE, Datta D, Morozov YM, Lightbourne TC, Lowet AS, Rakic P, Arnsten AFT, Wang M (2020b) Muscarinic M1 Receptors Modulate Working Memory Performance and Activity via KCNQ Potassium Channels in the Primate Prefrontal Cortex. Neuron 106:649-661.e4 Available at: https://doi.org/10.1016/j.neuron.2020.02.030.
Gamo NJ, Wang M, Arnsten AFT (2010) Methylphenidate and atomoxetine enhance prefrontal function through α2-adrenergic and dopamine D1 receptors. J Am Acad Child Adolesc Psychiatry 49:1011–1023.
Geerts H, Guillaumat PO, Grantham C, Bode W, Anciaux K, Sachak S (2005) Brain levels and acetylcholinesterase inhibition with galantamine and donepezil in rats, mice, and rabbits. Brain Res 1033:186–193.

Gershman SJ, Niv Y (2010) Learning latent structure: Carving nature at its joints. Curr Opin Neurobiol 20:251–256 Available at: http://dx.doi.org/10.1016/j.conb.2010.02.008.
Ghersi C, Bonfanti A, Manzari B, Feligioni M, Raiteri M, Pittaluga A (2003) Pharmacological heterogeneity of release-regulating presynaptic AMPA / kainate receptors in the rat brain : study with receptor antagonists. Neurochem Int 42:283–292.
Ghosh S, Maunsell JHR (2022) Locus coeruleus norepinephrine selectively controls visual attention. BioArxiv:1–13.
Ghoshal A, Rook JM, Dickerson JW, Roop GN, Morrison RD, Jalan-Sakrikar N, Lamsal A, Noetzel MJ, Poslusney MS, Wood MR, Melancon BJ, Stauffer SR, Xiang Z, Daniels JS, Niswender CM, Jones CK, Lindsley CW, Conn PJ (2016) Potentiation of M1 muscarinic receptor reverses plasticity deficits and negative and cognitive symptoms in a schizophrenia mouse model. Neuropsychopharmacology 41:598–610 Available at: http://dx.doi.org/10.1038/npp.2015.189.
Gläscher J, Adolphs R, Damasio H, Bechara A, Rudrauf D, Calamia M, Paul LK, Tranel D (2012) Lesion mapping of cognitive control and value-based decision making in the prefrontal cortex. Proc Natl Acad Sci U S A 109:14681–14686.
Glick SD, Jarvik ME (1970) Differential effects of amphetamine and scopolamine on matching performance of monkeys with lateral frontal lesions. J Comp Physiol Psychol 73:307–313.
Glimcher PW (2011) Understanding dopamine and reinforcement learning: The dopamine reward prediction error hypothesis. Proceedings of the National Academy of Sciences 108:17569.
Gobert A, Audinot V, Cistarelli L, Millan MJ (1998) Simultaneous quantification of serotonin, dopamine and noradrenaline levels in single frontal cortex dialysates of freely-moving rats reaveals a complex pattern of reciprocal auto- and heteroreceptor-mediated control of release. Neuroscience 84:413–429.
Goldman-Rakic PS, Lidow MS, Gallager DW (1990) Overlap of dopaminergic, adrenergic, and serotoninergic receptors and complementarity of their subtypes in primate prefrontal cortex. J Neurosci 10:2125–2138.
Gómez-Ríos GA, Tascon M, Reyes-garcés N, Boyacı E (2017) Quantitative analysis of biofluid spots by coated blade spray mass spectrometry , a new approach to rapid screening. Sci Rep 7:1–7.
Gould RW, Grannan MD, Gunter BW, Ball J, Bubser M, Bridges TM, Wess J, Wood MW, Brandon NJ, Duggan ME, Niswender CM, Lindsley CW, Conn PJ, Jones CK (2018) Cognitive enhancement and antipsychotic-like activity following repeated dosing with the selective M4 PAM VU0467154. Neuropharmacology 128:492–502.
Gould RW, Russell JK, Nedelcovych MT, Bubser M, Blobaum AL, Bridges TM, Newhouse PA, Lindsley CW, Conn PJ, Nader MA, Jones CK (2020) Modulation of arousal and sleep/wake architecture by M1 PAM VU0453595 across young and aged rodents and nonhuman primates. Neuropsychopharmacology 45:2219–2228 Available at: http://dx.doi.org/10.1038/s41386-020-00812-7.
Granger AJ, Mulder N, Saunders A, Sabatini BL (2016) Cotransmission of acetylcholine and GABA. Neuropharmacology 100:40–46.
Gratton C, Yousef S, Aarts E, Wallace DL, D'Esposito M, Silver MA (2017) Cholinergic, but not dopaminergic or noradrenergic, enhancement sharpens visual spatial perception in humans. Journal of Neuroscience 37:4405–4415.

Grilli M, Zappettini S, Zanardi A, Lagomarsino F, Pittaluga A, Zoli M, Marchi M (2009) Exposure to an enriched environment selectively increases the functional response of the pre-synaptic NMDA receptors which modulate noradrenaline release in mouse hippocampus. J Neurochem 110:1598–1606.
Grossman CD, Bari BA, Cohen JY (2022) Serotonin neurons modulate learning rate through uncertainty. Current Biology 32:586-599.e7 Available at: https://doi.org/10.1016/j.cub.2021.12.006.
Guihen E, Connor WTO (2009) Current separation and detection methods in microdialysis the drive towards sensitivity and speed. Electrophoresis 30:2062–2075.
H. Ferreira-Vieira T, M. Guimaraes I, R. Silva F, M. Ribeiro F (2016) Alzheimer's disease: Targeting the Cholinergic System. Curr Neuropharmacol 14:101–115.
Haber SN, Knutson B (2010) The reward circuit: Linking primate anatomy and human imaging. Neuropsychopharmacology 35:4–26 Available at: http://dx.doi.org/10.1038/npp.2009.129.
Hahn B (2015) Nicotinic Receptors and Attention.
Hains AB, Yabe Y, Arnsten AFT (2015) Chronic stimulation of alpha-2A-adrenoceptors with guanfacine protects rodent prefrontal cortex dendritic spines and cognition from the effects of chronic stress. Neurobiol Stress 2:1–9 Available at: http://dx.doi.org/10.1016/j.ynstr.2015.01.001.
Halliday GM, Leverenz JB, Schneider JS, Adler CH (2014) The Neurobiological Basis of Cognitive Impairment in Parkinson's Disease. Movement Disorders 29:634–650.
Halliday GM, Li YW, Blumbergs PC, Joh TH, Cotton PRGH, Howe PRC, Blessing WW, Geffen LB (1990) Neuropathology of Immunohstochemically Idendied Brainstem Neurons in Parkinson's Disease. American Neurological Association 27:373–385.
Hangya B, Ranade SP, Lorenc M, Kepecs A (2015) Central Cholinergic Neurons Are Rapidly Recruited by Reinforcement Feedback. Cell 162:1155–1168.
Hara M, Fukui R, Hieda E, Kuroiwa M, Bateup HS, Kano T, Greengard P, Nishi A (2010) Role of adrenoceptors in the regulation of dopamine/DARPP-32 signaling in neostriatal neurons. J Neurochem 113:1046–1059.
Harlé KM, Stewart JL, Zhang S, Tapert SF, Yu AJ, Paulus MP (2015) Bayesian neural adjustment of inhibitory control predicts emergence of problem stimulant use. Brain 138:3413–3426.
Hassan SF, Zumut S, Burke PG, Mcmullan S, Cornish JL, Goodchild AK (2015) Comparison of noradrenlaine, dopamine and serotonin in mediating the tachycardic and thermogenic effects of methamphetamine in the ventral medial prefrontal cortex. Neuroscience 295:209–220.
Hassani SA, Lendor S, Boyaci E, Pawliszyn J, Womelsdorf T (2019) Multineuromodulator measurements across fronto-striatal network areas of the behaving macaque using solid-phase microextraction. J Neurophysiol 122:1649–1660.
Hassani SA, Lendor S, Neumann A, Sinha Roy K, Banaie Boroujeni K, Hoffman KL, Pawliszyn J, Womelsdorf T (2021) Dose-Dependent Dissociation of Pro-cognitive Effects of Donepezil on Attention and Cognitive Flexibility in Rhesus Monkeys. Biological Psychiatry Global Open Science Available at: https://doi.org/10.1016/j.bpsgos.2021.11.012.
Hassani SA, Neumann A, Russell JK, Jones CK, Womelsdorf T (2023) M1 selective muscarinic allosteric modulation enhances cognitive flexibility and effective salience in nonhuman primates. in review.

Hassani SA, Oemisch M, Balcarras M, Westendorff S, Ardid S, van der Meer MA, Tiesinga P, Womelsdorf T (2017) A computational psychiatry approach identifies how alpha-2A noradrenergic agonist Guanfacine affects feature-based reinforcement learning in the macaque. Sci Rep 7:40606 Available at: http://www.nature.com/articles/srep40606.
Hassani SA, Womelsdorf T (2023) alpha2A adrenoceptor stimulation in primates supports fronto-striatal functions by enhancing reward prediction error encoding. in prep.
Hegedüs P, Sviatkó K, Király B, Martínez-Bellver S, Hangya B (2023) Cholinergic activity reflects reward expectations and predicts behavioral responses. iScience 26.
Heien MLA v, Johnson MA, Wightman RM (2004) Resolving neurotransmitters detected by fast-scan cyclic voltammetry. Anal Chem 76:5697–5704.
Heilbronner SR, Hayden BY (2016) Dorsal Anterior Cingulate Cortex: A Bottom-Up View. Annu Rev Neurosci 39:annurev-neuro-070815-013952 Available at: http://www.annualreviews.org/doi/10.1146/annurev-neuro-070815-013952.
Heilbronner SR, Hayden BY, Platt ML (2011) Decision salience signals in posterior cingulate cortex. Front Neurosci 5:1–9.
Herrero JL, Roberts MJ, Delicato LS, Gieselmann MA, Dayan P, Thiele A (2008) Acetylcholine contributes through muscarinic receptors to attentional modulation in V1. Nature 454:1110–1114.
Hersch SM, Gutekunst CA, Rees HD, Heilman CJ, Levey AI (1994) Distribution of m1-m4 muscarinic receptor proteins in the rat striatum: Light and electron microscopic immunocytochemistry using subtype-specific antibodies. Journal of Neuroscience 14:3351–3363.
Higgins GA, Silenieks LB, MacMillan C, Thevarkunnel S, Parachikova AI, Mombereau C, Lindgren H, Bastlund JF (2020) Characterization of Amphetamine, Methylphenidate, Nicotine, and Atomoxetine on Measures of Attention, Impulsive Action, and Motivation in the Rat: Implications for Translational Research. Front Pharmacol 11.
Hikosaka O, Ghazizadeh A, Griggs W, Amita H (2017) Parallel basal ganglia circuits for decision making. J Neural Transm:1–15.
Hikosaka O, Kim HF, Amita H, Yasuda M, Isoda M, Tachibana Y, Yoshida A (2019) Direct and indirect pathways for choosing objects and actions. European Journal of Neuroscience 49:637–645.
Hillmer AT, Wooten DW, Moirano JM, Slesarev M, Barnhart TE, Engle JW, Nickles RJ, Murali D, Schneider ML, Mukherjee J, Christian BT (2011) Specific α4β2 nicotinic acetylcholine receptor binding of [F-18]nifene in the rhesus monkey. Synapse 65:1309–1318.
Hirayama J, Yoshimoto J, Ishii S (2004) Bayesian representation learning in the cortex regulated by acetylcholine. Neural Networks 17:1391–1400.
Hock C, Müller-Spahn F, Schuh-Hofer S, Hofmann M, Dirnagl U, Villringer A (1995) Age dependency of changes in cerebral hemoglobin oxygenation during brain activation: A near-infrared spectroscopy study. Journal of Cerebral Blood Flow and Metabolism 15:1103–1108.
Holloway ZR, Freels TG, Comstock JF, Nolen HG, Sable HJ, Lester DB (2019) Comparing phasic dopamine dynamics in the striatum, nucleus accumbens, amygdala, and medial prefrontal cortex. Synapse 73:1–15.
Howe WM, Gritton HJ, Lusk NA, Roberts EA, Hetrick VL, Berke JD, Sarter M (2017) Acetylcholine Release in Prefrontal Cortex Promotes Gamma Oscillations and Theta–Gamma Coupling during Cue Detection. The Journal of Neuroscience 37:3215–3230.

Howlett JR, Huang H, Hysek CM, Paulus MP (2017) The effect of single-dose methylphenidate on the rate of error-driven learning in healthy males: a randomized controlled trial. Psychopharmacology (Berl) 234:3353–3360.
Huys QJ, Pizzagalli DA, Bogdan R, Dayan P (2013) Mapping anhedonia onto reinforcement learning: a behavioural meta-analysis. Biol Mood Anxiety Disord 3:1–16.
Huys QJM, Maia T v, Frank MJ (2016) Computational psychiatry as a bridge from neuroscience to clinical applications. Nat Neurosci 19:404–413 Available at: http://dx.doi.org/10.1038/nn.4238.
Iglesias S, Kasper L, Harrison SJ, Manka R, Mathys C, Stephan KE (2021) Cholinergic and dopaminergic effects on prediction error and uncertainty responses during sensory associative learning. Neuroimage 226.
Imbimbo B pietro (2001) Pharmacodynamic-tolerability relationships of cholinesterase inhibitors for Alzheimer's disease. CNS Drugs 15:375–390.
Irwin S (1968) Comprehensive observational assessment: Ia. A systematic, quantitative procedure for assessing the behavioral and physiologic state of the mouse. Psychopharmacologia 13:222–257.
Izquierdo A, Brigman JL, Radke AK, Rudebeck PH, Holmes A (2016) The neural basis of reversal learning: An updated perspective. Neuroscience Available at: http://linkinghub.elsevier.com/retrieve/pii/S030645221600244X.
Izquierdo A, Brigman JL, Radke AK, Rudebeck PH, Holmes A (2017) The neural basis of reversal learning: An updated perspective. Neuroscience 345:12–26 Available at: http://dx.doi.org/10.1016/j.neuroscience.2016.03.021.
Jacobs CB, Peairs MJ, Venton BJ (2010) Review: Carbon nanotube based electrochemical sensors for biomolecules. Anal Chim Acta 662:105–127.
Jäkälä P, Riekkinen M, Sirviö J, Koivisto E, Kejonen K, Matti, Riekkinen P (1999a) Guanfacine, but not clonidine, improves planning and working memory performance in humans. Neuropsychopharmacology 20:460–470.
Jäkälä P, Sirviö J, Riekkinen M, Koivisto E, Kejonen K, Vanhanen M, Riekkinen P (1999b) Guanfacine and clonidine, alpha2-agonists, improve paired associates Learning, but not delayed matching to sample, in humans. Neuropsychopharmacology 20:119–130.
Jentsch JD, Sanchez D, Elsworth JD, Roth RH (2008) Clonidine and guanfacine attenuate phencyclidine-induced dopamine overflow in rat prefrontal cortex: Mediating influence of the alpha-2A adrenoceptor subtype. Brain Res 1246:41–46 Available at: http://dx.doi.org/10.1016/j.brainres.2008.10.006.
Jepma M, Murphy PR, Nassar MR, Rangel-Gomez M, Meeter M, Nieuwenhuis S (2016) Catecholaminergic Regulation of Learning Rate in a Dynamic Environment. PLoS Comput Biol 12:1–24.
Ji X-H, Ji J-Z, Zhang H, Li B-M (2008) Stimulation of alpha2-adrenoceptors suppresses excitatory synaptic transmission in the medial prefrontal cortex of rat. Neuropsychopharmacology 33:2263–2271.
Jin LE, Wang M, Galvin VC, Lightbourne TC, Conn PJ, Arnsten AFT, Paspalas CD (2018) MGluR2 versus mGluR3 Metabotropic Glutamate Receptors in Primate Dorsolateral Prefrontal Cortex: Postsynaptic mGluR3 Strengthen Working Memory Networks. Cerebral Cortex 28:974–987.
Jing M, Zhang Y, Wang H, Li Y (2019) G-protein-coupled receptor-based sensors for imaging neurochemicals with high sensitivity and specificity. J Neurochem 151:279–288.

Jones BE, Cuello AC (1989) Afferents to the basal forebrain cholinergic cell area from pontomesencephalic-catecholamine, serotonin, and acetylcholine-neurons. Neuroscience 31:37–61.
Jones CK, Byun N, Bubser M (2012) Muscarinic and nicotinic acetylcholine receptor agonists and allosteric modulators for the treatment of schizophrenia. Neuropsychopharmacology 37:16–42.
Jones RW, Soininen H, Hager K, Aarsland D, Passmore P, Murthy A, Zhang R, Bahra R (2004) A multinational, randomised, 12-week study comparing the effects of donepezil and galantamine in patients with mild to moderate Alzheimer's disease. Int J Geriatr Psychiatry 19:58–67.
Joshi S, Gold JI (2022) Context-Dependent Relationships between Locus Coeruleus Firing Patterns and Coordinated Neural Activity in the Anterior Cingulate Cortex. Elife.
Joshi S, Li Y, Kalwani R, Gold JI (2016) Relationships between pupil diameter and neuronal activity in the locus coeruleus, colliculi, and cingulate cortex. 89:221–234.
Kaasinen V, Någren K, Järvenpää T, Roivainen A, Yu M, Oikonen V, Kurki T, Rinne JO (2002) Regional effects of donepezil and rivastigmine on cortical acetylcholinesterase activity in Alzheimer's disease. J Clin Psychopharmacol 22:615–620.
Kao C-Y, Anderzhanova E, Asara JM, Wotjak CT, Turrck CW (2015) NextGen Brain Microdialysis : Applying Modern Metabolomics Technology to the Analysis of Extracellular Fluid in the Central Nervous System. Mol Neuropsychiatry 1:60–67.
Kaping D, Vinck M, Hutchison RM, Everling S, Womelsdorf T (2011) Specific contributions of ventromedial, anterior cingulate, and lateral prefrontal cortex for attentional selection and stimulus valuation. PLoS Biol 9:e1001224 Available at: http://www.pubmedcentral.nih.gov/articlerender.fcgi?artid=3246452&tool=pmcentrez&rendertype=abstract [Accessed August 22, 2014].
Karasova JZ, Hrabinova M, Krejciova M, Jun D, Kuca K (2020) Donepezil and rivastigmine: Pharmacokinetic profile and brain-targeting after intramuscular administration in rats. Iranian Journal of Pharmaceutical Research 19:95–102.
Kawaguchi Y, Shindou T (1998) Noradrenergic excitation and inhibition of GABAergic cell types in rat frontal cortex. Journal of Neuroscience 18:6963–6976.
Kawaura K, Karasawa J ichi, Chaki S, Hikichi H (2014) Stimulation of postsynapse adrenergic alpha2A receptor improves attention/cognition performance in an animal model of attention deficit hyperactivity disorder. Behavioural Brain Research 270:349–356 Available at: http://dx.doi.org/10.1016/j.bbr.2014.05.044.
Kennedy RT (2013) Emerging trends in in vivo neurochemical monitoring by microdialysis. Curr Opin Chem Biol 17:860–867 Available at: http://dx.doi.org/10.1016/j.cbpa.2013.06.012.
Kennerley SW, Dahmubed AF, Lara AH, Wallis JD (2009) Neurons in the frontal lobe encode the value of multiple decision variables. J Cogn Neurosci 21:1162–1178.
Kennerley SW, Walton ME, Behrens TEJ, Buckley MJ, Rushworth MFS (2006) Optimal decision making and the anterior cingulate cortex. Nat Neurosci 9:940–947.
Khalighinejad N, Bongioanni A, Verhagen L, Folloni D, Attali D, Aubry JF, Sallet J, Rushworth MFS (2020) A Basal Forebrain-Cingulate Circuit in Macaques Decides It Is Time to Act. Neuron 105:370-384.e8 Available at: https://doi.org/10.1016/j.neuron.2019.10.030.
Kiechel JR (1980) Pharmacokinetics and metabolism of guanfacine in man: a review. Br J Clin Pharmacol 10:25S-32S.

Kikuchi T, Okamura T, Arai T, Obata T, Fukushi K, Irie T, Shiraishi T (2010) Use of a novel radiometric method to assess the inhibitory effect of donepezil on acetylcholinesterase activity in minimally diluted tissue samples. Br J Pharmacol 159:1732–1742.
Kim HF, Hikosaka O (2013) Distinct Basal Ganglia Circuits Controlling Behaviors Guided by Flexible and Stable Values. Neuron 79:1001–1010 Available at: http://dx.doi.org/10.1016/j.neuron.2013.06.044.
Kim HF, Hikosaka O (2015) Parallel basal ganglia circuits for voluntary and automatic behaviour to reach rewards. Brain 138:1776–1800.
Kim S, Bobeica I, Gamo NJ, Arnsten AFT, Lee D (2012) Effects of α-2A adrenergic receptor agonist on time and risk preference in primates. Psychopharmacology (Berl) 219:363–375.
Knakker B, Oláh V, Trunk A, Lendvai B, Lévay G, Hernádi I (2021) Delay-dependent cholinergic modulation of visual short-term memory in rhesus macaques. Behavioural Brain Research 396.
Koda K, Ago Y, Cong Y, Kita Y, Takuma K, Matsuda T (2010) Effects of acute and chronic administration of atomoxetine and methylphenidate on extracellular levels of noradrenaline, dopamine and serotonin in the prefrontal cortex and striatum of mice. J Neurochem 114:259–270.
Kodama T, Hikosaka K, Honda Y, Kojima T, Tsutsui K, Watanabe M (2015) Dopamine and glutamate release in the anterior default system during rest : A monkey microdialysis study. Behavioural Brain Research 294:194–197.
Kodama T, Hikosaka K, Watanabe M (2002) Differential changes in glutamate concentration in the primate prefrontal cortex during spatial delayed alternation and sensory-guided tasks. Exp Brain Res 145:133–141.
Kodama T, Kojima T, Honda Y, Hosokawa T, Tsutsui K, Watanabe M (2017) Oral Administration of Methylphenidate (Ritalin) Affects Dopamine Release Differentially Between the Prefrontal Cortex and Striatum: A Microdialysis Study in the Monkey. The Journal of Neuroscience 37:2387–2394 Available at: http://www.jneurosci.org/lookup/doi/10.1523/JNEUROSCI.2155-16.2017.
Kolta A, Diop L, Reader TA (1987) Noradrenergic effects on rat visual cortex: Single-cell microiontophoretic studies of alpha-2 adrenergic receptors. Life Sci 41:281–289.
König M, Thinnes A, Klein J (2018) Microdialysis and its use in behavioural studies: Focus on acetylcholine. J Neurosci Methods 300:206–215.
Korczyn AD (2000) Muscarinic M1 agonists in the treatment of Alzheimer's disease. Expert Opin Investig Drugs 9:2259–2267.
Kossl M, Vater M (1989) Noradrenaline enhances temporal auditory contrast and neuronal timing precision in the cochlear nucleus of the mustached bat. Journal of Neuroscience 9:4169–4178.
Kreitzer AC (2009) Physiology and pharmacology of striatal neurons. Annu Rev Neurosci 32:127–147.
Kucinski A, Phillips KB, Koshy Cherian A, Sarter M (2020) Rescuing the attentional performance of rats with cholinergic losses by the M1 positive allosteric modulator TAK-071. Psychopharmacology (Berl) 237:137–153.
Kume T, Sugimoto M, Takada Y, Yamaguchi T, Yonezawa A, Katsuki H, Sugimoto H, Akaike A (2005) Up-regulation of nicotinic acetylcholine receptors by central-type acetylcholinesterase inhibitors in rat cortical neurons. Eur J Pharmacol 527:77–85.

Kuwabara M, Mansouri FA, Buckley MJ, Tanaka K (2014) Cognitive control functions of anterior cingulate cortex in macaque monkeys performing a wisconsin card sorting test analog. Journal of Neuroscience 34:7531–7547.
Lange HS, Cannon CE, Drott JT, Kuduk SD, Uslaner JM (2015a) The M1 muscarinic positive allosteric modulator PQCA improves performance on translatable tests of memory and attention in rhesus monkeys. Journal of Pharmacology and Experimental Therapeutics 355:442–450.
Lange HS, Cannon CE, Drott JT, Kuduk SD, Uslaner JM (2015b) The M1 muscarinic positive allosteric modulator PQCA improves performance on translatable tests of memory and attention in rhesus monkeys. Journal of Pharmacology and Experimental Therapeutics 355:442–450.
Langmead CJ, Watson J, Reavill C (2008) Muscarinic acetylcholine receptors as CNS drug targets. Pharmacol Ther 117:232–243.
Lansink CS, Goltstein PM, Lankelma J v., Pennartz CMA (2010) Fast-spiking interneurons of the rat ventral striatum: Temporal coordination of activity with principal cells and responsiveness to reward. European Journal of Neuroscience 32:494–508.
Lapiz MDS, Morilak DA (2006) Noradrenergic modulation of cognitive function in rat medial prefrontal cortex as measured by attentional set shifting capability. Neuroscience 137:1039–1049.
Lee M, Mueller A, Moore T (2020) Differences in Noradrenaline Receptor Expression Across Different Neuronal Subtypes in Macaque Frontal Eye Field. Front Neuroanat 14:1–15.
Lendor S, Gómez-Ríos GA, Boyacl E, vander Heide H, Pawliszyn J (2019a) Space-resolved tissue analysis by solid-phase microextraction coupled to high-resolution mass spectrometry via desorption electrospray ionization. Anal Chem 91:10141–10148.
Lendor S, Hassani S-A, Boyaci E, Singh V, Womelsdorf T, Pawliszyn J (2019b) Solid Phase Microextraction-Based Miniaturized Probe and Protocol for Extraction of Neurotransmitters from Brains in Vivo. Anal Chem 91:4896–4905.
Leo G de, Gulino R, Coradazzi M (2023) Acetylcholine and noradrenaline differentially regulate hippocampus-dependent spatial learning and memory. Brain Commun 5:1–15 Available at: https://doi.org/10.1093/braincomms/fcac338.
Levey AI (1996) Muscarinic acetylcholine receptor expression in memory circuits: Implications for treatment of Alzheimer disease. Proc Natl Acad Sci U S A 93:13541–13546.
Levey AI, Kitt CA, Simonds WF, Price DL, Brann MR (1991) Identification and localization of muscarinic acetylcholine receptor proteins in brain with subtype-specific antibodies. Journal of Neuroscience 11:3218–3226.
Levin ED, Bushnell PJ, Rezvani AH (2011) Attention-modulating effects of cognitive enhancers. Pharmacol Biochem Behav 99:146–154 Available at: http://dx.doi.org/10.1016/j.pbb.2011.02.008.
Li BM, Mei ZT (1994) Delayed-response deficit induced by local injection of the alpha2-adrenergic antagonist yohimbine into the dorsolateral prefrontal cortex in young adult monkeys. Behav Neural Biol 62:134–139.
Li DD, Zhang YH, Zhang W, Zhao P (2019) Meta-analysis of randomized controlled trials on the efficacy and safety of donepezil, galantamine, rivastigmine, and memantine for the treatment of Alzheimer's disease. Front Neurosci 13.
Li J, von Pföstl V, Zaldivar D, Zhang X, Logothetis NK, Rauch A (2012) Measuring multiple neurochemicals and related metabolites in blood and brain of the rhesus monkey by using

dual microdialysis sampling and capillary hydrophilic interaction chromatography-mass spectrometry. Anal Bioanal Chem 402:2545–2554.
Lin SC, Gervasoni D, Nicolelis MAL (2006) Fast modulation of prefrontal cortex activity by basal forebrain noncholinergic neuronal ensembles. J Neurophysiol 96:3209–3219.
Liu Y, Liang X, Ren WW, Li BM (2014) Expression of β1- and β2-adrenoceptors in different subtypes of interneurons in the medial prefrontal cortex of mice. Neuroscience 257:149–157.
Ljubojevic V, Luu P, de Rosa E (2014) Cholinergic contributions to supramodal attentional processes in rats. Journal of Neuroscience 34:2264–2275.
Lucas-Meunier E, Fossier P, Baux G, Amar M (2003) Cholinergic modulation of the cortical neuronal network. Pflugers Arch 446:17–29.
Luccini E, Musante V, Neri E, Brambilla Bas M, Severi P, Raiteri M, Pittaluga A (2007) Functional interactions between presynaptic NMDA receptors and metabotropic glutamate receptors co-expressed on rat and human noradrenergic terminals. Br J Pharmacol 151:1087–1094.
Luine VN, Mohan G, Tu Z, Efange SMN (2002) Chromaproline and Chromaperidine, nicotine agonists, and Donepezil, cholinesterase inhibitor, enhance performance of memory tasks in ovariectomized rats. Pharmacol Biochem Behav 74:213–220.
Luo M, Zhou J, Liu Z (2015) Reward processing by the dorsal raphe nucleus: 5-HT and beyond. Learning and Memory 22:452–460.
Lustig C, Sarter M (2015) Attention and the Cholinergic System: Relevance to Schizophrenia. In: Current Topics in Behavioral Neurosciences, pp 327–362 Available at: http://link.springer.com/10.1007/7854_2015_5009.
Ma L et al. (2009) Selective activation of the M1 muscarinic acetylcholine receptor achieved by allosteric potentiation. Proc Natl Acad Sci U S A 106:15950–15955.
Maia T v, Frank MJ (2011) From reinforcement learning models to psychiatric and neurological disorders. Nat Neurosci 14:154–162 Available at: http://dx.doi.org/10.1038/nn.2723.
Major AJ, Vijayraghavan S, Everling S (2015) Muscarinic attenuation of mnemonic rule representation in macaque dorsolateral prefrontal cortex during a pro-and anti-saccade task. Journal of Neuroscience 35:16064–16076.
Major AJ, Vijayraghavan S, Everling S (2018) Cholinergic overstimulation attenuates rule selectivity in macaque prefrontal cortex. Journal of Neuroscience 38:1137–1150.
Mansouri FA, Buckley MJ, Fehring DJ, Tanaka K (2020) The Role of Primate Prefrontal Cortex in Bias and Shift between Visual Dimensions. Cerebral Cortex 30:85–99.
Mansouri FA, Buckley MJ, Tanaka K (2007) Mnemonic Function of the Dorsolateral Prefrontal Cortex in Conflict-Induced Behavioral Adjustment. Science (1979) 318:987–990 Available at: https://www.science.org/doi/10.1126/science.1146384.
Mao ZM, Arnsten AFT, Li BM (1999) Local infusion of an α-1 adrenergic agonist into the prefrontal cortex impairs spatial working memory performance in monkeys. Biol Psychiatry 46:1259–1265.
Marder E (2012) Overview Neuromodulation of Neuronal Circuits: Back to the Future. Neuron 76:1–11 Available at: http://dx.doi.org/10.1016/j.neuron.2012.09.010.
Marder E, O'Leary T, Shruti S (2014) Neuromodulation of Circuits with Variable Parameters: Single Neurons and Small Circuits Reveal Principles of State-Dependent and Robust Neuromodulation. Annu Rev Neurosci 37:329–346 Available at: http://www.annualreviews.org/doi/10.1146/annurev-neuro-071013-013958.

Marshall L, Mathys C, Ruge D, de Berker AO, Dayan P, Stephan KE, Bestmann S (2016a) Pharmacological Fingerprints of Contextual Uncertainty. PLoS Biol 14:1–31.
Marshall L, Mathys C, Ruge D, de Berker AO, Dayan P, Stephan KE, Bestmann S (2016b) Pharmacological Fingerprints of Contextual Uncertainty. PLoS Biol 14:1–31.
Marucci G, Buccioni M, Ben DD, Lambertucci C, Volpini R, Amenta F (2021) Efficacy of acetylcholinesterase inhibitors in Alzheimer's disease. Neuropharmacology:108352 Available at: https://doi.org/10.1016/j.neuropharm.2020.108352.
Mather M, Clewett D, Sakaki M, Harley CW (2016) Norepinephrine ignites local hotspots of neuronal excitation: How arousal amplifies selectivity in perception and memory. Behavioral and Brain Sciences 39:e200 Available at: https://www.cambridge.org/core/product/identifier/S0140525X15000667/type/journal_article.
Matsumoto M, Matsumoto K, Abe H, Tanaka K (2007) Medial prefrontal cell activity signaling prediction errors of action values. Nat Neurosci 10:647–656.
McBurney-Lin J, Vargova G, Garad M, Zagha E, Yang H (2022) The locus coeruleus mediates behavioral flexibility. Cell Rep 41:111534 Available at: https://doi.org/10.1016/j.celrep.2022.111534.
McGaughy J, Ross RS, Eichenbaum H (2008) Noradrenergic, but not cholinergic, deafferentation of prefrontal cortex impairs attentional set-shifting. Neuroscience 153:63–71.
McGinley MJ, Vinck M, Reimer J, Batista-Brito R, Zagha E, Cadwell CR, Tolias AS, Cardin JA, McCormick DA (2015) Waking State: Rapid Variations Modulate Neural and Behavioral Responses. Neuron 87:1143–1161.
Megemont M, McBurney-Lin J, Yang H (2022) Pupil diameter is not an accurate real-time readout of locus coeruleus activity. Elife 11:1–17.
Melancon BJ, Tarr JC, Panarese JD, Wood MR, Lindsley CW (2013) Allosteric modulation of the M1 muscarinic acetylcholine receptor: Improving cognition and a potential treatment for schizophrenia and Alzheimer's disease. Drug Discov Today 18:1185–1199 Available at: http://dx.doi.org/10.1016/j.drudis.2013.09.005.
Mesulam M -Marsel, Mufson EJ, Levey AI, Wainer BH (1983) Cholinergic innervation of cortex by the basal forebrain: Cytochemistry and cortical connections of the septal area, diagonal band nuclei, nucleus basalis (Substantia innominata), and hypothalamus in the rhesus monkey. Journal of Comparative Neurology 214:170–197.
Millan MJ et al. (2012) Cognitive dysfunction in psychiatric disorders: characteristics, causes and the quest for improved therapy. Nat Rev Drug Discov 11:141–168 Available at: http://dx.doi.org/10.1038/nrd3628\npapers3://publication/doi/10.1038/nrd3628\nhttp://www.nature.com/doifinder/10.1038/nrd3628.
Millan MJ, Goodwin GM, Meyer-lindenberg A, Ove S (2015) Learning from the past and looking to the future : Emerging perspectives for improving the treatment of psychiatric disorders. European Neuropsychopharmacology 25:599–656.
Minamimoto T, Saunders RC, Richmond BJ (2010) Monkeys quickly learn and generalize visual categories without lateral prefrontal cortex. Neuron 66:501–507 Available at: http://dx.doi.org/10.1016/j.neuron.2010.04.010.
Mirenowicz J, Schultz W (1994) Importance of unpredictability for reward responses in primate dopamine neurons. J Neurophysiol 72:1024–1027.

Mirza NR, Stolerman IP (2000) The role of nicotinic and muscarinic acetylcholine receptors in attention. Psychopharmacology (Berl) 148:243–250.
Moehle MS, Conn PJ (2019) Roles of the M4 acetylcholine receptor in the basal ganglia and the treatment of movement disorders. Movement Disorders 34:1089–1099.
Moehle MS, Pancani T, Byun N, Yohn SE, Wilson GH, Dickerson JW, Remke DH, Xiang Z, Niswender CM, Wess J, Jones CK, Lindsley CW, Rook JM, Conn PJ (2017) Cholinergic Projections to the Substantia Nigra Pars Reticulata Inhibit Dopamine Modulation of Basal Ganglia through the M4Muscarinic Receptor. Neuron 96:1358–1372.
Moghaddam B (1993) Stress Preferentially Increases Extraneurona Levels of Excitatory Amino Acids in the Prefrontal Cortex : Comparison to Hippocampus and Basal Ganglia. J Neurochem 60:1650–1657.
Mohebi A, Collins VL, Berke JD (2022) Cholinergic Interneurons Drive Motivation by Promoting Dopamine Release in the Nucleus Accumbens. bioRxiv:2022.11.06.515335 Available at: https://www.biorxiv.org/content/10.1101/2022.11.06.515335v1%0Ahttps://www.biorxiv.org/content/10.1101/2022.11.06.515335v1.abstract.
Monosov IE (2017) Anterior cingulate is a source of valence-specific information about value and uncertainty. Nat Commun 8:1–11 Available at: http://dx.doi.org/10.1038/s41467-017-00072-y.
Monosov IE, Haber SN, Leuthardt EC, Jezzini A (2020) Anterior Cingulate Cortex and the Control of Dynamic Behavior in Primates. Current Biology 30:R1442–R1454 Available at: https://doi.org/10.1016/j.cub.2020.10.009.
Monosov IE, Leopold DA, Hikosaka O (2015) Neurons in the primate medial basal forebrain signal combined information about reward uncertainty, value, and punishment anticipation. Journal of Neuroscience 35:7443–7459.
Moore TL, Killiany RJ, Herndon JG, Rosene DL, Moss MB (2006) Executive system dysfunction occurs as early as middle-age in the rhesus monkey. Neurobiol Aging 27:1484–1493.
Moran SP, DIckerson JW, Cho HP, Xiang Z, Maksymetz J, Remke DH, Lv X, Doyle CA, Rajan DH, Niswender CM, Engers DW, Lindsley CW, Rook JM, Conn PJ (2018) M1-positive allosteric modulators lacking agonist activity provide the optimal profile for enhancing cognition. Neuropsychopharmacology 43:1763–1771 Available at: http://dx.doi.org/10.1038/s41386-018-0033-9.
Mori S (2002) Responses to donepezil in Alzheimer's disease and Parkinson's disease. Ann N Y Acad Sci 977:493–500.
Moritz S, Hottenrott B, Randjbar S, Klinge R, von Eckstaedt FV, Lincoln TM, Jelinek L (2009) Perseveration and not strategic deficits underlie delayed alternation impairment in obsessive-compulsive disorder (OCD). Psychiatry Res 170:66–69 Available at: http://dx.doi.org/10.1016/j.psychres.2008.09.003.
Morón JA, Brockington A, Wise RA, Rocha BA, Hope BT (2002) Dopamine uptake through the norepinephrine transporter in brain regions with low levels of the dopamine transporter: Evidence from knock-out mouse lines. Journal of Neuroscience 22:389–395.
Morris LS, Kundu P, Dowell N, Mechelmans DJ, Favre P, Irvine MA, Robbins TW, Daw N, Bullmore ET, Harrison NA, Voon V (2016) Fronto-striatal organization: Defining functional and microstructural substrates of behavioural flexibility. Cortex 74:118–133 Available at: http://dx.doi.org/10.1016/j.cortex.2015.11.004.

Moussawi K, Riegel A, Nair S, Kalivas PW, Bargas J, Nacional U (2011) Extracellular glutamate : functional compartments operate in different concentration ranges. Front Syst Neurosci 5:1–9.

Mrzljak L, Levey AI, Goldman-Rakic PS (1993) Association of m1 and m2 muscarinic receptor proteins with asymmetric synapses in the primate cerebral cortex: Morphological evidence for cholinergic modulation of excitatory neurotransmission. Proc Natl Acad Sci U S A 90:5194–5198.

Mrzljak L, Pappy M, Leranth C, Goldman-Rakic PS (1995) Cholinergic synaptic circuitry in the macaque prefrontal cortex. J Comp Neurol 357:603–617 Available at: https://onlinelibrary.wiley.com/doi/10.1002/cne.903570409.

Muir JL, Dunnett SB, Robbins TW, Everitt BJ (1992) Attentional functions of the forebrain cholinergic systems: effects of intraventricular hemicholinium, physostigmine, basal forebrain lesions and intracortical grafts on a multiple-choice serial reaction time task. Exp Brain Res 89:611–622.

Müller U, Clark L, Lam ML, Moore RM, Murphy CL, Richmond NK, Sandhu RS, Wilkins IA, Menon DK, Sahakian BJ, Robbins TW (2005) Lack of effects of guanfacine on executive and memory functions in healthy male volunteers. Psychopharmacology (Berl) 182:205–213.

Murphy PR, O'Connell RG, O'Sullivan M, Robertson IH, Balsters JH (2014) Pupil diameter covaries with BOLD activity in human locus coeruleus. Hum Brain Mapp 35:4140–4154.

Nácher V, Hassani SA, Womelsdorf T (2018) Asymmetric effective connectivity between primate anterior cingulate and lateral prefrontal cortex revealed by electrical microstimulation. Brain Struct Funct 224:779–793 Available at: http://dx.doi.org/10.1007/s00429-018-1806-y.

Nai Q, Dong HW, Hayar A, Linster C, Ennis M (2009) Noradrenergic regulation of GABAergic inhibition of main olfactory bulb mitral cells varies as a function of concentration and receptor subtype. J Neurophysiol 101:2472–2484.

Nassar MR, Rumsey KM, Wilson RC, Parikh K, Heasly B, Gold JI (2012) Rational regulation of learning dynamics by pupil-linked arousal systems. Nat Neurosci 15:1040–1046 Available at: http://dx.doi.org/10.1038/nn.3130.

Newman EL, Gupta K, Climer JR, Monaghan CK, Hasselmo ME (2012) Cholinergic modulation of cognitive processing: Insights drawn from computational models. Front Behav Neurosci 6:1–19.

Nishiyama S, Tsukada H, Sato K, Kakiuchi T, Ohba H, Harada N, Takahashi K (2001) Evaluation of PET ligands (+) N-[11C]ethyl-3-piperidyl benzilate and (+) N-[11C]propyl-3-piperidyl benzilate for muscarinic cholinergic receptors: A PET study with microdialysis in comparison with (+)N-[11C]methyl-3-piperidyl benzilate in the conscious mo. Synapse 40:159–169.

Niv Y, Daniel R, Geana A, Gershman SJ, Leong YC, Radulescu A, Wilson RC (2015) Reinforcement learning in multidimensional environments relies on attention mechanisms. Journal of Neuroscience 35:8145–8157 Available at: http://www.ncbi.nlm.nih.gov/pubmed/26019331\nhttp://www.jneurosci.org/cgi/doi/10.1523/JNEUROSCI.2978-14.2015.

Nomura S, Bouhadana M, Morel C, Faure P, Cauli B, Lambolez B, Hepp R (2014) Noradrenalin and dopamine receptors both control cAMP-PKA signaling throughout the cerebral cortex. Front Cell Neurosci 8:1–12.

Noonan MAP, Crittenden BM, Jensen O, Stokes MG (2018) Selective inhibition of distracting input. Behavioural Brain Research 355:36–47 Available at: https://doi.org/10.1016/j.bbr.2017.10.010.
Oemisch M, Westendorff S, Azimi M, Hassani SA, Ardid S, Tiesinga P, Womelsdorf T (2019) Feature-specific prediction errors and surprise across macaque fronto-striatal circuits. Nat Commun 10:1–15 Available at: http://dx.doi.org/10.1038/s41467-018-08184-9.
Oemisch M, Westendorff S, Everling S, Womelsdorf T (2015) Interareal spike-train correlations of anterior cingulate and dorsal prefrontal cortex during attention shifts. Journal of Neuroscience 35:13076–13089.
Ohshima M, Itami C, Kimura F (2017) The α2A-adrenoceptor suppresses excitatory synaptic transmission to both excitatory and inhibitory neurons in layer 4 barrel cortex. Journal of Physiology 595:6923–6937.
Okada M, Fukuyama K, Kawano Y, Shiroyama T, Suzuki D, Ueda Y (2018) Effects of acute and sub-chronic administrations of guanfacine on catecholaminergic transmissions in the orbitofrontal cortex. Neuropharmacology 156:107547 Available at: https://doi.org/10.1016/j.neuropharm.2019.02.029.
O'Neill J, Fitten LJ, Siembieda DW, Ortiz F, Halgren E (2000) Effects of guanfacine on three forms of distraction in the aging macaque. Life Sci 67:877–885.
O'Neill J, Siembieda DW, Crawford KC, Halgren E, Fisher A, Fitten LJ (2003) Reduction in distractibility with AF102B and THA in the macaque. Pharmacol Biochem Behav 76:301–306.
O'Reilly JX, Schüffelgen U, Cuell SF, Behrens TEJ, Mars RB, Rushworth MFS (2013) Dissociable effects of surprise and model update in parietal and anterior cingulate cortex. Proc Natl Acad Sci U S A 110.
Ouyang G, Pawliszyn J (2007) Configurations and calibration methods for passive sampling techniques. J Chromatogr A 1168:226–235.
Padoa-Schioppa C, Assad JA (2006) Neurons in the orbitofrontal cortex encode economic value. Nature 441:223–226.
Palmer D, Dumont JR, Dexter TD, Prado MAM, Finger E, Bussey TJ, Saksida LM (2021) Touchscreen cognitive testing: Cross-species translation and co-clinical trials in neurodegenerative and neuropsychiatric disease. Neurobiol Learn Mem 182:107443 Available at: https://doi.org/10.1016/j.nlm.2021.107443.
Palomero-Gallagher N, Mohlberg H, Zilles K, Vogt B (2008) Cytology and receptor architecture of human anterior cingulate cortex. Journal of Comparative Neurology 508:906–926.
Parikh V, Ji J, Decker MW, Sarter M (2010) Prefrontal β2 subunit-containing and α7 nicotinic acetylcholine receptors differentially control glutamatergic and cholinergic signaling. Journal of Neuroscience 30:3518–3530.
Parikh V, Kozak R, Martinez V, Sarter M (2007) Prefrontal Acetylcholine Release Controls Cue Detection on Multiple Timescales. Neuron 56:141–154.
Parikh V, Pomerleau F, Huettl P, Gerhardt GA, Sarter M, Bruno JP (2004) Rapid assessment of in vivo cholinergic transmission by amperometric detection of changes in extracellular choline levels. European Journal of Neuroscience 20:1545–1554.
Passingham R (2021) Understanding the Prefrontal Cortex: Selective Advantage, Connectivity, and Neural Operations. Oxford University Press. Available at: https://books.google.com/books?id=jOEsEAAAQBAJ.
Passingham RE, Wise SP (2015) The Neurobiology of the Prefrontal Cortex.

Patel S et al. (1997) Biological profile of L-745,870, a selective antagonist with high affinity for the dopamine D4 receptor. Journal of Pharmacology and Experimental Therapeutics 283:636–647.
Patriarchi T, Cho JR, Merten K, Howe MW, Marley A, Xiong W, Folk RW, Broussard GJ, Liang R, Jang MJ, Zhong H, Dombeck D, von Zastrow M, Nimmerjahn A, Gradinaru V, Williams JT, Tian L (2018) Ultrafast neuronal imaging of dopamine dynamics with designed genetically encoded sensors. Science (1979) 360:1–22 Available at: https://www.science.org/doi/10.1126/science.aat4422.
Pawliszyn J (2000) Theory of Solid-Phase Microextraction. J Chromatogr Sci 38:270–278.
Pawliszyn J (2012) Theory of Solid-Phase Microextraction. In: Handbook of Solid Phase Microextraction (Pawliszyn J, ed), pp 13–59. Elsevier.
Paxinos G, Huang X, Toga A (2000) The Rhesus Monkey Brain in Stereotaxic Coordinates.
Perry M, Li Q, Kennedy RT (2009) Review of recent advances in analytical techniques for the determination of neurotransmitters. Anal Chim Acta 653:1–22.
Perry RH, Tomlinson BE, Blessed G, Bergmann K, Gibson PH (1978) Correlation of cholinergic abnormalities with senile plaques and mental test scores in senile dementia. Br Med J 2:1457–1459.
Perry RJ, Hodges JR (1999) Attention and executive deficits in Alzheimer's disease. A critical review. Brain 122:383–404.
Phillips JM, McAlonan K, Robb WGK, Brown VJ (2000) Cholinergic neurotransmission influences covert orientation of visuospatial attention in the rat. Psychopharmacology (Berl) 150:112–116.
Pittaluga A (2016) Presynaptic release-regulating mGlu1 receptors in central nervous system. Front Pharmacol 7:1–15.
Pittaluga A, Feligioni M, Longordo F, Luccini E, Raiteri M (2006) Trafficking of presynaptic AMPA receptors mediating neurotransmitter release : Neuronal selectivity and relationships with sensitivity to cyclothiazide. Neuropharmacology 50:286–296.
Podkowa A, Malikowska N, Salat K, Mogilski S, Gdula-Argasinska J, Librowski T (2015) Effect of Donepezil, an acetylcholinesterase inhibitor, on spatial learning and memory in mice. Journal of Shanghai Jiaotong University (Medical Science) 57:47–54.
Pratt RD, Perdomo CA (2002) Donepezil-treated patients with probable vascular dementia demonstrate cognitive benefits. In: Annals of the New York Academy of Sciences, pp 513–522.
Prickaerts J, Şık A, van der Staay FJ, de Vente J, Blokland A (2005) Dissociable effects of acetylcholinesterase inhibitors and phosphodiesterase type 5 inhibitors on object recognition memory: Acquisition versus consolidation. Psychopharmacology (Berl) 177:381–390.
Quik M, Polonskaya Y, Gillespie A, Jakowec M, Lloyd GK, Langston JW (2000) Localization of nicotinic receptor subunit mRNAs in monkey brain by in situ hybridization. Journal of Comparative Neurology 425:58–69.
Quintero JE, Day BK, Zhang Z, Grondin R, Stephens ML, Huettl P, Pomerleau F, Gash DM, Gerhardt GA (2007) Amperometric measures of age-related changes in glutamate regulation in the cortex of rhesus monkeys. Exp Neurol 208:238–246.
Radulescu A, Daniel R, Niv Y (2016) The effects of aging on the interaction between reinforcement learning and attention. Psychol Aging 31:747–757 Available at: https://www.researchgate.net/publication/269107473_What_is_governance/link/548173090cf22525dcb61443/download%0Ahttp://www.econ.upf.edu/~reynal/Civil

wars_12December2010.pdf%0Ahttps://think-asia.org/handle/11540/8282%0Ahttps://www.jstor.org/stable/41857625.
Rajkowski J, Kubiak P, Aston-Jones G (1994) Locus coeruleus activity in monkey: Phasic and tonic changes are associated with altered vigilance. Brain Res Bull 35:607–616.
Ramos BP, Colgan L, Nou E, Ovadia S, Wilson SR, Arnsten AFT (2005) The beta-1 adrenergic antagonist, betaxolol, improves working memory performance in rats and monkeys. Biol Psychiatry 58:894–900.
Rapan LJ, Froudist-walsh S, Niu M, Xu T, Zhao L (2022) Cytoarchitectonic, receptor distribution and functional connectivity analyses of the macaque frontal lobe. bioRxiv.
Rauch HE, Tung F, Striebel CT (1965) Maximum likelihood estimates of linear dynamic systems. AIAA Journal 3:1445–1450 Available at: https://arc.aiaa.org/doi/10.2514/3.3166.
Redish AD, Jensen S, Johnson A, Kurth-Nelson Z (2007) Reconciling Reinforcement Learning Models With Behavioral Extinction and Renewal: Implications for Addiction, Relapse, and Problem Gambling. Psychol Rev 114:784–805.
Reimer J, Froudarakis E, Cadwell CR, Yatsenko D, Denfield GH, Tolias AS (2014) Pupil Fluctuations Track Fast Switching of Cortical States during Quiet Wakefulness. Neuron 84:355–362.
Reimer J, McGinley MJ, Liu Y, Rodenkirch C, Wang Q, McCormick DA, Tolias AS (2016) Pupil fluctuations track rapid changes in adrenergic and cholinergic activity in cortex. Nat Commun 7:1–7 Available at: http://dx.doi.org/10.1038/ncomms13289.
Remy P, Doder M, Lees A, Turjanski N, Brooks D (2005) Depression in Parkinson ' s disease: loss of dopamine and noradrenaline innervation in the limbic system. Brain 128:1314–1322.
Reyes-Garcés N, Diwan M, Boyacl E, Gómez-Ríos GA, Bojko B, Nobrega JN, Bambico FR, Hamani C, Pawliszyn J (2019) In vivo brain sampling using a microextraction probe reveals metabolic changes in rodents after deep brain stimulation. Anal Chem 91:9875–9884.
Reyes-garcés N, Gionfriddo E, Gómez-Ríos GA, Alam MdN, Boyaci E, Bojko B, Singh V, Grandy J, Pawliszyn J (2018) Advances in Solid Phase Microextraction and Perspective on Future Directions. Anal Chem 90:302–360.
ROBBINS TW, GRANON S, MUIR JL, DURANTOU F, HARRISON A, EVERITT BJ (1998) Neural Systems Underlying Arousal and Attention: Implications for Drug Abuse. Ann N Y Acad Sci 846:222–237 Available at: https://onlinelibrary.wiley.com/doi/10.1111/j.1749-6632.1998.tb09740.x.
Rogers SL, Doody RS, Mohs RC, Friedhoff LT (1998) Donepezil Improves Cognition and Global Function in Alzheimer Disease. Clin Chem 158:1021–1031.
Rohlf H, Jucksch V, Gawrilow C, Huss M, Hein J, Lehmkuhl U, Salbach-Andrae H (2012) Set shifting and working memory in adults with attention-deficit/ hyperactivity disorder. J Neural Transm 119:95–106.
Romberg C, Mattson MP, Mughal MR, Bussey TJ, Saksida LM (2011) Impaired attention in the 3xTgAD mouse model of Alzheimer's disease: Rescue by donepezil (Aricept). Journal of Neuroscience 31:3500–3507.
Rook JM, Abe M, Cho HP, Nance KD, Luscombe VB, Adams JJ, Dickerson JW, Remke DH, Garcia-Barrantes PM, Engers DW, Engers JL, Chang S, Foster JJ, Blobaum AL, Niswender CM, Jones CK, Conn PJ, Lindsley CW (2017) Diverse Effects on M1 Signaling and Adverse Effect Liability within a Series of M1 Ago-PAMs. ACS Chem Neurosci 8:866–883.

Rook JM, Bertron JL, Cho HP, Garcia-Barrantes PM, Moran SP, Maksymetz JT, Nance KD, Dickerson JW, Remke DH, Chang S, Harp JM, Blobaum AL, Niswender CM, Jones CK, Stauffer SR, Conn PJ, Lindsley CW (2018a) A Novel M 1 PAM VU0486846 Exerts Efficacy in Cognition Models without Displaying Agonist Activity or Cholinergic Toxicity. ACS Chem Neurosci 9:2274–2285.

Rook JM, Bertron JL, Cho HP, Garcia-Barrantes PM, Moran SP, Maksymetz JT, Nance KD, Dickerson JW, Remke DH, Chang S, Harp JM, Blobaum AL, Niswender CM, Jones CK, Stauffer SR, Conn PJ, Lindsley CW (2018b) A Novel M 1 PAM VU0486846 Exerts Efficacy in Cognition Models without Displaying Agonist Activity or Cholinergic Toxicity. ACS Chem Neurosci 9:2274–2285.

Rossi AF, Bichot NP, Desimone R, Ungerleider LG (2007) Top-down attentional deficits in Macaques with lesions of lateral prefrontal cortex. Journal of Neuroscience 27:11306–11314.

Rothenhoefe KM, Costa VD, Bartolo R, Vicario-Feliciano R, Murray EA, Averbeck BB (2017) Effects of ventral striatum lesions on stimulus-based versus action-based reinforcement learning. Journal of Neuroscience 37:6902–6914.

Rouse ST, Thomas TM, Levey AI (1997) Muscarinic acetylcholine receptor subtype, m2: Diverse functional implications of differential synaptic localization. Life Sci 60:1031–1038.

Rudebeck PH, Saunders RC, Lundgren DA, Murray EA (2017) Specialized Representations of Value in the Orbital and Ventrolateral Prefrontal Cortex: Desirability versus Availability of Outcomes. Neuron 95:1208-1220.e5 Available at: http://dx.doi.org/10.1016/j.neuron.2017.07.042.

Rupniak NMJ, Tye SJ, Field MJ (1997) Enhanced performance of spatial and visual recognition memory tasks by the selective acetylcholinesterase inhibitor E2020 in rhesus monkeys. Psychopharmacology (Berl) 131:406–410.

Salgado H, Garcia-Oscos F, Martinolich L, Hall S, Restom R, Tseng KY, Atzori M (2012) Pre- and postsynaptic effects of norepinephrine on γ-aminobutyric acid-mediated synaptic transmission in layer 2/3 of the rat auditory cortex. Synapse 66:20–28.

Salgado H, Garcia-Oscos F, Patel A, Martinolich L, Nichols JA, Dinh L, Roychowdhury S, Tseng KY, Atzori M (2011) Layer-specific noradrenergic modulation of inhibition in cortical layer II/III. Cerebral Cortex 21:212–221.

Salinas AG, Lee JO, Augustin SM, Zhang S, Patriarchi T, Tian L, Morales M, Mateo Y, Lovinger DM (2022) Sub-second striatal dopamine dynamics assessed by simultaneous fast-scan cyclic voltammetry and fluorescence biosensor. bioRxiv:2022.01.09.475513 Available at: https://www.biorxiv.org/content/10.1101/2022.01.09.475513v1%0Ahttps://www.biorxiv.org/content/10.1101/2022.01.09.475513v1.abstract.

Sallee FR, McGough J, Wigal T, Donahue J, Lyne A, Biederman J (2009) Guanfacine extended release in children and adolescents with attention-deficit/hyperactivity disorder: A placebo-controlled trial. J Am Acad Child Adolesc Psychiatry 48:155–165 Available at: http://dx.doi.org/10.1097/CHI.0b013e318191769e.

Santana N, Mengod G, Artigas F (2018) Expression of a1-adrenergic receptors in rat prefrontal cortex: cellular co-localization with 5-HT2A receptors. International journal of neuropsychopharmacology 16:1139–1151.

Santello M, Calì C, Bezzi P (2012) Gliotransmission and the Tripartite Synapse. In: Synaptic Plasticity. Advances in Experimental Medicine and Biology (Kreutz M, Sala C, eds), pp 307–331.
Sara SJ (2009) The locus coeruleus and noradrenergic modulation of cognition. Nat Rev Neurosci 10:211–223.
Sarter M, Lustig C (2019) Cholinergic double duty: cue detection and attentional control. Curr Opin Psychol 29:102–107 Available at: https://doi.org/10.1016/j.copsyc.2018.12.026.
Sarter M, Lustig C (2020) Forebrain cholinergic signaling: Wired and phasic, not tonic, and causing behavior. Journal of Neuroscience 40:712–719.
Sarter M, Lustig C, Blakely RD, Koshy Cherian A (2016) Cholinergic genetics of visual attention: Human and mouse choline transporter capacity variants influence distractibility. J Physiol Paris 110:10–18 Available at: http://dx.doi.org/10.1016/j.jphysparis.2016.07.001.
Scahill L, Chappell PB, Kim YS, Schultz RT, Katsovich L, Shepherd E, Arnsten AFT, Cohen DJ, Leckman JF (2001) A Placebo-Controlled Study of Guanfacine in the Treatment of Children With Tic Disorders and Attention Deficit Hyperactivity Disorder. American Journal of Psychiatry 158:1067–1074 Available at: http://psychiatryonline.org/doi/abs/10.1176/appi.ajp.158.7.1067.
Schlagenhauf F, Huys QJM, Deserno L, Rapp MA, Beck A, Heinze HJ, Dolan R, Heinz A (2014) Striatal dysfunction during reversal learning in unmedicated schizophrenia patients. Neuroimage 89:171–180 Available at: http://dx.doi.org/10.1016/j.neuroimage.2013.11.034.
Schluter EW, Mitz AR, Cheer JF, Averbeck BB (2014) Real-time dopamine measurement in awake monkeys. PLoS One 9.
Schmitz TW, Nathan Spreng R (2016) Basal forebrain degeneration precedes and predicts the cortical spread of Alzheimer's pathology. Nat Commun 7:1–13.
Schultz W, Dayan P, Montague PR (1997) A Neural Substrate of Prediction and Reward. Science (1979) 275:1593–1599 Available at: https://www.science.org/doi/10.1126/science.275.5306.1593.
Schwartz J, Javitch J (2013) Neurotransmitters. In: Principles of Neural Science (Kandel E, Schwartz J, Jessell T, Siegelbaum S, Hudspeth A, eds), pp 289–306.
Schwarz RD, Callahan MJ, Coughenour LL, Dickerson MR, Kinsora JJ, Lipinski WJ, Raby CA, Spencer CJ, Tecle H (1999) Milameline (CI-979/RU35926): A muscarinic receptor agonist with cognition-activating properties: Biochemical and in vivo characterization. Journal of Pharmacology and Experimental Therapeutics 291:812–822.
Schwerdt HN, Shimazu H, Amemori K, Amemori S, Tierney PL, Gibson DJ, Hong S, Yoshida T, Langer R, Cima MJ, Graybiel AM (2017) Long-term dopamine neurochemical monitoring in primates. Proceedings of the National Academy of Sciences 114:13260–13265.
Seu E, Lang A, Rivera RJ, Jentsch JD (2009) Inhibition of the norepinephrine transporter improves behavioral flexibility in rats and monkeys. Psychopharmacology (Berl) 202:505–519.
Sharma P, Tripathi MK, Shrivastava SK (2020) Targeting Enzymes for Pharmaceutical Development. Available at: http://link.springer.com/10.1007/978-1-0716-0163-1.
Shenhav A, Botvinick MM, Cohen JD (2013) The expected value of control: An integrative theory of anterior cingulate cortex function. Neuron 79:217–240 Available at: http://dx.doi.org/10.1016/j.neuron.2013.07.007.

Sheth SA, Mian MK, Patel SR, Asaad WF, Williams ZM, Dougherty DD, Bush G, Eskandar EN (2012) Human dorsal anterior cingulate cortex neurons mediate ongoing behavioural adaptation. Nature 488:218–221.
Shin CY, Kim HS, Cha KH, Won DH, Lee JY, Jang SW, Sohn UD (2018) The effects of donepezil, an acetylcholinesterase inhibitor, on impaired learning and memory in rodents. Biomol Ther (Seoul) 26:274–281.
Shinomoto S, Miura K, Koyama S (2005) A measure of local variation of inter-spike intervals. BioSystems 79:67–72.
Shinomoto S, Shima K, Tanji J (2003) Differences in Spiking Patterns among Cortical Neurons. Neural Comput 15:2823–2842.
Shiraishi T, Kikuchi T, Fukushi K, Shinotoh H, Nagatsuka SI, Tanaka N, Ota T, Sato K, Hirano S, Tanada S, Iyo M, Irie T (2005) Estimation of plasma IC50 of donepezil hydrochloride for brain acetylcholinesterase inhibition in monkey using N-[11C] methylpiperidin-4-yl acetate ([11C]MP4A) and PET. Neuropsychopharmacology 30:2154–2161.
Shirey JK, Brady AE, Jones PJ, Davis AA, Bridges TM, Kennedy JP, Jadhav SB, Menon UN, Xiang Z, Watson ML, Christian EP, Doherty JJ, Quirk MC, Snyder DH, Lah JJ, Levey AI, Nicolle MM, Lindsley CW, Conn PJ (2009) A selective allosteric potentiator of the M1 muscarinic acetylcholine receptor increases activity of medial prefrontal cortical neurons and restores impairments in reversal learning. Journal of Neuroscience 29:14271–14286.
Silvetti M, Seurinck R, van Bochove ME, Verguts T (2013) The influence of the noradrenergic system on optimal control of neural plasticity. Front Behav Neurosci 7:1–6.
Smith AC, Brown EN (2003) Estimating a State-Space Model from Point Process Observations. Neural Comput 15:965–991 Available at: http://www.mitpressjournals.org/doi/abs/10.1162/089976603765202622.
Smith AC, Frank LM, Wirth S, Yanike M, Hu D, Kubota Y, Graybiel AM, Suzuki WA, Brown EN (2004) Dynamic Analysis of Learning in Behavioral Experiments. J Neurosci 24:447–461 Available at: http://www.jneurosci.org/cgi/content/abstract/24/2/447\nhttp://www.jneurosci.org/cgi/reprint/24/2/447.pdf.
Spowart-Manning L, van der Staay FJ (2005) Spatial discrimination deficits by excitotoxic lesions in the Morris water escape task. Behavioural Brain Research 156:269–276.
Steere JC, Arnsten AF (1997) The alpha-2A noradrenergic receptor agonist guanfacine improves visual object discrimination reversal performance in aged rhesus monkeys. BehavNeurosci 111:883–891.
Stephan KE, Schlagenhauf F, Huys QJM, Raman S, Aponte EA, Brodersen KH, Rigoux L, Moran RJ, Daunizeau J, Dolan RJ, Friston KJ, Heinz A (2015) Computational neuroimaging strategies for single patient predictions. Neuroimage Available at: http://dx.doi.org/10.1016/j.neuroimage.2016.06.038.
Su Z, Cohen JY (2022) Two types of locus coeruleus norepinephrine neurons drive reinforcement learning. BioArxiv:1–24.
Sugimoto H (2001) Donepezil hydrochloride: A treatment drug for alzheimer s disease. Chemical Records 1:63–73.
Sun Y, Yang Y, Galvin VC, Yang S, Arnsten AF, Wang M (2017) Nicotinic α4β2 cholinergic receptor influences on dorsolateral prefrontal cortical neuronal firing during a working memory task. Journal of Neuroscience 37:5366–5377.

Swanson CJ, Perry KW, Koch-Krueger S, Katner J, Svensson KA, Bymaster FP (2006) Effect of the attention deficit/hyperactivity disorder drug atomoxetine on extracellular concentrations of norepinephrine and dopamine in several brain regions of the rat. Neuropharmacology 50:755–760.

Swanson JM, Volkow ND (2002) Pharmacokinetic and pharmacodynamic properties of stimulants: Implications for the design of new treatments for ADHD. Behavioural Brain Research 130:73–78.

Syková E (2004) Extrasynaptic volume transmission and diffusion parameters of the extracellular space. Neuroscience 129:861–876.

Taffe MA, Weed MR, Gold LH (1999) Scopolamine alters rhesus monkey performance on a novel neuropsychological test battery. Cognitive Brain Research 8:203–212.

Taffe MA, Weed MR, Gutierrez T, Davis SA, Gold LH (2002) Differential muscarinic and NMDA contributions to visuo-spatial paired-associate learning in rhesus monkeys. Psychopharmacology (Berl) 160:253–262.

Tamiji J, Crawford A (2011) The Neurobiology of Lipid Metabolism in. Europe PMC 18:98–112.

Terry A v., Callahan PM (2019) Nicotinic acetylcholine receptor ligands, cognitive function, and preclinical approaches to drug discovery. Nicotine and Tobacco Research 21:383–394.

Terry A v., Plagenhoef M, Callahan PM (2016) Effects of the nicotinic agonist varenicline on the performance of tasks of cognition in aged and middle-aged rhesus and pigtail monkeys. Psychopharmacology (Berl) 233:761–771.

Tervo DGR, Proskurin M, Manakov M, Kabra M, Vollmer A, Branson K, Karpova AY (2014) Behavioral variability through stochastic choice and its gating by anterior cingulate cortex. Cell 159:21–32 Available at: http://dx.doi.org/10.1016/j.cell.2014.08.037.

Thiele A (2013) Muscarinic signaling in the brain. Annu Rev Neurosci 36:271–294.

Thiele A, Bellgrove MA (2018) Neuromodulation of Attention. Neuron 97:769–785 Available at: https://doi.org/10.1016/j.neuron.2018.01.008.

Thienel R, Kellermann T, Schall U, Voss B, Reske M, Halfter S, Sheldrick AJ, Radenbach K, Habel U, Jon Shah N, Kircher T (2009) Muscarinic antagonist effects on executive control of attention. International Journal of Neuropsychopharmacology 12:1307–1317.

Thorn CA, Moon J, Bourbonais CA, Harms J, Edgerton JR, Stark E, Steyn SJ, Butter CR, Lazzaro JT, O'Connor RE, Popiolek M (2019) Striatal, Hippocampal, and Cortical Networks Are Differentially Responsive to the M4- and M1-Muscarinic Acetylcholine Receptor Mediated Effects of Xanomeline. ACS Chem Neurosci 10:1753–1764.

Tobin AB (2018) Targeting the M1 muscarinic receptor in Alzheimer's Disease. Proceedings for Annual Meeting of The Japanese Pharmacological Society WCP2018:SY85-2 Available at: https://www.jstage.jst.go.jp/article/jpssuppl/WCP2018/0/WCP2018_SY85-2/_article.

Totah NK, Neves RM, Panzeri S, Logothetis NK, Eschenko O (2018) The Locus Coeruleus Is a Complex and Differentiated Neuromodulatory System. Neuron 99:1055-1068.e6 Available at: https://doi.org/10.1016/j.neuron.2018.07.037.

Trendelenburg AU, Starke K, Limberger N (1994) Presynaptic α2A-adrenoceptors inhibit the release of endogenous dopamine in rabbit caudate nucleus slices. Naunyn Schmiedebergs Arch Pharmacol 350:473–481.

Tsolias A, Medalla M (2022) Muscarinic Acetylcholine Receptor Localization on Distinct Excitatory and Inhibitory Neurons Within the ACC and LPFC of the Rhesus Monkey. Front Neural Circuits 15:1–25.

Tsukada H, Kakiuchi T, Ando I, Ouchi Y (1997) Functional activation of cerebral blood flow abolished by scopolamine is reversed by cognitive enhancers associated with cholinesterase inhibition: A positron emission tomography study in unanesthetized monkeys. Journal of Pharmacology and Experimental Therapeutics 281:1408–1414.

Tsukada H, Nishiyama S, Fukumoto D, Ohba H, Sato K, Kakiuchi T (2004a) Effects of Acute Acetylcholinesterase Inhibition on the Cerebral Cholinergic Neuronal System and Cognitive Function: Functional Imaging of the Conscious Monkey Brain Using Animal PET in Combination with Microdialysis. Synapse 52:1–10.

Tsukada H, Nishiyama S, Fukumoto D, Ohba H, Sato K, Kakiuchi T (2004b) Effects of Acute Acetylcholinesterase Inhibition on the Cerebral Cholinergic Neuronal System and Cognitive Function: Functional Imaging of the Conscious Monkey Brain Using Animal PET in Combination with Microdialysis. Synapse 52:1–10.

Tsukada H, Nishiyama S, Ohba H, Sato K, Harada N, Kakiuchi T (2001) Cholinergic neuronal modulations affect striatal dopamine transporter activity: PET studies in the conscious monkey brain. Synapse 42:193–195.

Tsukada H, Sato K, Kakiuchi T, Nishiyama S (2000) Age-related impairment of coupling mechanism between neuronal activation and functional cerebral blood flow response was restored by cholinesterase inhibition: PET study with microdialysis in the awake monkey brain. Brain Res 857:158–164.

Turchi J, Sarter M (1997) Cortical acetylcholine and processing capacity: Effects of cortical cholinergic deafferentation on crossmodal divided attention in rats. Cognitive Brain Research 6:147–158.

Turchi J, Sarter M (2000) Cortical cholinergic inputs mediate processing capacity: Effects of 192 IgG-saporin-induced lesions on olfactory span performance. European Journal of Neuroscience 12:4505–4514.

Uhlen S, Muceniece R, Rangel N, Tiger G, Wikberg JE (1995) Comparison of the binding activities of some drugs on alpha 2A, alpha 2B and alpha 2C-adrenoceptors and non-adrenergic imidazoline sites in the guinea pig. Pharmacol Toxicol 76:353–364 Available at: http://www.ncbi.nlm.nih.gov/pubmed/7479575.

Uhlen S, Porter AC, Neubig RR (1994) The novel alpha-2 adrenergic radioligand [3H]-MK912 is alpha-2C selective among human alpha-2A, alpha-2B and alpha-2C adrenoceptors. Journal of Pharmacology and Experimental Therapeutics 271:1558–1565.

Uhlen S, Wikberg JE (1991) Delineation of rat kidney alpha 2A- and alpha 2B-adrenoceptors with [3H]RX821002 radioligand binding: computer modelling reveals that guanfacine is an alpha 2A-selective compound. Eur J Pharmacol 202:235–243 Available at: http://www.ncbi.nlm.nih.gov/pubmed/1666366\nhttp://www.sciencedirect.com/science/article/pii/0014299991902996.

Umbriaco D, Watkins KC, Descarries L, Cozzari C, Hartman BK (1994) Ultrastructural and morphometric features of the acetylcholine innervation in adult rat parietal cortex: An electron microscopic study in serial sections. Journal of Comparative Neurology 348:351–373.

U'Prichard DC, Bechtel WD, Rouot BM, Snyder SH (1979) Multiple apparent alpha-noradrenergic receptor binding sites in rat brain: Effect of 6-hydroxydopamine. Mol Pharmacol 16:47–60.

Uslaner JM, Eddins D, Puri V, Cannon CE, Sutcliffe J, Chew CS, Pearson M, Vivian JA, Chang RK, Ray WJ, Kuduk SD, Wittmann M (2013) The muscarinic M1 receptor positive

allosteric modulator PQCA improves cognitive measures in rat, cynomolgus macaque, and rhesus macaque. Psychopharmacology (Berl) 225:21–30.
Uslaner JM, Kuduk SD, Wittmann M, Lange HS, Fox S v., Min C, Pajkovic N, Harris D, Cilissen C, Mahon C, Mostoller K, Warrington S, Beshore DC (2018) Preclinical to human translational pharmacology of the novel M1positive allosteric modulator MK-7622. Journal of Pharmacology and Experimental Therapeutics 365:556–566.
Vardigan JD, Cannon CE, Puri V, Dancho M, Koser A, Wittmann M, Kuduk SD, Renger JJ, Uslaner JM (2015) Improved cognition without adverse effects: Novel M1 muscarinic potentiator compares favorably to donepezil and xanomeline in rhesus monkey. Psychopharmacology (Berl) 232:1859–1866.
Vartak D, Togt C Van Der, Vugt B Van, Roelfsema PR (2017) Electrochemical measurement of acetylcholine in the dorsolateral prefrontal cortex : A technical report. BioRXiv:1–25.
Venkatesan S, Jeoung H-S, Chen T, Power SK, Liu Y, Lambe EK (2020) Endogenous Acetylcholine and Its Modulation of Cortical Microcircuits to Enhance Cognition. In: Behavioral Pharmacology of the Cholinergic System, pp 47–69 Available at: http://link.springer.com/10.1007/7854_2020_138.
Verma S, Kumar A, Tripathi T, Kumar A (2018) Muscarinic and nicotinic acetylcholine receptor agonists: current scenario in Alzheimer's disease therapy. Journal of Pharmacy and Pharmacology 70:985–993.
Vijayraghavan S, Major AJ, Everling S (2016) Dopamine D1 and D2 Receptors Make Dissociable Contributions to Dorsolateral Prefrontal Cortical Regulation of Rule-Guided Oculomotor Behavior. Cell Rep 16:805–816 Available at: http://dx.doi.org/10.1016/j.celrep.2016.06.031.
Vijayraghavan S, Major AJ, Everling S (2018) Muscarinic M1 Receptor Overstimulation Disrupts Working Memory Activity for Rules in Primate Prefrontal Cortex. Neuron 98:1256-1268.e4 Available at: https://doi.org/10.1016/j.neuron.2018.05.027.
Vijayraghavan S, Wang M, Birnbaum SG, Williams G v., Arnsten AFTT (2007) Inverted-U dopamine D1 receptor actions on prefrontal neurons engaged in working memory. Nat Neurosci 10:376–384.
Vizi ES (2000) Role of high-affinity receptors and membrane transporters in nonsynaptic communication and drug action in the central nervous system. Pharmacol Rev 52:63–89.
Vo K, Rutledge RB, Chatterjee A, Kable JW (2014) Dorsal striatum is necessary for stimulus-value but not action-value learning in humans. Brain 137:3129–3135.
Voon V, Derbyshire K, Rück C, Irvine MA, Worbe Y, Enander J, Schreiber LRN, Gillan C, Fineberg NA, Sahakian BJ, Robbins TW, Harrison NA, Wood J, Daw ND, Dayan P, Grant JE, Bullmore ET (2015) Disorders of compulsivity: A common bias towards learning habits. Mol Psychiatry 20:345–352.
Vossel S, Bauer M, Mathys C, Adams RA, Dolan RJ, Stephan KE, Friston KJ (2014) Cholinergic stimulation enhances Bayesian belief updating in the deployment of spatial attention. Journal of Neuroscience 34:15735–15742.
Voytko M lou, Olton DS, Richardson RT, Gorman LK, Tobin JR, Price DL (1994) Basal forebrain lesions in monkeys disrupt attention but not learning and memory. Journal of Neuroscience 14:167–186.
Wallis JD, Kennerley SW (2011) Contrasting reward signals in the orbitofrontal cortex and anterior cingulate cortex. Ann N Y Acad Sci 1239:33–42.

Waltz JA (2017) The neural underpinnings of cognitive flexibility and their disruption in psychotic illness. Neuroscience 345:203–217 Available at: http://dx.doi.org/10.1016/j.neuroscience.2016.06.005.
Wang HX, Waterhouse BD, Gao WJ (2013) Selective suppression of excitatory synapses on GABAergic interneurons by norepinephrine in juvenile rat prefrontal cortical microcircuitry. Neuroscience 246:312–328 Available at: http://dx.doi.org/10.1016/j.neuroscience.2013.05.009.
Wang JKT, Andrews H, Thukral V (1992) Presynaptic Glutamate Receptors Regulate Noradrenaline Release from Isolated Nerve Terminals. J Neurochem 58:204–211.
Wang JX, Kurth-Nelson Z, Kumaran D, Tirumala D, Soyer H, Leibo JZ, Hassabis D, Botvinick M (2018) Prefrontal cortex as a meta-reinforcement learning system. Nat Neurosci 21:860–868 Available at: http://dx.doi.org/10.1038/s41593-018-0147-8.
Wang M, Datta D, Enwright J, Galvin V, Yang ST, Paspalas C, Kozak R, Gray DL, Lewis DA, Arnsten AFT (2019) A novel dopamine D1 receptor agonist excites delay-dependent working memory-related neuronal firing in primate dorsolateral prefrontal cortex. Neuropharmacology 150:46–58 Available at: https://doi.org/10.1016/j.neuropharm.2019.03.001.
Wang M, Gamo NJ, Yang Y, Jin LE, Wang XJ, Laubach M, Mazer JA, Lee D, Arnsten AFT (2011) Neuronal basis of age-related working memory decline. Nature 476:210–213.
Wang M, Ji J-Z, Li B-M (2004) The α2A-Adrenergic Agonist Guanfacine Improves Visuomotor Associative Learning in Monkeys. Neuropsychopharmacology 29:86–92 Available at: http://www.nature.com/doifinder/10.1038/sj.npp.1300278.
Wang M, Ramos BP, Paspalas CD, Shu Y, Simen A, Duque A, Vijayraghavan S, Brennan A, Dudley A, Nou E, Mazer J a., McCormick D a., Arnsten a. FT (2007) alpha2A-Adrenoceptors Strengthen Working Memory Networks by Inhibiting cAMP-HCN Channel Signaling in Prefrontal Cortex. Cell 129:397–410.
Wang XJ, Krystal JH (2014) Computational psychiatry. Neuron 84:638–654 Available at: http://dx.doi.org/10.1016/j.neuron.2014.10.018.
Ward N, Zinke W, Coppola J, Disney A (2018) Variations in neuromodulatory chemical signatures define compartments in macaque cortex. bioRxiv:272849.
Watanabe M, Kodama T, Hikosaka K (1997) Increase of Extracellular Dopamine in Primate Prefrontal Cortex During a Working Memory Task. J Neurophysiol 78:2795–2798.
Waterhouse BD, Azizi S a, Burne R a, Woodward DJ (1990) Modulation of rat cortical area 17 neuronal responses to moving visual stimuli during norepinephrine and serotonin microiontophoresis. Brain Res 514:276–292.
Waterhouse BD, Navarra RL (2018) The locus coeruleus-norepinephrine system and sensory signal processing: A historical review and current perspectives. Brain Res:1–15 Available at: https://doi.org/10.1016/j.brainres.2018.08.032.
Watson CJ, Venton BJ, Kennedy RT (2006) In Vivo Measurements of Neurotransmitters by Microdialysis Sampling. Anal Chem 78:1391–1399.
Watson MR, Voloh B, Naghizadeh M, Womelsdorf T (2019a) Quaddles: A multidimensional 3-D object set with parametrically controlled and customizable features. Behav Res Methods 51:2522–2532.
Watson MR, Voloh B, Thomas C, Hasan A, Womelsdorf T (2019b) USE: An integrative suite for temporally-precise psychophysical experiments in virtual environments for human, nonhuman, and artificially intelligent agents. J Neurosci Methods 326.

Weed MR, Taffe MA, Polis I, Roberts AC, Robbins TW, Koob GF, Bloom FE, Gold LH (1999) Performance norms for a rhesus monkey neuropsychological testing battery: Acquisition and long-term performance. Cognitive Brain Research 8:185–201.

Whitehouse PJ, Price DL, Clark AW, Coyle JT, DeLong MR (1981) Alzheimer disease: Evidence for selective loss of cholinergic neurons in the nucleus basalis. Ann Neurol 10:122–126.

Wiecki T v., Antoniades CA, Stevenson A, Kennard C, Borowsky B, Owen G, Leavitt B, Roos R, Durr A, Tabrizi SJ, Frank MJ (2016) A computational cognitive biomarker for early-stage Huntington's disease. PLoS One 11.

Wilkinson DG, Passmore AP, Bullock R, Hopker SW, Smith R, Potocnik FC v, Maud CM, Engelbrecht I, Hock C, Ieni JR, Bahra RS (2002) A multinational, randomised, 12-week, comparative study of donepezil and rivastigmine in patients with mild to moderate Alzheimer's disease. Int J Clin Pract 56:441–446 Available at: http://www.ncbi.nlm.nih.gov/pubmed/12166542.

Williams ZM, Eskandar EN (2006) Selective enhancement of associative learning by microstimulation of the anterior caudate. Nat Neurosci 9:562–568.

Wilson RC, Niv Y (2012) Inferring Relevance in a Changing World. Front Hum Neurosci 5:1–14 Available at: http://journal.frontiersin.org/article/10.3389/fnhum.2011.00189/abstract.

Wither RG, Boehnke SE, Lablans A, Armitage-Brown B, Munoz DP (2020) Behavioral shaping of rhesus macaques using the Cambridge neuropsychological automated testing battery. J Neurosci Methods 342:108803 Available at: https://doi.org/10.1016/j.jneumeth.2020.108803.

Woicik PA, Urban C, Alia-Klein N, Henry A, Maloney T, Telang F, Wang GJ, Volkow ND, Goldstein RZ (2011) A pattern of perseveration in cocaine addiction may reveal neurocognitive processes implicit in the Wisconsin Card Sorting Test. Neuropsychologia 49:1660–1669 Available at: http://dx.doi.org/10.1016/j.neuropsychologia.2011.02.037.

Womelsdorf T, Everling S (2015) Long-Range Attention Networks: Circuit Motifs Underlying Endogenously Controlled Stimulus Selection. Trends Neurosci 38:682–700 Available at: http://dx.doi.org/10.1016/j.tins.2015.08.009.

Womelsdorf T, Thomas C, Neumann A, Watson M, Boroujeni KB, Hassani SA, Parker JM, Hoffman KL (2021a) A Kiosk Station for the Assessment of Multiple Cognitive Domains and Enrichment of Monkeys. Front Behav Neurosci 15:721069 Available at: https://doi.org/10.1101/2021.03.06.434198.

Womelsdorf T, Watson MR, Tiesinga P (2021b) Learning at variable attentional load requires cooperation of working memory, meta-learning, and attention-augmented reinforcement learning. J Cogn Neurosci 34:79–107.

Xing B, Li YC, Gao WJ (2016) Norepinephrine versus dopamine and their interaction in modulating synaptic function in the prefrontal cortex. Brain Res 1641:217–233 Available at: http://dx.doi.org/10.1016/j.brainres.2016.01.005.

Yang Y, Paspalas CD, Jin LE, Picciotto MR, Arnsten AFT, Wang M (2013) Nicotinic α7 receptors enhance NMDA cognitive circuits in dorsolateral prefrontal cortex. Proc Natl Acad Sci U S A 110:12078–12083.

Yehuda S, Rabinovitz S, Mostofsky DI (1999) Mini-Review Essential Fatty Acids Are Mediators of Brain Biochemistry and Cognitive Functions. J Neurosci Res 56:565–570.

Yerkes RM, Dodson JD (1908) The Relation of Strength of Stimulus to Rapidity of Habit-Formation. Journal of Comparative Neurology and Psychology 18:459–482 Available at: http://psychclassics.yorku.ca/Yerkes/Law/.

Yi F, Liu S-S, Luo F, Zhang X-H, Li B-M (2013) Signaling mechanism underlying α2A -adrenergic suppression of excitatory synaptic transmission in the medial prefrontal cortex of rats. Eur J Neurosci 38:2364–2373.

Yoo JH, Valdovinos MG, Williams DC (2007) Relevance of donepezil in enhancing learning and memory in special populations: A review of the literature. J Autism Dev Disord 37:1883–1901.

Yoshimi K, Kumada S, Weitemier A, Jo T, Inoue M (2015) Reward-induced phasic dopamine release in the monkey ventral striatum and putamen. PLoS One 10:1–22.

Yu AJ, Dayan P (2005) Uncertainty, Neuromodulation, and Attention. Neuron 46:681–692 Available at: https://linkinghub.elsevier.com/retrieve/pii/S0896627305003624.

Zapata A, Chefer VI, Parrot S, Denoroy L (2013) Detection and Quantification of Neurotransmitters in Dialysates. Curr Protoc Neurosci 63:1–35.

Zhang H, Sulzer D (2004) Frequency-dependent modulation of dopamine release by nicotine. Nat Neurosci 7:581–582.

Zhang H, Sulzer D (2012) Regulation of striatal dopamine release by presynaptic auto- and heteroreceptors. Basal Ganglia 2:5–13 Available at: http://dx.doi.org/10.1016/j.baga.2011.11.004.

Zhang J, Rittman T, Nombela C, Fois A, Coyle-Gilchrist I, Barker RA, Hughes LE, Rowe JB (2016) Different decision deficits impair response inhibition in progressive supranuclear palsy and Parkinson's disease. Brain 139:161–173.

Zhang X, Es-haghi A, Musteata FM, Ouyang G, Pawliszyn J (2007a) Quantitative in Vivo Microsampling for Pharmacokinetic Studies Based on an Integrated Solid-Phase Microextraction System. Anal Chem 79:4507–4513.

Zhang X, Rauch A, Lee H, Xiao H, Rainer G, Logothetis N (2007b) Capillary hydrophilic interaction chromatography/mass spectrometry for simultaneous determination of multiple neurotransmitters in primate cerebral cortex. Rapid Commun Mass Spectrom 21:3621–3628.

Zhou X, Qi XL, Douglas K, Palaninathan K, Kang HS, Buccafusco JJ, Blake DT, Constantinidis C (2011) Cholinergic modulation of working memory activity in primate prefrontal cortex. J Neurophysiol 106:2180–2188.

Zilles K, Palomero-Gallagher N, Grefkes C, Scheperjans F, Boy C, Amunts K, Schleicher A (2002) Architectonics of the human cerebral cortex and transmitter receptor fingerprints: Reconciling functional neuroanatomy and neurochemistry. European Neuropsychopharmacology 12:587–599.

Zilles K, Palomero-Gallagher N, Schleicher A (2004) Transmitter receptors and functional anatomy of the cerebral cortex. J Anat 205:417–432.